Fifteen Lectures on

Laminar and Turbulent Combustion

N. Peters

RWTH Aachen

Ercoftac Summer School
September 14-28, 1992
Aachen, Germany

Draft version April 1995, may contain some type errors and misprints

Contents

Introduction

This text is a revised version of the material prepared for a lecture series at the ERCOFTAC-summer school at Aachen 1992. It was intended as an introduction to the fundamentals of combustion science with the aim to supply the basic notions and equations for more detailed numerical exercises in calculating combustion phenomena. With modern computational tools and facilities numerical calculations with large codes aiming to predict the performance of combustion devices such as furnaces, reciprocative engines and gas turbines are feasable and start to compete with practical experimentation. Whether they will partly or fully replace experimental investigations will largely depend on the efficiency of the numerical methods and on the reliability of the turbulence and the combustion models. While there is a large scientific community concerned with Computational Fluid Dynamics and the improvement of turbulence models, the know-how in combustion modeling seems to be restricted to a small number of specialists. The reason for this is the complexity of the subject which requires knowledge in thermodynamics, chemical kinetics and fluid mechanics. At the interface of these disciplines combustion lately emerges as an exact science which is able to predict rather than to merely describe experimentally observed phenomena. This is due to the introduction of modern mathematical tools such as large activation energy asymptotics and, more recently, rate-ratio asymptotics in combination with numerical calculations of one-dimensional flame structures.

In order to classify combustion phenomena it has been useful to introduce two types of flames: **Premixed and Diffusion Flames.** For laminar flames issuing from a tube burner these two models of combustion are shown in Fig. A. If fuel and air are already mixed within the tube, as in the case of a Bunsen burner, and the gas is ignited downstream a premixed flame front will propagate towards the burner until it finds its steady state position in the form of the well-known Bunsen cone. The fundamental quantity which describes this mode of combustion is the laminar burning velocity. It is the velocity with which the flame front propagates normal to itself into the unburned mixture. For the steady state Bunsen cone it therefore must be equal to the flow velocity v_n normal to the flame front. Behind the flame front yet unburnt intermediates as CO and H_2 will mix with the air entrained from outside the burner and lead to post flame oxidation and radiation.

The other mode of combustion is that in a diffusion flame. Here no air is mixed with the fuel within the tube of the burner. This may be achieved in a Bunsen burner shown in Lecture 6 in Fig. 6.2 by closing the air inlet into the mixing chamber. Then only fuel issues from the tube as shown in the second picture in Fig. A. It mixes with the surrounding air by convection and diffusion while combustion occurs already. Optimal conditions for combustion, however, are restricted to the vicinity of the surface of stoichiometric mixture. This is the surface where fuel and air exist locally at a proportion that allows both to be entirely consumed. This will lead to the highest flame temperature and due to the temperature sensitivity of the chemical reactions to the fastest reaction rates. In most cases combustion is much faster than diffusion and diffusion is the rate limiting step that controls the entire process. This is the reason why those flames, where the reactants are non-premixed, are called diffusion flames.

Premixed flames appear with a blue to bluish-green color, while diffusion flames radiate in a bright yellow. The blue color of premixed flames is due to chemiluminescence

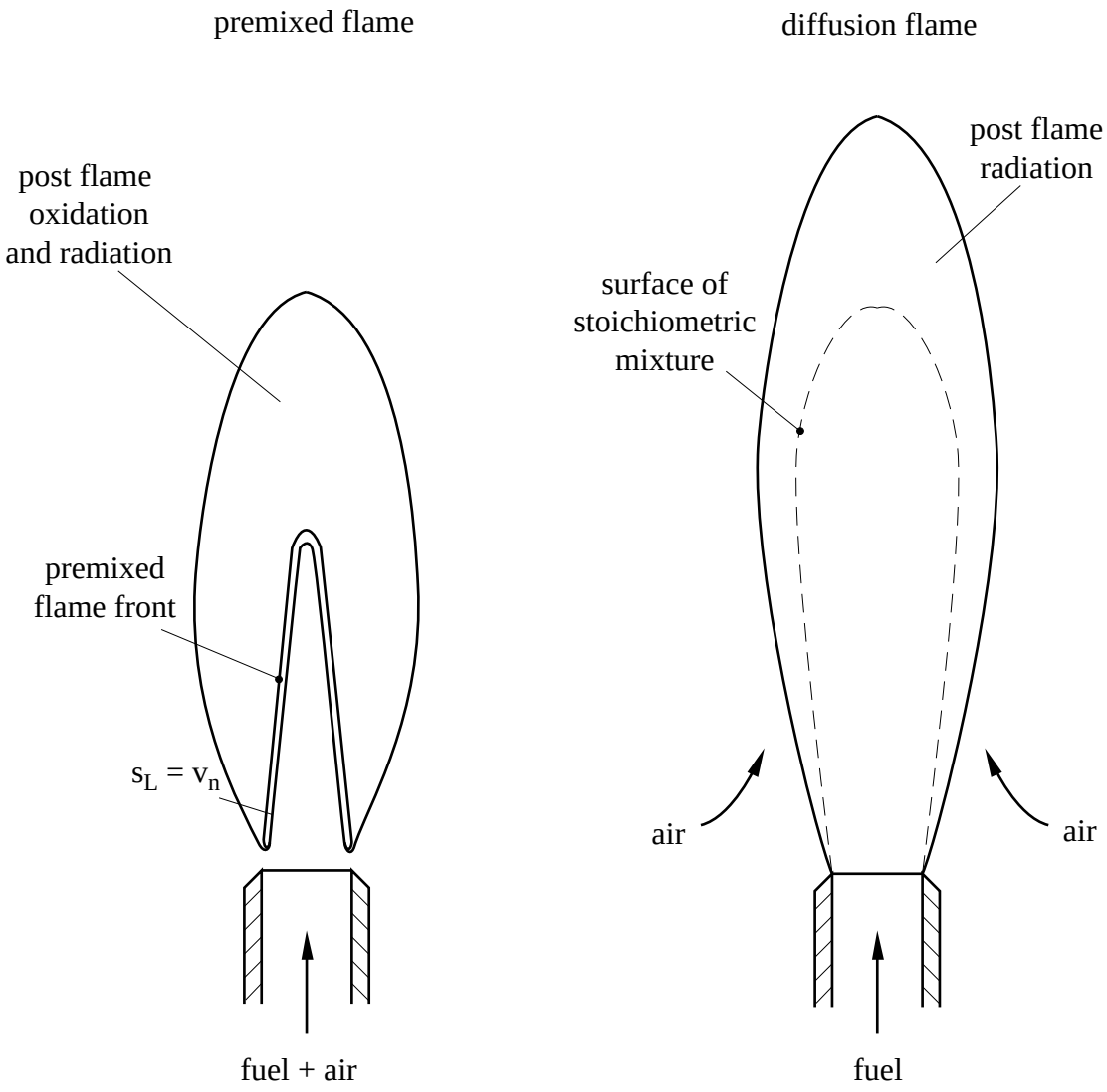

Fig. A: Different modes of laminar combustion

of some exited species (C_2 and CH radicals), while the yellow color of diffusion flames is caused by radiating soot particles which dominate over the chemiluminescence that is also present in non-pemixed combustion. Highly stretched diffusion flames, in fact, also appear blue since the local residence time is too short for soot particles to be formed. This leads to the conclusion that the color of a flame is characteristic for the available residence time rather than the mode of mixing.

Premixed Flames are used whenever intense combustion within a small volume is required. This is the case in household appliances and spark ignition engines. Another example for non-premixed combustion are Diesel engines, where a liquid fuel spray is injected into the compressed hot air within the cylinder. Large combustion devices such as furnaces, on the contrary, operate under non-premixed conditions with diffusion flames

since the premixing of large volumes of fuel and air represents a serious safety problem. Sometimes combustion is partially premixed in order to have a better control over flame stability and pollutant emissions, as it is the case in jet engine combustion chambers, in gas-boilers or in stratified-charge spark ignition engines.

The classification of combustion phenomena into premixed and non-premixed combustion is used throughout this text. After an introduction into the basic thermodynamics in Lecture 1, chemical kinetics in Lecture 2 and 3, ignition and extinction phenomena in Lecture 4 and the balance equations of fluid dynamics in Lecture 5 laminar premixed flames are treated in Lecture 6–8 and laminar diffusion flames in Lectures 9 and 10. Then an introduction into turbulent combustion is given in Lecture 11. Non-premixed turbulent combustion is presented in Lectures 12 and 13 while premixed turbulent combustion is treated in Lecture 14. Finally, a Lecture on partially premixed turbulent combustion closes the text.

In preparing these lectures and the revised text I have enjoyed the support from many of my students and friends. I am particular endebted to Peter Terhoeven for cross-reading the manuscript and for the preparation of many of the figures. I could also rely on the efficiency of ??? in preparing the manuscript.

Lecture 1: Mass and Energy Balance in Combustion Systems

Combustion is a mass and energy conversion process during which chemical bond energy is transformed to thermal energy. The fuel reacts with the oxygen of the air to form products such as carbon dioxide and water which have a lower chemical bond energy than the reactants. The details of the reaction mechanism that leads from the reactants to the products will be presented in Lecture 2. Here we will only consider the initial and the final state of a homogeneous system and use the classical balance laws of thermodynamics. This global view is much simpler and leads to some useful results such as the adiabatic flame temperature, but it contains less physics than the dynamic description of combustion processes, governed by differential equations, that will be considered in the subsequent lectures. We will first present definitions of concentrations and other thermodynamic variables and present the mass and energy balance for multicomponent systems.

1.1 Mole Fractions and Mass Fractions

When chemical species react with each other to form other species, their basic constituents, the chemical elements are conserved. The particular atom defining the element, a C-atom within a CH_4 molecule, for example, will be found within the CO_2 molecule after combustion is completed. In order to describe the chemical transformation between species quantitatively, we need to introduce definitions for concentrations. Since different descriptions are being used in the combustion literature, it is useful to present these first and to relate them to each other.

The Mole Fraction

We consider a multi-component system with n different chemical species that contains a large number of molecules. Then $6.0236 \cdot 10^{23}$ molecules are defined as one mole. The number of moles of species i denoted by n_i and its sum is the total number of moles n_s

$$n_s = \sum_{i=1}^{n} n_i \ . \tag{1.1}$$

The mole fraction of species i is now defined

$$X_i = \frac{n_i}{n_s}, \quad i = 1, 2, \ldots, n \ . \tag{1.2}$$

The Mass Fraction

The mass m_i of all molecules of species i is related to its number of moles by

$$m_i = W_i n_i \tag{1.3}$$

where W_i is the molecular weight of species i. For some important species in combustions W_i is given in Table 1.1. The total mass of all molecules in the mixture is

$$m = \sum_{i=1}^{n} m_i \ . \tag{1.4}$$

The mass fraction of species i is now defined

$$Y_i = \frac{m_i}{m}, \quad i = 1, 2, \ldots, n \ . \tag{1.5}$$

Defining the mean molecular weight W by

$$m = W n_s \tag{1.6}$$

one obtains the relation between mole fractions and mass fractions as

$$Y_i = \frac{W_i}{W} X_i \ . \tag{1.7}$$

The mean molecular weight may be calculated if either the mole fractions or the mass fractions are known

$$W = \sum_{i=1}^{n} W_i X_i = \left[\sum_{i=1}^{n} \frac{Y_i}{W_i} \right]^{-1} \ . \tag{1.8}$$

The Mass Fraction of Elements

In addition, the mass fraction of elements is very useful in combustion. While the mass of the species changes due to chemical reactions, the mass of the elements is conserved. We denote by m_j the mass of all atoms of element j contained in all molecules of the system. If a_{ij} is the number of atoms of element j in a molecule of species i and W_j is the molecular weight of that atom, the mass of all atoms j in the system is

$$m_j = \sum_{i=1}^{n} \frac{a_{ij} W_j}{W_i} m_i \ . \tag{1.9}$$

The mass fraction of element j is then

$$Z_j = \frac{m_j}{m} = \sum_{i=1}^{n} \frac{a_{ij} W_j}{W_i} Y_i = \frac{W_j}{W} \sum_{i=1}^{n} a_{ij} X_i, \quad j = 1, 2, \ldots, n_e \tag{1.10}$$

No.	Species	W_i [kg/kmol]	$H_{i,\mathrm{ref}}$ [kJ/mol]	$S_{i,\mathrm{ref}}$ [kJ/kmolK]	$\pi_{A,i}$	$\pi_{B,i}$
1	H	1.008	217.986	114.470	-1.2261	1.9977
2	HNO	31.016	99.579	220.438	-1.0110	4.3160
3	OH	17.008	39.463	183.367	3.3965	2.9596
4	HO_2	33.008	20.920	227.358	- .1510	4.3160
5	H_2	2.016	0.000	130.423	-2.4889	2.8856
6	H_2O	18.016	-241.826	188.493	-1.6437	3.8228
7	H_2O_2	34.016	-136.105	233.178	-8.4782	5.7218
8	N	14.008	472.645	153.054	5.8661	1.9977
9	NO	30.008	90.290	210.442	5.3476	3.1569
10	NO_2	46.008	33.095	239.785	-1.1988	4.7106
11	N_2	28.016	0.000	191.300	3.6670	3.0582
12	N_2O	44.016	82.048	219.777	-5.3523	4.9819
13	O	16.000	249.194	160.728	6.8561	1.9977
14	O_2	32.000	0.000	204.848	4.1730	3.2309
15	O_3	48.000	142.674	238.216	-3.3620	5.0313
16	NH	15.016	331.372	180.949	3.0865	2.9596
17	NH_2	16.024	168.615	188.522	-1.9835	3.8721
18	NH_3	17.032	-46.191	192.137	-8.2828	4.8833
19	N_2H_2	30.032	212.965	218.362	-8.9795	5.4752
20	N_2H_3	31.040	153.971	228.513	-17.5062	6.9796
21	N_2H_4	32.048	95.186	236.651	-25.3185	8.3608
22	C	12.011	715.003	157.853	6.4461	1.9977
23	CH	13.019	594.128	182.723	2.4421	3.0829
24	HCN	27.027	130.540	201.631	-5.3642	4.6367
25	HCNO	43.027	-116.733	238.048	-10.1563	6.0671
26	HCO	29.019	-12.133	224.421	-. 2313	4.2667
27	CH_2	14.027	385.220	180.882	-5.6013	4.2667
28	CH_2O	30.027	-115.896	218.496	-8.5350	5.4012
29	CH_3	15.035	145.686	193.899	-10.7155	5.3026
30	CH_2OH	31.035	-58.576	227.426	-15.3630	6.6590
31	CH_4	16.043	-74.873	185.987	-17.6257	6.1658
32	CH_3OH	32.043	-200.581	240.212	-18.7088	7.3989
33	CO	28.011	-110.529	197.343	4.0573	3.1075
34	CO_2	44.011	-393.522	213.317	-5.2380	4.8586
35	CN	26.019	456.056	202.334	4.6673	3.1075
36	C_2	24.022	832.616	198.978	1.9146	3.5268
37	C_2H	25.030	476.976	207.238	-4.6242	4.6367
38	C_2H_2	26.038	226.731	200.849	-15.3457	6.1658
39	C_2H_3	27.046	279.910	227.861	-17.0316	6.9056
40	CH_3CO	43.046	-25.104	259.165	-24.2225	8.5334
41	C_2H_4	28.054	52.283	219.468	-26.1999	8.1141
42	CH_3COH	44.054	-165.979	264.061	-30.7962	9.6679
43	C_2H_5	29.062	110.299	228.183	-32.8633	9.2980
44	C_2H_6	30.070	-84.667	228.781	-40.4718	10.4571
45	C_3H_8	44.097	-103.847	269.529	-63.8077	14.7978
46	C_4H_2	50.060	465.679	250.437	-34.0792	10.0379
47	C_4H_3	51.068	455.847	273.424	-36.6848	10.8271
48	C_4H_8	56.108	16.903	295.298	-72.9970	16.7215
49	C_4H_{10}	58.124	-134.516	304.850	-86.8641	19.0399
50	C_5H_{10}	70.135	-35.941	325.281	-96.9383	20.9882
51	C_5H_{12}	72.151	-160.247	332.858	-110.2702	23.3312
52	C_6H_{12}	84.152	-59.622	350.087	-123.2381	25.5016
53	C_6H_{14}	86.178	-185.560	380.497	-137.3228	28.2638
54	C_7H_{14}	98.189	-72.132	389.217	-147.4583	29.6956
55	C_7H_{16}	100.205	-197.652	404.773	-162.6188	32.6045
56	C_8H_{16}	112.216	-135.821	418.705	-173.7077	34.5776
57	C_8H_{18}	114.232	-223.676	430.826	-191.8158	37.6111
58	C_2H_{40}	44.054	-51.003	243.044	-34.3705	9.7912
59	HNO_3	63.016	-134.306	266.425	-19.5553	9.7912
60	HE	4.003	0.000	125.800		
61	A	39.944	0.000	154.599		
62	C_{solid}	12.011	0.000	0.000	-9.975	1.719

Table 1.1: Molecular constants for some important species in combustion at $T_{\mathrm{ref}} = 298.16\mathrm{K}$

where n_e is the total number of elements in the system. Notice that no meaningful definition for the mole fraction of elements can be given because only the mass of the elements is conserved. From the definitions above it follows that

$$\sum_{i=1}^{n} X_i = 1, \quad \sum_{i=1}^{n} Y_i = 1, \quad \sum_{j=1}^{n_e} Z_j = 1 \ . \tag{1.11}$$

The Partial Molar Density

An additional variable defining a concentration, that is frequently used in chemical kinetics, is the number of moles per unit volume or partial molar density

$$[X_i] = \frac{n_i}{V} \tag{1.12}$$

where V is the volume of the system. The molar density of the system is then

$$\frac{n_s}{V} = \sum_{i=1}^{n} [X_i] \ . \tag{1.13}$$

The Partial Density

The density and the partial density are defined

$$\rho = \frac{m}{V}, \quad \rho_i = \frac{m_i}{V} = \rho Y_i \ . \tag{1.14}$$

The partial molar density is related to the partial density and the mass fraction by

$$[X_i] = \frac{\rho_i}{W_i} = \frac{\rho Y_i}{W_i} \ . \tag{1.15}$$

The Thermal Equation of State

In most combustion systems of technical interest the law of ideal gases is valid. Even for high pressure combustion this is a sufficiently accurate approximation because the temperatures are typically also very high. In a mixture of ideal gases the molecules of species i exert on the surrounding walls of the vessel the partial pressure p_i

$$p_i = \frac{n_i \mathrm{R}\ T}{V} = [X_i] \mathrm{R}\ T = \frac{\rho Y_i}{W_i} \mathrm{R}\ T \ . \tag{1.16}$$

Here R is the universal gas constant equal to 8.3143 J/mol K or 82.05 atm cm^3 / mol K. Dalton's law states that for an ideal gas the total pressure is equal to the sum of the partial pressures. This leads to the thermal equation of state for a mixture of ideal gases

$$p = \sum_{i=1}^{n} p_i = n_s \frac{\mathrm{R}\ T}{V} = \frac{\rho \mathrm{R}\ T}{W} \tag{1.17}$$

where (1.6) and (1.14) have been used. From (1.16), (1.17), and (1.2) it follows that the partial pressure is equal to the total pressure times the mole fraction

$$p_i = pX_i \ . \tag{1.18}$$

Furthermore, defining the partial volume by

$$V_i = \frac{n_i \mathrm{R}\ T}{p} \tag{1.19}$$

it follows that an equivalent relation exists for the partial volume

$$V_i = V\ X_i \ . \tag{1.20}$$

1.2 Stoichiometry

Equations describing chemical reactions such as

$$\mathrm{H_2} + \frac{1}{2}\mathrm{O_2} = \mathrm{H_2O}$$

or

$$\mathrm{H} + \mathrm{O_2} \underset{k_b}{\overset{k_f}{\rightleftharpoons}} \mathrm{OH} + \mathrm{O}$$

are based on the principle of element conservation during reaction and define the stoichiometric coefficients ν_i' of the reactant i on the left hand side and ν_i'' of the product i on the right hand side. The first example above corresponds to a global reaction while the second one, where the equal sign is replaced by arrows, denotes an elementary reaction that takes place with a finite reaction rate (conf. Lecture 2). Formally a reaction equation may be cast into the form

$$\sum_{i=1}^{n} \nu_i'\ \mathcal{M}_i = \sum_{i=1}^{n} \nu_i''\ \mathcal{M}_i \tag{1.21}$$

where $\mathcal{M}_i$ stands for the chemical symbol of species i. The net stoichiometric coefficient

$$\nu_i = \nu_i'' - \nu_i' \tag{1.22}$$

is positive for products and negative for reactants. A system of r elementary reactions may formally then be written

$$\sum_{i=1}^{n} \nu_{ik}\ \mathcal{M}_i = 0, \quad k = 1, 2, \ldots, r \tag{1.23}$$

where ν_{ik} is the net stoichiometric coefficient of species i in reaction k.

The stoichiometry defined by the reaction equation relates the molar production or consumption of species to each other. The change of the number of moles of species i to that of species 1 is

$$\frac{\mathrm{d}n_i}{\nu_i} = \frac{\mathrm{d}n_1}{\nu_1} \ . \tag{1.24}$$

With (1.3) the relation between the partial masses is

$$\frac{\mathrm{d}m_i}{\nu_i W_i} = \frac{\mathrm{d}m_1}{\nu_1 W_1} \ . \tag{1.25}$$

Since the total mass in the system is independent of the chemical reaction (while the total number of moles is not), the relation between mass fractions is

$$\frac{\mathrm{d}Y_i}{\nu_i W_i} = \frac{\mathrm{d}Y_1}{\nu_1 W_1} \ . \tag{1.26}$$

A fuel-air mixture is called stoichiometric, if the fuel-to-oxygen ratio is such that both are entirely consumed when combustion to CO_2 and H_2O is completed. For example, the global reaction describing the combustion of a single component hydrocarbon fuel C_mH_n (subscript F) is

$$\nu'_F \ \mathrm{C}_m \ \mathrm{H}_n + \nu'_{\mathrm{O}_2} \ \mathrm{O}_2 = \nu''_{\mathrm{CO}_2} \ \mathrm{CO}_2 + \nu''_{\mathrm{H}_2\mathrm{O}} \ \mathrm{H}_2\mathrm{O}$$

the stoichiometric coefficients are

$$\nu'_F = 1, \quad \nu'_{\mathrm{O}_2} = m + \frac{n}{4}, \quad \nu''_{\mathrm{CO}_2} = m, \quad \nu''_{\mathrm{H}_2\mathrm{O}} = \frac{n}{2} \tag{1.27}$$

where ν'_F may be chosen arbitrarily to unity. Stoichiometric mixture requires that the ratio of the number of moles of fuel and oxidizer in the unburnt mixture is equal to the ratio of the stoichiometric coefficients

$$\left.\frac{n_{\mathrm{O}_2,u}}{n_{F,u}}\right|_{\mathrm{st}} = \frac{\nu'_{\mathrm{O}_2}}{\nu'_F} \tag{1.28}$$

or in terms of mass fractions

$$\left.\frac{Y_{\mathrm{O}_2,u}}{Y_{F,u}}\right|_{\mathrm{st}} = \frac{\nu'_{\mathrm{O}_2} \ W_{\mathrm{O}_2}}{\nu'_F \ W_F} = \nu \tag{1.29}$$

where ν is called the stoichiometric mass ratio. Then fuel and oxidizer are both consumed when combustion is completed. Integrating (1.26) with $i = \mathrm{O}_2$, $1 = F$ between the initial unburnt state (subscript u) and any later state leads to

$$\frac{Y_{\mathrm{O}_2} - Y_{\mathrm{O}_2,u}}{\nu'_{\mathrm{O}_2} \ W_{\mathrm{O}_2}} = \frac{Y_F - Y_{F,u}}{\nu'_F \ W_F} \ . \tag{1.30}$$

This may be written as

$$\nu \ Y_F - Y_{\mathrm{O}_2} = \nu \ Y_{F,u} - Y_{\mathrm{O}_2,u} \tag{1.31}$$

For a stoichiometric mixture fuel and oxygen are completely consumed at the end of combustion, $Y_F = Y_{\mathrm{O}_2} = 0$. Introducing this into (1.31), (1.29) is recovered.

1.3 The Mixture Fraction

The mixture fraction is an extremely useful variable in combustion, in particular for diffusion flames (Lectures 9, 10, 12, and 13). Here we present it first for a homogeneous system. In a two-feed system, where a fuel stream (subscript 1) with mass flux $\dot{m}_1$ is mixed with an oxidizer stream (subscript 2) with mass flux $\dot{m}_2$, the mixture fraction represents the mass fraction of the fuel stream in the mixture

$$Z \;=\; \frac{\dot{m}_1}{\dot{m}_1 + \dot{m}_2} \;. \tag{1.32}$$

Both fuel and oxidizer streams may contain inerts such as nitrogen. The mass fraction $Y_{F,u}$ of the fuel in the mixture is proportional to the mass fraction in the original fuel stream, so

$$Y_{F,u} \;=\; Y_{F,1} Z \;, \tag{1.33}$$

where $Y_{F,1}$ denotes the mass fraction of fuel in the fuel stream. Similarly, since $1 - Z$ represents the mass fraction of the oxidizer stream in the mixture, one obtains for the mass fraction of oxygen in the mixture

$$Y_{\mathrm{O}_2,u} \;=\; Y_{\mathrm{O}_2,2}(1 - Z) \;, \tag{1.34}$$

where $Y_{\mathrm{O}_2,2}$ represents the mass fraction of oxygen in the oxidizer stream ($Y_{\mathrm{O}_2,2} = 0.232$ for air). Introducing (1.33) and (1.34) into (1.31) one obtains the mixture fraction as a variable that couples the mass fractions of the fuel and the oxygen

$$Z \;=\; \frac{\nu Y_F - Y_{\mathrm{O}_2} + Y_{\mathrm{O}_2,2}}{\nu Y_{F,1} + Y_{\mathrm{O}_2,2}} \;. \tag{1.35}$$

For a stoichiometric mixture one obtains with $\nu Y_F = Y_{\mathrm{O}_2}$ the stoichiometric mixture fraction

$$Z_{\mathrm{st}} \;=\; \left[1 + \frac{\nu Y_{F,1}}{Y_{\mathrm{O}_2,2}}\right]^{-1} \;. \tag{1.36}$$

If $Z < Z_{\mathrm{st}}$ fuel is deficient and the mixture is called fuel lean. Then, combustion terminates when all the fuel is consumed, $Y_{F,b} = 0$ in the burnt gas (subscript b). The remaining oxygen mass fraction in the burnt gas is calculated from (1.35) as

$$Y_{\mathrm{O}_2,b} = Y_{\mathrm{O}_2,2}\left(1 - \frac{Z}{Z_{\mathrm{st}}}\right), \quad Z \le Z_{\mathrm{st}} \tag{1.37}$$

where (1.36) was used. Similarly, if $Z > Z_{\mathrm{st}}$ oxygen is deficient and the mixture is called fuel rich. Combustion then terminates when all the oxygen is consumed, $Y_{\mathrm{O}_2,b} = 0$, leading to

$$Y_{F,b} = Y_{F,1}\,\frac{Z - Z_{\mathrm{st}}}{1 - Z_{\mathrm{st}}}, \quad Z \ge Z_{\mathrm{st}} \;. \tag{1.38}$$

For the hydrocarbon fuel considered above the element mass fractions in the unburnt mixture are

$$Z_{\mathrm{C}} = m\,\frac{W_{\mathrm{C}}}{W_F}\,Y_{F,u} \;, \quad Z_{\mathrm{H}} = n\,\frac{W_{\mathrm{H}}}{W_F}\,Y_{F,u} \;, \quad Z_{\mathrm{O}} = Y_{\mathrm{O}_2,u} \tag{1.39}$$

Because elements are conserved during combustion, the element mass fractions calculates from (1.10) do not change. For the burnt gas they are

$$\begin{aligned} Z_{\mathrm{C}} &= m\ \frac{W_{\mathrm{C}}}{W_F}\ Y_{F,b} + \frac{W_{\mathrm{C}}}{W_{\mathrm{CO_2}}}\ Y_{\mathrm{CO_2},b} \\ Z_{\mathrm{H}} &= n\ \frac{W_{\mathrm{H}}}{W_F}\ Y_{F,b} + 2\ \frac{W_{\mathrm{H}}}{W_{\mathrm{H_2O}}}\ Y_{\mathrm{H_2O},b} \\ Z_{\mathrm{O}} &= 2\ \frac{W_{\mathrm{O}}}{W_{\mathrm{O_2}}}\ Y_{\mathrm{O_2},b} + 2\ \frac{W_{\mathrm{O}}}{W_{\mathrm{CO_2}}}\ Y_{\mathrm{CO_2},b} + \frac{W_{\mathrm{O}}}{W_{\mathrm{H_2O}}}\ Y_{\mathrm{H_2O},b}\ . \end{aligned} \tag{1.40}$$

This leads with (1.33) and $Y_{F,b} = 0$ for $Z \leq Z_{\mathrm{st}}$ and (1.38) for $Z \geq Z_{\mathrm{st}}$ to piecewise linear relations of the product mass fractions in terms of Z

$$\begin{aligned} Z \leq Z_{\mathrm{st}}: \quad Y_{\mathrm{CO_2},b} &= Y_{\mathrm{CO_2,st}}\ \frac{Z}{Z_{\mathrm{st}}} \\ Y_{\mathrm{H_2O},b} &= Y_{\mathrm{H_2O,st}}\ \frac{Z}{Z_{\mathrm{st}}} \\ Z \geq Z_{\mathrm{st}}: \quad Y_{\mathrm{CO_2},b} &= Y_{\mathrm{CO_2,st}}\ \frac{1-Z}{1-Z_{\mathrm{st}}} \\ Y_{\mathrm{H_2O},b} &= Y_{\mathrm{H_2O,st}}\ \frac{1-Z}{1-Z_{\mathrm{st}}}\ . \end{aligned} \tag{1.41}$$

where

$$\begin{aligned} Y_{\mathrm{CO_2,st}} &= Y_{F,1}\ Z_{\mathrm{st}}\ \frac{m\ W_{\mathrm{CO_2}}}{W_F} \\ Y_{\mathrm{H_2O,st}} &= Y_{F,1}\ Z_{\mathrm{st}}\ \frac{n\ W_{\mathrm{H_2O}}}{2\ W_F}\ . \end{aligned} \tag{1.42}$$

Profiles of Y_F and $Y_{\mathrm{O_2}}$ in the unburnt and in the burnt gas and product profiles are shown in Fig. 1.1.

The fuel-air equivalence ratio is the ratio of fuel-air ratio in the unburnt to that of a stoichiometric mixture

$$\phi = \frac{Y_{F,u}\ /\ Y_{\mathrm{O_2},u}}{(Y_{F,u}\ /\ Y_{\mathrm{O_2},u})_{\mathrm{st}}} = \frac{\nu\ Y_{F,u}}{Y_{\mathrm{O_2},u}}\ . \tag{1.43}$$

Introducing (1.33) and (1.34) into (1.43) leads with (1.36) to a unique relation between the equivalence ratio and the mixture fraction

$$\phi = \frac{Z}{1-Z}\ \frac{(1-Z_{\mathrm{st}})}{Z_{\mathrm{st}}}\ . \tag{1.44}$$

This relation is also valid for multicomponent fuels (conf. Exercise 1.1). It illustrates that the mixture fraction is simply another expression for the local equivalence ratio. It may also be interpreted as a combination of element mass fractions. For example, the fuel mass fraction $Y_{F,u}$ of a hydrocarbon fuel $\mathrm{C}_m\mathrm{H}_n$ is equal to

$$Y_{F,u} = W_F\ \left(n\ \frac{Z_{\mathrm{C}}}{W_{\mathrm{C}}} + m\ \frac{Z_{\mathrm{H}}}{W_{\mathrm{H}}}\right) \tag{1.45}$$

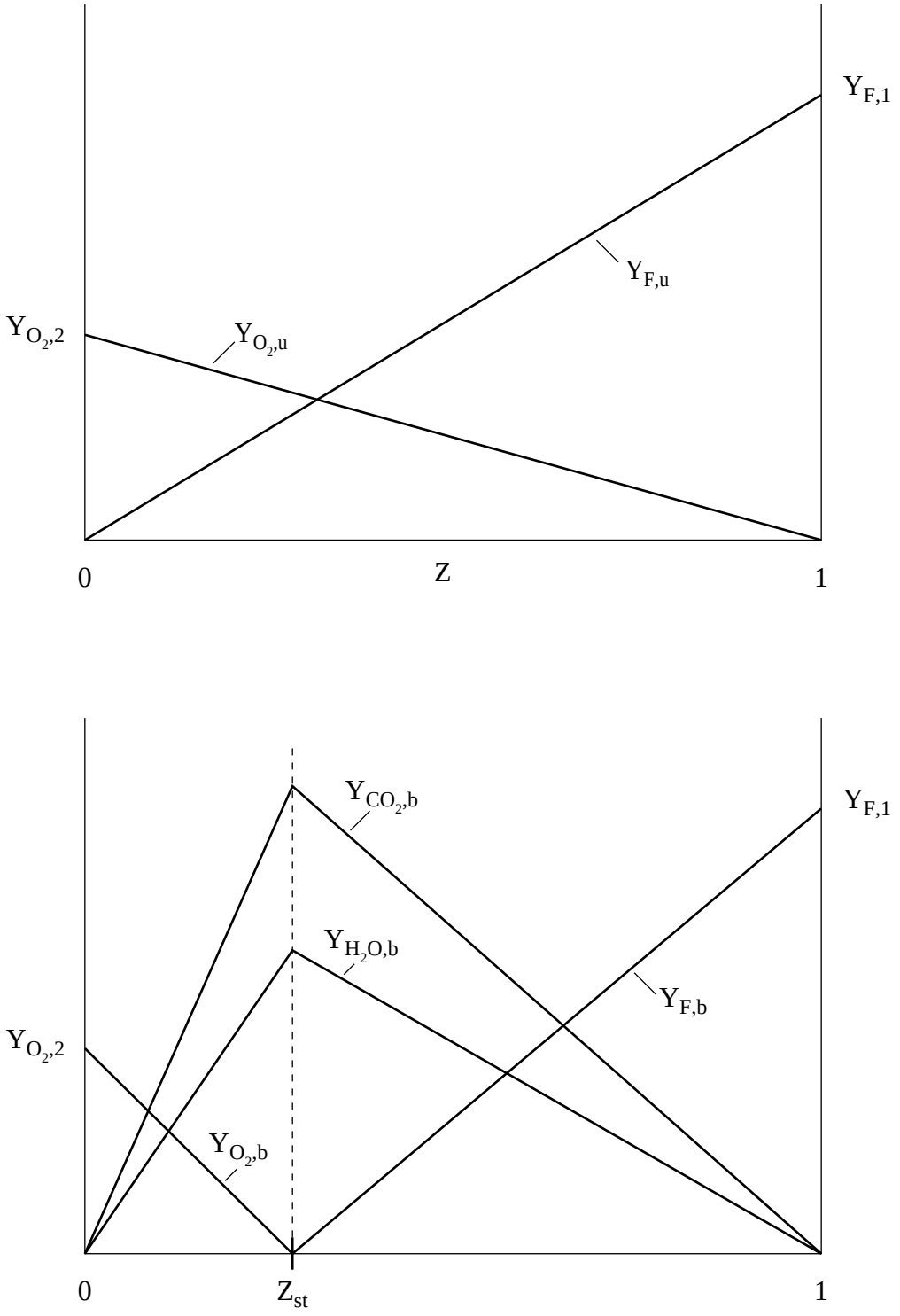

Fig. 1.1: Profiles of Y_F, Y_{O_2}, Y_{CO_2}, and Y_{H_2O} in the unburnt and the burnt gas

Equation (1.33) then shows that Z is related to a linear combination of Z_{C} and Z_{H}.

1.4 Energy Conservation During Combustion

The first law of thermodynamics describes the balance between different forms of energy and thereby defines the internal energy.

$$\mathrm{d}u + p\mathrm{d}v = \mathrm{d}h - v\mathrm{d}p = \mathrm{d}q + \mathrm{d}w_R \,. \tag{1.46}$$

Here $\mathrm{d}q$ is the heat transfer from the surroundings, $\mathrm{d}w_R$ is the frictional work, $\mathrm{d}u$ is the change of internal energy and $p\mathrm{d}v$ is the work due to volumetric changes. The specific enthalpy h is related to the specific inner energy u by

$$h = u + pv = u + \frac{\mathrm{R}\ T}{W} \tag{1.47}$$

where $v = 1/\rho$ is the specific volume.

In a multicomponent system, the specific internal energy and specific enthalpy are the mass weighted sums of the specific quantities of all species

$$u = \sum_{i=1}^{n} Y_i\ u_i, \quad h = \sum_{i=1}^{n} Y_i\ h_i \ . \tag{1.48}$$

For an ideal gas the partial specific enthalpy is related to the partial specific internal energy by

$$h_i = u_i + \frac{\mathrm{R}\ T}{W_i} \tag{1.49}$$

and both depend only on temperature. The temperature dependence of the partial specific enthalpy is given by

$$h_i = h_{i,\mathrm{ref}} + \int_{T_{\mathrm{ref}}}^{T} c_{pi}\ \mathrm{d}T \ . \tag{1.50}$$

Here c_{pi} is the specific heat capacity at constant pressure and $h_{i,\mathrm{ref}}$ is the reference enthalpy at the reference temperature T_{ref}. This temperature may be arbitrarily chosen, most frequently $T_{\mathrm{ref}} = 0$ K or $T_{\mathrm{ref}} = 298.16$ K are being used. The partial molar enthalpy is

$$H_i = W_i\ h_i \tag{1.51}$$

and its temperature dependence is

$$H_i = H_{i,\mathrm{ref}} + \int_{T_{\mathrm{ref}}}^{T} C_{pi}\ \mathrm{d}T \tag{1.52}$$

where the molar heat capacity at constant pressure is

$$C_{pi} = W_i\ c_{pi} \ . \tag{1.53}$$

In a multicomponent system, the specific heat capacity at constant pressure of the mixture is

$$c_p = \sum_{i=1}^{n} Y_i c_{pi} \,. \tag{1.54}$$

In Table 1.1 the molar reference enthalpies at $T_{\rm ref} = 298.16$ K of a number of species are listed. It should be noted that the reference enthalpies of H_2, O_2, N_2, and solid carbon were chosen as zero, because they represent the chemical elements. Reference enthalpies of combustion products such as CO_2 and H_2O are typically negative. The temperature dependence of C_{pi} and H_i may be calculated from the NASA polynomials documented in a paper by A. Burcat [1].

1.5 The Adiabatic Flame Temperature

Let us consider the first law for an adiabatic system ($\mathrm{d}q = 0$) at constant pressure ($\mathrm{d}p = 0$) and neglect the work done by friction ($\mathrm{d}w_R = 0$). From (1.46) we then have $\mathrm{d}h = 0$ which may be integrated from the unburnt to the burnt state as

$$h_u = h_b \tag{1.55}$$

or

$$\sum_{i=1}^{n} Y_{i,u} h_{i,u} = \sum_{i=1}^{n} Y_{i,b} h_{i,b} \,. \tag{1.56}$$

With the temperature dependence of the specific enthalpy (1.50) this may be written as

$$\sum_{i=1}^{n} (Y_{i,u} - Y_{i,b}) h_{i,\rm ref} = \int_{T_{\rm ref}}^{T_b} c_{p,b} \mathrm{d}T - \int_{T_{\rm ref}}^{T_u} c_{p,u} \mathrm{d}T \,. \tag{1.57}$$

Here the specific heat capacities are those of the mixture, to be calculated with the mass fractions of the burnt and unburnt gases, respectively

$$c_{p,b} = \sum_{i=1}^{n} Y_{i,b} c_{p_i}(T), \quad c_{p,u} = \sum_{i=1}^{n} Y_{i,u} c_{p_i}(T) \,. \tag{1.58}$$

For a one-step global reaction the left hand side of (1.57) may be calculated by integrating (1.26) as

$$Y_{i,u} - Y_{i,b} = (Y_{F,u} - Y_{F,b}) \frac{\nu_i W_i}{\nu_F W_F} \tag{1.59}$$

such that

$$\sum_{i=1}^{n} (Y_{i,u} - Y_{i,b}) h_{i,\rm ref} = \frac{(Y_{F,u} - Y_{F,b})}{\nu_F W_F} \sum_{i=1}^{n} \nu_i W_i h_{i,\rm ref} \,. \tag{1.60}$$

Here it is convenient to define the heat of combustion as

$$Q = -\sum_{i=1}^{n} \nu_i W_i h_i = -\sum_{i=1}^{n} \nu_i H_i \,. \tag{1.61}$$

This quantity changes very little with temperature and is often set equal to

$$Q_{\rm ref} = -\sum_{i=1}^{n} \nu_i H_{i,\rm ref} \tag{1.62}$$

For simplicity, let us set $T_u = T_{\rm ref}$ and assume $c_{p,b}$ to be approximately constant. For combustion in air, the contribution of nitrogen is dominant in calculating $c_{p,b}$. At temperatures around 2000 K its specific heat is approximately 1.30 kJ/kg K. The value of c_{pi} is somewhat larger for CO_2 and somewhat smaller for O_2 while that for H_2O is twice as large. A first aproximation for the specific heat of the burnt gas for lean and stoichiometric mixtures is then $c_p = 1.40$ kJ/kg K. Assuming c_p constant and $Q = Q_{\rm ref}$, the adiabatic flame temperature for a lean mixture ($Y_{F,b} = 0$) is calculated from (1.57) and (1.60) with $\nu_F = -\nu'_F$ as

$$T_b - T_u = \frac{Q_{\rm ref} Y_{F,u}}{c_p \nu'_F W_F} \,. \tag{1.63}$$

For a rich mixture (1.59) must be replaced by

$$Y_{i,u} - Y_{i,b} = (Y_{\rm O_2,u} - Y_{\rm O_2,b}) \frac{\nu_i W_i}{\nu_{\rm O_2} W_{\rm O_2}} \tag{1.64}$$

and one obtains similarly for complete consumption of the oxygen ($\rm Y_{O_2,b} = 0$)

$$T_b - T_u = \frac{Q_{\rm ref} Y_{\rm O_2,u}}{c_p \nu'_{\rm O_2} W_{\rm O_2}} \,. \tag{1.65}$$

Equations (1.63) and (1.65) may be expressed in terms of the mixture fraction by introducing (1.33) and (1.34) and by specifying the temperature of the unburnt mixture by

$$T_u(Z) = T_2 - Z(T_2 - T_1) \tag{1.66}$$

where T_2 is the temperature of the oxidizer stream and T_1 that of the fuel stream. Equation (1.66) describes mixing of the two streams with c_p assumed to be constant. Equations (1.63) and (1.65) then take the form

$$\begin{aligned} T_b(Z) &= T_u(Z) + \frac{Q_{\rm ref} Y_{F,1}}{c_p \nu'_F W_F} Z, \qquad && Z \le Z_{\rm st} \\ T_b(Z) &= T_u(Z) + \frac{Q_{\rm ref} Y_{\rm O_2,2}}{c_p \nu'_{\rm O_2} W_{\rm O_2}} (1 - Z) \qquad && Z \ge Z_{\rm st} \,. \end{aligned} \tag{1.67}$$

The adiabatic temperature is plotted over mixture fraction in Fig. 1.2. The maximum temperature at $Z = Z_{\rm st}$ is calculated from either one of (1.67) as

$$\begin{aligned} T_{\rm st} &= T_u(Z_{\rm st}) + \frac{Y_{F,1} Z_{\rm st} Q_{\rm ref}}{\nu'_F W_F c_p} \\ &= T_u(Z_{\rm st}) + \frac{Y_{\rm O_2,2}(1 - Z_{\rm st}) Q_{\rm ref}}{\nu'_{\rm O_2} W_{\rm O_2} c_p} \,. \end{aligned} \tag{1.68}$$

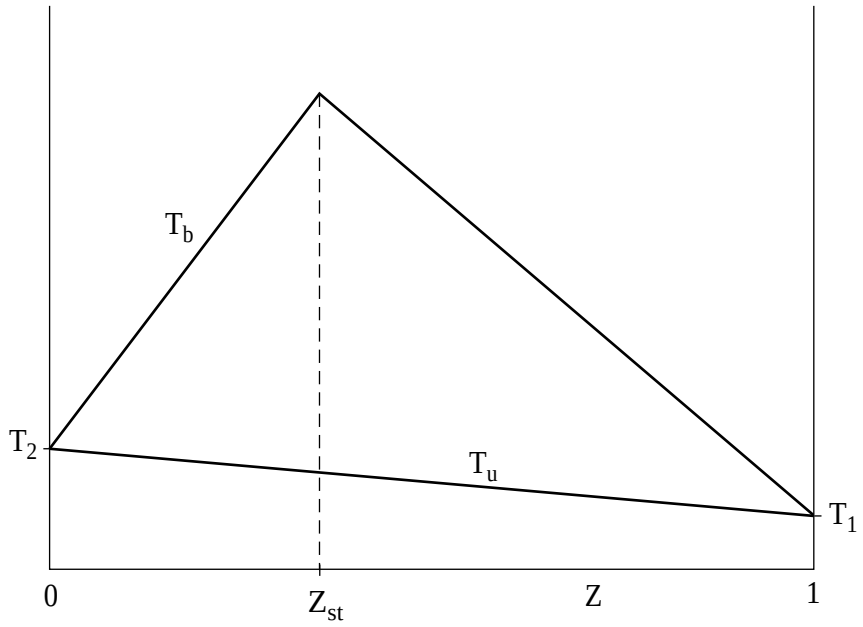

Fig. 1.2: The adiabatic temperature over mixture fraction

Fuel	Z_{st}	T_{st} [K]
CH_4	0.05496	2263.3
C_2H_6	0.05864	2288.8
C_2H_4	0.06349	2438.5
C_2H_2	0.07021	2686.7
C_3H_8	0.06010	2289.7

Table 1.2: Stoichiometric mixture fractions and stoichiometric flame temperatures for some hydrocarbon-air mixtures

For the combustion of a pure fuel ($Y_{F,1} = 1$) in air ($Y_{\mathrm{O}_2,2} = 0.232$) with $T_{u,\mathrm{st}} = 300\mathrm{K}$ values for T_{st} are given in Table 1.2 using $c_p = 1.40$ kJ/kg K.

1.6 Chemical Equilibrium

From the standpoint of thermodynamics, the assumption of complete combustion is incorrect because it disregards the possibility of dissociation of combustion products. A more general formulation is the assumption of chemical equilibrium. In that context complete combustion represents the limit of an infinite equilibrium constant as will be shown below. Both approximations, chemical equilibrium and complete combustion, are valid in the limit of infinitely fast reaction rates only, a condition which will seldomly be valid in combustion systems. We will consider finite rate chemical kinetics in lecture 2. Only for hydrogen diffusion flames complete chemical equilibrium is a good approximation, while for hydrocarbon diffusion flames finite kinetic rates are needed. In the latter the fast chemistry assumption overpredicts the formation of intermediates such as CO and H_2 due to the

dissociation of fuel on the rich side by large amounts. Nevertheless, since the equilibrium assumption represents an exact thermodynamic limit, it shall be considered here.

The Chemical Potential and the Law of Mass Action

Differently from the enthalpy, the partial molar entropy of a chemical species in a mixture of ideal gases depends on the partial pressure

$$S_i = S_i^0 - \mathrm{R}\ln\frac{p_i}{p_0} \tag{1.69}$$

where $p_0 = 1\,\mathrm{atm}$ and

$$S_i^0 = S_{i,\mathrm{ref}}^0 + \int_{T_{\mathrm{ref}}}^{T} \frac{C_{p_i}}{T}\mathrm{d}T \tag{1.70}$$

depends only on temperature. Values for the reference entropy $S_{i,\mathrm{ref}}$ are also listed in Table 1.1. The partial molar entropy may now be used to define the chemical potential

$$\mu_i = H_i - TS_i = \mu_i^0 + \mathrm{R}T\ln\frac{p_i}{p_0} \tag{1.71}$$

where

$$\mu_i^0 = H_{i,\mathrm{ref}} - TS_{i,\mathrm{ref}}^0 + \int_{T_{\mathrm{ref}}}^{T} C_{p_i}\mathrm{d}T - T\int_{T_{\mathrm{ref}}}^{T} \frac{C_{p_i}}{T}\mathrm{d}T \tag{1.72}$$

is the chemical potential at 1 atm. As it is shown in standard textbooks of thermodynamics the condition for chemical equilibrium for the k-th reaction is given by

$$\sum_{i=1}^{n} \nu_{ik}\mu_i = 0, \qquad k = 1, 2, \cdots, r \tag{1.73}$$

Using (1.71) in (1.73) leads to

$$-\sum_{i=1}^{n} \nu_{ik}\mu_i^0 = \mathrm{R}T\ln\prod_{i=1}^{n}\left(\frac{p_i}{p_0}\right)^{\nu_{ik}} . \tag{1.74}$$

Defining the equilibrium constant K_{pk} by

$$\mathrm{R}T\ln K_{pk} = -\sum_{i=1}^{n} \nu_{ik}\mu_i^0 \tag{1.75}$$

one obtains the law of mass action

$$\prod_{i=1}^{n}\left(\frac{p_i}{p_0}\right)^{\nu_{ik}} = K_{pk}(T)\,. \tag{1.76}$$

An approximation of equilibrium constants may be derived by introducing the quantity

$$\pi_i = \frac{H_{i,\mathrm{ref}} - \mu_i^0}{\mathrm{R}T} = \frac{S_{i,\mathrm{ref}}^0}{\mathrm{R}} + \int_{T_{\mathrm{ref}}}^{T} \frac{C_{p_i}}{\mathrm{R}T}\mathrm{d}T - \frac{1}{\mathrm{R}T}\int_{T_{\mathrm{ref}}}^{T} C_{p_i}\mathrm{d}T\,. \tag{1.77}$$

For constant C_{p_i} the second term in this expression would yield a logarithm of the temperature, while the last term does not vary much if $T \gg T_{\mathrm{ref}}$. Therefore $\pi_i(T)$ may be approximated by

$$\pi_i(T) = \pi_{iA} + \pi_{iB}\ln T\,. \tag{1.78}$$

Introducing this into (1.75) one obtains

$$K_{pk} = B_{pk}T^{n_{pk}} \exp\left(\frac{Q_{k,\mathrm{ref}}}{\mathrm{R}T}\right) \tag{1.79}$$

where (1.62) was used and

$$B_{pk} = \exp\left(\sum_{i=1}^{n} \nu_{ik}\pi_{iA}\right), \qquad n_{pk} = \sum_{i=1}^{n} \nu_{ik}\pi_{iB}\,. \tag{1.80}$$

Values for π_{iA} and π_{iB} are also listed in Table 1.1.

An example: Equilibrium Calculation of the H_2-air system

Using the law of mass action one obtains for the reaction

$$(1) \qquad 2\mathrm{H_2} + \mathrm{O_2} = 2\mathrm{H_2O} \tag{1.81}$$

the relation between partial pressures

$$p_{\mathrm{H_2}}^2 p_{\mathrm{O_2}} = p_{\mathrm{H_2O}}^2 K_{p_1} \cdot p_{\mathrm{O}} \tag{1.82}$$

where

$$K_{p_1} = 0.0835T^{-1.3565}\exp(58171/T) \tag{1.83}$$

was approximated using (1.79) and the values from Table 1.1. Introducing the definition

$$\Gamma_i = \frac{Y_i}{W_i} \tag{1.84}$$

the partial pressure is written with (1.18) as

$$p_i = pX_i = p\Gamma_i W \tag{1.85}$$

where the mean molecular weight is

$$W = \left(\Gamma_{\mathrm{H_2}} + \Gamma_{\mathrm{O_2}} + \Gamma_{\mathrm{H_2O}} + \Gamma_{\mathrm{N_2}}\right)^{-1}\,. \tag{1.86}$$

Furthermore, we need to consider the element mass balance. The element mass fractions of the unburnt mixture are

$$Z_{\mathrm{H}} = Y_{F,1} Z, \qquad Z_{\mathrm{O}} = Y_{\mathrm{O}_2,2}(1-Z), \qquad Z_{\mathrm{N}} = Y_{\mathrm{N}_2} = Y_{\mathrm{N}_2,2}(1-Z)\,. \tag{1.87}$$

These are equal to those in the equilibrium gas where

$$\begin{aligned} \frac{Z_{\mathrm{H}}}{W_{\mathrm{H}}} &= 2\Gamma_{\mathrm{H}_2,b} + 2\Gamma_{\mathrm{H}_2\mathrm{O},b} \\ \frac{Z_{\mathrm{O}}}{W_{\mathrm{O}}} &= 2\Gamma_{\mathrm{O}_2,b} + \Gamma_{\mathrm{H}_2\mathrm{O},b} \end{aligned} \tag{1.88}$$

while Z_{N} remains unchanged. Combining (1.82)–(1.88) leads to the following nonlinear equation for $\Gamma_{\mathrm{H}_2\mathrm{O},b}$

$$\begin{aligned} f\left(\Gamma_{\mathrm{H}_2\mathrm{O},b}\right) \equiv & \left(\Gamma_{\mathrm{H}_2\mathrm{O},b} - \frac{Z_{\mathrm{H}}}{2W_{\mathrm{H}}}\right)^2 \left(\frac{Z_{\mathrm{O}}}{W_{\mathrm{O}}} - \Gamma_{\mathrm{H}_2\mathrm{O},b}\right) \\ & - \frac{\Gamma^2_{\mathrm{H}_2\mathrm{O},b}}{K^2_{p_1} p} \left(\frac{Z_{\mathrm{H}}}{W_{\mathrm{H}}} + \frac{Z_{\mathrm{O}}}{W_{\mathrm{O}}} + 2\Gamma_{\mathrm{N}_2} - \Gamma_{\mathrm{H}_2\mathrm{O},b}\right) = 0\,. \end{aligned} \tag{1.89}$$

This equation has one root between $\Gamma_{\mathrm{H}_2\mathrm{O},b} = 0$ and the maximum values $\Gamma_{\mathrm{H}_2\mathrm{O},b} = Z_{\mathrm{H}}/2W_{\mathrm{H}}$ and $\Gamma_{\mathrm{H}_2\mathrm{O},b} = Z_{\mathrm{O}}/W_{\mathrm{O}}$ which correspond to complete combustion for lean and rich conditions in the limit $K_{p_1} \to \infty$, respectively. The solution, which is a function of the temperature, may be found by successively bracketing the solution within this range. The temperature is then calculated by employing a Newton iteration on (1.55) leading to the equation

$$f_T(T) = h_u - \sum_{i=1}^{n} Y_{i,b} h_{i,\mathrm{ref}} - \int_{T_{\mathrm{ref}}}^{T} C_{p_b} \mathrm{d}T\,. \tag{1.90}$$

The iteration converges readily following

$$T = T^{\nu} + \frac{f_T(T^{\nu})}{C_{p_b}(T^{\nu})} \tag{1.91}$$

where ν is the iteration index. The solution is shown in Fig. 1.3 for a hydrogen-air flame as a function of the mixture fraction for $T_u = 300$ K.

Another Example: Equilibrium Calculation for Lean Hydrocarbon-Air Mixtures

The procedure is similar to that for hydrogen air mixtures, except that we must include CO and CO_2 as additional species. The additional equilibrium reaction

$$(2) \qquad \mathrm{CO} + \mathrm{H_2O} = \mathrm{CO_2} + \mathrm{H_2} \tag{1.92}$$

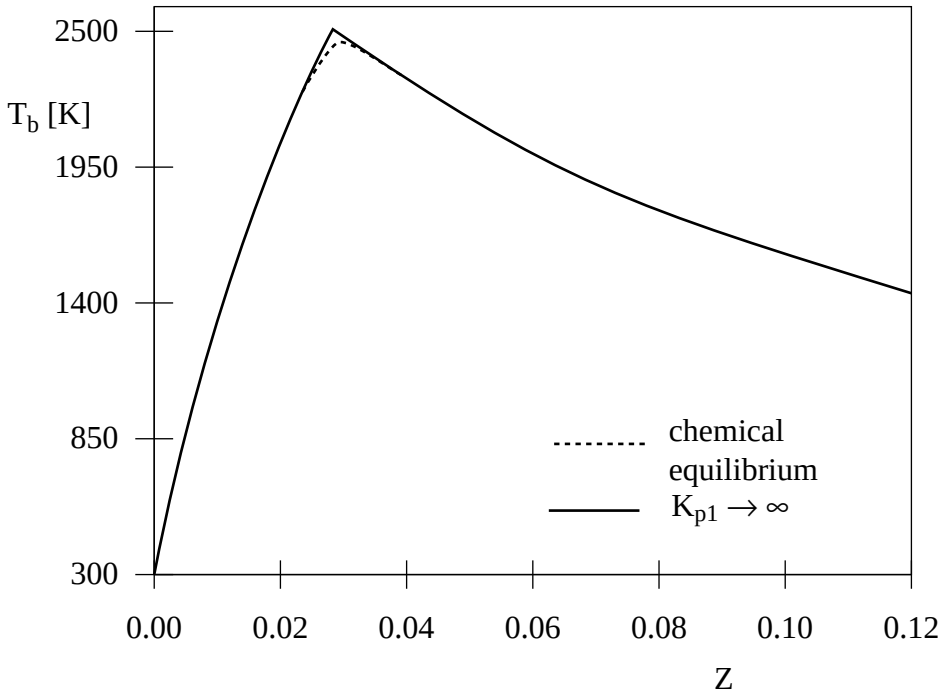

Fig. 1.3: Equilibrium flame temperature for a hydrogen-air mixture

leads to an additional relation between partial pressures

$$p_{\mathrm{CO_2}} p_{\mathrm{H_2}} = K_{p_2} p_{\mathrm{CO}} p_{\mathrm{H_2O}} \tag{1.93}$$

where

$$K_{p_2} = 3.9449 \cdot 10^{-5} T^{0.8139} \exp(4951/T)\,. \tag{1.94}$$

For a hydrocarbon fuel $\mathrm{C}_m\mathrm{H}_n$ the element mass fractions in the unburnt mixture are

$$\begin{aligned} Z_{\mathrm{C}} &= \frac{m M_{\mathrm{C}}}{M_F} Y_{F,1} Z \\ Z_{\mathrm{H}} &= \frac{n M_{\mathrm{H}}}{M_F} Y_{F,1} Z \end{aligned} \tag{1.95}$$

while those of Z_{O} and Z_{N} are the same as in (1.87). In the equilibrium gas we have the relations

$$\begin{aligned} \frac{Z_{\mathrm{H}}}{M_{\mathrm{H}}} &= 2\Gamma_{\mathrm{H_2},b} + 2\Gamma_{\mathrm{H_2O},b} \\ \frac{Z_{\mathrm{O}}}{M_{\mathrm{O}}} &= 2\Gamma_{\mathrm{O_2},b} + \Gamma_{\mathrm{H_2O},b} + \Gamma_{\mathrm{CO},b} + 2\Gamma_{\mathrm{CO_2},b} \\ \frac{Z_{\mathrm{C}}}{M_{\mathrm{C}}} &= \Gamma_{\mathrm{CO},b} + \Gamma_{\mathrm{CO_2},b}\,. \end{aligned} \tag{1.96}$$

Eliminating $\Gamma_{H_2,b}$ and $\Gamma_{CO,b}$ and using (1.93) leads to an expression for Γ_{CO_2},b as a function of Γ_{H_2O},b and K_{p_2}

$$\Gamma_{CO_2,b} = \frac{2K_{p_2}\Gamma_{H_2O,b}Z_C/W_C}{Z_H/W_H - 2(1-K_{p_2})\Gamma_{H_2O,b}}\,. \tag{1.97}$$

This must be introduced into the nonlinear equation for $\Gamma_{H_2O,b}$ derived from (1.82)

$$\begin{aligned} f\left(\Gamma_{H_2O,b}\right) \equiv & \left(\Gamma_{H_2O,b} - \frac{Z_H}{2W_H}\right)^2 \left(\frac{Z_O}{W_O} - \frac{Z_C}{W_C} - \Gamma_{H_2O,b} - \Gamma_{CO_2,b}\right) \\ & - \frac{\Gamma^2_{H_2O,b}}{K^2_{p_1}p}\left(\frac{Z_H}{W_H} + \frac{Z_O}{W_O} + \frac{Z_C}{W_C} + 2\Gamma_{N_2,b} - \Gamma_{H_2O,b} - \Gamma_{CO_2,b}\right) = 0\,. \end{aligned} \tag{1.98}$$

This equation may be solved in the same way as (1.89). The Newton iteration for the flame temperature follows the procedure given by (1.90) and (1.91).

Temperature profiles for lean methane, acetylene and propane flames as a function of the equivalence ratio for $T_u = 300$K are shown in Fig. 1.4.

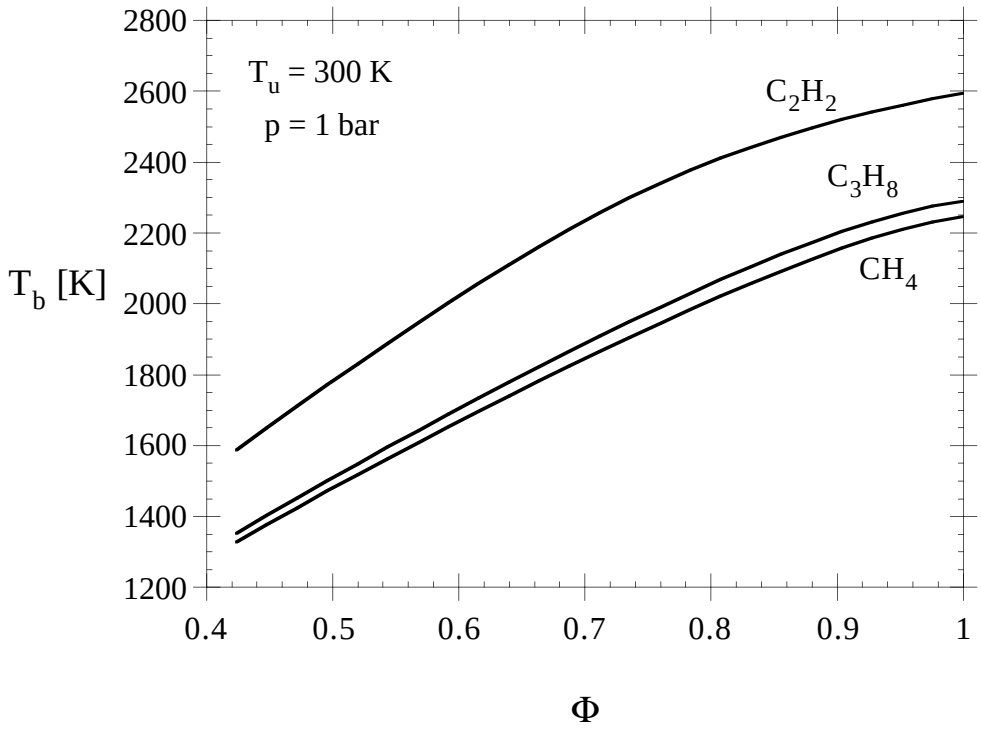

Fig. 1.4: Adiabatic flame temperatures for lean methane, acetylene and propane flames as a function of the equivalence ratio for $T_u = 300$K

Exercise 1.1

The element mass fractions $Z_{\mathrm{H},F}$, $Z_{\mathrm{C},F}$, $Z_{\mathrm{O},F}$, $Z_{\mathrm{N},F}$ of a fuel are assumed to be known. Determine the stoichiometric mixture fraction.

Exercise 1.2

Calculate the equilibrium mole fraction of NO in air at $T = 1000\mathrm{K}$ and $T = 1500\mathrm{K}$ by assuming that the mole fractions of O_2 ($X_{O_2} = 0.21$) and N_2 ($X_{N_2} = 0.79$) remain unchanged.

Solution:
The equilibrium constant of the reaction

$$N_2 + O_2 = 2\,NO$$

is with the values in table 1.1

$$K_p(T) = 17.38\,T^{0.0247}\,\exp(-21719/T)$$

of NO is the partial pressure

$$p_{NO} = (p_{N_2} p_{O_2} K_p)^{1/2}\,.$$

Neglecting the consumption of N_2 and O_2 as a first approximation, their partial pressures may be approximated with (1.18) as $p_{N_2} = 0.79\,p$, $p_{O_2} = 0.21\,p$ in air. The equilibrium mole fraction of NO is then

$$X_{NO} = 1.7\,T^{0.01235}\,\exp(-10856/T)\,.$$

At $T = 1000$ K one obtains 38 ppv (parts per volume = $X_i \cdot 10^{-6}$) and at $T = 1500\,\mathrm{K}$ 230 ppv. This indicates that at high temperatures equilibrium NO-levels exceed by far those that are accepted by modern emission standards which are around 100 ppv or lower. Equilibrium considerations therefore suggest that in low temperature exhaust gases NO is above the equilibrium value and can be removed by catalysts.

References

[1] Penner, S.S., Chemistry Problems in Jet Propulsion, Pergamon Press, New York 1957.

[2] Burcat, A., Thermochemical Data for Combustion Calculations, in "Combustion Chemistry", Gardiner jr., W.C., (Ed.), Springer-Verlag 1984.

Lecture 2: Chemical Kinetics of Gas Phase Combustion Reactions

Chemical equilibrium considerations consider the initial and the final state only, thereby leaving an important question unanswered: How much **time** is needed for the conversion from reactants to products? In real combustion systems, the rate of reaction must to be compared with that of other processes, such convection and diffusion. Furthermore, the overall rate is the sum of a sequence of single reaction steps since combustion typically proceeds in reaction chains. The estimate of a global reaction time is further complicated by the fact that many of the individual reaction steps depend strongly on temperature: At low temperatures those steps that are able to initiate a reaction chain are very slow. Therefore our environment, in which air and fuel (such as wood) coexist, can remain in an unstable, the so-called chemically "frozen" state. Only when the temperature exceeds a critical value of the order of 1000K, the transition to the stable equilibrium state is possible.

2.1 The Chemical Reaction Rate

The quantity to describe the advancement of a reaction with time is the reaction rate. In lecture 1 we have already noted that reaction equations describe the stoichiometry of either global or elementary reactions. Elementary reactions occur due to collisions between specific molecules in the gas phase, while global reactions may be viewed as a result of many of these elementary processes. From a rigorous point of view, a reaction rate may only be attributed to elementary reactions. The assumption of a single rate for a one-step global reaction, which is very often used to describe the structure of ignition and flame phenomena (conf. lectures 4 and 6, for example), can therefore not be justified on the basis of chemical kinetics. It nevertheless represents a useful ad-hoc approximation in order to simplify the mathematical analysis.

When a molecule A reacts with a molecule B to form the molecules C and D

$$\mathrm{A} + \mathrm{B} \overset{k_f}{\rightarrow} \mathrm{C} + \mathrm{D}\,,$$

species A is consumed at the same rate as B, while C and D are formed at that rate. The elementary collision process is schematically illustrated in Fig. 2.1, where $(\mathrm{AB})^*$ represents an intermediate excited state or activated complex. The rate of consumption of species A in proportional to the molar densities of A and of B. Since A is consumed the time derivative of its molar density is negative. Introducing the reaction rate coefficient k_f as a constant of proportionality, it may be written as

$$\left(\frac{\mathrm{d}[\mathrm{A}]}{\mathrm{d}t}\right)_f = -k_f[\mathrm{A}][\mathrm{B}]\,. \tag{2.1}$$

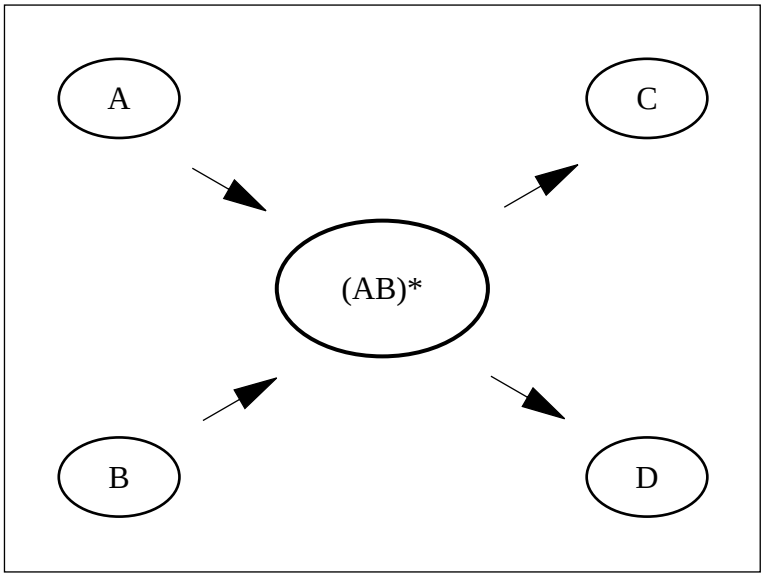

Fig. 2.1: Schematic presentation of a bimolecular reaction between molecules A and B passing through an intermediate unstable molecule $(AB)^*$ which decomposes to C and D.

Here the subscript f denotes the forward reaction and k_f is the reaction rate coefficient of the forward reaction. If two molecules A combine to A_2

$$A + A \overset{k_f}{\rightarrow} A_2$$

the rate of consumption of A is

$$\frac{d[A]}{dt} = -2k_f[A]^2 \,. \tag{2.2}$$

The factor 2 appears here because two molecules are consumed and the square follows from (2.1) if both reactants are identical. This reasoning may be extended to the generalized reaction equation

$$\nu'_A A + \nu'_B B \overset{k_f}{\rightarrow} \nu''_C C + \nu''_D D \,.$$

The time derivative of the molar density of A is then

$$\left(\frac{d[A]}{dt}\right)_f = -\nu'_A k_f [A]^{\nu'_A}[B]^{\nu'_B} = \nu_A w_f \tag{2.3}$$

where the second equation defines the reaction rate w_f of the forward reaction since $\nu_A = -\nu'_A$. For an elementary reaction containing an arbitrary number of reactants n we write the reaction rate w_f as

$$w_f = k_f \prod_{j=1}^{n} [X_j]^{\nu'_j} \,. \tag{2.4}$$

The time rate of change due to the forward reaction of any species participating in the reaction is then with $\nu_i = \nu_i'' - \nu_i'$

$$\frac{1}{\nu_i}\left(\frac{\mathrm{d}[X_i]}{\mathrm{d}t}\right)_f = \frac{1}{\nu_j}\left(\frac{\mathrm{d}[X_j]}{\mathrm{d}t}\right)_f = w_f\,. \tag{2.5}$$

For every elementary reaction there is, in principle, the possibility that it proceeds in the backward direction as well. When C and D react to form A and B, this may be written as

$$\nu_\mathrm{A}'\mathrm{A} + \nu_\mathrm{B}'\mathrm{B} \underset{k_b}{\leftarrow} \nu_\mathrm{C}''\mathrm{C} + \nu_\mathrm{D}''\mathrm{D}$$

where the previous stoichiometric coefficients were maintained. The time rate of formation of A by the backward reaction is here

$$\left(\frac{\mathrm{d}[\mathrm{A}]}{\mathrm{d}t}\right)_b = \nu_\mathrm{A}' k_b [\mathrm{C}]^{\nu_\mathrm{C}''}[\mathrm{D}]^{\nu_\mathrm{D}''} = -\nu_\mathrm{A} w_b \tag{2.6}$$

The subscript b denotes the backward reaction and k_b is its rate coefficient. The net rate of change of the molar density of A is the sum of the forward and the backward step

$$\frac{\mathrm{d}[\mathrm{A}]}{\mathrm{d}t} = \left(\frac{\mathrm{d}[\mathrm{A}]}{\mathrm{d}t}\right)_f + \left(\frac{\mathrm{d}[\mathrm{A}]}{\mathrm{d}t}\right)_b = \nu_\mathrm{A}(w_f - w_b) = \nu_\mathrm{A} w \tag{2.7}$$

The net reaction rate for a reaction with arbitrary numbers of reactants and products is finally

$$w = k_f \prod_{j=1}^{n} [X_j]^{\nu_j'} - k_b \prod_{j=1}^{n} [X_j]^{\nu_j''}\,. \tag{2.8}$$

Rate coefficients of some of the most important reactions necessary to calculate hydrocarbon flames up to propane are listed in Table 2.1.

2.2 Classification of Elementary Reactions

Elementary reactions exchange atoms or atomic groups between the molecules that are involved. For example, the elementary reaction

$38f$ $$\mathrm{CH_4 + H \rightarrow CH_3 + H_2}$$

which appears in table 2.1 as reaction 38f describes the collision of a CH_4 molecule with an H radical, in which a C-H bond of the methane molecule is broken and the free H radical from the methane molecule forms with the original H radical a stable H_2 molecule. The CH_3 radical may react in a consecutive step with an O radical

35 $$\mathrm{CH_3 + O \rightarrow CH_2O + H}$$

to form a stable formaldehyd molecule CH_2O and an H radical. Reactions 38f and 35 are bimolecular since two reactants are present. Most elementary combustion reactions are

bimolecular reactions. The constant B in the rate coefficient of a bimolecular reaction in table 2.1 has the dimension $\mathrm{cm}^3/(\mathrm{mole\ sec})\ \mathrm{K}^{-n}$. Other possibilities are unimolecular or trimolecular reactions. Reactions between more then 3 molecules are so unlikely that they do not play any role in gas phase reactions.

Unimolecular reactions occur when the large molecules decompose spontaneously into smaller radicals. An example for a unimolecular reaction is the dissociation of the n-propyl-radical

73 $$n\text{-}\mathrm{C_3H_7} \rightarrow \mathrm{C_2H_4} + \mathrm{CH_3}\,.$$

Here the energy stored within vibrational modes is used to break the bond between the second and the third C-atom in the linear structure of the n-$\mathrm{C_3H_7}$-radical. The breaking of the second bond in such radicals is called the β-fission. The constant B of a unimolecular reaction has the dimension $\mathrm{sec}^{-1}\ \mathrm{K}^{-n}$. Examples for trimolecular reactions are the steps

15 $$\mathrm{H + H + M \rightarrow H_2 + M}$$

$5f$ $$\mathrm{H + O_2 + M \rightarrow HO_2 + M}$$

34 $$\mathrm{CH_3 + H + M \rightarrow CH_4 + M}\,. \quad \text{(limit for } p \rightarrow 0.\text{)}$$

In the first two of these the inert third body M is needed to remove the bond energy that is liberated during recombination. If it was not present, the products $\mathrm{H_2}$ and $\mathrm{HO_2}$ would immediately dissociate again. In the third example the low pressure limit of reaction 34 is considered. Since $\mathrm{CH_4}$ is more likely than H or $\mathrm{O_2}$ to store energy as vibrational and rotational energy the bimolecular reaction

34 $$\mathrm{CH_3 + H \rightarrow CH_4}\,, \quad \text{(limit for } p \rightarrow \infty\,.\text{)}$$

valid in the high pressure limit, competes with the trimolecular reaction $\mathrm{CH_3 + H + M \rightarrow CH_4 + M}$. This will be discussed below when the pressure dependence of reactions is addressed. The constant B in the rate coefficient of a trimolecular reaction in Table 2.1 has the dimension $\mathrm{cm}^6/(\mathrm{mole}^2\ \mathrm{sec})\ \mathrm{K}^{-n}$.

The third body in a trimolecular reaction may be any other molecule within the system that remains chemically inert during that reaction. Different molecules promote the reaction, however, at a different rate. This is accounted for by so-called catalytic efficiencies for different molecules as compared to a specific one, say $\mathrm{H_2}$, in a reaction. The reaction rate of the reaction

$$\mathrm{A + B + M} \underset{k_b}{\overset{k_f}{\rightleftarrows}} \mathrm{AB + M}$$

is then

$$w = k_f[\mathrm{A}][\mathrm{B}][\mathrm{M}] - k_b[\mathrm{AB}][\mathrm{M}] \tag{2.9}$$

where the molecular density of the third body is the sum of molar densities of all species, weighted with their catalytic efficiency z_i

$$[\mathrm{M}]' = \sum_{i=1}^{n} z_i[X_i]\,. \tag{2.10}$$

For the reactions 5 and 24 the catalytic efficiencies are given by Warnatz [2.1] as

$$\begin{array}{llll} z_{\mathrm{H_2}} = 1.0\,, & z_{\mathrm{CH_4}} = 6.5\,, & z_{\mathrm{H_2O}} = 6.5\,, & z_{\mathrm{CO}} = 0.75 \\ z_{\mathrm{O_2}} = 0.4\,, & z_{\mathrm{N_2}} = 0.4\,, & & z_{\mathrm{Ar}} = 0.35\,. \end{array} \tag{2.11}$$

Since no data exist for the catalytic efficiencies of many other species, z_i is set equal to unity for these species. If all z_i's were set equal to unity, one obtains for the third body

$$[\mathrm{M}] = \sum_{i_1}^{n} [X_i] = \frac{p}{\mathcal{R}T}\,. \tag{2.11}$$

If $[X_i]$ is used in units of moles/cm^3 and the pressure in units of atmospheres, $\mathcal{R}$ takes the value $\mathcal{R} = 82.05$ atm cm^3/mol K.

2.3 Temperature Dependence of Reaction Rate Coefficients

The forward rate coefficient k_f defined in (2.1) and the backward rate coefficient k_b defined in (2.6) are, in principle, only functions of temperature. These coefficients describe the frequency at molecular collisions between molecules and the probability that a collision will lead a chemical reaction. A reaction will take place if the kinetic energy of the colliding molecules is larger than a threshold energy which is specific for the reaction considered. This energy is called the activation energy E_f of the forward reaction or E_b of the backward reaction. In Fig. 2.2 the chemical energy E_{chem} contained in the different species is plotted schematically over time during the reaction progress.

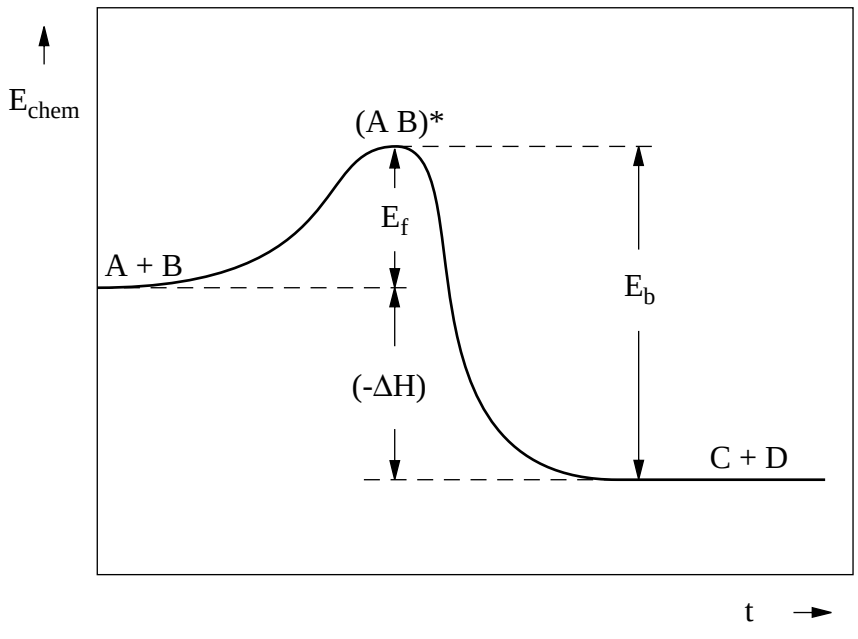

Fig. 2.2: Schematic representation of the chemical energy contained in the reactants, the intermediate activated complex and the products of the reaction shown in Fig. 2.1.

According to Fig. 2.2, reactants A and B form an activated complex $(AB)^*$ at an energy level which is by the amount E_f larger than the chemical energy contained in the reactants. Here it is assumed that the reaction is exothermic. Then the energy of the products is by the amount $(-\Delta H)$ lower than that of the reactants. The activation energy of the backward reaction, needed to reach the energy level of the activated complex, is then

$$E_b = E_f + (-\Delta H)\,. \tag{2.12}$$

On the basis of statistical thermodynamics [2.2] it can be shown that the temperature dependence of the rate coefficients follows an modified Arhenius law

$$\begin{aligned} k_f(T) &= B_f T^{n_f} \exp(-\frac{E_f}{\mathcal{R}T}) \\ k_b(T) &= B_b T^{n_b} \exp(-\frac{E_b}{\mathcal{R}T})\,. \end{aligned} \tag{2.13}$$

Here B_f and B_b are the frequency factors (containing additional information about spatial configurations of the molecules during the reaction). The exponential terms $\exp(-E_f/\mathcal{R}T)$ and $\exp(-E_b/\mathcal{R}T)$ are in general the dominant terms describing the temperature dependence of the reaction rate coefficients. The algebraic power dependencies T^{n_f} and T^{n_b} only modify the exponential temperature dependence. They are referred to as the pre-exponential temperature dependence. For radical-radical recombination reactions such as reactions 15–17 in Table 2.1 the activation energy E_f is zero, since no activation energy is needed to reach the activated complex. Then the preexponential term is dominant in describing the temperature dependence.

By inserting (2.13) into (2.7) and (2.8) and considering the limiting case of chemical equilibrium on may derive a relation between the rate coefficients $k_f(T)$ and $k_b(T)$.

$$\frac{\mathrm{d}[A]}{\mathrm{d}t} = \nu_A k_f(T) \prod_{j=0}^{n} [X_j]^{\nu'_j} \left\{ 1 - \frac{k_b(T)}{k_f(T)} \prod_{j=1}^{n} [X_j]^{\nu_j} \right\} \tag{2.14}$$

In an isolated homogeneous system equilibrium is reached for large times. Then all $[X_j]$ are equal to the equilibrium value $[X_j]_{\mathrm{eq}}$ and the l.h.s as well as the curly brackets on the r.h.s. vanish. This leads by comparison with (1.76) using (1.16) to the requirement at equilibrium

$$\frac{k_f(T)}{k_b(T)} = \frac{K_p(T)}{(\mathcal{R}T)^{\nu_s}}\,, \quad \nu_s = \sum_{j=1}^{n} \nu_j \tag{2.15}$$

This relation is generally used also far from chemical equilibrium. For a scheme of $k = 1, 2, \ldots r$ chemical reactions the following relations between rate coefficients are valid

$$\begin{aligned} B_{bk} &= B_{fk} \mathcal{R}^{\nu_{ks}} / B_{pk}\,, \quad \nu_{ks} = \sum_{j=1}^{n} \nu_{jk} \\ n_{bk} &= n_{fk} - n_{pk} + \nu_{ks}\,, \quad E_{bk} = E_{fk} + (-\Delta H_{k,ref})\,. \end{aligned} \tag{2.16}$$

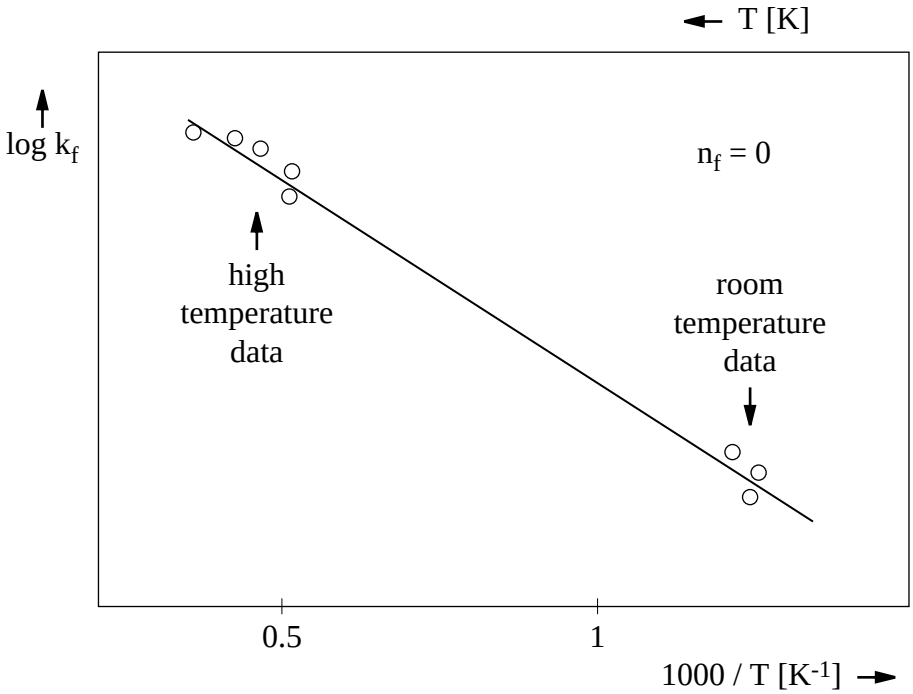

Fig. 2.3: Arrhenius plot of temperature dependence of the reaction rate coefficient k_f for the case $n_f = 0$. Measurements exist often for room temperature or, from shock tube data, at high temperatures around 2000 K and above.

Here the coefficients from (1.80) have been used.

It may be noted here in non-homogeneous systems local chemical equilibrium is approached by assuming that the term in front of the curly brackets in (2.14) tends to infinity while the l.h.s., generalized to contain convective and diffusive terms, remains finite. Then the curly brackets vanish but the reaction rate remains finite. Mathematically it is the limit of the product of two terms, one approaching infinity and the other one zero.

2.4 Pressure Dependence of Reaction Rate Coefficients

As the example of the two reaction paths 34

$$\mathrm{CH_3 + H + M \rightleftarrows CH_4 + M}$$
$$\mathrm{CH_3 + H \rightleftarrows CH_4}$$

has shown, the same reactants may react simultaneously in bimolecular and trimolecular reactions and yield the same products. Similarly, considering the backward reactions of this example, monomolecular and bimolecular reactions may occur simultaneously. Which one of these two competing paths will be favored depends on the pressure. This may be illustrated by considering the formation of the activated complex and the collision of this complex with the third body as two consecutive steps

1 $$\mathrm{A + B} \underset{k_{b1}}{\overset{k_{f1}}{\rightleftarrows}} \mathrm{(AB)^*}$$

2 $$\mathrm{(AB)^* + M} \underset{k_{b2}}{\overset{k_{f2}}{\rightleftarrows}} \mathrm{AB + M}$$

If the pressure is low the concentration of the third body M is low according to (2.11) and therefore the second reaction as the slower one in the sequence of reactions 1 and 2 becomes rate determining. Therefore the concentration of the third body is important and the overall reaction tends to a three-body reaction in the limit of low pressure. On the other hand, if the pressure is high, the second one in the sequence occurs almost immediately after the activated complex $(AB)^*$ has been formed. Therefore the overall reaction does not depend on the concentration of M and behaves as a bimolecular reaction in the limit of high pressures.

A simplified approach to calculate the transition from one limit to the other goes back to Lindemann (conf. [2.3]). The balance equations for A, $(AB)^*$, and AB are written

$$\begin{aligned}
\frac{\mathrm{d[A]}}{\mathrm{d}t} &= -k_{f1}[\mathrm{A}][\mathrm{B}] + k_{b1}[(\mathrm{AB})^*] \\
\frac{\mathrm{d}[(\mathrm{AB})^*]}{\mathrm{d}t} &= k_{f1}[\mathrm{A}][\mathrm{B}] - k_{b1}[(\mathrm{AB})^*] - k_{f2}[(\mathrm{AB})^*][\mathrm{M}] + k_{b2}[\mathrm{AB}][\mathrm{M}] \\
\frac{\mathrm{d[AB]}}{\mathrm{d}t} &= k_{f2}[(\mathrm{AB})^*][\mathrm{M}] - k_{b2}[\mathrm{AB}][\mathrm{M}]\,.
\end{aligned} \tag{2.17}$$

One may now assume that the reactions $1b$ and $2f$ by which the activated complex is consumed, are much faster than reaction $1f$ by which it is formed. Then the concentration of $(AB)^*$ remains always very low and the time derivative in the second equation of (2.17) may be neglected. (This is the so called "steady state approximation" that will be used extensively in lecture 3 to derive reduced mechanisms). The concentration at $(AB)^*$ is then

$$[(\mathrm{AB})^*] = \frac{k_{f1}[\mathrm{A}][\mathrm{B}] + k_{b2}[\mathrm{AB}][\mathrm{M}]}{k_{b1} + k_{f2}[\mathrm{M}]}\,. \tag{2.18}$$

Introducing this into the first and third equation of (2.17) leads after some algebra to

$$-\frac{\mathrm{d}[A]}{\mathrm{d}t} = \frac{\mathrm{d[AB]}}{\mathrm{d}t} = k_{f1}[\mathrm{A}][\mathrm{B}]F(T,p)\left(1 - \frac{k_{b1}k_{b2}}{k_{f1}k_{f2}}\frac{[\mathrm{AB}]}{[\mathrm{A}][\mathrm{B}]}\right) . \tag{2.19}$$

Here

$$F(T,p) = \frac{k_{f2}(T)p}{RTk_{b1}(T) + k_{f2}(T)p} \tag{2.20}$$

describes the pressure dependence of the step

$$\mathrm{A} + \mathrm{B} + (\mathrm{M}) \rightarrow \mathrm{AB} + (\mathrm{M})$$

where (2.11) has been used. In the limit of large pressures $F(T,p)$ tends to unity and k_f corresponds to $k_{f\infty}$ in Table 2.1, while for low pressures the forward rate becomes

$$\lim_{p\to 0} k_{f1}F(T,p) = \frac{k_{f1}k_{f2}}{k_{b1}}[\mathrm{M}] = k_{f0}[\mathrm{M}] \tag{2.21}$$

where k_{f0} is that of a three body reaction $\mathrm{A} + \mathrm{B} + \mathrm{M} \rightarrow \mathrm{AB} + \mathrm{M}$. Finally the ratio $(k_{b1}k_{b2})/(k_{f1}k_{f2})$ in (2.19) may be interpreted as the inverse of the equilibrium constant of the global reaction, $\mathrm{A} + \mathrm{B} = \mathrm{AB}$.

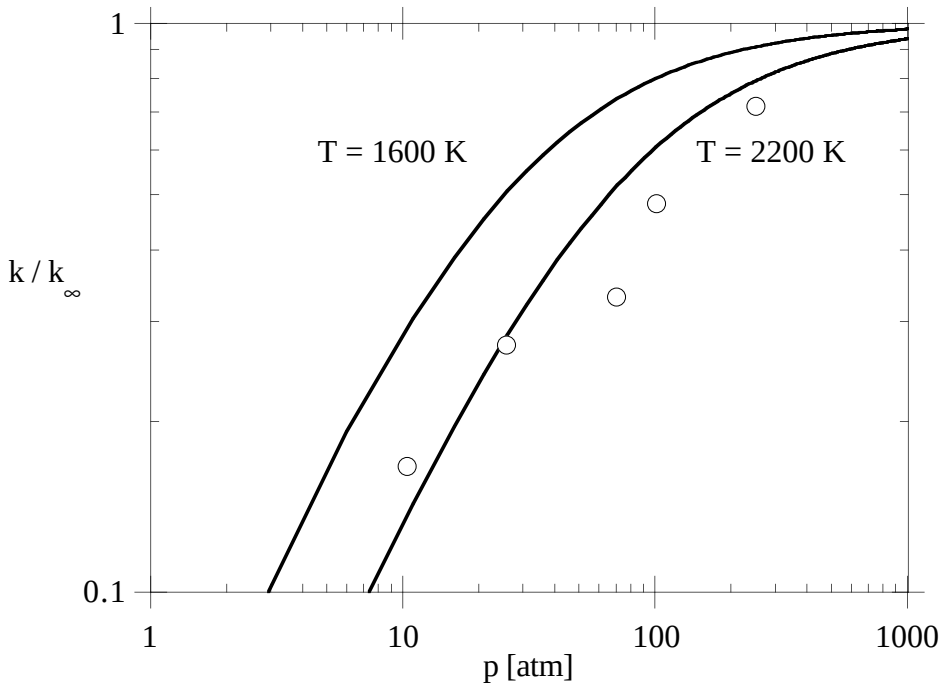

Fig. 2.4: Pressure dependence of the reaction 34: $\mathrm{CH_3} + \mathrm{H} + (\mathrm{M}) = \mathrm{CH_4} + (\mathrm{M})$

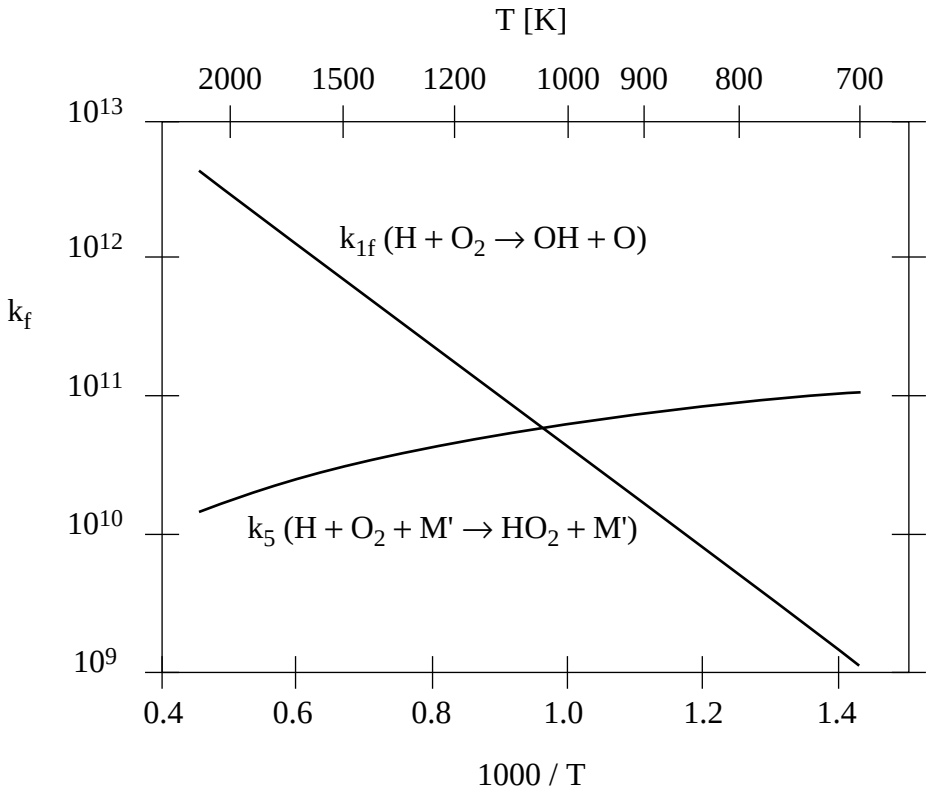

Fig. 2.5: Comparison of rate coefficients of the competing reactions between H and O_2 at one atmosphere.

References

[2.1] Warnatz, J. (in Gardiner)

[2.2] Vincenti, Kruger

[2.3] Troe (in Gardiner)

Table 2.1 Constants in the expression $k = \mathrm{B}T^n \exp(-E/\mathcal{R}T)$ in the rate coefficients of some important elementary reactions

Nr.	Reaction	B mole, cm^3, sec	n	E kJ/mole
1.1 H_2/O_2 Chain Reactions				
1f	O_2+H→OH+O	2.000E+14	0.00	70.30
1b	OH+O→O_2+H	1.568E+13	0.00	3.52
2f	H_2+O→OH+H	5.060E+04	2.67	26.30
2b	OH+H→H_2+O	2.222E+04	2.67	18.29
3f	H_2+OH→H_2O+H	1.000E+08	1.60	13.80
3b	H_2O+H→H_2+OH	4.312E+08	1.60	76.46
4f	OH+OH→H_2O+O	1.500E+09	1.14	0.42
4b	H_2O+O→OH+OH	1.473E+10	1.14	71.09
1.2 HO_2 Formation and Consumption				
5f	O_2+H+M'→HO_2+M'	2.300E+18	-0.80	0.00
5b	HO_2+M'→O_2+H+M'	3.190E+18	-0.80	195.39
6	HO_2+H→OH+OH	1.500E+14	0.00	4.20
7	HO_2+H→H_2+O_2	2.500E+13	0.00	2.90
8	HO_2+OH→H_2O+O_2	6.000E+13	0.00	0.00
9	HO_2+H→H_2O+O	3.000E+13	0.00	7.20
10	HO_2+O→OH+O_2	1.800E+13	0.00	-1.70
1.3 H_2O_2 Formation and Consumption				
11	HO_2+HO_2→H_2O_2+O_2	2.500E+11	0.00	-5.20
12f	OH+OH+M'→H_2O_2+M'	3.250E+22	-2.00	0.00
12b	H_2O_2+M'→OH+OH+M'	1.692E+24	-2.00	202.29
13	H_2O_2+H→H_2O+OH	1.000E+13	0.00	15.00
14f	H_2O_2+H→H_2+HO_2	1.700E+12	0.00	15.70
14b	H_2+HO_2→H_2O_2+H	1.150E+12	0.00	80.88

Table 2.1 continued

Nr.	Reaction	B mole, cm^3, sec	n	E kJ/mole
1.4 Recombination Reactions				
15	H+H+M'→H_2+M'	1.800E+18	-1.00	0.00
16	OH+H+M'→H_2O+M'	2.200E+22	-2.00	0.00
17	O+O+M'→O_2+M'	2.900E+17	-1.00	0.00
2. CO/CO_2 Mechanism				
18f	CO+OH→CO_2+H	4.400E+06	1.50	-3.10
18b	CO_2+H→CO+OH	4.956E+08	1.50	89.76
3.1 CH Consumption				
19	CH+O_2→CHO+O	3.000E+13	0.00	0.00
20	CO_2+CH→CHO+CO	3.400E+12	0.00	2.90
3.2 CHO Consumption				
21	CHO+H→CO+H_2	2.000E+14	0.00	0.00
22	CHO+OH→CO+H_2O	1.000E+14	0.00	0.00
23	CHO+O_2→CO+HO_2	3.000E+12	0.00	0.00
24f	CHO+M'→CO+H+M'	7.100E+14	0.00	70.30
24b	CO+H+M'→CHO+M'	1.136E+15	0.00	9.97
3.3 CH_2 Consumption				
25f	CH_2+H→CH+H_2	8.400E+09	1.50	1.40
25b	CH+H_2→CH_2+H	5.830E+09	1.50	13.08
26	CH_2+O→CO+H+H	8.000E+13	0.00	0.00
27	CH_2+O_2→CO+OH+H	6.500E+12	0.00	6.30
28	CH_2+O_2→CO_2+H+H	6.500E+12	0.00	6.30

Table 2.1 continued

Nr.	Reaction	B mole, cm^3, sec	n	E kJ/mole
3.4 CH_2O Consumption				
29	$CH_2O+H \rightarrow CHO+H_2$	2.500E+13	0.00	16.70
30	$CH_2O+O \rightarrow CHO+OH$	3.500E+13	0.00	14.60
31	$CH_2O+OH \rightarrow CHO+H_2O$	3.000E+13	0.00	5.00
32	$CH_2O+M' \rightarrow CHO+H+M'$	1.400E+17	0.00	320.00
3.5 CH_3 Consumption				
33f	$CH_3+H \rightarrow CH_2+H_2$	1.800E+14	0.00	63.00
33b	$CH_2+H_2 \rightarrow CH_3+H$	3.680E+13	0.00	44.30
34	$CH_3+H+(M) \rightarrow CH_4+(M)$ k_∞ k_0	2.108E+14 6.257E+23	0.00 -1.80	0.00 0.00
35	$CH_3+O \rightarrow CH_2O+H$	7.000E+13	0.00	0.00
36	$CH_3+CH_3+(M) \rightarrow C_2H_6+(M)$ k_∞ k_0	3.613E+13 1.270E+41	0.00 -7.00	0.00 11.56
37	$CH_3+O_2 \rightarrow CH_2O+OH$	3.400E+11	0.00	37.40
38f	$CH_4+H \rightarrow CH_3+H_2$	2.200E+04	3.00	36.60
38b	$CH_3+H_2 \rightarrow CH_4+H$	8.391E+02	3.00	34.56
39	$CH_4+O \rightarrow CH_3+OH$	1.200E+07	2.10	31.90
40f	$CH_4+OH \rightarrow CH_3+H_2O$	1.600E+06	2.10	10.30
40b	$CH_3+H_2O \rightarrow CH_4+OH$	2.631E+05	2.10	70.92
4.1 C_2H Consumption				
41f	$C_2H+H_2 \rightarrow C_2H_2+H$	1.100E+13	0.00	12.00
41b	$C_2H_2+H \rightarrow C_2H+H_2$	5.270E+13	0.00	119.95
42	$C_2H+O_2 \rightarrow CHCO+O$	5.000E+13	0.00	6.30

Table 2.1 continued

Nr.	Reaction	B mole, cm^3, sec	n	E kJ/mole
4.2 CHCO Consumption				
43f	$CHCO+H \rightarrow CH_2+CO$	3.000E+13	0.00	0.00
43b	$CH_2+CO \rightarrow CHCO+H$	2.361E+12	0.00	-29.39
44	$CHCO+O \rightarrow CO+CO+H$	1.000E+14	0.00	0.00
4.3 C_2H_2 Consumption				
45	$C_2H_2+O \rightarrow CH_2+CO$	4.100E+08	1.50	7.10
46	$C_2H_2+O \rightarrow CHCO+H$	4.300E+14	0.00	50.70
47f	$C_2H_2+OH \rightarrow C_2H+H_2O$	1.000E+13	0.00	29.30
47b	$C_2H+H_2O \rightarrow C_2H_2+OH$	9.000E+12	0.00	-15.98
48	$C_2H_2+CH \rightarrow C_3H_3$	2.100E+14	0.00	-0.50
4.4 C_2H_3 Consumption				
49	$C_2H_3+H \rightarrow C_2H_2+H_2$	3.000E+13	0.00	0.00
50	$C_2H_3+O_2 \rightarrow C_2H_2+HO_2$	5.400E+11	0.00	0.00
51f	$C_2H_3+(M) \rightarrow C_2H_2+H+(M)$ k_∞ k_0	2.000E+14 1.187E+42	0.00 -7.50	166.29 190.40
51b	$C_2H_2+H \rightarrow C_2H_3$ k_∞	1.053E+14	0.00	3.39
4.5 C_2H_4 Consumption				
52f	$C_2H_4+H \rightarrow C_2H_3+H_2$	1.500E+14	0.00	42.70
52b	$C_2H_3+H_2 \rightarrow C_2H_4+H$	9.605E+12	0.00	32.64
53	$C_2H_4+O \rightarrow CH_3+CO+H$	1.600E+09	1.20	3.10
54f	$C_2H_4+OH \rightarrow C_2H_3+H_2O$	3.000E+13	0.00	12.60
54b	$C_2H_3+H_2O \rightarrow C_2H_4+OH$	8.283E+12	0.00	65.20
55	$C_2H_4+M' \rightarrow C_2H_2+H_2+M'$	2.500E+17	0.00	319.80

Table 2.1 continued

Nr.	Reaction	B mole, cm^3, sec	n	E kJ/mole
4.6 C_2H_5 Consumption				
56f	$C_2H_5+H \rightarrow CH_3+CH_3$	3.000E+13	0.00	0.00
56b	$CH_3+CH_3 \rightarrow C_2H_5+H$	3.547E+12	0.00	49.68
57	$C_2H_5+O_2 \rightarrow C_2H_4+HO_2$	2.000E+12	0.00	20.90
58f	$C_2H_5+(M) \rightarrow C_2H_4+H+(M)$ k_∞ k_0	2.000E+13 1.000E+17	0.00 0.00	166.00 130.00
58b	$C_2H_4+H \rightarrow C_2H_5$ k_∞	3.189E+13	0.00	12.61
4.7 C_2H_6 Consumption				
59	$C_2H_6+H \rightarrow C_2H_5+H_2$	5.400E+02	3.50	21.80
60	$C_2H_6+O \rightarrow C_2H_5+OH$	3.000E+07	2.00	21.40
61	$C_2H_6+OH \rightarrow C_2H_5+H_2O$	6.300E+06	2.00	2.70
5.1 C_3H_3 Consumption				
62	$C_3H_3+O_2 \rightarrow CHCO+CH_2O$	6.000E+12	0.00	0.00
63	$C_3H_3+O \rightarrow C_2H_3+CO$	3.800E+13	0.00	0.00
64f	$C_3H_4 \rightarrow C_3H_3+H$	5.000E+14	0.00	370.00
64b	$C_3H_3+H \rightarrow C_3H_4$	1.700E+13	0.00	19.88
5.2 C_3H_4 Consumption				
65	$C_3H_4+O \rightarrow C_2H_2+CH_2O$	1.000E+12	0.00	0.00
66	$C_3H_4+O \rightarrow C_2H_3+CHO$	1.000E+12	0.00	0.00
67	$C_3H_4+OH \rightarrow C_2H_3+CH_2O$	1.000E+12	0.00	0.00
68	$C_3H_4+OH \rightarrow C_2H_4+CHO$	1.000E+12	0.00	0.00

Table 2.1 continued

Nr.	Reaction	B mole, cm^3, sec	n	E kJ/mole
5.3 C_3H_5 Consumption				
69f	$C_3H_5 \rightarrow C_3H_4+H$	3.980E+13	0.00	293.10
69b	$C_3H_4+H \rightarrow C_3H_5$	1.267E+13	0.00	32.48
70	$C_3H_5+H \rightarrow C_3H_4+H_2$	1.000E+13	0.00	0.00
5.4 C_3H_6 Consumption				
71f	$C_3H_6 \rightarrow C_2H_3+CH_3$	3.150E+15	0.00	359.30
71b	$C_2H_3+CH_3 \rightarrow C_3H_6$	2.511E+12	0.00	-34.69
72	$C_3H_6+H \rightarrow C_3H_5+H_2$	5.000E+12	0.00	6.30
5.5 C_3H_7 Consumption				
73	n-$C_3H_7 \rightarrow C_2H_4+CH_3$	9.600E+13	0.00	129.80
74f	n-$C_3H_7 \rightarrow C_3H_6+H$	1.250E+14	0.00	154.90
74b	$C_3H_6+H \rightarrow$ n-C_3H_7	4.609E+14	0.00	21.49
75	i-$C_3H_7 \rightarrow C_2H_4+CH_3$	6.300E+13	0.00	154.50
76	i-$C_3H_7+O_2 \rightarrow C_3H_6+HO_2$	1.000E+12	0.00	20.90
5.6 C_3H_8 Consumption				
77	$C_3H_8+H \rightarrow$ n-$C_3H_7+H_2$	1.300E+14	0.00	40.60
78	$C_3H_8+H \rightarrow$ i-$C_3H_7+H_2$	1.000E+14	0.00	34.90
79	$C_3H_8+O \rightarrow$ n-C_3H_7+OH	3.000E+13	0.00	24.10
80	$C_3H_8+O \rightarrow$ i-C_3H_7+OH	2.600E+13	0.00	18.70
81	C_3H_8+OH $\rightarrow$ n-$C_3H_7+H_2O$	3.700E+12	0.00	6.90
82	C_3H_8+OH $\rightarrow$ i-$C_3H_7+H_2O$	2.800E+12	0.00	3.60

[M'] = 6.5[CH_4]+6.5[H_2O]+1.5[CO_2]+0.75[CO]+0.4[O_2]+0.4[N_2]+1.0[Other]

Lecture 3: Systematic Reduction of Reaction Kinetics for Hydrogen and Methane Flames

The general idea of reducing complex kinetic schemes by the introduction of steady state assumptions has been known to chemists for a long time. However, it has become fruitful for combustion applications only very recently [3.1]–[3.4]. Interestingly enough, it was the application to hydrocarbon flames rather than to the much simpler hydrogen flames that first showed the full potential of the methodology.

The key to the success in combustion applications lies in the fact that flame chemistry for most of the hydrocarbon species proceeds in reaction chains, where each intermediate species is produced and consumed by only a few major reactions. This allows to derive algebraic expressions for these species from their steady state relations. If these expressions involve other steady state species, a non-linear system of algebraic equations results. Consequently, its solution is not unique and among all the possible roots of this system, the right one must be singled out. Fortunately, this coupling occurs only rarely between intermediate hydrocarbon species. A way to overcome the difficulties introduced by the non-uniqueness of the system of algebraic equations is the truncation of some steady state relations.

Reduced mechanisms are useful for at least two applications:

1. they reduce the computational effort in numerical calculations of flames by replacing the differential equations for those intermediate species that are assumed as being in steady state by algebraic relations;
2. they allow to study the flame structure by asymptotic methods and thereby help to identify the relatively few kinetic parameters that mainly influence global properties such as the burning velocity or extinction strain rates.

3.1 Steady state approximations as an asymptotic limit

Steady state approximations for intermediate species can be justified in many different ways. They first were derived for zero dimensional homogeneous systems that depend only on time, and the term "steady state" was introduced because the time derivative of these species is set to zero

$$\frac{d[C_i]}{dt} = 0 = \sum_{k=1}^{r} \nu_{ik} w_k \,. \tag{3.1}$$

Here, t denotes the time, and w_k the reaction rate. The justification for this approximation is generally provided in physical terms by stating that the rate at which species i is consumed is much faster than the rate by which it is produced. Therefore its concentration always stays much smaller than those of the initial reactants and the final products. Since the concentration always stays small, its time derivative also stays small compared to the time derivatives of the other species, as (3.1) implies.

As an example, one may look at the well-known Zeldovich mechanism for thermal production of NO

$$\text{A} \qquad \mathrm{O} + \mathrm{N_2} \rightarrow \mathrm{N} + \mathrm{NO}$$
$$\text{B} \qquad \mathrm{N} + \mathrm{O_2} \rightarrow \mathrm{O} + \mathrm{NO}\,.$$

Here, we assume that the level of atomic oxygen O is given as a result of the oxidation reactions in a combustion system. Now we assume that atomic nitrogen N is in steady state because reaction B is faster than reaction A. One then can add both reactions, and cancel N to obtain the global reaction

$$\text{(I)} \qquad \mathrm{N_2} + \mathrm{O_2} = 2\mathrm{NO}\,.$$

In this case the O also cancels, but this is fortuitous. The rate of the overall reaction is that of the first reaction which is slow and therefore rate-determining. Since two moles of NO are formed according to reaction I, the time change of NO is

$$\frac{dC_{\mathrm{NO}}}{dt} = 2k_A(T)C_{\mathrm{O}}C_{\mathrm{N_2}}\,. \tag{3.2}$$

This shall now be derived in a more systematic way. The balance equations for NO and N are

$$\begin{aligned} \frac{dC_{\mathrm{NO}}}{dt} &= k_A C_{\mathrm{O}} C_{\mathrm{N_2}} + k_B C_{\mathrm{N}} C_{\mathrm{O_2}} \\ \frac{dC_{\mathrm{N}}}{dt} &= k_A C_{\mathrm{O}} C_{\mathrm{N_2}} - k_B C_{\mathrm{N}} C_{\mathrm{O_2}}\,. \end{aligned} \tag{3.3}$$

These equations will be non-dimensionalized by introducing reference values for all concentrations and the temperature. We define

$$c_{\mathrm{NO}} = C_{\mathrm{NO}}/C_{\mathrm{NO\,ref}}, \quad c_{\mathrm{N}} = C_{\mathrm{N}}/C_{\mathrm{N\,ref}} \tag{3.4}$$

and a non-dimensional time as

$$\tau = tk_A(T_{\mathrm{ref}})C_{\mathrm{O\,ref}}C_{\mathrm{N_2\,ref}}/C_{\mathrm{NO\,ref}}\,. \tag{3.5}$$

For simplicity, we assume the temperature and the concentrations of $\mathrm{O_2}, \mathrm{O}$ and $\mathrm{N_2}$ to be constant equal to their reference value. Then the reference value for N must be chosen as

$$C_{\mathrm{N\,ref}} = \frac{k_A(T_{\mathrm{ref}})C_{\mathrm{O\,ref}}C_{\mathrm{N_2\,ref}}}{k_B(T_{\mathrm{ref}})C_{\mathrm{O_2\,ref}}} \tag{3.6}$$

in order to obtain the non-dimensional equations

$$\begin{aligned} \frac{dc_{\mathrm{NO}}}{d\,\tau} &= 1 + c_{\mathrm{N}} \\ \varepsilon\frac{dc_{\mathrm{N}}}{d\,\tau} &= 1 - c_{\mathrm{N}}\,. \end{aligned} \tag{3.7}$$

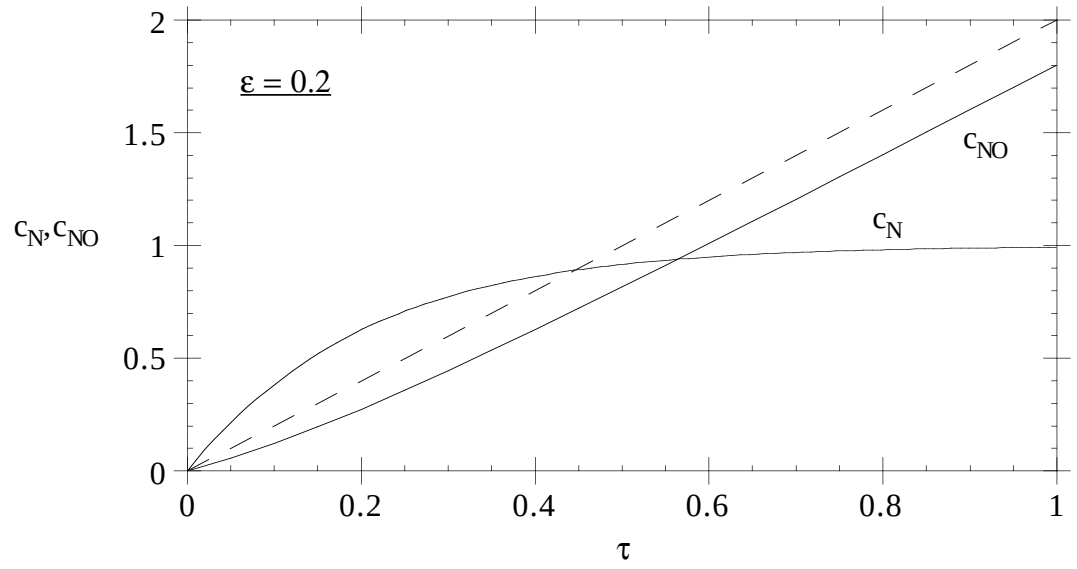

Fig. 3.1: Solution of (3.9) for the non-dimensional concentrations of N and NO as a function of the non-dimensional time. The steady state solution for c_{NO}, (3.10), is also shown (dashed line).

Here, ε denotes a small parameter defined by

$$\varepsilon = \frac{C_{\mathrm{N}\,\mathrm{ref}}}{C_{\mathrm{NO}\,\mathrm{ref}}} = \frac{k_A(T_{\mathrm{ref}})C_{\mathrm{O}\,\mathrm{ref}}C_{\mathrm{N_2}\,\mathrm{ref}}}{k_B(T_{\mathrm{ref}})C_{\mathrm{O_2}\,\mathrm{ref}}C_{\mathrm{NO}\,\mathrm{ref}}}\,. \tag{3.8}$$

The two parts of this equation suggest that ε may be assumed small based on two different kinds of reasoning:

1. the concentration of the intermediate species in (3.7) is small compared to the typical concentration of the product, which is NO in this case,

or

2. the rate constant k_A by which the intermediate N is formed is much smaller than the rate k_B at which it is consumed. This argument assumes that the ratio of the reference concentrations is of order unity.

The solution of the system (3.7) is readily obtained as

$$\begin{aligned} c_{\mathrm{N}} &= 1 - \exp(-\tau/\varepsilon) \\ c_{\mathrm{NO}} &= 2\tau + \varepsilon(\exp(-\tau/\varepsilon) - 1) \end{aligned} \tag{3.9}$$

showing that there are two time scales in this problem, namely τ and τ/ε. In the limit $\varepsilon \to 0$ the solution simplifies to

$$c_{\mathrm{N}} = 1, \quad c_{\mathrm{NO}} = 2\tau\,. \tag{3.10}$$

This is equivalent to setting C_{N} equal to the reference solution, equation (3.6). Then C_{NO} is in dimensional terms

$$C_{\mathrm{NO}} = 2tk_A(T_{\mathrm{ref}})C_{\mathrm{O}\,\mathrm{ref}}C_{\mathrm{N_2}\,\mathrm{ref}}\,, \tag{3.11}$$

which is equivalent to the solution, which is obtained by integrating (3.2).

It should be noted that (3.10) does not satisfy the initial conditions $c_{\mathrm{N}} = 0$ at $\tau = 0$. Therefore, the steady state solution breaks down in an initial layer of thickness ε, where the short time scale τ/ε is of order unity.

For the case $\varepsilon = 0.2$ the solution (3.9) has been plotted in Fig. 3.1. It is seen that the concentration of c_{N} grows in the initial layer to the steady state value $c_N = 1$, which then is valid for large times. The concentration of c_{NO} grows initially slower than the linear time dependence of the steady state solution. There also is an order $O(\varepsilon)$ difference that remains in the solution for long times due to neglecting the second term in the solution for c_{NO}. This is again due to the initial boundary condition for c_{N}, which is not satisfied by the steady state solution.

This example illustrates that steady state assumption may be analyzed rigorously by asymptotic methods and how the error that they introduce may be estimated. In a more complicated chemical system, where many steady state assumptions apply, this methodology can become cumbersome, since many small parameters that relate rate constants to each other, will appear. These parameters then must be ordered in a specific way to obtain a reasonable and self-consistent result. Very often it is easier to analyze numerical results from a complete solution and compare the magnitude of the concentrations of the intermediates to the concentrations of the initial reactants or the final products. This corresponds to the reasoning associated with the first of equations (3.8). The error introduced by each steady state assumption is then typically of the order of this concentration ratio. For many engineering purposes it will be acceptable to assume those intermediate species in steady state, whose concentration is significantly less than 10% of the initial fuel concentration.

3.2 Reduced Mechanisms for Hydrogen Flames

The steady state assumption for a species i leads to an algebraic equation between reaction rates. Therefore each of these equations can be used to eliminate rates in the remaining balance equations for the non-steady state species. The stoichiometry of the resulting balance equations defines the global mechanism between the non-steady state species. Therefore the global mechanism depends on the choice of the reaction rates that were eliminated. The rule is that one should choose for each species the fastest rate by which it is consumed. Although this choice may be arbitrary sometimes, it has no consequence as far as the balance equations for the non-steady state species are concerned. We will illustrate this for the case of a hydrogen-oxygen mechanism involving only the first 8 reactions in Table 3.1. The balance equations are

$$\begin{aligned}
L(C_{\mathrm{H}}) &= -w_1 + w_2 + w_3 - w_5 - w_6 - w_7 \\
0 = L(C_{\mathrm{OH}}) &= w_1 + w_2 - w_3 - 2w_4 + 2w_6 - w_8 \\
0 = L(C_{\mathrm{O}}) &= w_1 - w_2 + w_4 \\
L(C_{\mathrm{H_2}}) &= -w_2 - w_3 + w_7 \\
L(C_{\mathrm{O_2}}) &= -w_1 - w_5 + w_7 + w_8 \\
L(C_{\mathrm{H_2O}}) &= w_3 + w_4 + w_8 \\
0 = L(C_{\mathrm{HO_2}}) &= w_5 - w_6 - w_7 - w_8 \,.
\end{aligned} \tag{3.12}$$

Here, $L(C_i)$ denotes a linear differential operator which may contain not only the time

derivative as the one on the l.h.s. of (3.3) but also, for a non-homogeneous system, convective and diffusive terms. The specific form for flames will be introduced below. The species OH, O and HO_2 are assumed in steady state in (3.12) and the corresponding L-operators were set equal to zero that leads to three algebraic equations between the reaction rates w_k. After choosing to eliminate rate w_2 for O, w_3 for OH and w_7 for HO_2 as their respectively fastest consumption rates, one can find linear combinations such that those rates do no longer appear on the r.h.s. of the balance equations for H, H_2, O_2 and H_2O. These combinations read

$$\begin{aligned} L(C_{\mathrm{H}}) + \{L(C_{\mathrm{OH}}) + 2L(C_{\mathrm{O}}) - L(C_{\mathrm{HO_2}})\} &= 2w_1 - 2w_5 + 2w_6 \\ L(C_{\mathrm{H_2}}) + \{-L(C_{\mathrm{OH}}) - 2L(C_{\mathrm{O}}) + L(C_{\mathrm{HO_2}})\} &= -3w_1 + w_5 - 3w_6 \\ L(C_{\mathrm{O_2}}) + \{L(C_{\mathrm{HO_2}})\} &= -w_1 - w_6 \\ L(C_{\mathrm{H_2O}}) + \{L(C_{\mathrm{OH}}) + L(C_{\mathrm{O}})\} &= 2w_1 + 2w_6\,. \end{aligned} \tag{3.13}$$

Here, the terms in braces are L-operators of steady state species and are to be neglected. By arranging the r.h.s. such that those rates with equal stoichiometric coefficients are added, one obtains

$$\begin{aligned} L(C_{\mathrm{H}}) &= 2(w_1 + w_6) - 2w_5 \\ L(C_{\mathrm{H_2}}) &= -3(w_1 + w_6) + w_5 \\ L(C_{\mathrm{O_2}}) &= -(w_1 + w_6) \\ L(C_{\mathrm{H_2O}}) &= 2(w_1 + w_6)\,. \end{aligned} \tag{3.14}$$

The stoichiometry of these balance equations corresponds to the global mechanism

$$\begin{array}{lrcl} \text{(I)} & 3\mathrm{H_2} + \mathrm{O_2} & = & 2\mathrm{H} + 2\mathrm{H_2O} \\ \text{(II)} & 2\mathrm{H} + \mathrm{M} & = & \mathrm{H_2} + \mathrm{M} \end{array} \tag{3.15}$$

with the rates

$$\begin{aligned} w_{\mathrm{I}} &= w_1 + w_6 \\ w_{\mathrm{II}} &= w_5\,. \end{aligned} \tag{3.16}$$

In the second of the global reactions the inert body M has been added as a reminder of the third body that appears in reaction 5 of the original scheme in Table 3.1. This shall illustrate the role of reaction II as a chain breaking global reaction where the only remaining radical, namely H, is being consumed. The role of the first global reaction is that of an overall chain branching step. It also could have been derived by adding reaction 2 and twice reaction 3 to reaction 1 and canceling the steady state species O and OH. Similarly, the global step II could have been derived by adding reaction 7 to reaction 5 and eliminating HO_2 (and fortuitously also O_2).

Alternatively to choosing w_7 to be eliminated by the steady state equation for HO_2, one could have chosen to eliminate w_6, which is, in fact, about five times faster than w_7 at typical flame temperatures. Employing the same procedure as before, this would result in the alternate global steps

$$\begin{array}{lrcl} \text{(I}') & 3\mathrm{H_2} + \mathrm{O_2} & = & 2\mathrm{H} + 2\mathrm{H_2O} \\ \text{(II}') & 2\mathrm{H_2} + \mathrm{O_2} & = & 2\mathrm{H_2O} \end{array} \tag{3.17}$$

	Reaction			A	β	E
$1f$	$H + O_2$	$\rightarrow$	$O + OH$	2.0×10^{14}	0.0	16800
$1b$	$O + OH$	$\rightarrow$	$O_2 + H$	1.575×10^{13}	0.0	690
$2f$	$O + H_2$	$\rightarrow$	$OH + H$	1.8×10^{10}	1.0	8826
$2b$	$OH + H$	$\rightarrow$	$O + H_2$	8.0×10^{9}	1.0	6760
$3f$	$H_2 + OH$	$\rightarrow$	$H_2O + H$	1.17×10^{9}	1.3	3626
$3b$	$H_2O + H$	$\rightarrow$	$H_2 + OH$	5.09×10^{9}	1.3	18588
$4f$	$OH + OH$	$\rightarrow$	$H_2O + O$	6.0×10^{8}	1.3	0
$4b$	$H_2O + O$	$\rightarrow$	$OH + OH$	5.9×10^{9}	1.3	17029
5	$H + O_2 + M^a$	$\rightarrow$	$HO_2 + M^a$	2.3×10^{18}	-0.8	0
6	$H + HO_2$	$\rightarrow$	$OH + OH$	1.5×10^{14}	0.0	1004
7	$H + HO_2$	$\rightarrow$	$H_2 + O_2$	2.5×10^{13}	0.0	700
8	$OH + HO_2$	$\rightarrow$	$H_2O + O_2$	2.0×10^{13}	0.0	1000
$9f$	$CO + OH$	$\rightarrow$	$CO_2 + H$	1.51×10^{7}	1.3	-758
$9b$	$CO_2 + H$	$\rightarrow$	$CO + OH$	1.57×10^{9}	1.3	22337
$10f$	CH_4 (+ M)^b	$\rightarrow$	$CH_3 + H$ (+ M)^b	6.3×10^{14}	0.0	104000
$10b$	$CH_3 + H$ (+ M)^b	$\rightarrow$	CH_4 (+ M)^b	5.20×10^{12}	0.0	-1310
$11f$	$CH_4 + H$	$\rightarrow$	$CH_3 + H_2$	2.2×10^{4}	3.0	8750
$11b$	$CH_3 + H_2$	$\rightarrow$	$CH_4 + H$	9.57×10^{2}	3.0	8750
$12f$	$CH_4 + OH$	$\rightarrow$	$CH_3 + H_2O$	1.6×10^{6}	2.1	2460
$12b$	$CH_3 + H_2O$	$\rightarrow$	$CH_4 + OH$	3.02×10^{5}	2.1	17422
13	$CH_3 + O$	$\rightarrow$	$CH_2O + H$	6.8×10^{13}	0.0	0
14	$CH_2O + H$	$\rightarrow$	$HCO + H_2$	2.5×10^{13}	0.0	3991
15	$CH_2O + OH$	$\rightarrow$	$HCO + H_2O$	3.0×10^{13}	0.0	1195
16	$HCO + H$	$\rightarrow$	$CO + H_2$	4.0×10^{13}	0.0	0
17	$HCO + M$	$\rightarrow$	$CO + H + M$	1.6×10^{14}	0.0	14700
18	$CH_3 + O_2$	$\rightarrow$	$CH_3O + O$	7.0×10^{12}	0.0	25652
19	$CH_3O + H$	$\rightarrow$	$CH_2O + H_2$	2.0×10^{13}	0.0	0
20	$CH_3O + M$	$\rightarrow$	$CH_2O + H + M$	2.4×10^{13}	0.0	28812
21	$HO_2 + HO_2$	$\rightarrow$	$H_2O_2 + O_2$	2.0×10^{12}	0.0	0
$22f$	$H_2O_2 + M$	$\rightarrow$	$OH + OH + M$	1.3×10^{17}	0.0	45500
$22b$	$OH + OH + M$	$\rightarrow$	$H_2O_2 + M$	9.86×10^{14}	0.0	-5070
$23f$	$H_2O_2 + OH$	$\rightarrow$	$H_2O + HO_2$	1.0×10^{13}	0.0	1800
$23b$	$H_2O + HO_2$	$\rightarrow$	$H_2O_2 + OH$	2.86×10^{13}	0.0	32790
24	$OH + H + M^a$	$\rightarrow$	$H_2O + M^a$	2.2×10^{22}	-2.0	0
25	$H + H + M^a$	$\rightarrow$	$H_2 + M^a$	1.8×10^{18}	-1.0	0

[a] Third body efficiencies: $CH_4 = 6.5$, $H_2O = 6.5$, $CO_2 = 1.5$, $H_2 = 1.0$, $CO = 0.75$, $O_2 = 0.4$, $N_2 = 0.4$. All other species = 1.0 .

[b] Lindemann form, $k = k_\infty/(1 + k_{f\,\mathrm{all}}/[\mathrm{M}])$ where $k_{f\,\mathrm{all}} = 0.0063 \exp(-18000/RT)$.

Table 3.1: Methane-Air reaction mechanism:
rate coefficients in the form $k_j = A\,T^\beta \exp(-E/\mathrm{R}T)$.
Units are moles, cubic centimeters, seconds, Kelvins, and calories/mole.

with the rates

$$\begin{aligned} w'_{\mathrm{I}} &= w_1 - w_7 - w_8 \\ w'_{\mathrm{II}} &= w_5 \,. \end{aligned} \tag{3.18}$$

After writing the balance equations for this scheme

$$\begin{aligned} L(C_{\mathrm{H}}) &= 2(w_1 - w_7 - w_8) \\ L(C_{\mathrm{H_2}}) &= -3(w_1 - w_7 - w_8) - 2w_5 \\ L(C_{\mathrm{O_2}}) &= -(w_1 - w_7 - w_8) - w_5 \\ L(C_{\mathrm{H_2O}}) &= 2(w_1 - w_7 - w_8) + 2w_5 \end{aligned} \tag{3.19}$$

and using the steady state relation for HO_2

$$w_5 - w_6 - w_7 - w_8 = 0 \tag{3.20}$$

one finds that the balance equations are identical with those in (3.14). The balance equations therefore remain independent of the choice of the rates that were eliminated. Different global mechanisms therefore lead to the same solution for a given problem.

The reason that reaction 7 has been chosen in the reduced 4-step mechanism for methane flames, which will be derived below, is essentially tutorial. Since in the methane mechanism many chain breaking steps besides reactions 5 and 7 will play an important role in reducing the H-atom concentration, a chain breaking step was retained to illustrate the general behavior of the global mechanism.

Sometimes, for instance for the asymptotic analysis of the flame structure, one may choose to disregard some rates in the remaining global reaction scheme. In a first asymptotic analysis of methane flames, which is presented in lecture 7, only reaction rates w_1 and w_5 were retained in (3.16) as principal rates of the global reactions IV and III corresponding to I and II in (3.15), respectively. The same choice in (3.18) would then lead to different balance equations. Therefore the form of the global mechanism may become important, if not all rates are retained in the final formulation.

3.3 A Reduced Mechanism for Methane Flames

The first step in deriving a reduced mechanism is to define a suitable starting mechanism. This may be viewed as an already reduced form of a much larger "full" mechanism available in the literature. For the specific problem considered, a numerical solution must be obtained using the full mechanism and a sensitivity analysis must be carried out to identify the influence of each individual reaction on the solution. The starting mechanism should contain only those elementary reactions that are necessary to reproduce a characteristic quantity, such as the burning velocity, within about less than five percent accuracy. This simplifies the algebra of the following steps considerately. In addition, the sensitivity analysis helps to choose the fast reactions that are to be eliminated later.

For hydrocarbon flames typically about fifty elementary reactions are necessary to reproduce the burning velocity over the whole range of equivalence ratios and pressures up to 50 atm with reasonable accuracy. For lean-to-stoichiometric methane flames the "skeletal"

mechanism of 25 elementary reactions in Table 3.1, was identified as a sufficiently good representation of the elementary kinetics. This mechanism only contains hydrocarbons of the C_1-chain and is therefore expected to be insufficient for rich methane flames. Here, we will use this mechanism as a starting mechanism for the reduction procedure.

The second step in this procedure is to identify steady state species. Following the first of the two alternate reasonings described following (3.8), we have analyzed the outcome of a numerical calculation for premixed methane flames (3.8) based on the starting mechanism and determined the relative order of magnitude of the intermediate species concentrations.

The choice of retaining H rather than OH or O as a non-steady-state species is justified because H appears as a reactant in the first reaction $H + O_2 \rightarrow O + OH$ which is the most important one for flame calculations. It competes with $H + O_2 + M \rightarrow HO_2 + M$ as the most important chain breaking reaction. Therefore it is crucial to calculate the H concentration more accurately than those of O and OH.

It is now possible to use the eight steady-state conditions to eliminate eight reaction rates from the system. We want to eliminate the fastest reactions that consume each steady-state species and by that construct what will be called the main chain. From a sensitivity analysis it is found that for the oxidation of CH_4 via CH_3, CH_2O and CHO to CO, this main chain is

$$\begin{array}{lrcl} 11 & CH_4 + H & \rightarrow & CH_3 + H_2 \\ 13 & CH_3 + O & \rightarrow & CH_2O + H \\ 14 & CH_2O + H & \rightarrow & HCO + H_2 \\ 17 & HCO + M & \rightarrow & CO + H + M\,. \end{array} \tag{3.21}$$

We will therefore use the steady-state relations for CH_3, CH_2O and HCO to eliminate the rates w_{13}, w_{14}, and w_{17} from the balance equations. In addition, we will use the steady-state relations for O, OH, and H_2O to eliminate the rates w_2, w_3, and w_7 and by that define the main chain for the chain branching reactions

$$\begin{array}{lrcl} 1 & H + O_2 & \rightarrow & OH + O \\ 2 & O + H_2 & \rightarrow & H + OH \\ 3 & OH + H_2 & \rightarrow & H + H_2O \end{array} \tag{3.22}$$

as well as for the chain breaking reactions

$$\begin{array}{lrcl} 5 & H + O_2 + M & \rightarrow & HO_2 + M \\ 7 & H + HO_2 & \rightarrow & H_2 + O_2\,. \end{array} \tag{3.23}$$

Finally, the main chain for the conversion of CO to CO_2 consists of the two reactions

$$\begin{array}{lrcl} 9 & CO + OH & \rightarrow & CO_2 + H \\ 3 & OH + H_2 & \rightarrow & H_2O + H\,. \end{array} \tag{3.24}$$

By adding the reactions in (3.21)–(3.24) and canceling the steady state species where reaction 3 is used twice in (3.22) one obtains the global four step mechanism for methane flames

$$\begin{array}{lrcl} \mathrm{I} & CH_4 + 2H + H_2O & \rightleftharpoons & CO + 4H_2 \\ \mathrm{II} & CO + H_2O & \rightleftharpoons & CO_2 + H_2 \\ \mathrm{III} & H + H + M & \rightleftharpoons & H_2 + M \\ \mathrm{IV} & O_2 + 3H_2 & \rightleftharpoons & 2H + 2H_2O\,. \end{array} \tag{3.25}$$

Differently from the more systematic procedure used above for the H_2-O_2 system the consideration of the main chain by itself does not provide the rates of the global reactions as in (3.16). It only provides as principal rates the rate determining steps, which are the first ones in each of the sequences (3.21)–(3.25), namely w_{11} for I, w_9 for II, w_5 for III and w_1 for IV. These are also the only ones that were not eliminated by the steady state relations. The next step is to add to these appropriate additional reaction rates. To gain some more insight into the properties of the remaining reactions and to avoid linear algebra one may consider each of them as part of an alternate chain that is to be compared to the respective main chain. We will call the remaining reactions side reactions. Beginning with reaction 4 one realizes that it is linearly dependent on reactions 2 and 3 since the addition of reactions 2 and 4 leads to reaction 3. Since reactions 2 and 3 were eliminated the rate w_4 will also not appear in the rates of the global reactions. This was already found in (3.16).

The effect of side reaction 6 is determined by comparing it to reaction 7. Subtracting reaction 7 from reaction 6 and adding reaction 3 twice leads to the global step IV

$$
\begin{array}{ll}
6 & \mathrm{H + HO_2 \rightarrow OH + OH} \\
7 & -(\mathrm{H + HO_2 \rightarrow H_2 + O_2}) \\
3 & +2\,(\mathrm{H_2 + OH \rightarrow H_2O + H}) \\
\hline
 & \mathrm{O_2 + 3H_2 = 2H + 2H_2O}\,.
\end{array}
$$

Therefore the rate w_6 should be added in w_{IV} as it was already found in (3.16). The effect of reaction 8 is found by subtracting reaction 3

$$
\begin{array}{ll}
8 & \mathrm{OH + HO_2 \rightarrow H_2O + O_2} \\
3 & -(\mathrm{H_2 + OH \rightarrow H_2O + H}) \\
\hline
7 & \mathrm{H + HO_2 = H_2 + O_2}\,,
\end{array}
$$

which leads to reaction 7. Therefore reaction 8 has the same chain breaking effect as reaction 7 and w_8 disappears as w_7 from the global rates.

In a similar way the side reactions of the C_1-hydrocarbon chain may be analyzed. For reactions 10 and 12 the main chain reaction that they should be compared with is reaction 11. Reaction 10 may be obtained by subtracting the global reaction III from reaction 11.

$$
\begin{array}{ll}
11 & \mathrm{CH_4 + H \rightarrow CH_3 + H_2} \\
\mathrm{III} & -(\mathrm{H + H + M \rightarrow H_2 + M}) \\
\hline
10 & \mathrm{CH_4 + M = CH_3 + H + M}
\end{array}
$$

while subtracting reaction 3 from reaction 12 leads to reaction 11

$$\begin{array}{ll} 12 & \mathrm{CH_4 + OH \rightarrow CH_3 + H_2O} \\ 3 & -(\mathrm{H_2 + OH \rightarrow H_2O + H}) \\ \hline \mathrm{II} & \mathrm{CH_4 + H = CH_3 + H_2}\,. \end{array}$$

This indicates that reaction 10 acts as reaction 11 but it has a chain branching effect that is stoichiometrically the inverse of the global reaction III. It should therefore be added in w_{I} and be subtracted in w_{III}. On the other hand, reaction 12 has the similar effect as reaction 11 and should only be added in w_I.

The next side reaction in Table 3.1 is reaction 15. Subtracting reaction 3 from it shows that it has the same effect as 14 and should therefore not appear. But reaction 16 may be obtained by adding the global reaction III to 17. Therefore it has, when compared to reaction 17, a chain breaking effect and should be added in w_{III}.

Reaction 18 initiates a side chain leading from CH_3 to CH_2O. If one chooses reaction 20 as the fastest intermediate step, which consumes CH_3O in this side chain and adds it to 18, one observes a chain branching effect since two radicals are formed

$$\begin{array}{ll} 18 & \mathrm{CH_3 + O_2 \rightarrow CH_3O + O} \\ 20 & \mathrm{CH_3O + M \rightarrow CH_2O + H + M} \\ \hline \mathrm{II} & \mathrm{CH_3 + O_2 = CH_2O + O + H}\,. \end{array}$$

Adding reactions 2 and 3 twice to this one obtains

$$\begin{array}{ll} & \mathrm{CH_3 + O_2 \rightarrow CH_2O + O + H} \\ 2 & 2(\mathrm{O + H_2 \rightarrow OH + H}) \\ 3 & 2(\mathrm{H_2 + OH \rightarrow H_2O + H}) \\ \hline & \mathrm{CH_3 + O_2 + 4H_2 + O = CH_2O + 5H + 2H_2O}\,. \end{array}$$

This may be decomposed into the reaction 13 plus global reaction IV minus the global reaction III. This suggests that w_{18} as the principal rate of this side chain should be added to w_{IV} and be subtracted from w_{III}. Then, within this side chain, reaction 19 must be compared to reaction 20, which shows that it has a chain breaking effect corresponding to the stoichiometry of the global step III. Its rate therefore must be added to w_{III}.

Another side chain is initiated by reaction 21. Considering reaction 22 as the fastest step to consume H_2O_2 and adding this as well as twice reaction 3 and subtracting twice reaction 7 one obtains

$$\begin{array}{ll} 21 & \mathrm{HO_2 + HO_2 \rightarrow H_2O_2 + O_2} \\ 22 & \mathrm{H_2O_2 + M \rightarrow OH + OH + M} \\ 3 & 2(\mathrm{H_2 + OH \rightarrow H_2O + H}) \\ 7 & -2(\mathrm{H + H_2O \rightarrow H_2 + O_2}) \\ \hline \end{array}$$

$$4H_2 + O_2 = 4H + 2H_2O\,,$$

which corresponds to reaction IV from which reaction III is subtracted. Therefore w_{21} should be added in $w_{\rm IV}$ and subtracted in $w_{\rm III}$. When the effect of reaction 23 is compared to 22 in this side chain, one obtains by adding reaction 23 plus reaction 7 minus 3 times reaction 3

23	$H_2O_2 + OH \rightarrow H_2O + HO_2$
7	$H + HO_2 \rightarrow H_2 + O_2$
3	$-3(H_2 + OH \rightarrow H_2O + H)$

$$H_2O_2 + 2H_2O + 4H = 2OH + 4H_2 + O_2\,.$$

This is an overall step that may be decomposed into reaction 22 plus the global step III minus the global step IV. This implies that w_{23} should be added in $w_{\rm III}$ and be subtracted in $w_{\rm IV}$.

Finally, reactions 24 and 25 are three body chain breaking reactions whose rates should be added in $w_{\rm III}$. This is immediately evident for reaction 25 and also by subtraction of reaction 3 from reaction 25. We may therefore summarize the rates of the global reactions as

$$\begin{aligned} w_{\rm I} &= w_{10} + w_{11} + w_{12} \\ w_{\rm II} &= w_9 \\ w_{\rm III} &= w_5 - w_{10} + w_{16} - w_{18} + w_{19} \\ &\quad - w_{21} + w_{23} + w_{24} + w_{25} \\ w_{\rm IV} &= w_1 + w_6 + w_{18} + w_{21} - w_{23}\,. \end{aligned} \tag{3.26}$$

3.4 Truncation of steady state relations

The reaction rates must be expressed in terms of the rate constants and the concentrations. Some concentrations are those of steady state species. As shown in equation (3.12), these may be calculated from their balance equations with the L operator set equal to zero, which will be called steady state relations. Therefore a system of non-linear algebraic equation complements the remaining balance equations for the non-steady state species.

The most important step in reducing mechanisms is a systematic truncation of some steady state relations such that the system of non-linear algebraic equations becomes explicit. A numerical calculation for a premixed methane flame based on the starting mechanism (Table 3.1) was performed. In Fig. 3.2 we have plotted the forward and backward rates of reactions 1–4 and in Fig. 3.3 those of reactions 9–13. The origin in these figures is at the maximum of production of H. Downstream of the origin the rates $3f$ and $3b$ are dominant in the steady state equation for OH. Therefore to leading order OH can be calculated from the partial equilibrium of reaction 3

$$C_{\rm OH} = \frac{k_{3b} C_{\rm H_2O} C_{\rm H}}{k_{3f} C_{\rm H_2}}\,. \tag{3.27}$$

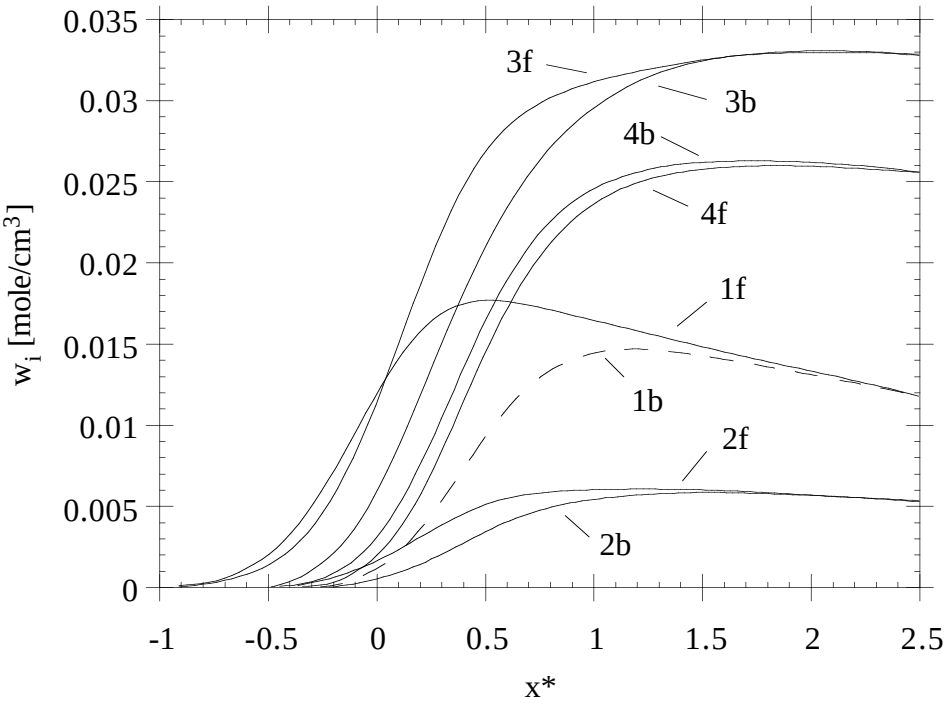

Fig. 3.2: Reaction rates 1–4 in a stoichiometric methane-air flame at 1 atm as a function of the non-dimensional coordinate $x^* = \rho_u s_L \int_0^x (\lambda/c_p)^{-1}\, dx$.

A first order approximation would need to include reaction $1f$ since its rate is large close to the inner layer. To satisfy the transition to equilibrium far downstream, the backward reaction $1b$ also would have been considered, although its rate is small near the inner layer. It may therefore be viewed as a second order term that is retained only for consistency with the downstream equilibrium condition. Since the concentration of O appears in $1b$, an ad-hoc approximation for C_{O} satisfying the downstream equilibrium is given by partial equilibrium of reaction 4

$$C_{\mathrm{O}} = \frac{k_{4f} C_{\mathrm{OH_{eq}}}^2}{k_{4b} C_{\mathrm{H_2O}}} \,. \tag{3.28}$$

Here $C_{\mathrm{OH_{eq}}}$ is the partial equilibrium concentration obtained from eq. (3.27). If the steady state relation for C_{OH} is truncated such that only the forward and backward rates of reactions 1 and 3 appear and the above approximation for C_{O} is inserted, one obtains

$$C_{\mathrm{OH}} = \frac{k_{3b} C_{\mathrm{H_2O}} C_{\mathrm{H}} + k_{1f} C_{\mathrm{H}} C_{\mathrm{O_2}}}{k_{3f} C_{\mathrm{H_2}} + k_{1b} k_{4f} k_{3b}^2 C_{\mathrm{H}}^2 C_{\mathrm{H_2O}} / (k_{4b} k_{3f}^2 C_{\mathrm{H_2}}^2)} \,. \tag{3.29}$$

Since the third reaction does not appear in the steady state relation for O and CH_3, only first and second order terms are to be balanced here.

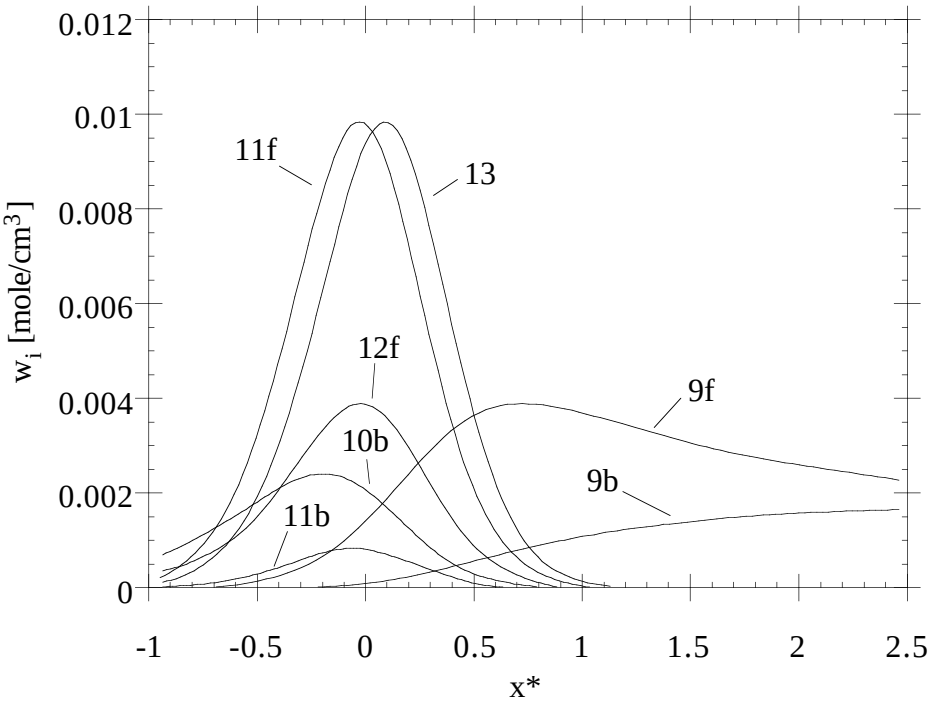

Fig. 3.3: Reaction rates 9–13 in a stoichiometric methane-air flame at 1 atm as a function of the non-dimensional coordinate $x^* = \rho_u s_L \int_0^x (\lambda/c_p)^{-1}\, dx$.

O:

$$\begin{aligned} &k_{1f}C_{\mathrm{H}}C_{\mathrm{O}_2} + k_{2b}C_{\mathrm{OH}}C_{\mathrm{H}} + k_{4f}C_{\mathrm{OH}}^2 \\ &= C_{\mathrm{O}}\{k_{1b}C_{\mathrm{OH}} + k_{2f}C_{\mathrm{H}_2} + k_{4b}C_{\mathrm{H}_2\mathrm{O}} + k_{13}C_{\mathrm{CH}_3}\} \end{aligned} \tag{3.30}$$

CH_3:

$$\begin{aligned} &\{k_{11f}C_{\mathrm{H}} + k_{12f}C_{\mathrm{OH}}\}C_{\mathrm{CH}_4} \\ &= C_{\mathrm{CH}_3}\{k_{10b}C_{\mathrm{H}}C_{\mathrm{M}} + k_{11b}C_{\mathrm{H}_2} + k_{12b}C_{\mathrm{H}_2\mathrm{O}} + k_{13}C_{\mathrm{O}}\}\,. \end{aligned} \tag{3.31}$$

These are again truncated steady state relations based on the comparison of magnitude of the rates in Figs. 3.2 and 3.3. Rates of other reactions not shown here are very much smaller.

Since reaction 13 appears in both expressions, C_{CH_3} must be eliminated and a quadratic equation is obtained for C_{O}

$$C_{\mathrm{O}} = \frac{-b + \sqrt{b^2 - 4ac}}{2a} \tag{3.32}$$

where

$$\begin{aligned} &a = k_{13}\,B, \quad b = BD + k_{13}(C - A) \\ &c = -AD \end{aligned} \tag{3.33}$$

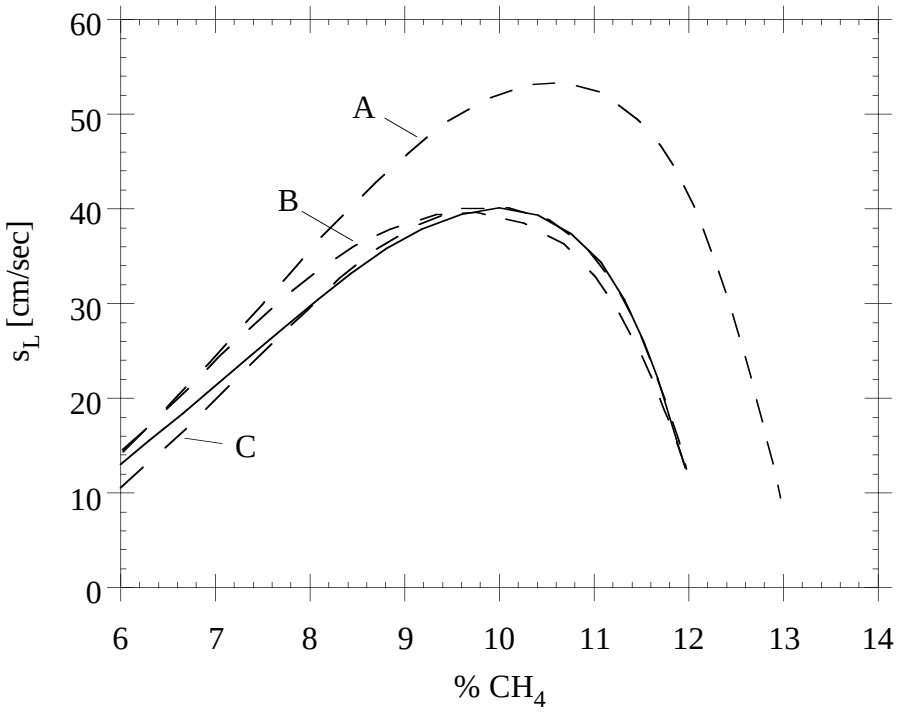

Fig. 3.4: Burning velocity s_L as a function of the mole fraction of CH_4 in the unburnt gas (starting mechanism: solid line, cases A, B, and C of reduced mechanism formulations: dashed lines).

and

$$\begin{aligned} A &= k_{1f}C_{\rm H}C_{\rm O_2} + k_{2b}C_{\rm OH}C_{\rm H} + k_{4f}C_{\rm OH}^2 \\ B &= k_{1b}C_{\rm OH} + k_{2f}C_{\rm H_2} + k_{4b}C_{\rm H_2O} \\ C &= \{k_{11f}C_{\rm H} + k_{12f}C_{\rm OH}\}C_{\rm CH_4} \\ D &= k_{10b}C_{\rm H}C_{\rm M} + k_{11b}C_{\rm H_2} + k_{12b}C_{\rm H_2O}\,. \end{aligned} \tag{3.34}$$

Once solutions to these truncated steady states have been obtained, it is easy to resolve the steady state relations for $C_{\rm CH_3O}, C_{\rm CH_2O}$ and $C_{\rm HCO}$ in terms of $C_{\rm OH}, C_{\rm O}$ and $C_{\rm CH_3}$

$$\begin{aligned} C_{\rm CH_3O} &= \frac{k_{18}C_{\rm CH_3}C_{\rm O_2}}{k_{19}C_{\rm H} + k_{20}C_{\rm M}} \\ C_{\rm CH_2O} &= \frac{k_{13}C_{\rm CH_3}C_{\rm O} + (k_{19}C_{\rm H} + k_{20}C_{\rm M})C_{\rm CH_3O}}{k_{14}C_{\rm H} + k_{15}C_{\rm OH}} \\ C_{\rm HCO} &= \frac{(k_{14}C_{\rm H} + k_{15}C_{\rm OH})C_{\rm CH_2O}}{k_{16}C_{\rm H} + k_{17}C_{\rm M}}\,. \end{aligned} \tag{3.35}$$

The steady state relation for $C_{\rm HO_2}$ may again be truncated by considering only the rates of reactions 5–8, since the others involving $C_{\rm HO_2}$ are small. This leads to

$$C_{\rm HO_2} = \frac{k_5 C_{\rm H}C_{\rm O_2}C_{\rm M}}{(k_6 + k_7)C_{\rm H} + k_8 C_{\rm OH}}\,. \tag{3.36}$$

Finally, the steady state relation for $C_{\mathrm{H_2O_2}}$ leads to

$$C_{\mathrm{H_2O_2}} = \frac{k_{21}C^2_{\mathrm{HO_2}} + k_{22b}C^2_{\mathrm{OH}}C_M + k_{23b}C_{\mathrm{H_2O}}C_{\mathrm{HO_2}}}{k_{22f}C_{\mathrm{M}} + k_{23f}C_{\mathrm{OH}}} \,. \tag{3.37}$$

3.5 Comparison of Truncated Steady State Relations

The explicit algebraic relations derived above have been used in a numerical calculation based on the reduced mechanism for methane flames. They are tested against the solution based on the starting mechanism. Three different formulations of reduced mechanisms were calculated:

A) uses partial equilibrium of reaction 3 for C_{OH} according to eq. (3.27) and neglects the term involving k_{13} in the steady state relation for C_{O}, such that only reactions of the H_2O_2-system are being balanced there

B) uses partial equilibrium of reaction 3 for C_{OH} and the quadratic equation (3.32) for C_{O}

C) uses the first order correction, eq. (3.29) for C_{OH} and the quadratic equation (3.22) for C_{O}.

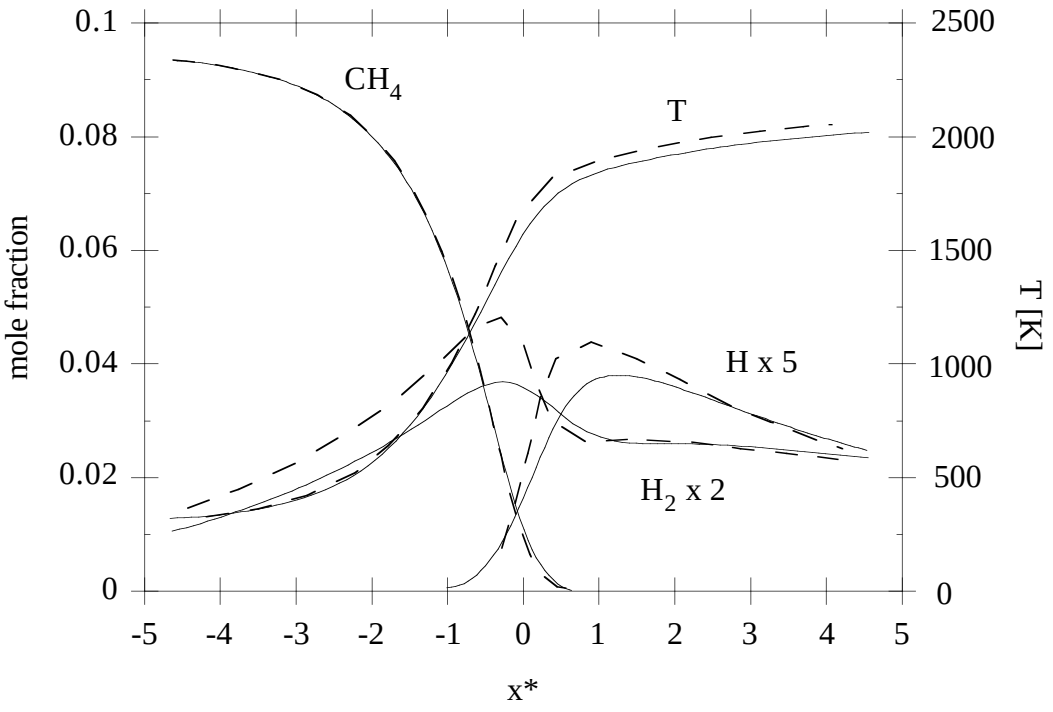

Fig. 3.5: Mole fractions and temperature for a stoichiometric methane-air flame at 1 atm as a function of the non-dimensional coordinate $x^* = \rho_u s_L \int_0^x (\lambda/c_p)^{-1}\, dx$ (starting mechanism: solid line, reduced mechanism: dashed line).

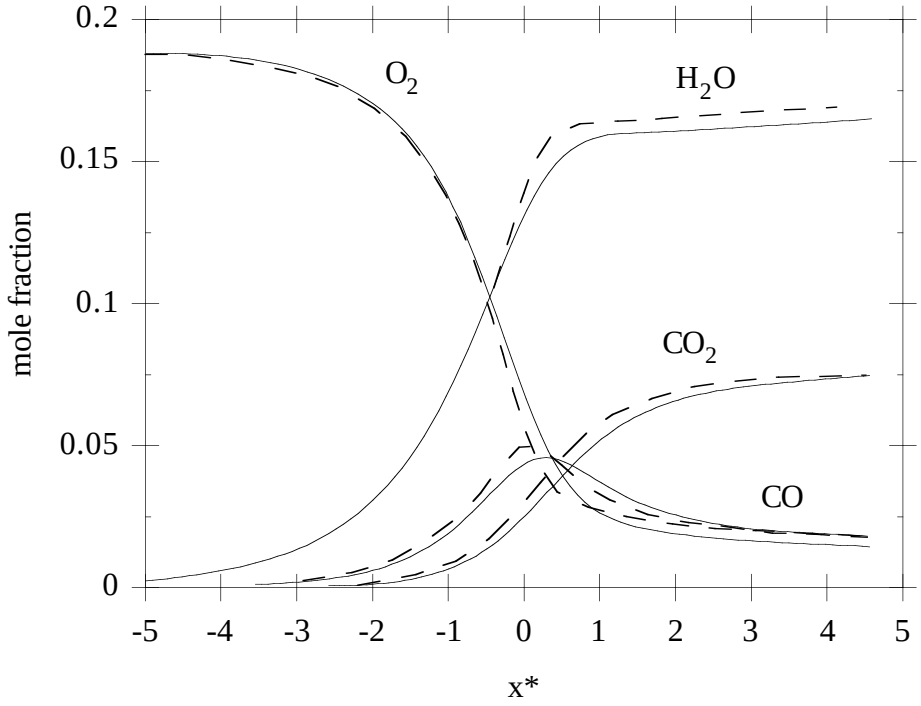

Fig. 3.6: Mole fractions for a stoichiometric methane-air flame at 1 atm as a function of the non-dimensional coordinate $x^* = \rho_u s_L \int_0^x (\lambda/c_p)^{-1}\, dx$ (starting mechanism: solid line, reduced mechanism C: dashed line).

In Fig. 3.4 the burning velocity at 1 atm is plotted as a function of the mole fraction of CH_4 in the unburnt mixture and the three cases are compared with the starting mechanism. The mechanism in Table 3.1 has been used for these calculations. While case A gives very high burning velocities, which, at $\phi = 1$, corresponding to $C_{\mathrm{CH_4}\,u} = 9.5\%$, is around 50 cm/sec, the cases B and C do well. In case C the burning velocity differs from that of the starting mechanism by less than 1.5 cm/sec over the entire range of equivalence ratios while case B shows maximum derivations of 3 cm/sec or 10% on the lean side.

The mole fractions of the non-steady state species and the temperature for a stoichiometric flame at 1 atm are plotted in Figs. 3.5 and 3.6. Here the reduced mechanism formulation based on case C has been used. It is seen, that except for H and H_2 the agreement is quite good, but not as good as for the burning velocity. Even larger deviations are found for the steady state species $C_{\mathrm{O}}, C_{\mathrm{OH}}$, and $C_{\mathrm{CH_3}}$ shown in Fig. 3.7. The larger differences for these species are expected since the steady state assumptions enter their balance equations directly.

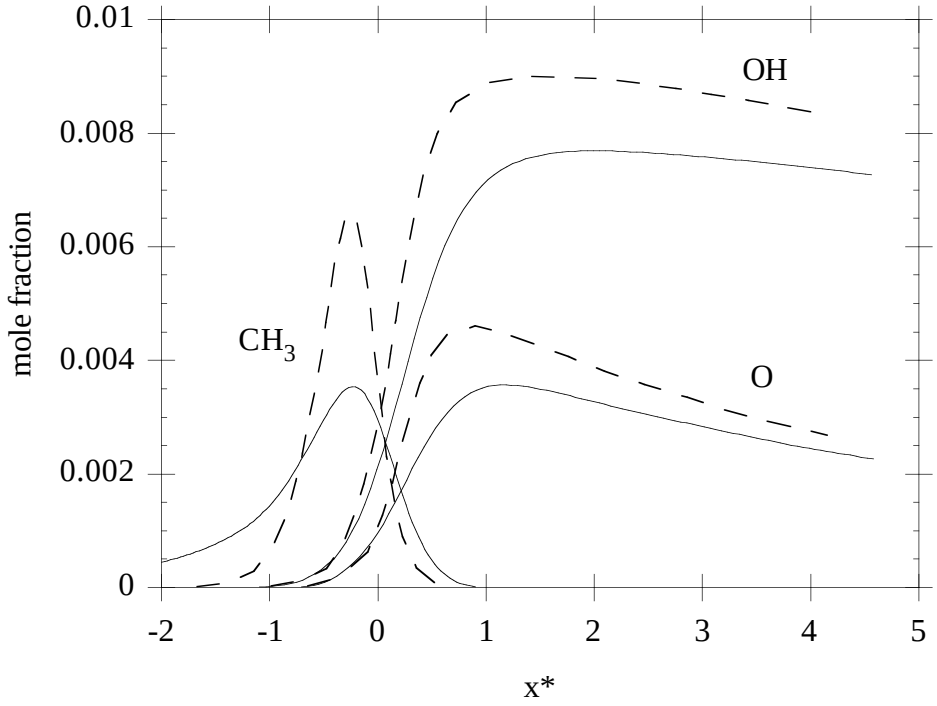

Fig. 3.7: Mole fractions of steady state species for a stoichiometric methane-air flame at 1 atm as a function of the non-dimensional coordinate $x^* = \rho_u s_L \int_0^x (\lambda/c_p)^{-1}\, dx$ (starting mechanism: solid line, reduced mechanism C: dashed line).

References

[3.1] Peters, N., "Numerical and Asymptotic Analysis of Systematically Reduced Reaction Schemes for Hydrocarbon Flames", Numerical Simulation of Combustion Phenomena, Lecture Notes in Physics **241**, pp. 90–109, 1985.

[3.2] Paczko, G., Lefdal, P.M. and Peters, N., "Reduced Reaction Schemes for Methane, Methanol and Propane Flames", 21st Symposium (International) on Combustion, The Combustion Institute, pp. 739–748, 1988.

[3.3] Peters, N. and Kee, R.J.,"The Computation of Stretched Laminar Methane-Air Diffusion Flames Using a Reduced Four-Step Mechanism", Combustion and Flame **68**, pp. 17–30, 1987.

[3.4] Peters, N. and Rogg, B. (Eds.), "Reduced Kinetic Mechanisms for Combustion Applications", Springer-Verlag, to appear 1993.

Lecture 4: Ignition and Extinction in Homogeneous Systems

If a spatially homogeneous premixed fuel-air mixture is preheated to temperatures of the order of 750 K and higher, there is a possibility that chain branching reactions accelerate the generation of radicals and heat which subsequently leads to a thermal runaway. This process, called autoignition is of technical importance, for example in Diesel engines. A fundamental quantity that describes autoignition is the ignition delay time t_i, which is the time span of the induction process preceeding the thermal runaway in a homogeneous system. The ignition delay time depends on the kinetic properties of the reaction process and on the initial temperature and pressure. There are conditions of pressure and temperature where the ignition delay time tends to infinity and autoignition is chemically inhibited. These conditions are called explosion limits.

We will also consider the case of a well-stirred reactor which has a continuous in-flow of reactants and out-flow of products. If the residence time within the reactor is sufficiently long, auto-ignition will take place. Once ignition has occurred in the reactor, in-flowing reactants are rapidly burned. If the flow rate is increased and thereby the residence time within the reactor decreases, combustion may be extinguished. The simplified analysis to be presented in this lecture will also allow us to discuss extinction conditions.

4.1 Theory of Thermal Explosions

It is convenient to assume that during the ignition process either the density or the pressure remains constant. Here we want to consider the constant density case. Let us consider a closed adiabatic vessel at constant volume V containing a given mass m such that the density $\rho = m/V$ remains constant during the ignition process as shown in Fig. 4.1.

With $dq = 0$ and neglecting the frictional work, $dw_R = 0$, (1.46) states that the change of internal energy vanishes

$$\frac{\mathrm{d}u}{\mathrm{d}t} = 0\,. \tag{4.1}$$

With $\rho = \text{const}$ the equations for the chemical species are written as

$$\rho\frac{\mathrm{d}Y_i}{\mathrm{d}t} = W_i \sum_{k=1}^{r} \nu_{ik} w_k\,. \tag{4.2}$$

With (4.1) and the definition (1.48) for the internal energy one obtains

$$\mathrm{d}u = \sum_{i=1}^{n} u_i \mathrm{d}Y_i + \sum_{i=1}^{n} Y_i \mathrm{d}u_i \tag{4.3}$$

where

$$\sum_{i=1}^{n} Y_i \mathrm{d}u_i = \left(\sum_{i=1}^{n} Y_i c_{vi}\right) \mathrm{d}T = c_v \mathrm{d}T \tag{4.4}$$

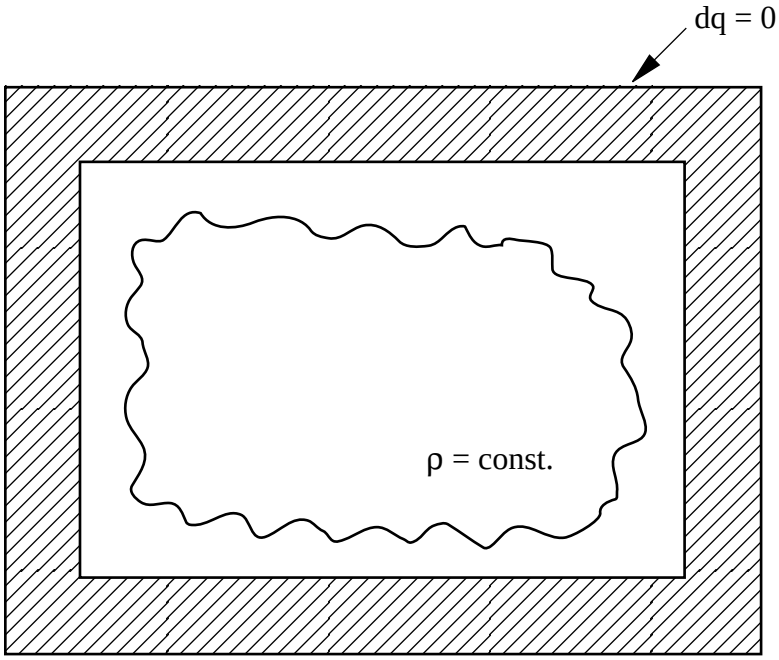

Fig. 4.1: Autoignition in a closed volume

which defines the mean specific heat capacity at constant volume c_v. With (4.2) this leads to the temperature equation

$$\rho c_v \frac{\mathrm{d}T}{\mathrm{d}t} = \sum_{k=1}^{r} Q_{vk} w_k \tag{4.5}$$

where

$$Q_{vk} = -\sum_{i=1}^{n} \nu_{ik} W_i u_i \tag{4.6}$$

is the heat of combustion for a constant volume process.

Let us, for simplicity, assume a one-step reaction with a large activation energy E and the reaction rate

$$\omega = B \left(\frac{\rho Y_F}{W_F}\right) \left(\frac{\rho Y_{\mathrm{O}_2}}{W_{\mathrm{O}_2}}\right) \exp\left(-\frac{E}{\mathcal{R}T}\right) . \tag{4.7}$$

The governing equations then simplify to

$$\rho \frac{\mathrm{d}Y_i}{\mathrm{d}t} = \nu_i W_i \omega \,, \tag{4.8}$$

$$\rho c_v \frac{\mathrm{d}T}{\mathrm{d}t} = Q_v \omega \,. \tag{4.9}$$

Assuming constant c_v and Q_v and multiplying (4.8) with Q_v and (4.9) with $\nu_i W_i$ leads after integration to the coupling relation between the species mass fractions and the temperature

$$\frac{c_v (T - T_0)}{Q_v} = \frac{(Y_i - Y_{i0})}{\nu_i W_i} \tag{4.10}$$

where T_0 is the initial temperature before thermal runaway and Y_{i0} is the initial mass fraction. We will, for simplicity, assume that Q_v/c_v is large compared to $T - T_0$ during the ignition process and set $Y_i = Y_{i0}$ which corresponds to the neglection of reactant consumption. With the modified reaction rate

$$\omega = B' \exp\left(-\frac{E}{\mathcal{R}T}\right), \qquad B' = B\,\frac{Y_{F,0}}{W_F}\,\frac{\rho Y_{\mathrm{O}_2,0}}{W_{\mathrm{O}_2}} \tag{4.11}$$

the temperature equation becomes

$$\frac{\mathrm{d}T}{\mathrm{d}t} = \frac{Q_v}{c_v} B' \exp\left(-\frac{E}{\mathcal{R}T}\right). \tag{4.12}$$

The temperature is expanded as

$$T = T_0(1 + \varepsilon y) \tag{4.13}$$

where ε is a small parameter. A Taylor expansion of the inverse of the temperature

$$\frac{1}{T} = \frac{1}{T_0} - \frac{T - T_0}{T_0^2} = \frac{1}{T_0}(1 - \varepsilon y) \tag{4.14}$$

leads to an expansion of the exponential term in (4.12) as

$$\exp\left(-\frac{E}{\mathcal{R}T}\right) = \exp\left(-\frac{E}{\mathcal{R}T_0}\right) \exp\left(\frac{E}{\mathcal{R}T_0}\varepsilon y\right). \tag{4.15}$$

This suggests the definition of ε as

$$\varepsilon = \frac{\mathcal{R}T_0}{E} \tag{4.16}$$

which implies that the activation energy is large as it was assumed above. When the expansion (4.13) together with (4.15) is introduced into (4.12) one obtains

$$\frac{\mathrm{d}y}{\mathrm{d}t} = \frac{e^y}{t_i} \tag{4.17}$$

with the ignition delay time defined as

$$t_i = \frac{\mathcal{R}T_0^2}{E}\,\frac{c_v}{Q_v B'} \exp\left(\frac{E}{\mathcal{R}T_0}\right). \tag{4.18}$$

The solution of (4.17) is with the initial condition $y = 0$ at $t = 0$ using the transformation $x = e^{-y}$ which leads to $\mathrm{d}x/\mathrm{d}t = -1/t_i$ with the solution $x = 1 - t/t_i$. In terms of T this is

$$T = T_0 - \frac{\mathcal{R}T_0^2}{E} \log\left(1 - \frac{t}{t_i}\right) \tag{4.19}$$

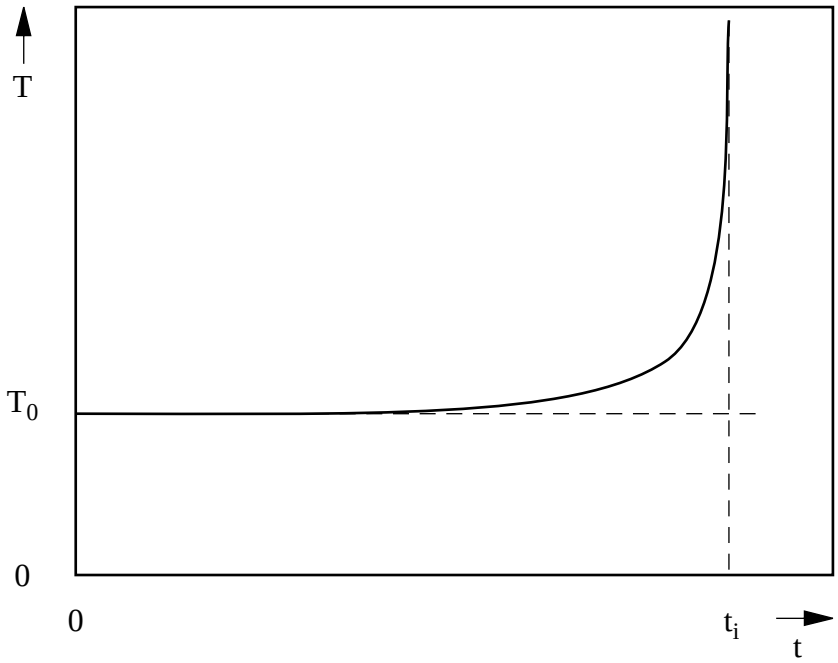

Fig. 4.2: Thermal runaway illustrated by the solution (4.19)

which is plotted in Fig. 4.2 and shows a thermal runaway at $t = t_i$. The solution is valid only as long as ε is small and T does not exceed the order of $T_0(1 + \mathcal{R}T_0^2/E)$, since y was assumed of order unity.

4.2 Ignition of Hydrogen-Oxygen Mixtures

In order to analyze the competition between chain-branching and chain-breaking reactions we will follow [4.1] and consider a simplified mechanism for the ignition of hydrogen-oxygen or hydrogen-air mixtures

$$\begin{array}{lcl} (1) & \mathrm{H + O_2} & \rightarrow \quad \mathrm{OH + O} \\ (2) & \mathrm{O + H_2} & \rightarrow \quad \mathrm{OH + H} \\ (3) & \mathrm{OH + H_2} & \rightarrow \quad \mathrm{H_2O + H} \\ (5) & \mathrm{H + O_2 + M} & \rightarrow \quad \mathrm{HO_2 + M} \\ (7b) & \mathrm{H_2 + O_2} & \rightarrow \quad \mathrm{H + HO_2\,.} \end{array} \tag{4.20}$$

Assuming reactions (2) and (3) very fast and thereby O and OH in steady state we can combine the first three reactions to a global step.

$$\text{(I)} \qquad \mathrm{3H_2 + O_2} \xrightarrow{k_1} \mathrm{2H + 2H_2O\,.} \tag{4.21}$$

as shown in Lecture 3. As it is easily calculated from Table 1.1 the heat of combustion of reaction I is 48 kJ/mol while reaction (7b) is slightly endothermic with -21 kJ/mol.

Reaction (5) releases most of the heat with 197 kJ/mol. Only this contribution will be retained in the temperature equation which then reads

$$\rho c_v \frac{\mathrm{d}T}{\mathrm{d}t} = Q_{v5}\omega_5 \,. \tag{4.22}$$

Therefore a significant change of temperature will only occur when reaction (5) becomes important. The balance equation for the formation of H-radicals is

$$\rho \frac{\mathrm{d}Y_\mathrm{H}}{\mathrm{d}t} = W_\mathrm{H}(2\omega_I + \omega_{7b} - \omega_5) \,. \tag{4.23}$$

It will be assumed for simplicity that during the first stage of ignition the temperature change is small and the reactants and the rate coefficients remain constant. Introducing non-dimensional variables

$$\begin{aligned} x &= \frac{Y_\mathrm{H}\, k_1(T_0)}{(Y_{\mathrm{H}_2})_0\, k_{7b}(T_0)} \\ \tau &= t k_1(T_0)\rho_0 Y_{\mathrm{O}_2,0}/W_{\mathrm{O}_2} \\ \kappa &= k_5(T_0) z_5 p/(k_1(T_0)\mathcal{R}T_0) \end{aligned} \tag{4.24}$$

(4.23) becomes

$$\frac{\mathrm{d}x}{\mathrm{d}\tau} = (2-\kappa)x + 1 \tag{4.25}$$

with the initial conditions $x = 0$ at $\tau = 0$. The solution is

$$x = \frac{\exp[(2-\kappa)\tau] - 1}{2-\kappa} \,. \tag{4.26}$$

The non-dimensional radical concentration is plotted for $\kappa = 0.1$, $\kappa = 2$ and $\kappa = 10$ in Fig. 4.3. This shows that it increases exponentially if $\kappa < 2$, linearly for $\kappa = 2$ and reaches a constant value $x = 1/(\kappa - 2)$ for $\kappa > 2$.

While (4.19) readily suggests a definition of the ignition delay time as $t = t_i$ where $y \to \infty$, such a definition is not evident for the solution (4.26). Here the initially exponential growth of the radical concentration for $\kappa < 2$ and the existence of a threshold at $\kappa = 2$ are the main results. The condition $\kappa = 2$ defines a cross-over temperature T_c between the first and the fifth reaction

$$2k_1(T_c) = \frac{z_5 p}{\mathcal{R}T_c} k_5(T_c) \,. \tag{4.27}$$

Here z_5 is the effective third body efficiency

$$z_5 = X_{\mathrm{H}_2,0} + 0.4\, X_{\mathrm{O}_2,0} + 0.4\, X_{\mathrm{N}_2,0}$$

of the initial fuel air mixture. It is around 0.6 for stoichiometric hydrogen-air flames and around 0.8 for stoichiometric hydrogen-oxygen flames. The pressure dependence of T_c was evaluated using $z_5 = 0.7$ and the rates from Table 2.1 and is plotted in Fig. 4.5 below. For $p = 1\,\mathrm{atm}$ T_c is close to 1000 K. Below this temperature the chain breaking effect of reaction 5 dominates as compared to the chain-branching effect of reaction 1.

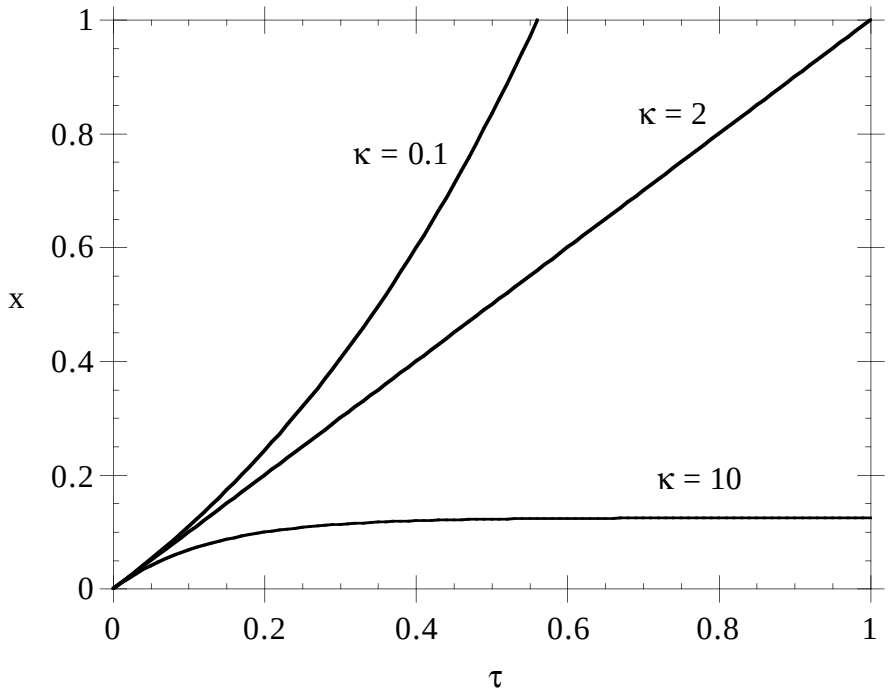

Fig. 4.3: Solutions of (4.26) for $\kappa = 0.1$, $\kappa = 2$, $\kappa = 10$.

For a homogeneous stochiometric hydrogen-oxygen mixture at 0.1 bar the onset of ignition was calculated using a 17-step-mechanism or 8-step-mechanism and the 3-step-mechanism of (4.20) and (4.21). Ignition delay times for both cases are calculated numerically and are compared at different initial temperatures and are shown in an Arrhenius diagram in Fig. 4.4. It is seen that the ignition delay time increases with decreasing temperature in the range from 1500 K to around 800 K. Then, at 790 K which corresponds to the cross-over temperature T_c at $p = 0.1$ bar, it suddenly increases to very large values, making ignition in technical systems quasi impossible.

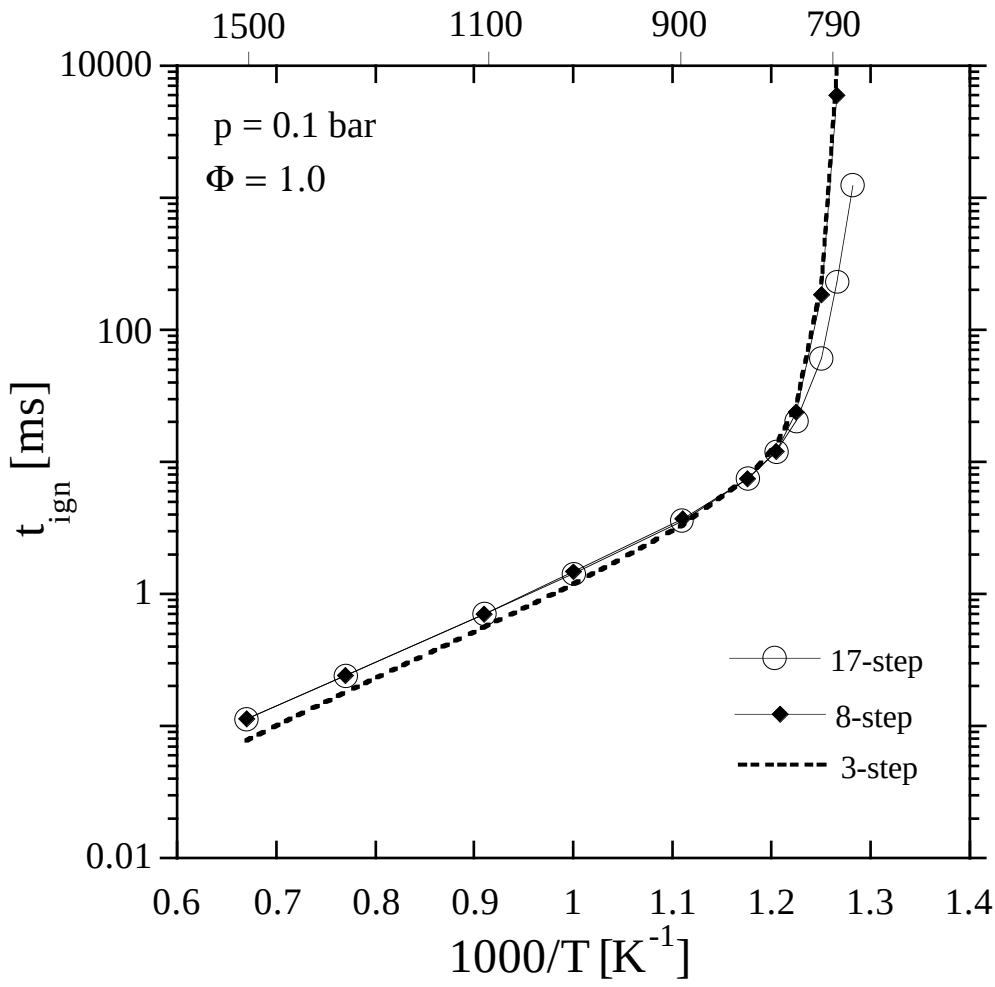

Fig. 4.4: Ignition delay times for stoichiometric hydrogen-oxygen mixtures. The lines show the full mechanism containing the first 17 steps in Table 2.1, the first 8 steps and the simplified 3-step mechanism of reactions 5, 7b and I given in (4.20) and (4.21).

4.3 Explosion Limits for Hydrogen-Oxygen Mixtures

The onset of a homogeneous explosion in a closed vessel depends on additional influences, in particular the heat loss to the walls and thereby on the dimensions of the vessel. Fig. 4.5 taken from [4.2] shows the explosion limits for a stoichiometric hydrogen oxygen mixture as a function of pressure and temperature. For a time range between 750 K and 840 K there are three branches separating non-explosive to explosive conditions. The low and the high pressure branch are influenced by the depletion of chain carrier on the walls of the vessel. Different coatings with KCl give different values for the explosion limits. The middle branch is essentially determined by the competition between reaction (1) and (5). It agrees well with T_c evaluated from (4.27).

The lower branch may be explained as follows: For low temperatures the initial chain

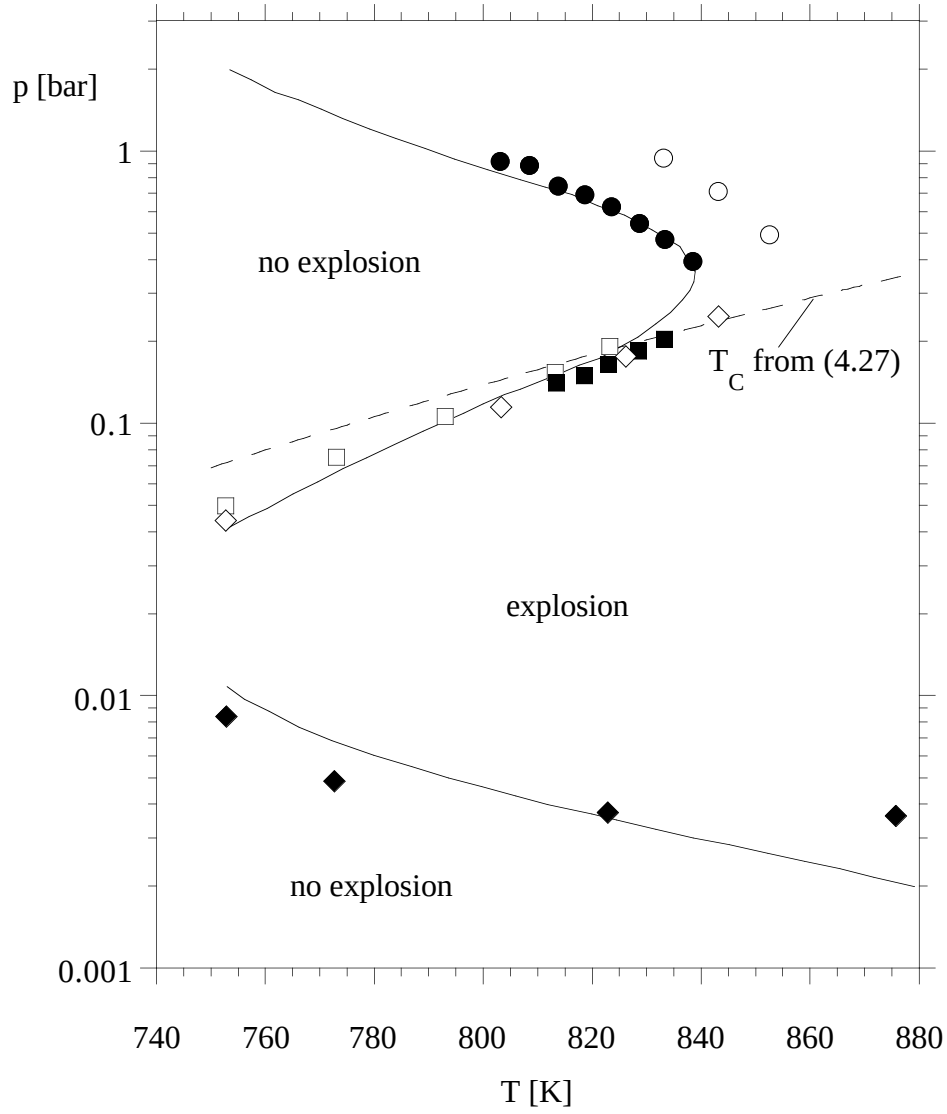

Fig. 4.5: Explosion limits for a stoichiometric hydrogen oxygen mixture in a spherical vessel. Solid line: numerical calculations using a full kinetic mechanism by Stahl and Warnatz [4.2] data points referenced therein, dashed line: (4.27) with $z_5 = 0.7$

branching proceeds through the reaction:

$$\begin{aligned} \mathrm{H_2 + O_2 + M} &\rightarrow \mathrm{H_2O_2 + M} \\ \mathrm{H_2O_2 + M} &\rightarrow \mathrm{OH + OH + M}\,. \end{aligned}$$

Since the first of these reactions is trimolecular with a large activation energy, it increases relatively to the other bimolecular reactions as the pressure increases but decreases with temperature. A line of constant rate should then have a negative slope in the p-T dia-

gram 4.5. The explosion limit is then given by the condition that the rate of removal of radicals by wall reactions equals that of production by the two reactions above.

For pressures above the middle branch in Fig. 4.5, chain braking by reaction (5), leads to a massive formation of HO_2. This reacts with H and OH as

$$\begin{array}{lrcl} (6) & H + HO_2 & \rightarrow & OH + OH \\ (7) & H + HO_2 & \rightarrow & H_2 + O_2 \\ (8) & OH + HO_2 & \rightarrow & H_2O + O_2\,. \end{array}$$

Only the first of these is radical conserving, while reaction (7) and (8) are chain breaking. This was already discussed in Lecture 3. Therefore HO_2 is not a chain carrier at typical combustion conditions. When large amounts of HO_2 are being formed, however, there is a chain branching effect through the reactions

$$\begin{array}{lrcl} (9) & H_2 + HO_2 & \rightarrow & H_2O_2 + H \\ (10) & H_2O_2 + M & \rightarrow & OH + OH + M\,. \end{array}$$

Whether chain branching by reactions (9) and (10) dominates over chain breaking by reactions (7) and (8) depends on the ratio of H and OH versus H_2 and on temperature. In addition, the possibility of chain branching in a closed vessel depends again on the vessel diameter. The larger the vessel and therefore the volume to wall area ratio, the less radicals are removed compared to those that are being formed. Therefore an increase of pressure beyond the second explosion limit will eventually lead to the third explosion limit, the upper branch in Fig 4.5. Since reactions (9) and (10) increase with temperature, the third branch is reached later at lower temperatures, which explains its negative slope in Fig 4.5.

4.4 Ignition of Higher Hydrocarbon-Oxygen System

While the ignition delay time of lower hydrocarbons increases monotonically with decreasing temperature in a similar way as that of hydrogen-oxygen mixtures, higher hydrocarbons behave differently. There is a high temperature regime where the fuel is rapidly decomposed into small C_2- and C_1-hydrocarbons, which are subsequently oxidized leading to a thermal runaway as for small hydrocarbons. At intermediate temperatures, the ignition delay time decreases with decreasing temperature. At temperatures below typically 700 K the ignition delay time decreases again with increasing temperature. In this low temperature regime the fuel is oxidized by O_2-addition in a degenerated chain branching mechanism. Fig. 4.6 shows the ignition delay time for *n*-heptane. Rather detailed mechanisms have been proposed to model the ignition delay times of fuels like *n*-heptane and iso-octane over a large temperature range [4.3]. While n-heptane may be considered as a reference fuel for the (desired) auto-ignition in a Diesel engine, iso-octane may represent a gasoline fuel, where auto-ignition leads to (undesired) engine knock.

The high temperature oxidation of *n*-heptane proceeds from the attack of the fuel by H, OH and HO_2 radicals to form *n*-heptyl radicals and through the break-up of these into C_2H_4, CH_3 and H radicals. These are oxidized by reactions of the C_1-C_2-chemistry. The

low temperature chemistry of lower aliphatic hydrocarbons is characterized by degenerated chain branching which may be illustrated by the following sequence of reaction steps:

$$
\begin{aligned}
RH + O_2 &\longrightarrow R + HO_2 && \text{(initiation)}\\
RH + OH &\longrightarrow R + H_2O && \text{(initiation)}\\
R + O_2 &\rightleftharpoons RO_2 && \text{(first } O_2\text{-addition)}\\
RO_2 &\longrightarrow R'O_2H && \text{(internal H-abstraction)}\\
R'O_2H + O_2 &\rightleftharpoons O_2R'O_2H && \text{(second } O_2\text{-addition)}\\
O_2R'O_2H &\longrightarrow HO_2R''O_2H && \text{(internal H-abstraction)}\\
HO_2R''O_2H &\longrightarrow HO_2R''O + OH && \text{(chain propagation)}\\
HO_2R''O &\longrightarrow OR''O + OH\,. && \text{(chain branching)}
\end{aligned}
$$

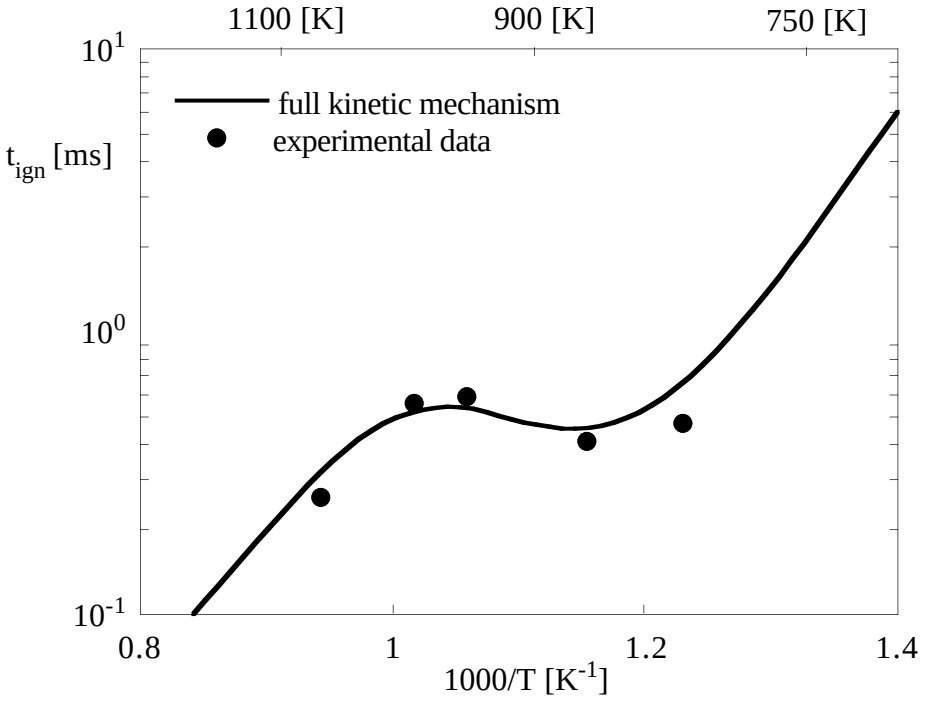

Fig. 4.6: Comparison of calculated ignition delay times for stoichiometric n-heptane-air mixtures by a full kinetic mechanism of 1011 elementary reactions with experimental data [4.4] at 40 atm.

For *n*-heptane R is represented by C_7H_{15}, $R' = C_7H_{14}$ and $R'' = C_7H_{13}$. This low temperature mechanism is no longer valid when the temperature increases beyond about 800 K. The competition of the reverse reactions of the first and second O_2-addition with the subsequent internal H-abstraction reaction is the key to the understanding of the negative temperature dependence of ignition delay. With increasing temperature these

reverse reactions become faster than their forward reactions, thereby stopping the reaction sequence. A transition to the high temperature mechanism must occur.

The apparent negative temperature dependence of the intermediate branch shall be explained by discussing a simplified 4-step ad-hoc model with adjusted rate constants of n-heptane ignition [4.5], which is written as

$$\begin{aligned} \mathrm{F} &\xrightarrow{1} \mathrm{X} \\ \mathrm{X} + 11\,\mathrm{O_2} &\xrightarrow{2} \mathrm{P} \\ \mathrm{F} + 2\,\mathrm{O_2} &\underset{3b}{\overset{3f}{\rightleftharpoons}} \mathrm{I} \\ \mathrm{I} + 9\,\mathrm{O_2} &\xrightarrow{4} \mathrm{P}\,. \end{aligned}$$

Here F stands for the fuel, with $\mathrm{F} = n\text{-}\mathrm{C_7H_{16}}$. X and I represent the combined intermediates, where $\mathrm{X} = 3\mathrm{C_2H_4} + \mathrm{CH_3} + \mathrm{H}$ and $\mathrm{I} = \mathrm{HO_2R''O} + \mathrm{H_2O}$. P represents a combination of the products, with $\mathrm{P} = 7\mathrm{CO_2} + 8\mathrm{H_2O}$.

The first two reactions correspond to a two-step high temperature scheme containing an endothermic fuel decomposition into small hydrocarbons and the exothermic oxidation of these into the final combustion products. The last two steps represent the degenerated chain branching mechanism discussed above. Combining all steps up to the formulation of $\mathrm{HO_2R''O}$ leads to the third global step of the model. The fourth step contains the chain branching and the oxidation to the combustion products. Only the third reaction is considered to be reversible. The activation energy of the backward reaction $3b$ is assumed much larger than that of the forward reaction $3f$. Therefore, at low temperatures the backward reaction $3b$ is unimportant. However, at temperatures around 800 K and higher, the backward reaction dominates over the forward reaction and thereby decreases the relative importance of reactions 3 and 4 in the mechanism. This shall explain the transition from the low temperature to the high temperature branch.

Let us, for the moment, neglect the effects of reactions 1 and 2. The conservation equations for the mole fractions X_F and X_I of the fuel F and the intermediate I then simplify to

$$\begin{aligned} \frac{\mathrm{d}}{\mathrm{d}t} X_\mathrm{F} &= -k_{3f}\, X_\mathrm{F}\, X_{\mathrm{O_2}} + k_{3b}\, X_\mathrm{I} \\ \frac{\mathrm{d}}{\mathrm{d}t} X_\mathrm{I} &= k_{3f}\, X_\mathrm{F}\, X_{\mathrm{O_2}} - k_{3b}\, X_\mathrm{I} - k_4\, X_\mathrm{I}\, X_{\mathrm{O_2}}\,. \end{aligned} \tag{4.28}$$

For temperatures above 800 K the rate of reaction 4 is small compared to the rates of the two reactions 3. Under these conditions, there are two stages in the ignition process: In a first stage, with a characteristic time determined by the reactions 3, we can neglect the effect of reaction 4. No significant change of temperature occurs during this stage because the heat release of reaction 3 is small compared to that of reaction 4. The consumption of oxygen during this stage is also small because the stoichiometric coefficient 2 of reaction 3 is small compared to 9 of reaction 4. The temperature rise can only occur during the second stage, when the fast reactions 3 are in partial equilibrium. Therefore, assuming

partial equilibrium of reaction 3, (4.28) simplifies to

$$\begin{aligned} k_{3f}\, X_{\mathrm{O}}\, X_{\mathrm{F}} &= k_{3b}\, X_{\mathrm{I}} \\ \frac{\mathrm{d}}{\mathrm{d}t}\,(X_{\mathrm{I}} + X_{\mathrm{F}}) &= -k_4\, X_{\mathrm{I}}\, X_{\mathrm{O}_2}\,. \end{aligned} \tag{4.29}$$

The reaction rate constants appearing in (4.29) are given by

$$k_{3f} = B_{3f}\, e^{-E_{3f}/\mathcal{R}T}\,, \quad k_{3b} = B_{3b}\, e^{-E_{3b}/\mathcal{R}T}\,, \quad k_4 \ = B_4\, e^{-E_4/\mathcal{R}T}\,.$$

If we define $X_{\mathrm{S}} = X_{\mathrm{I}} + X_{\mathrm{F}}$, the mole fraction of the pool formed by I and F, we can express X_{I} as a function of X_{S} as

$$X_{\mathrm{I}} = X_{\mathrm{S}}\, \frac{K X_{\mathrm{O}_2}}{1 + K X_{\mathrm{O}_2}} \tag{4.30}$$

where K is the equilibrium constant of the third reaction

$$K = \frac{k_{3f}}{k_{3b}} = \frac{B_{3f}}{B_{3b}}\, \exp\left(\,(E_{3b} - E_{3f})\,/\mathcal{R}T\right)\,. \tag{4.31}$$

Thus the second of (4.29) becomes

$$\frac{\mathrm{d}}{\mathrm{d}t}\, X_{\mathrm{S}} = -k_4\, \frac{K\, X_{\mathrm{O}_2}}{1 + K\, X_{\mathrm{O}_2}}\, X_{\mathrm{O}_2}\, X_{\mathrm{S}}\,. \tag{4.32}$$

For values of T larger than the cross-over temperature of approximately 800 K, $K\, X_{\mathrm{O}_2}$ becomes small compared to 1. In this case the reverse reaction 3 is so fast that the concentration of I cannot grow, $X_{\mathrm{I}} \ll 1$ according to (4.30) and remains in steady state. Then $X_{\mathrm{S}} = X_{\mathrm{F}}$ and (4.32) simplifies to

$$\frac{\mathrm{d}}{\mathrm{d}t}\, X_{\mathrm{F}} = -k_4\, K\, X_{\mathrm{F}}\, X_{\mathrm{O}_2}^2\,. \tag{4.33}$$

corresponding to the overall kinetic scheme

$$\mathrm{F} + 11\,\mathrm{O}_2 \longrightarrow \mathrm{P}\,.$$

The combined reaction rate constant

$$k_4\, K = \frac{B_{3f}}{B_{3b}}\, B_4\, \exp\left[-\left(E_4 + E_{3f} - E_{3b}\right)/\mathcal{R}T\right] \tag{4.34}$$

is associated with the apparent activation energy $E_{3f} + E_4 - E_{3b}$, which is negative if E_{3b} is sufficiently larger than the sum of E_{3f} and E_4 as it was assumed in [4.5].

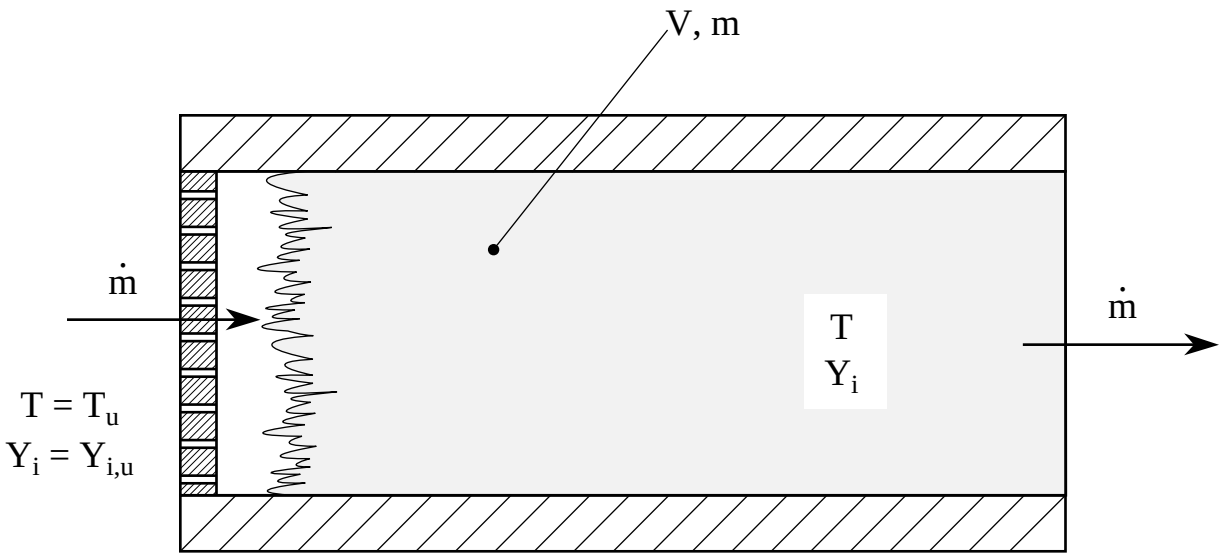

Fig. 4.7: Schematic representation of a continuously stirred flow reactor

4.5 The Continuously Stirred Flow Reactor, Steady State Solutions

We now want to consider an idealized flow reactor of constant mass m and volume V shown in Fig. 4.7. The mass flow rate $\dot{m}$ enters with reactants $Y_i = Y_{iu}$ at temperature $T = T_u$. The reactants are immediately mixed with combustion products at the entrance of the reactor where the flow is assumed to be highly stirred by many incoming turbulent jets.

The temperature and the concentrations within the reaction are assumed to be uniform equal to T and Y_i, respectively. The reactor is assumed adiabatic for simplicity.

The time rate of change $\mathrm{d}m_i/\mathrm{d}t$ of the partial mass m_i of species i within the reactor is equal to the difference between it inflowing and outflowing mass flow rate of species i, $\dot{m}(Y_{i,u} - Y_i)$ and the change by chemical reactions $(\mathrm{d}m_i/\mathrm{d}t)_{\mathrm{chem}}$. Using $m_i = mY_i$ and

$$\left(\frac{\mathrm{d}m_i}{\mathrm{d}t}\right)_{\mathrm{chem}} = V\dot{m}_i = VW_i \sum_{k=1}^{r} \nu_{ik} w_k \tag{4.35}$$

where $\dot{m}_i$ is the chemical mass production rate per unit volume, one obtains

$$m\frac{\mathrm{d}Y_i}{\mathrm{d}t} = \dot{m}\,(Y_{iu} - Y_i) + VW_i \sum_{k=1}^{r} \nu_{ik} w_k\,. \tag{4.36}$$

For an open adiabatic system at constant pressure the first law of thermodynamics yields $\mathrm{d}h = 0$. Similar to (4.3) and (4.4) one now obtains

$$\mathrm{d}h = \sum_{i=1}^{n} h_i \mathrm{d}Y_i + \sum_{i=1}^{n} Y_i \mathrm{d}h_i = 0 \tag{4.37}$$

and

$$\sum_{k=1}^{n} Y_i \mathrm{d}h_i = \left(\sum_{i=1}^{n} Y_i c_{p_i} \right) \mathrm{d}T = c_p \mathrm{d}T \,. \tag{4.38}$$

Combining this with (4.36) leads to the temperature equation

$$mc_p \frac{\mathrm{d}T}{\mathrm{d}t} = \dot{m} c_p \left(T_u - T \right) + V \sum_{k=1}^{r} Q_k w_k \tag{4.39}$$

where

$$Q_k = - \sum_{i=1}^{n} \nu_{ik} W_i h_i \tag{4.40}$$

is the heat of combustion for a constant pressure process. We will now consider a single one-step reaction with a large activation energy governed by the reaction rate

$$\omega = B \frac{\rho Y_F}{W_F} \exp \left(- \frac{E}{\mathcal{R} T} \right) \,. \tag{4.41}$$

In assuming a dependence on the concentration of the fuel F only, but not on that of the oxidizer, we implicitly consider a sufficiently lean mixture with a large excess of oxygen. Therefore the concentration of oxygen does not change much during combustion and therefore does not affect the reaction rate. (This will be discussed in more detail in Lecture 6.) In (4.41) B has the dimension sec^{-1} and therefore represents the inverse of a reaction time. It must be compared to the residence time t_ν within the reactor which is

$$t_\nu = \frac{m}{\dot{m}} \tag{4.42}$$

Using $\rho = m/V$ and introducing the nondimensional quantities

$$\begin{aligned} Y^* &= \frac{Y_F}{Y_{F,u}} \,, \quad T^* = \frac{T}{T_u} \,, \quad t^* = \frac{t}{t_\nu} \,, \\ \mathrm{Da} &= B t_\nu \,, \quad E^* = \frac{E}{\mathcal{R} T_u} \,, \quad Q^* = \frac{Q Y_u}{c_p W_F T_u} \,, \end{aligned} \tag{4.43}$$

one obtains the non-dimensional reactor equations (with the asterisk removed)

$$\begin{aligned} \frac{\mathrm{d}Y}{\mathrm{d}t} &= 1 - Y - \mathrm{Da}\, Y \exp\left(-E/T\right) \\ \frac{\mathrm{d}T}{\mathrm{d}t} &= 1 - T + Q\, \mathrm{Da}\, Y \exp\left(-E/T\right) \end{aligned} \tag{4.44}$$

The parameters of these equations are the Damköhlers number Da, the non-dimensional heat of combustion Q and the non-dimensional activation energy E. (The definition of the Damköhler number differs here from the one to be used in subsequent lectures, where

the exponential term evaluated at a specific temperature will be included. Here we want to consider a large range of temperatures and therefore use the product of the reaction frequency B and the residence time to define Da.)

Multiplying the first of (4.44) by Q and adding both equations one obtains a linear equation $\mathrm{d}x/\mathrm{d}t = -x$ for $x = 1 - T + Q(1 - Y)$ which has the trivial solution $x = 0$. This leads to the following coupling relation between the temperature and the concentration

$$T + QY = 1 + Q \tag{4.45}$$

Introducing this into (4.44) the problem of the adiabatic reactor is described by a single equation for the temperature

$$\frac{\mathrm{d}T}{\mathrm{d}t} = 1 - T + \mathrm{Da}\,\mathbf{N}\,(T) \tag{4.46}$$

where the non-linear operator $\mathbf{N}$ defined by

$$\mathbf{N} = (1 + Q - T)\exp\,(-E/T) \tag{4.47}$$

From (4.45) it is seen that the minimum and the maximum values of the temperature are

$$\begin{aligned} Y = 1: &\quad T_{\min} = 1 \\ Y = 0: &\quad T_{\max} = 1 + Q \end{aligned} \tag{4.48}$$

We will now assume that the reactor has reached a steady state. The steady state temperature T_S is obtained from the algebraic equation

$$0 = 1 - T_S + \mathrm{Da}\,\mathbf{N}\,(T_S) \tag{4.49}$$

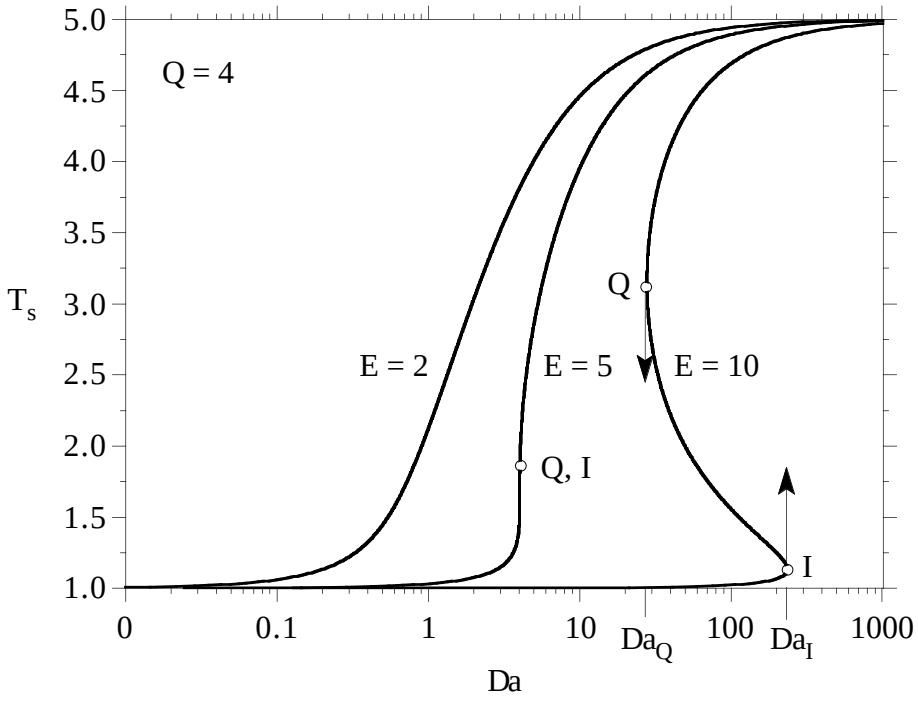

Fig. 4.8: Steady state solutions of the reactor equations

Solutions of (4.49) for $Q = 4$ and $E = 2$, $E = 5$ and $E = 10$ are shown in Fig. 4.8. For $E = 2$ one obtains a monotonous increase of T_S with increasing Damköhler number. For $E = 10$, however, there is a range of Damköhler numbers between Da_Q and Da_I where multiple solutions exist. The shape of this curve reminds vaguely of an S, it is often called the "S-shaped curve". At the points Q and I, corresponding to the Damköhler numbers Da_Q and Da_I the curve for $E = 10$ has a vertical tangent. If the reactor is originally operated with a low residence time and therefore a small Damköhler number, the solution remains close to the $T_S = 1$ corresponding to the non-reacting case. When the Damköhler number increases beyond $\mathrm{Da} = 100$ in the case $E = 10$, there is a small temperature increase. Beyond $\mathrm{Da} = \mathrm{Da}_I$, however, the low temperature solution does no longer exist and the only steady state solution at which the reactor can operate is the solution on the high temperature branch. The instationary transition from the low to the high temperature branch corresponds to an ignition process. It starts from the point I of the lower temperature branch, and is denoted by an arrow in Fig. 4.8.

When the upper branch is reached, steady state combustion is established. If one then reduces the residence time again, thereby lowering the Damköhler number, one follows the curve $E = 10$ to the left towards lower temperatures. This indicates that the available residence time is unsufficient for complete combustion and that an increasing amount of fuel will remain unreacted. When the Damköhler number becomes lower then Da_Q an unstationary transition from the upper to the lower temperature branch occurs. This corresponds to the extinction or quenching of the reaction. The temperature then drops from the value at the point Q to a value close to $T = 1$. This is again denoted by an arrow in Fig. 4.8. The ignition at a large Damköhler number Da_I and subsequent extinction at a lower Damköhler number Da_Q is a typical hysteresis process. We will show below that only the upper and the lower branch of the steady state solution are stable while the middle branch solution is unstable.

4.6 Ignition and Extinction of the Continuously Stirred Flow Reactor

In order to determine the conditions for which multiple solutions exist, we want to calculate the temperatures T_I and T_Q corresponding to the ignition and quenching points. At these points the curve has a vertical tangent leading to the condition

$$\frac{\mathrm{dDa}}{\mathrm{d}T_S} = 0\,. \tag{4.50}$$

Since (4.49) may be expressed as

$$\mathrm{Da} = \frac{T_S - 1}{\mathbf{N}\,(T_S)} \tag{4.51}$$

(4.50) leads to

$$\mathbf{N}\,(T_S) - (T_S - 1)\,\frac{\mathrm{d}\mathbf{N}\,(T_S)}{\mathrm{d}T_S} = 0 \tag{4.52}$$

with

$$\frac{\mathrm{d}\mathbf{N}\,(T_S)}{\mathrm{d}T_S} = \mathbf{N}\,(T_S)\left(\frac{E}{T_S^2} - \frac{1}{1 + Q - T_S}\right) \tag{4.53}$$

one obtains after some algebraic manipulations a quadratic equation which has the solution

$$T_{I,Q} = \frac{(2+Q) \pm Q\sqrt{1-4(1+Q)/EQ}}{2(1+Q/E)} \,. \tag{4.54}$$

The term under the square root vanishes for $E = 4(1+Q)/Q$. For this combustion of parameters the ignition and the quenching points coincide. For the value $Q = 4$ chosen in Fig. 4.8 this corresponds to $E = 5$. Two solutions and therefore ignition as well as quenching exist only if

$$E > 4(1+Q)/Q \,. \tag{4.55}$$

For smaller values of the activation energy a monotonous transition from lower to higher temperatures takes place. This is shown for $E = 2$ in Fig. 4.8. Typical combustion processes starting from ambient temperature are nearly always in the regime of large non-dimensional activation energies where ignition and quenching may occur.

Approximate expressions for the temperatures T_I and T_Q resulting from (4.54) may be obtained in the limit $E \to \infty$. Expanding the square root term and the term in the denominator of (4.53) up to first order as

$$\begin{aligned} \sqrt{1-4(1+Q)/EQ} &\approx 1 - 2(1+Q)/EQ \\ (1+Q/E)^{-1} &\approx 1 - Q/E \end{aligned} \tag{4.56}$$

one obtains

$$T_I = 1 + 1/E \,, \quad T_Q = 1 + Q - \frac{(1+Q)^2}{E} \,. \tag{4.57}$$

In terms of dimensional quantities this may be expressed as

$$T_I = T_{\min}\left(1 + \frac{\mathcal{R}T_{\min}}{E}\right) \,, \quad T_Q = T_{\max}\left(1 - \frac{\mathcal{R}T_{\max}}{E}\right) \tag{4.58}$$

It is easily seen that for ignition the temperature increment $\mathcal{R}T_{\min}/E$ corresponds to that used in (4.13).

Quenching occurs, when the temperature decreases by a small amount below the maximum temperature. For typical maximum combustion temperatures around 2000 K and activation energies corresponding to $E/\mathcal{R} = 20{,}000$ K, a temperature decrease of around 200 K would already lead to extinction.

It is worthwhile to study the upper branch of the steady state solution up to the extinction point by an asymptotic expansion. We write the non-dimensional temperature as

$$T_S = 1 + Q - \varepsilon y \tag{4.59}$$

where ε is yet to be determined. Expanding the inverse temperature in the exponential term in (4.47) as

$$\frac{1}{T_S} = \frac{1}{(1+Q)[1-\varepsilon y/(1+Q)]} = \frac{1}{1+Q} + \frac{\varepsilon y}{(1+Q)^2} \tag{4.60}$$

and inserting this into (4.49) one obtains

$$0 = -Q + \varepsilon y + \mathrm{Da}\,\varepsilon y \exp\left(-\frac{E}{1+Q}\right) \exp\left(-\frac{E\varepsilon}{(1+Q)^2} y\right) \tag{4.61}$$

In the limit $\varepsilon \to 0$ the second term in this equation vanishes. Assuming Q of order unity, a balance of the first with the third term then requires that the Damköhler number is sufficiently large. We shall now discuss (4.61). Depending on the magnitude of the activation energy there are two cases:

1. **The Non-dimensional activation energy E is of order unity.**
   This suggests the definition $\varepsilon = 1/\mathrm{Da}$ leading to a **large Damköhler number** analysis. The second exponential then vanishes in the limit $\varepsilon \to 0$ and with

   $$y = Q \exp\left(\frac{E}{1+Q}\right) \tag{4.62}$$

   the temperature expansion (4.59) becomes

   $$T_S = 1 + Q - \frac{Q}{\mathrm{Da}} \exp\left(\frac{E}{1+Q}\right) . \tag{4.63}$$

   This expression is able to approximate the upper branch of the S-shaped curve for the case $E = 2$ in Fig. 4.8. It is not suitable for the case $E = 10$ and is in particular not able to predict the turning point of this curve at extinction.

2. **The Non-dimensional activation energy E is asymptotically large.**
   The grouping in the second exponential in (4.61) then suggests the definition

   $$\varepsilon = \frac{(1+Q)^2}{E} \tag{4.64}$$

   equivalent to **large activation energy** asymptotics. In order to obtain a balance of the remaining terms in (4.61) one must now require that the quantity

   $$\delta = \frac{\mathrm{Da}\,(1+Q)^2}{EQ} \exp\left(-\frac{E}{1+Q}\right) \tag{4.65}$$

   is of order unity. This indicates that the Damköhler number must grow as

   $$\mathrm{Da} \sim \varepsilon^{-1} \exp((1+Q)/\varepsilon)$$

   in the limit $\varepsilon \to 0$. This linking of two asymptotically large parameters in a specific way is called a distinguished limit. Inserting (4.64) and (4.65) into (4.61) leads to the nonlinear equation

   $$1 = \delta y \exp(-y) \tag{4.66}$$

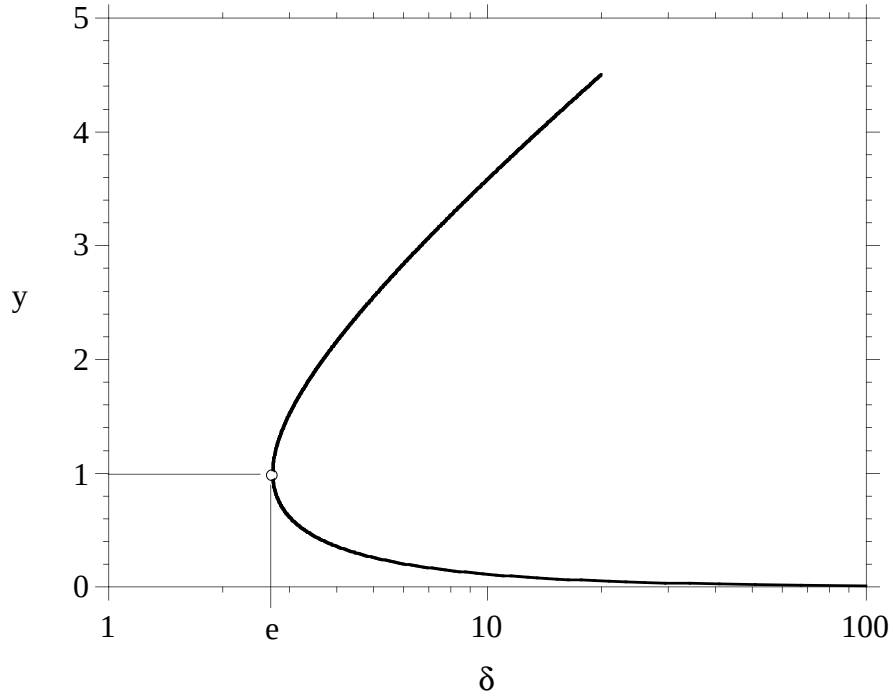

Fig. 4.9: Large activation energy asymptotic solution of the upper branch of the S-shaped curve showing a turning point which corresponds to extinction.

from which y may be determined. Its solution is plotted in Fig. 4.9 showing a turning point at $y = 1$, $\delta = e$. For values of $\delta > e$ there are two solutions, the lower one corresponding to the upper branch in Fig. 4.8, the upper one corresponding to the intermediate branch. The turning point characterizes the extinction condition.

It shall be noted that the analysis of extinction requires large activation energy rather than large Damköhler number asymptotics.

4.7 Stability of the Steady State Solutions

Finally, we want to show that, when multiple solutions exist, only the lower and the upper branches of the S-shaped curve are stable, while the intermediate branch is unstable. We go back to (4.46) and introduce the small temperature perturbation T' of the steady state solution

$$T = T_S + T'(t)\,. \tag{4.67}$$

When this is introduced into (4.46) and (4.49) is substracted, one obtains after linearisation

$$\frac{\mathrm{d}T'}{\mathrm{d}t} = -\lambda T' \tag{4.68}$$

where

$$\lambda = 1 - \mathrm{Da}\frac{\mathrm{d}\mathbf{N}(T_S)}{\mathrm{d}T_S} = \mathbf{N}(T_S)\frac{\mathrm{dDa}}{\mathrm{d}T_S}\,. \tag{4.69}$$

Here (4.51) has been used. The perturbation

$$T' = T'_0 \exp(-\lambda t) \tag{4.70}$$

where T'_0 is an arbitrary initial perturbation, clearly decays with time if it is positive, but it grows if λ is negative. Since the sign of λ equals the sign of $\mathrm{dDa}/\mathrm{d}T_S$, steady state solutions showing an increase of temperature with increasing Damköhler number are stable. This is true for the lower and the upper branch of the S-shaped curve. The opposite is true for the middle branch which therefore is unstable.

Exercise 4.1

Derive an approximate expression for the ignition delay time in the high and intermediate temperature range by assuming that the activation energy E_1 of reaction 1 is very large and the intermediate X in steady state.

Solution

With the steady state approximation reactions 1 and 2 can be replaced by the overall reaction

$$\mathrm{F} + 11\,\mathrm{O_2} \rightarrow \mathrm{P}$$

with the rate

$$\frac{\mathrm{d}}{\mathrm{d}t} X_\mathrm{F} = -k_1 X_\mathrm{F} .$$

Combining this with the contribution of reactions 3 and 4 according to (4.33) in the intermediate temperature range the rate of fuel consumption can be written as

$$\frac{\mathrm{d}}{\mathrm{d}t} X_\mathrm{F} = -k_1 X_\mathrm{F} - k_4 K X_\mathrm{F} X_{\mathrm{O_2}}^2 . \tag{$*$}$$

The corresponding temperature equation is

$$\frac{\mathrm{d}}{\mathrm{d}t} T = Q \left(k_1 X_\mathrm{F} + k_4 K X_\mathrm{F} X_{\mathrm{O_2}}^2 \right) . \tag{$**$}$$

where Q is the heat reduction of the overall reaction. Equations $(*)$ and $(**)$ are to be solved with the initial conditions $X_\mathrm{F} = X_{\mathrm{F},0}$ and $T = T_0$ at $t = 0$. Due to the large exothermicity of the reactions, small changes in the fuel and oxygen concentration are sufficient to increase the temperature significantly. Accounting for the fact that the activation energy E_1 is large compared to $E_{3f} - E_{3b} + E_4$, which then is of order unity, a suitable expansion of the temperature is

$$T = T_0(1 + \varepsilon y) , \quad \varepsilon = \frac{\mathcal{R}\, T_0}{E_1} .$$

Neglecting the reactant consumption in $(**)$ by setting $X_\mathrm{F} = X_{\mathrm{F},0}$ and $X_{\mathrm{O_2}} = X_{\mathrm{O_2},0}$ one obtains the equation for the non-dimensional temperature increment y

$$\frac{\mathrm{d}y}{\mathrm{d}t} = \frac{1}{t_1} e^y + \frac{1}{t_2} \tag{$***$}$$

with the initial condition $y(0) = 0$. Here the inverse characteristic times are defined as

$$\frac{1}{t_1} = \frac{E_1}{\mathcal{R}T_0^2}\, Q\, X_{\mathrm{F},0} B_1 \exp\left(-E_1/\mathcal{R}T_0\right)$$
$$\frac{1}{t_2} = \frac{E_1}{\mathcal{R}T_0^2}\, Q\, X_{\mathrm{F},0} X_{\mathrm{O}_2,0}^2 B_4\, \frac{B_{3f}}{B_{3b}}\, \exp\left(-(E_{3f} - E_{3b} + E_4)/\mathcal{R}T_0\right)$$

Equation $(***)$ may be transformed using $x = e^{-y}$. One then has to solve a linear differential equation which is easily integrated. The solution in terms of t as a function of y is finally

$$\frac{t}{t_2} = \log\left(1 + \frac{t_1}{t_2}\right) - \log\left(1 + \frac{t_1}{t_2} e^{-y}\right) .$$

When y becomes infinite, the ignition time is

$$t_{\mathrm{ign}} = t_2\, \log(1 + t_1/t_2)\,,$$

For small values of t_1 corresponding to large T_0, the log may by linearized leading to $t_{\mathrm{ign}} \to t_1$ describing the high temperature range. For large values of t_1 the 1 in the log may be neglected leading to a weak temperature dependence of t_{ign}.

References

[4.1] Trevino, C., "Progress in Astronautics and Aeronautics", **131**, pp. 19–43, 1989.

[4.2] Maas, U. and Warnatz, J., Combustion and Flame **74**, pp. 53–69, 1988.

[4.3] Westbrook, C.K., Warnatz, J. and Pitz, W.J., 22nd Symposium (International) on Combustion, p. 893, The Combustion Institute 1988.

[4.4] Cieski, H. and Adomeit, G., "Shock tube investigation of self-ignition of fuel/air mixtures under engine conditions", Combustion and Flame, to appear 1992.

[4.5] Müller, U.C., Peters, N. and Liñán, A., 24th Symposium on Combustion, to appear 1992.

Lecture 5: Fluid Dynamics and Basic Equations for Flames

The basic equations for calculating combustion processes in the gas phase are the equations of continuum mechanics. They include in addition to balance equations for mass and momentum those for the energy and the chemical species. Associated with the release of thermal energy and the increase in temperature is a local decrease in density which in turn affects the momentum balance. Therefore, all these equations are closely coupled to each other. Nevertheless, in deriving these equations we will try to point out how they can be simplified and partially uncoupled under certain assumptions.

5.1 Balance Equations

Let us consider a general quality per unit volume $f(\vec{x}, t)$. Its integral over the finite volume V, with the time-independent boundary A is given by

$$F(t) = \int_V f(\vec{x}, t)\, \mathrm{d}V \tag{5.1}$$

The temporal change of F

$$\frac{\partial F}{\partial t} = \int_V \frac{\partial f}{\partial t}\, \mathrm{d}V \tag{5.2}$$

is then due to the following three effects:

1. by the flux $\vec{\phi}_f$ across the boundary A. This flux may be due to convection or molecular transport. It is directed inwards and therefore opposite to the normal vector $\vec{n}$ on the surface, which is directed outwards. By integration over the boundary A we therefore obtain
$$-\int_A \vec{\phi}_f \vec{n}\, \mathrm{d}A\,;$$

2. by a local source σ_f within the volume. This is an essential production of partial mass by chemical reactions. Integrating the source term over the volume leads to
$$\int_V \sigma_f\, \mathrm{d}V\,;$$

3. by an external induced source. Examples are the gravitational force or thermal radiation. Integration of s_f over the volume yields
$$\int_V s_f\, \mathrm{d}V\,.$$

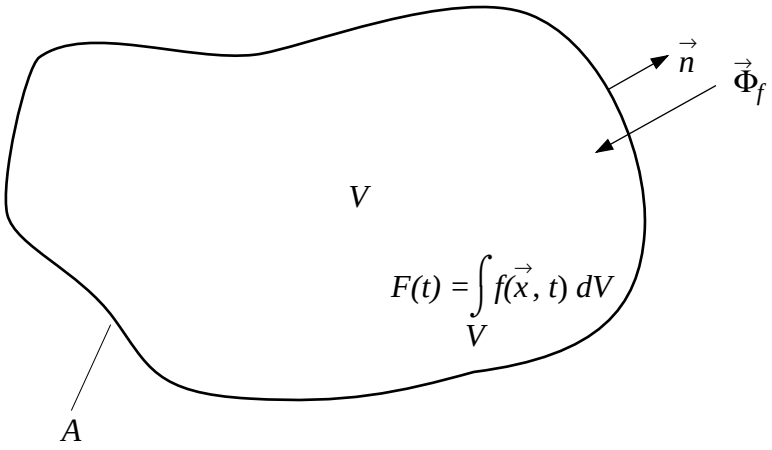

Fig. 5.1: Volume F with time-independent boundary A

We therefore have the balance equation

$$\int_V \frac{\partial f}{\partial t}\,\mathrm{d}V = -\int_A \vec{\phi}_f \vec{n}\,\mathrm{d}A + \int_V (\sigma_f + s_f)\,\mathrm{d}V$$

Changing the integral over the boundary A into a volume integral using Gauss' theorem

$$\int_A \vec{\phi}_f \vec{n}\,\mathrm{d}A = \int_V \mathrm{div}\,\vec{\phi}_f\,\mathrm{d}V$$

and realizing that the balance must be independent of the volume, we obtain the general balance equation in differential form

$$\frac{\partial f}{\partial t} = -\,\mathrm{div}\,\vec{\phi}_f + \sigma_f + s_f\,. \tag{5.3}$$

Mass Balance

Set the partial mass per unit volume $\rho_i = \rho Y_i = f$. The partial mass flux across the boundary is $\rho_i \vec{v}_i = \vec{\phi}_f$, where $\vec{v}_i$ the diffusion velocity. Summation over all components yields the mass flow

$$\rho\vec{v} = \sum_{i=1}^{n} \rho_i \vec{v}_i \tag{5.4}$$

where $\vec{v}$ is the mass average velocity. The difference between $\vec{v}_i$ defines the diffusion flux

$$\vec{v}_i - \vec{v} = \frac{\vec{j}_i}{\rho_i} \tag{5.5}$$

where the sum satisfies

$$\sum_{i=1}^{n} j_i = 0\,. \tag{5.6}$$

Setting the chemical source term

$$\sigma_f = \dot{m}_i = W_i \sum_{k=1}^{r} \nu_{ik} w_k$$

one obtains the equation for the partial density

$$\frac{\partial \rho_i}{\partial t} = -\operatorname{div}(\rho_i \vec{v}_i) + \dot{m}_i \quad (i = 1, 2, ..., n)\,. \tag{5.7}$$

The summation over i leads to the continuity equation

$$\frac{\partial \rho}{\partial t} = -\operatorname{div}(\rho \vec{v})\,. \tag{5.8}$$

Introducing the total derivative of a quantity a

$$\frac{Da}{Dt} = \frac{\partial a}{\partial t} + \vec{v} \cdot \operatorname{grad} a\,, \tag{5.9}$$

a combination with the continuity equation yields

$$\rho \frac{Da}{Dt} = \frac{\partial(\rho a)}{\partial t} + \operatorname{div}(\rho \vec{v} a)\,. \tag{5.10}$$

Then (5.7) may also be written using (5.5)

$$\rho \frac{DY_i}{Dt} = -\operatorname{div} \vec{j}_i + \dot{m}_i \quad (i = 1, 2, ..., n)\,. \tag{5.11}$$

Momentum Balance

Set the momentum per unit volume $\rho \vec{v} = f$. The momentum flux is the sum of the convective momentum in flow $\rho \vec{v}\vec{v}$ and the pressure tensor

$$\overline{\overline{P}} = p\, \overline{\overline{E}} + \overline{\overline{\tau}} \tag{5.12}$$

where $\overline{\overline{E}}$ is the unit tensor and $\overline{\overline{\tau}}$ is the viscous stress tensor. Therefore $\rho \vec{v}\vec{v} + \overline{\overline{P}} = \phi_f$. There is no local source of momentum but the gravitational force from outside $s_f = -\vec{i}\rho g$ where $\vec{i}$ is the unit vector and g the constant of gravity. The momentum equation then reads

$$\frac{\partial \rho \vec{v}}{\partial t} = -\operatorname{Div}(\rho \vec{v}\vec{v} + \overline{\overline{P}}) - \vec{i}\rho g \tag{5.13}$$

or with (5.7) and (5.11)

$$\rho \frac{D\vec{v}}{Dt} = -\operatorname{grad} p - \operatorname{Div} \overline{\overline{\tau}} - \vec{i}\rho g\,. \tag{5.14}$$

Kinetic Energy Balance

Multiplying (5.13) with $\vec{v}$ for each component of $\vec{v}$ one obtains the balance for the kinetic energy $v^2 = \vec{v} \cdot \vec{v}$

$$\frac{1}{2}\frac{\partial}{\partial t}(\rho v^2) = -\operatorname{div}(\overline{\overline{P}} \cdot \vec{v} + \frac{1}{2}\vec{v}\rho v^2) + \overline{\overline{P}} : \operatorname{Grad}\vec{v} - \vec{i}\rho g\vec{v}\,. \tag{5.15}$$

Potential Energy Balance

The gravitational force may be written as the derivative of the time-independent potential

$$\vec{i}g = \operatorname{grad}\psi, \quad \frac{\partial\psi}{\partial t} = 0\,. \tag{5.16}$$

Then with (5.8) the balance for the potential energy is

$$\frac{\partial(\rho\psi)}{\partial t} = -\operatorname{div}(\rho\vec{v}\psi) + \vec{i}\rho g\vec{v}\,. \tag{5.17}$$

Total and Internal Energy and Enthalpy Balance

The first law of thermodynamics states that the total energy must be conserved, such that the local source $\sigma_f = 0$. We set $\rho e = f$, where the total energy per unit mass is

$$e = u + \frac{1}{2}v^2 + \psi \tag{5.18}$$

this defines the internal energy introduced in (1.46). The total energy flux $\vec{j}_e = \vec{\phi}_f$ is

$$j_e = \rho e\vec{v} + \overline{\overline{P}} \cdot \vec{v} + \vec{j}_q \tag{5.19}$$

which defines the total heat flux $\vec{j}_q$. The externally induced source due to radiation is $q_R = s_f$. Then the total energy balance

$$\frac{\partial(\rho e)}{\partial t} = -\operatorname{div}\vec{j}_e + q_R \tag{5.20}$$

may be used to derive an equation for the internal energy

$$\frac{\partial(\rho u)}{\partial t} = -\operatorname{div}(\rho\vec{v}u + \vec{j}_q) - \overline{\overline{P}} : \operatorname{Grad}\vec{v} + q_R\,. \tag{5.21}$$

Using (5.10) this may be written with the total derivative

$$\rho\frac{Du}{Dt} = -\operatorname{div}\vec{j}_q - p\operatorname{div}\vec{v} + \overline{\overline{\tau}} : \operatorname{Grad}\vec{v} + q_R\,. \tag{5.22}$$

Since $\operatorname{div}\vec{v} = \rho\, D\rho^{-1}/Dt$ this may be written as

$$\underbrace{\frac{Du}{Dt}}_{\mathrm{d}u} + \underbrace{p\frac{D\rho^{-1}}{Dt}}_{p\,\mathrm{d}v} = \underbrace{\frac{1}{\rho}\left[-\operatorname{div}\vec{j}_q + q_R\right]}_{\mathrm{d}q} + \underbrace{\frac{1}{\rho}\,\overline{\overline{\tau}}\colon \operatorname{Grad}\vec{v}}_{\mathrm{d}w_R} \tag{5.23}$$

illustrating the equivalence with the first law introduced in a global thermodynamic balance in (1.46). With $h = u + p/\rho$ the enthalpy balance equation is then

$$\rho\frac{Dh}{Dt} = \frac{Dp}{Dt} - \operatorname{div}\vec{j}_q + \overline{\overline{\tau}}\colon \operatorname{Grad}\vec{v} + q_R\,. \tag{5.24}$$

5.2 Transport Processes

In its most general form Newton's law states that the stress tensor is proportional to the symmetric, trace-free part of the velocity gradient, more specifically

$$\overline{\overline{\tau}} = -\mu\left[\operatorname{Grad}\vec{v} - \frac{\overline{\overline{E}}}{3}\operatorname{div}\vec{v}\right]^s\,. \tag{5.25}$$

Here the suffix s denotes that only the symmetric part is taken and the second term in the brackets subtracts the trace elements from the tensor. Newton's law thereby defines the dynamic viscosity. Similarly Fick's law states that the diffusion flux is proportional to the concentration gradient. Due to thermodiffusion it is also proportional to the temperature gradient. The most general form for multicomponent diffusion is written as

$$\vec{j}_i = \frac{W_i}{W}\sum_{\substack{j=1\\ j\neq i}}^{n}\rho D_{ij} W_j \operatorname{grad} X_j - \frac{D_i^T}{T}\operatorname{grad} T \quad (i = 1, 2, \ldots n)\,. \tag{5.26}$$

For most combustion processes thermodiffusion can safely be neglected. For a binary mixture (5.26) then reduces to

$$\vec{j}_i = -\rho\mathcal{D}_{ij}\operatorname{grad} Y_i \tag{5.27}$$

where $\mathcal{D}_{ij} = \mathcal{D}_{ji}$ is the binary diffusion coefficient. For multicomponent mixtures where one component occurs in large amounts, as for the combustion in air where nitrogen is abundant, all other species may be treated as trace species and (5.27) with the binary diffusion coefficient with respect to the abundant component may be used as an approximation

$$\vec{j}_i = -\rho D_i \operatorname{grad} Y_i, \quad D_i = \mathcal{D}_{i,\mathrm{N}_2}\,. \tag{5.28}$$

A generalization for an effective diffusion coefficient D_i to be used for the minor species in (5.28) is

$$D_i = \frac{\sum\limits_{\substack{i=1\\ i\neq j}}^{n} X_i}{\sum\limits_{\substack{j=1\\ j\neq i}}^{n} X_i/\mathcal{D}_{ij}}\,. \tag{5.29}$$

Note that the use of (5.28) does not satisfy the condition (5.6). Finally, Fourier's law of thermal conductivity states that the heat flux should be proportional to the temperature gradient. The heat flux $\vec{j}_q$ includes the effect of partial enthalpy transport by diffusion and is written

$$\vec{j}_q = -\lambda \operatorname{grad} T + \sum_{i=1}^{n} h_i \vec{j}_i \tag{5.30}$$

which defines the thermal conductivity λ. In (5.30) the Dufour heat flux has been neglected. Transport coefficients for single components can be calculated on the basis of the theory of rarefied gases [5.1].

5.3 Different forms of the energy equation

We start from the enthalpy equation and neglect in the following the viscous dissipation term $\overline{\overline{\tau}}$: Grad $\vec{v}$ and the radiative heat transfer term q_R. Then, differentiating (1.48) as

$$\mathrm{d}h = c_p \mathrm{d}T + \sum_{i=1}^{n} h_i \mathrm{d}Y_i \tag{5.31}$$

where c_p is the heat capacity at constant pressure of the mixture, we can write the heat flux as

$$\vec{j}_q = -\frac{\lambda}{c_p} \operatorname{grad} h + \sum_{i=1}^{n} h_i \left(\vec{j}_i + \frac{\lambda}{c_p} \operatorname{grad} Y_i \right) . \tag{5.32}$$

For the special case that the diffusion flux can be approximated by (5.27) with an effective diffusion coefficient D_i we introduce the Lewis number

$$\mathrm{Le}_i = \frac{\lambda}{\rho c_p D_i} \tag{5.33}$$

and write the last term in (5.32) as

$$\sum_{i=1}^{n} h_i \left(1 - \frac{1}{\mathrm{Le}_i} \right) \frac{\lambda}{c_p} \operatorname{grad} Y_i \, . \tag{5.34}$$

This term vanishes if the Lewis numbers of all species can be assumed equal to unity. This is an interesting approximation because it leads to the following form of the enthalpy equation

$$\rho \frac{Dh}{Dt} = \frac{Dp}{Dt} + \operatorname{div} \left(\frac{\lambda}{c_p} \operatorname{grad} h \right) . \tag{5.35}$$

If furthermore the pressure is constant as it is approximately the case in all applications except in reciprocating engines, the enthalpy equation would be very much simplified. The assumption of unity Lewis numbers for all species is not justified in many combustion applications. In fact, deviations from that assumption lead to a number of interesting phenomena that have been studied recently in the context of flame stability and the response

of flames to external disturbances. We will address these questions in some of the lectures below.

Another important form of the energy equation is that in terms of the temperature. With (5.31) and (5.11) the total derivative of the enthalpy can be written as

$$\rho \frac{Dh}{Dt} = \rho c_p \frac{DT}{Dt} + \sum_{i=1}^{n} (-\operatorname{div} \vec{j}_i + \dot{m}_i) h_i \,. \tag{5.36}$$

Then with (5.30), the enthalpy equation (5.24) without the second last term yields the temperature equation

$$\rho c_p \frac{DT}{Dt} = \frac{Dp}{Dt} + \operatorname{div}(\lambda \operatorname{grad} T) - \sum_{i=1}^{n} c_{pi} \vec{j}_i \operatorname{grad} T - \sum_{i=1}^{n} h_i \dot{m}_i + q_R \,. \tag{5.37}$$

Here the last term describes the temperature change due to chemical reactions. It may be written as

$$-\sum_{i=1}^{n} h_i \dot{m}_i = -\sum_{k=1}^{r} \sum_{i=1}^{n} \nu_{ik} W_i h_i w_k = \sum_{k=1}^{r} Q_k w_k \tag{5.38}$$

where definition (2.7) has been used for each reaction. The second term on the right hand side may be neglected, if one assumes that all specific heats c_{pi} are equal. This assumption is very often justified since this term does not contribute as much to the change of temperature as the other terms in the equation, in particular the chemical source term. If one also assumes that spatial gradients of c_p may be neglected for the same reason, the temperature equation takes the form

$$\rho \frac{DT}{Dt} = \frac{1}{c_p} \frac{Dp}{Dt} + \operatorname{div} \left(\frac{\lambda}{c_p} \operatorname{grad} T \right) + \sum_{k=1}^{r} \frac{Q_k}{c_p} w_k + \frac{q_R}{c_p} \,. \tag{5.39}$$

For a constant pressure it is very similar to (5.10) with an effective diffusion coefficient for all reactive species and a spatially constant Lewis number Le_i may be written as

$$\rho \frac{DY_i}{Dt} = \frac{1}{\mathrm{Le}_i} \operatorname{div} \left(\frac{\lambda}{c_p} \operatorname{grad} Y_i \right) + W_i \sum_{k=1}^{r} \nu_{ik} w_k \,. \tag{5.40}$$

For unity Lewis numbers this and the temperature equation are easily combined to obtain the enthalpy equation (5.35). Since the use of (5.39) and (5.40) does not require the unity Lewis number assumption, this formulation is often used when non-unity Lewis number effects are to be analyzed. For flame calculations a sufficiently accurate approximation for the transport properties is [5.2]

$$\frac{\lambda}{c_p} = 2.58 \cdot 10^{-4} \frac{\mathrm{g}}{\mathrm{cm\,sec}} \left(\frac{T}{298\mathrm{K}} \right)^{0.7} \,, \tag{5.41}$$

a constant Prandtl number

$$\mathrm{Pr} = \frac{\mu c_p}{\lambda} = 0.75\,, \tag{5.42}$$

and constant Lewis numbers. For a number of species occurring in methane-air flames approximate values from [5.2] are listed in Table 5.1. A first approximation for other hydrocarbon species can be based on the assumption that the binary diffusion coefficients of species i with respect to nitrogen is approximately proportional to

$$D_i \sim \left(\frac{W_i + W_{\mathrm{N}_2}}{2W_i W_{\mathrm{N}_2}}\right)^{1/2}\,. \tag{5.43}$$

Then the ratio of its Lewis number to that of methane is

$$\frac{\mathrm{Le}_i}{\mathrm{Le}_{\mathrm{CH}_4}} = \left(\frac{W_i}{W_{\mathrm{CH}_4}}\,\frac{W_{\mathrm{CH}_4} + W_{\mathrm{N}_2}}{W_i + W_{\mathrm{N}_2}}\right)^{1/2}\,. \tag{5.44}$$

CH_4	O_2	H_2O	CO_2	H	O	OH	HO_2
0.97	1.11	0.83	1.39	0.18	0.70	0.73	1.10

H_2	CO	H_2O_2	HCO	CH_2O	CH_3	CH_3O
0.3	1.10	1.12	1.27	1.28	1.00	1.30

Table 5.1: Lewis numbers of some reacting species occurring in methane-air flames

5.3 Balance Equations for Element Mass Fractions

Summation of the balance equations for the mass fractions (5.11) according to (1.10) leads to the balance equations for Z_j

$$\rho\frac{DZ_j}{Dt} = -\,\mathrm{div}\sum_{i=1}^{n}\frac{a_{ij}W_j}{W_i}\vec{j}_i\,. \tag{5.45}$$

Here the summation over the chemical source terms vanishes

$$W_j\sum_{i=1}^{n}\sum_{k=1}^{r}a_{ij}\nu_{ik}w_k = W_j\sum_{k=1}^{r}w_k\sum_{i=1}^{n}a_{ij}\nu_{ik} = 0$$

since the last sum vanishes for each reaction. The diffusion term simplifies if one assumes that the diffusion coefficients of a species are equal. If one further more assumes a unity Lewis number this leads to

$$\rho\frac{DZ_j}{Dt} = \mathrm{div}\left(\frac{\lambda}{c_p}\,\mathrm{grad}\,Z_j\right)\,. \tag{5.47}$$

A similar equation may be derived for the mixture fraction Z. Since Z is defined according to (1.32) as the mass fraction of the fuel stream, it represents the sum of element mass fractions contained in the fuel stream. The mass fraction of the fuel is the sum of the element mass fractions

$$Y_{F,u} = \sum_{j=1}^{n_e} Z_{j,F} \tag{5.48}$$

where

$$Z_{j,F} = a_{F,j} \frac{W_j}{W_F} Y_{F,u} \,. \tag{5.49}$$

With (1.33) the mixture fraction may therefore be expressed as a sum of element mass fractions

$$Z = \frac{\sum_{j=1}^{n_e} Z_{j,F}}{Y_{F,1}} \,. \tag{5.50}$$

Then, with the assumption of unit Lewis numbers, a summation over (5.47) leads to a balance equation for the mixture fraction

$$\rho \frac{DZ}{Dt} = \operatorname{div}\left(\frac{\lambda}{c_p} \operatorname{grad} Z\right) \,. \tag{5.51}$$

For a one-step reaction with the reaction rate w this equation can also be derived using (1.35) and (5.40) for Y_F and Y_{O_2} with $\mathrm{Le}_F = L_{\mathrm{O}_2} = 1$ as

$$\begin{aligned} \rho \frac{DY_F}{Dt} &= \operatorname{div}\left(\frac{\lambda}{c_p} \operatorname{grad} Y_F\right) - \nu'_F W_F w \\ \rho \frac{DY_{\mathrm{O}_2}}{Dt} &= \operatorname{div}\left(\frac{\lambda}{c_p} \operatorname{grad} Y_{\mathrm{O}_2}\right) - \nu'_{\mathrm{O}_2} W_{\mathrm{O}_2} w \,. \end{aligned} \tag{5.52}$$

Dividing the first of these by $\nu'_{\mathrm{O}_2} W_{\mathrm{O}_2}$ and subtracting yields a source-free balance equation for the combination

$$\frac{Y_F}{\nu'_F W_F} = \frac{Y_{\mathrm{O}_2}}{\nu'_{\mathrm{O}_2} W_{\mathrm{O}_2}} \tag{5.53}$$

which is a linear function of Z according to (1.35). This leads again to (5.51). For constant pressure the enthalpy equation (5.35) has the same form as (5.51) and a coupling relation between the enthalpy and the mixture fraction may be derived

$$h = h_2 + Z(h_1 - h_2) \tag{5.54}$$

where h_1 is the enthalpy of the fuel stream and h_2 that of the oxidizer stream. Similarly, using (5.47) and (5.51) the element mass fractions may be expressed in terms of the mixture fraction

$$Z_j = Z_{j,2} + Z(Z_{j,1} - Z_{j,2}) \tag{5.55}$$

where $Z_{j,1}$ and $Z_{j,2}$ are the element mass fractions in the fuel and oxidizer stream, respectively. It should be noted that the coupling relations (5.54) and (5.55) required a two feed

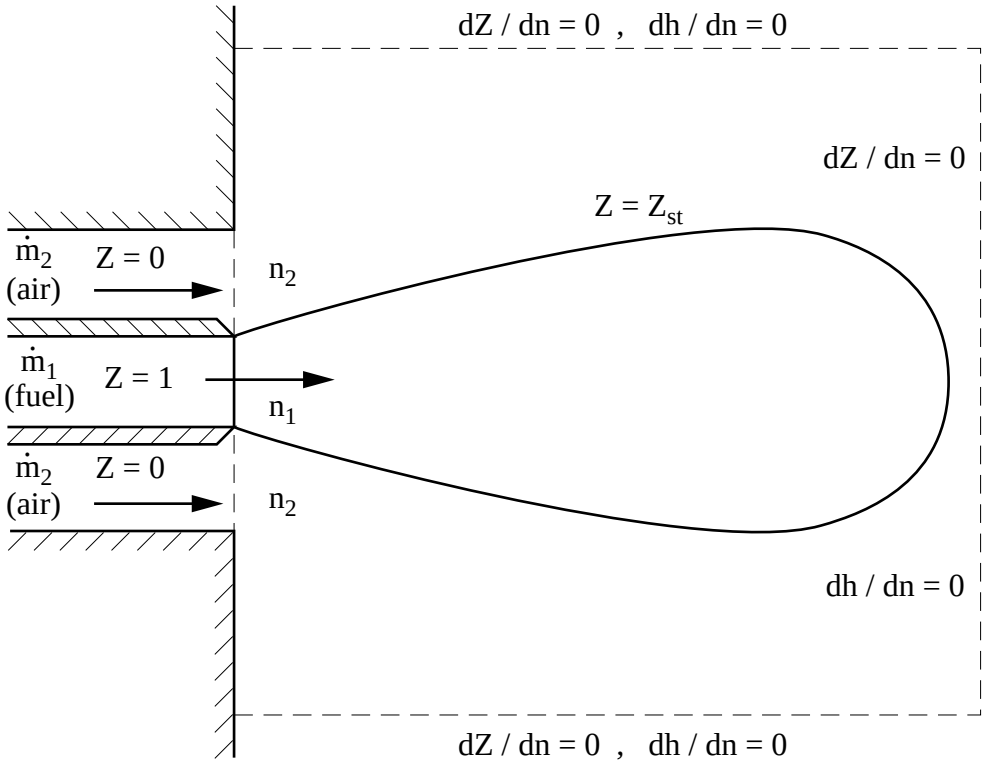

Fig. 5.2: Coflow diffusion flame

system with equivalent boundary conditions for the enthalpy and the mass fractions. A practical example is a single jet as fuel stream with co-flowing air as oxidizer stream into an open atmosphere, such that zero gradient boundary conditions apply everywhere except at the input streams as shown in Fig. 5.2. Once the mixture fraction field has been obtained by numerical solution of (5.51) the adiabatic flame temperature may be calculated using the methods of lecture 2 as a local function of Z.

References

[5.1] Hirschfelder, J.O., Curtiss, C.F. and Bird, R.B., "Molecular Theory of Gases and Liquids", Wiley New York 1954.

[5.2] Smooke, M.D. and Giovangigli, V., "Reduced Kinetic Mechanisms and Asymptotic Approximation for Methane-Air Flames", Lecture Notes in Physics **384**, p. 29, Springer-Verlag Berlin 1992.

Lecture 6: Laminar Premixed Flames: Burning Velocities and One-step Asymptotics

6.1 The Laminar Burning Velocity

The classical device to generate a laminar premixed flame is the Bunsen burner shown in Fig. 6.1. Gaseous fuel from the fuel supply enters through an orifice into the mixing chamber, into which air is entrained through adjustable openings from the outside. The cross sectional area of the fuel orifice may be adjusted by moving the needle through an adjustment screw into the orifice. Thereby the velocity of the jet entering into the mixing chamber may be varied and the entrainment of the air and the mixing can be optimized. The mixing chamber must be long enough to generate a premixed gas issuing from the Bunsen tube into the surroundings. If the velocity of the issuing flow is larger than the laminar burning velocity to be defined below, a Bunsen flame cone establishes itself at the top of the tube. It represents a steady premixed flame propagating normal to itself with the burning velocity s_L into the unburnt mixture.

The kinematic balance of this process is illustrated for a steady oblique flame in Fig. 6.2. The oncoming flow velocity vector v_u of the unburnt mixture (subscript u) is split into a component $v_{t,u}$ which is tangential to the flame and into a component $v_{n,u}$ normal to the flame front. Due to thermal expansion within the flame front the normal velocity component is increased, since the mass flow ρv through the flame must be the same in the unburnt mixture and in the burnt gas (subscript b)

$$(\rho v_n)_u = (\rho v_n)_b \,, \tag{6.1}$$

therefore

$$v_{n,b} = v_{n,u} \frac{\rho_u}{\rho_b} \,. \tag{6.2}$$

The tangential velocity component v_t is not affected by the gas expansion and remains the same

$$v_{t,b} = v_{t,u} \,. \tag{6.4}$$

Vector addition of the velocity components in the burnt gas in Fig. 6.2 then leads to $\vec{v}_b$ which points into a direction which is deflected from the flow direction of the unburnt mixture. Finally, since the flame front is stationary in this experiment, the burning velocity $s_{L,u}$ with respect to the unburnt mixture must be equal to the flow velocity of the unburnt mixture normal to the front.

$$s_{L,u} = v_{n,u} \tag{6.5}$$

With the Bunsen flame cone angle in Fig. 6.1 denoted by α the normal velocity is $v_{n,u} = v_u \cdot \sin\alpha$ and it follows

$$s_{L,u} = v_u \sin\alpha \,. \tag{6.6}$$

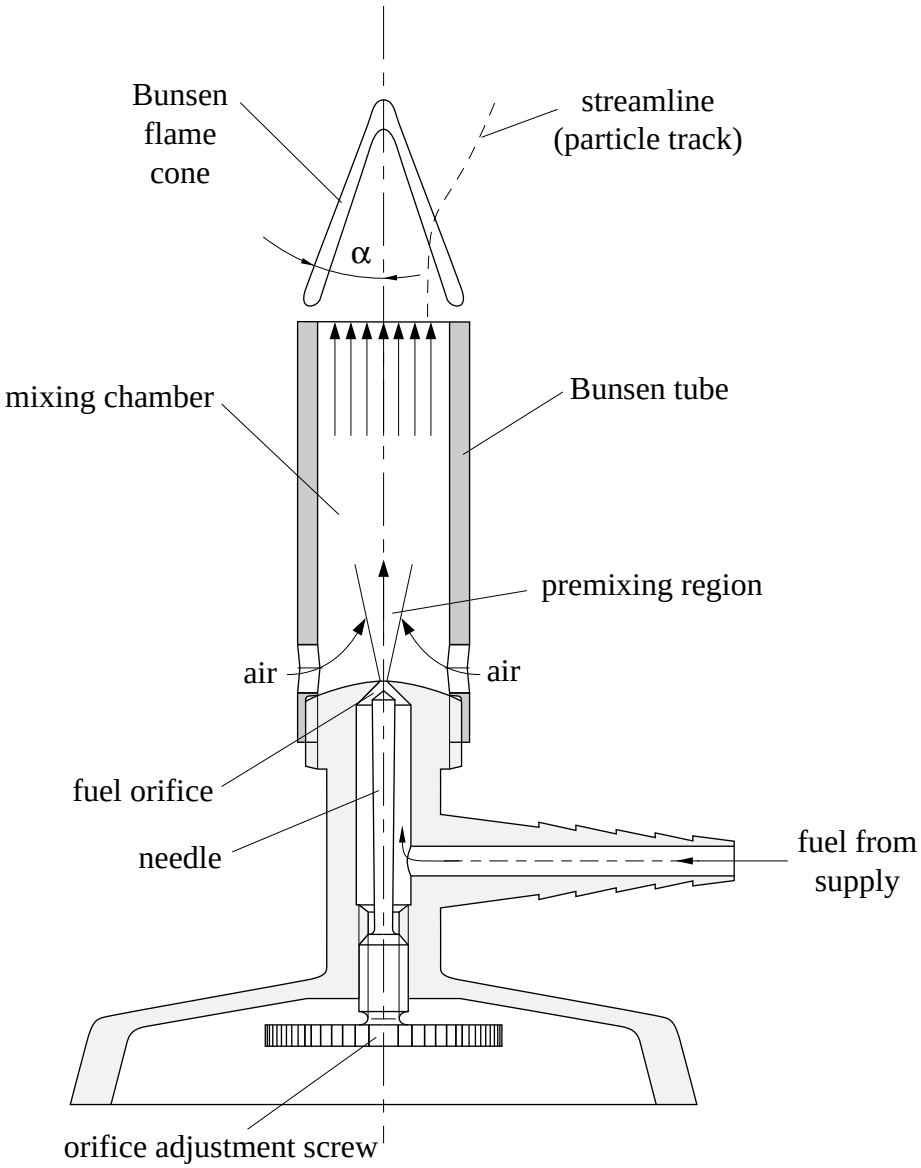

Fig. 6.1: The Bunsen burner

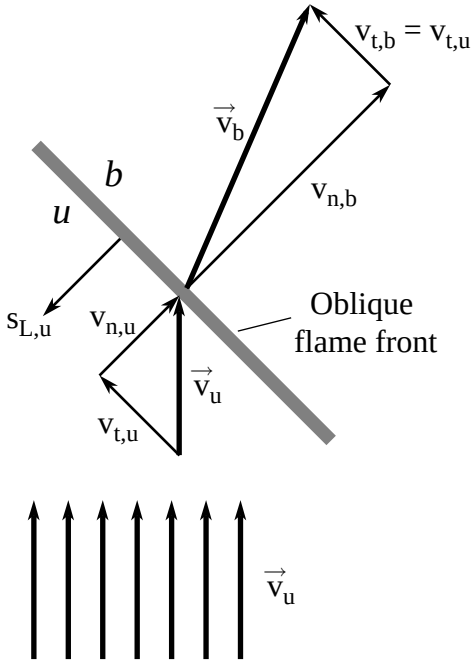

Fig. 6.2: Kinematic balance for a steady oblique flame

This allows to experimentally determine the burning velocity by measuring the cone angle α under the condition that the flow velocity v_u is uniform across the tube exit. If this is not the case the flame angle also varies with radial distance, since the burning velocity $s_{L,u}$ is essentially constant.

A particular phenomenon occurs at the flame tip. If the tip is closed, which is in general the case for hydrocarbon flames (but not necessarily for lean hydrogen flames) the burning velocity at the tip, being normal and therefore equal to the flow velocity, is by a factor $1/\sin\alpha$ larger than the burning velocity through the oblique part of the cone. This will be explained in Lecture 8 by the strong curvature of the flame front at the tip leading to a preheating by the lateral parts of the flame front and thereby to an increase in burning velocity. This analysis also includes the effect of non-unity Lewis numbers by which, for instance, the difference between lean hydrogen and lean hydrocarbon flames can be explained. Finally, it is shown in Fig. 6.1 that the flame is detached form the rim of the burner. This is due to conductive heat loss to the burner which leads in regions very close to the rim to temperatures, at which combustion cannot be sustained.

Another example for an experimental device to measure laminar burning velocities is the combustion bomb (Fig. 6.3) within which a flame is initiated by a central spark. Spherical propagation of a flame then takes place which may optically be detected through quartz windows and the flame propagation velocity $\mathrm{d}r_f/\mathrm{d}t$ may be recorded. Now the flame front is not stationary. If the radial flow velocities are defined positive in inward direction, the velocity of the front must be substracted from these in the mass flow balance

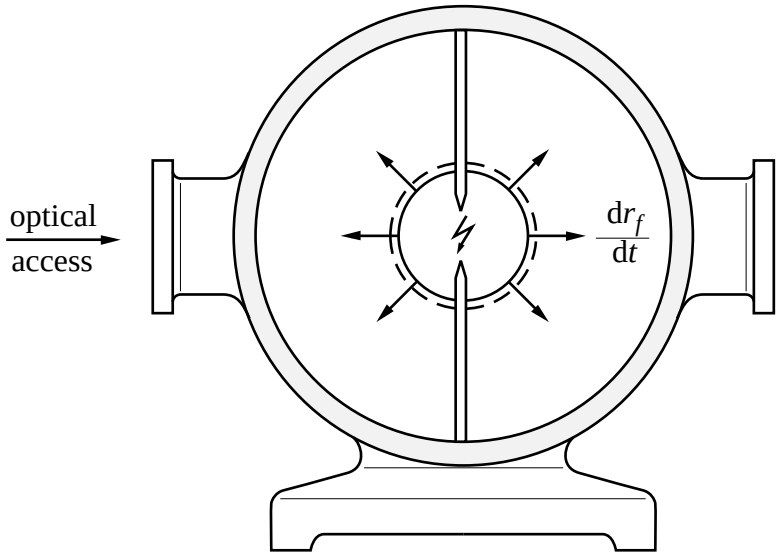

Fig. 6.3: Laminar spherical flame propagation in a combustion bomb

through the flame front

$$\rho_u \left(v_u - \frac{\mathrm{d}r_f}{\mathrm{d}t} \right) = \rho_b \left(v_b - \frac{\mathrm{d}r_f}{\mathrm{d}t} \right) \tag{6.7}$$

At the flame front the kinematic balance between propagation velocity, flow velocity and burning velocity with respect to the unburnt mixture is

$$\frac{\mathrm{d}r_f}{\mathrm{d}t} = v_u + s_{L,u} \,. \tag{6.8}$$

Similarly, the kinematic balance with respect to the burnt gas is

$$\frac{\mathrm{d}r_f}{\mathrm{d}t} = v_b + s_{L,b} \,. \tag{6.9}$$

In the present example the flow velocity v_b in the burnt gas behind the flame is zero due to symmetry. This leads with (6.7) and (6.8) to

$$\frac{\mathrm{d}r_f}{\mathrm{d}t} = \frac{\rho_u}{\rho_u - \rho_b} v_u = v_u + s_{L,u} \tag{6.10}$$

from which the velocity in the unburnt mixture is calculated as

$$v_u = \frac{\rho_u - \rho_b}{\rho_b} s_{L,u} \tag{6.11}$$

This velocity is induced by the expansion of the gas behind the flame front. Furthermore it follows that the flame propagation velocity is related to the burning velocity $s_{L,u}$ by

$$\frac{\mathrm{d}r_f}{\mathrm{d}t} = \frac{\rho_u}{\rho_b} s_{L,u} \tag{6.12}$$

Measuring the flame propagation velocity $\mathrm{d}r_f/\mathrm{d}t$ then allows to determine $s_{L,u}$. Furthermore, from (6.9) it follows with $v_b = 0$ that

$$\frac{\mathrm{d}r_f}{\mathrm{d}t} = s_{L,b}\,. \tag{6.13}$$

The comparison of (6.12) and (6.13) shows that the burning velocity with respect to the burnt gas is by a factor ρ_u/ρ_b larger than that with respect to the unburnt gas. This is equivalent to (6.2).

For convenience we will denote in the following the burning velocity with respect to the unburnt gas by s_L

$$s_L \equiv s_{L,u}\,. \tag{6.14}$$

while we keep the notation $s_{L,b}$ for the burning velocity with respect to the burnt gas.

6.2 Governing Equations for Steady Premixed Flames, Numerical Calculations and Experimental Data

Let us consider a planar steady state flame configuration normal to the x-direction with the unburnt mixture at $x \to -\infty$ and the burnt gas at $x \to +\infty$.

The flame structure is schematically shown in Fig. 6.4 for the case of a lean flame with a one-step reaction.

$$\nu'_F F + \nu'_{\mathrm{O}_2}\mathrm{O}_2 \to \nu''_P P\,. \tag{6.19}$$

The fuel and oxidizer are convected from upstream with the burning velocity s_L having the mass fractions $Y_{F,u}$ and $Y_{\mathrm{O}_2,u}$ at $x \to -\infty$ and diffuse into the reaction zone. Here the fuel is entirely depleted while the remaining oxygen is convected downstream where it has the mass fraction $Y_{\mathrm{O}_2,b}$. The chemical reaction forms the product P and releases heat which leads to a temperature rise. The mass fraction Y_P increases therefore in a similar way from zero to $Y_{P,b}$ as the temperature from T_u to T_b. The product diffuses upstream, and mixes with the fuel and the oxidizer. Heat conduction from the reaction zone is also directed upstream leading to a preheating of the fuel/air mixture. Therefore the region upstream of the reaction zone is called the preheat zone

We will now consider the general as with multi-step chemical kinetics. The fundamental property of a premixed flame, the burning velocity s_L may be calculated by solving the governing conservation equations for the overall mass, species and temperature

Continuity

$$\frac{\mathrm{d}(\rho u)}{\mathrm{d}x} = 0\,, \tag{6.15}$$

Species

$$\rho u\frac{\mathrm{d}Y_i}{\mathrm{d}x} = -\frac{\mathrm{d}j_i}{\mathrm{d}x} + \dot{m}_i\,, \tag{6.16}$$

Energy

$$\rho u c_p\frac{\mathrm{d}T}{\mathrm{d}x} = \frac{\mathrm{d}}{\mathrm{d}x}(\lambda\frac{\mathrm{d}T}{\mathrm{d}x}) - \sum_{i=1}^{n} h_i\dot{m}_i - \sum_{i=1}^{n} c_p j_i\frac{\mathrm{d}T}{\mathrm{d}x} + \frac{\partial p}{\partial t}\,. \tag{6.17}$$

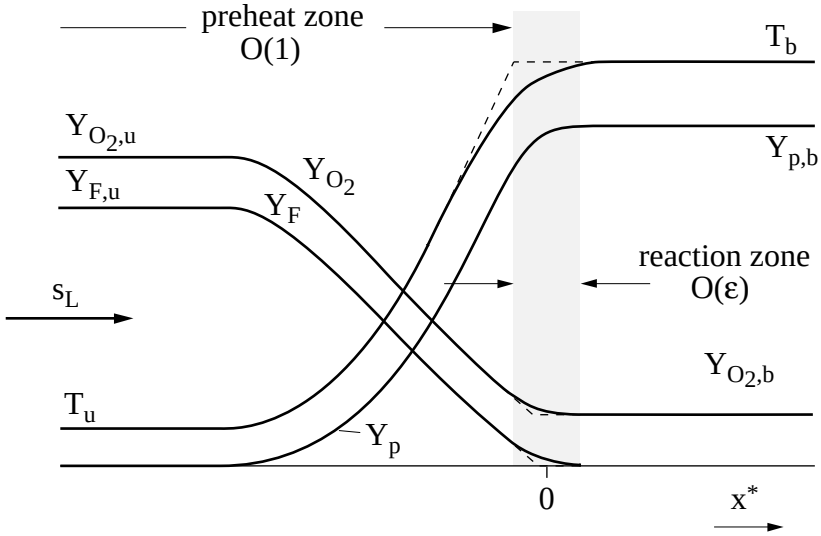

Fig. 6.4: Flame structure of a lean flame with one-step asymptotics

The continuity equation may be integrated once to yield

$$\rho u = \rho_u s_L \,, \tag{6.18}$$

where the subscript u denotes conditions in the fresh, unburnt mixture, and where s_L denotes the burning velocity. The latter is an eigenvalue, which must be determined as part of the solution. For flame propagation with burning velocities much smaller than the velocity of sound, the pressure is spatially constant and is determined from the thermal equation of state. Therefore spatial pressure gradients are neglected in (6.17) while temporal pressure gradients have been retained.

The system of equations (6.16)–(6.18) may be solved numerically with the appropriate upstream boundary conditions for the mass fractions and the temperature and zero gradient boundary conditions downstream. As an example taken from [6.1] calculations of the burning velocity of premixed methane-air flames using a mechanism that contains only C_1-hydrocarbons and a mechanism that includes the C_2-species are shown in Fig. 6.5 as a function of the equivalence ratio Φ. The two curves are compared with compilations of various data from the literature. It is seen that the calculations with the C_2-mechanism shows a better agreement than the C_1-mechanism. As an other example burning velocities of propane flames taken from [6.4] are shown in Fig. 6.6.

6.3 Premixed Flames Based on One-step Asymptotics

A classical example of an asymptotic description of the structure of a premixed flame is due to Zeldovich and Frank-Kamenetzki in 1938. It is known as the thermal flame theory and considers the single one-step reaction (6.19)

We will assume that reaction rate is first order with respect to fuel and to oxygen

$$w = B \frac{\rho Y_F}{W_F} \frac{\rho Y_{\mathrm{O}_2}}{W_{\mathrm{O}_2}} \exp\left(\frac{-E}{\mathcal{R}T}\right) \tag{6.20}$$

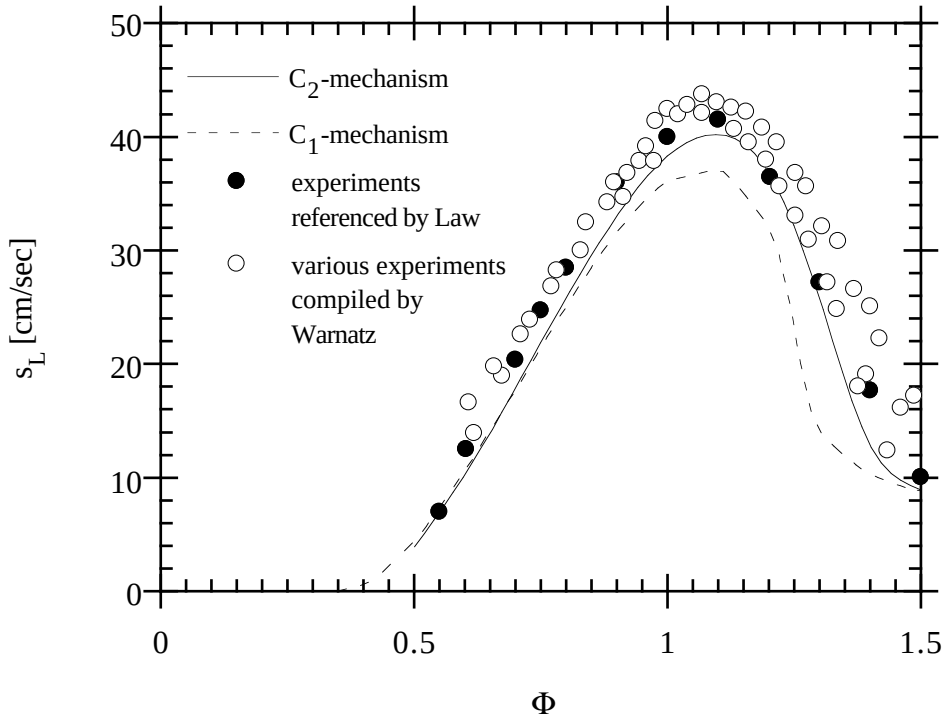

Fig. 6.5: Burning velocities calculated with a starting C_1-mechanism and a starting C_2-mechanism, several data compiled by Warnatz [6.2], and recent data referenced by Law [6.3] for atmospheric methane-air-flames

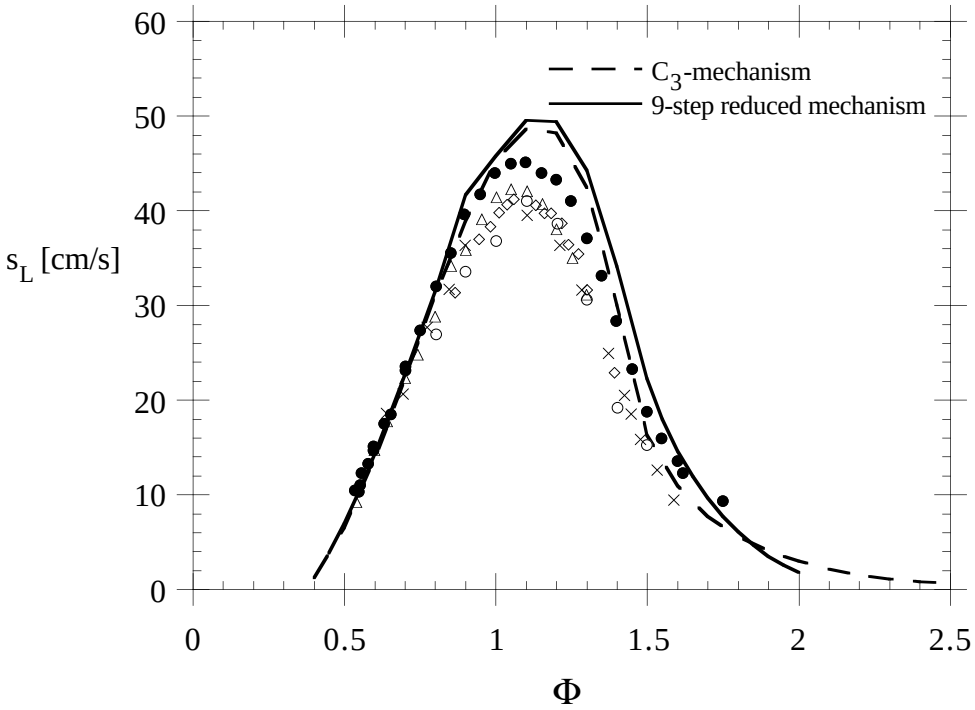

Fig. 6.6: Burning velocity of propane-air flames vs. equivalence ratio Φ obtained with an elementary mechanism containing only species up to C_3 hydrocarbons from Table 3.1 and a reduced 9-step mechanism and from experimental results (◯: Metghalchi et al, [6.5], ×: Smith et al., [6.6], ◇: Scholte et al., [6.7], △: Yamaoka et al., [6.8], •: C.K. Law, [6.3])

Alternative forms, in particular a rate which is first order with respect to the fuel only, may also be considered. We will show that this case will be contained as a limit for extremely lean flames in the expression above. The most important feature in (6.20) is the Arrhenius type temperature dependence where the activation energy E is assumed to be large. Both the activation energy and the frequency factor B are adjustable parameters and cannot be deduced from elementary kinetic data. The one-step model has widely been used in descriptions of flame stability where it essentially serves as model that produces a thin flame with a strong temperature sensitivity. In this lecture we will derive an explicit expression for the burning velocity. This is to be compared in lecture 7 to results derived from a four-step reduced mechanism for methane-air flames.

The flame structure was already shown schematically in Fig. 6.4. Since the reaction is assumed to be irreversible, the reaction rate must vanish in the burnt gas. Therefore one of the reactants must be entirely depleted: the fuel in the case of lean flames, the oxidizer for rich flames and both for stoichiometric flames. This leads to the condition in the burnt gas

$$Y_{F,b} \cdot Y_{\mathrm{O}_2,b} = 0\,. \tag{6.21}$$

The combustion of the reactants in the reaction zone leads to an increase in temperature and therefore an increase of the reaction rate. In the asymptotic analysis to be developed, the large temperature dependence of the reaction rate, expressed by the large activation energy will play a crucial role.

Let us assume at first that (5.28) for the diffusion flux can be employed and that the Lewis number is unity. Then, using $\rho u = \rho_u s_L$ the species balance equation (5.40) is for the mass fractions of fuel and oxygen

$$\begin{aligned} \rho_u s_L \frac{\mathrm{d}Y_F}{\mathrm{d}x} &= \frac{\mathrm{d}}{\mathrm{d}x}\left(\frac{\lambda}{c_p}\frac{\mathrm{d}Y_F}{\mathrm{d}x}\right) - \nu'_F W_F w \\ \rho_u s_L \frac{\mathrm{d}Y_{\mathrm{O}_2}}{\mathrm{d}x} &= \frac{\mathrm{d}}{\mathrm{d}x}\left(\frac{\lambda}{c_p}\frac{\mathrm{d}Y_{\mathrm{O}_2}}{\mathrm{d}x}\right) - \nu'_{\mathrm{O}_2} W_{\mathrm{O}_2} w \end{aligned}\,. \tag{6.22}$$

These can be combined with the temperature equation (5.39) in the form

$$\rho_u s_L \frac{\mathrm{d}T}{\mathrm{d}x} = \frac{\mathrm{d}}{\mathrm{d}x}\left(\frac{\lambda}{c_p}\frac{\mathrm{d}T}{\mathrm{d}x}\right) + \frac{Q}{c_p} w\,. \tag{6.23}$$

This leads to algebraic coupling relations between the mass fractions and the temperature which may be integrated from the burnt state to any state within the flame as

$$\begin{aligned} Y_F &= -\frac{\nu'_F W_F c_p}{Q}(T - T_b) + Y_{F,b} \\ Y_{\mathrm{O}_2} &= -\frac{\nu'_{\mathrm{O}_2} W_{\mathrm{O}_2} c_p}{Q}(T - T_b) + Y_{\mathrm{O}_2,b}\,. \end{aligned} \tag{6.24}$$

Here Q and c_p have been assumed constant for simplicity. With (6.24) the reaction rate is a function of temperature and only (6.23) needs to be considered in the following.

We will now introduce the non-dimensional coordinate

$$x^* = \rho_u s_L \int_0^x \frac{c_p}{\lambda}\, dx \tag{6.25}$$

and a non-dimensional temperature

$$T^* = \frac{T - T_u}{T_b - T_u} \tag{6.26}$$

where $T_b - T_u$ is given by (2.9) or by (2.11) for lean or rich flames, respectively. Then the nondimensional reaction rate takes the form

$$w^* = \frac{\lambda Q}{\rho_u^2 s_L^2 c_p^2 (T_b - T_u)} w(T) \tag{6.27}$$

and the temperature equation may be written (with the asterisks removed)

$$\frac{\mathrm{d}T^*}{\mathrm{d}x^*} = \frac{\mathrm{d}^2 T^*}{\mathrm{d}x^{*\,2}} + w^*\,, \tag{6.28}$$

subject to the boundary condition

$$T^* = 0 \quad \text{at} \quad x^* \to -\infty, \quad T^* = 1 \quad \text{at} \quad x^* \to \infty\,. \tag{6.29}$$

Since the temperature decreases towards the unburnt mixture and the activation energy is large, there is only a small region where the reaction rate is close to its maximum value. Only in a thin region the reaction rate is non-negligible and it is therefore called the reaction zone. Its thickness is of order $\mathrm{O}(\varepsilon)$ in terms of the non-dimensional coordinate x^*, where ε is a smaller parameter to be determined during the analysis.

In order to analyze the flame structure in the reaction zone, we introduce a stretched coordinate

$$\zeta = \frac{x^*}{\varepsilon} \tag{6.30}$$

and expand the temperature around its maximum value as

$$T^* = 1 - \varepsilon y\,. \tag{6.31}$$

Similarly, the mass fractions and ρ as well as λ may be expanded to first order as

$$\begin{aligned}
Y_F &= Y_{F,b} + \varepsilon \frac{c_p (T_b - T_u) \nu_F' W_F}{Q} y\,, \\
Y_{\mathrm{O}} &= Y_{\mathrm{O},b} + \varepsilon \frac{c_p (T_b - T_u) \nu_{\mathrm{O}_2}' W_{\mathrm{O}_2}}{Q} y\,, \\
\rho &= \rho_b - \varepsilon (T_b - T_u) \left.\frac{\partial \rho}{\partial T}\right|_b y\,, \\
\lambda &= \lambda_b - \varepsilon (T_b - T_u) \left.\frac{\partial \lambda}{\partial T}\right|_b y\,.
\end{aligned} \tag{6.32}$$

With the dimensional temperature $T = T_u + T^*(T_b - T_u)$ the expansion of the exponential term to first order is

$$\begin{aligned} \exp\left(-\frac{E}{\mathcal{R}T}\right) &= \exp\left(\frac{-E/\mathcal{R}}{T_b - (T_b - T_u)\varepsilon y}\right) \\ &= \exp\left(-\frac{E}{\mathcal{R}T_b}\right) \exp\left(-\varepsilon \frac{E(T_b - T_u)}{\mathcal{R}T_b^2} y\right) . \end{aligned} \tag{6.33}$$

This suggests the following definition of ε

$$\varepsilon = \frac{\mathcal{R}T_b^2}{E(T_b - T_u)} \tag{6.34}$$

which is therefore the inverse of a non-dimensional activation energy. The quantity

$$\mathrm{Ze} = \frac{E(T_b - T_u)}{\mathcal{R}T_b^2} \tag{6.35}$$

will be called the Zeldovich number. Introducing (6.32)–(6.34) into the non-dimensional reaction rate leads to

$$w = \mathrm{Da}\, \varepsilon (y + by^2) \exp(-y) . \tag{6.36}$$

Here Da is the Damköhler number

$$\mathrm{Da} = \frac{B\rho_b^2 \lambda_b}{(\rho v)_u^2} \frac{\left(Y_{\mathrm{O}_2,b} \nu'_F W_F + Y_{F,b} \nu'_{\mathrm{O}_2} W_{\mathrm{O}_2}\right)}{W_F W_{\mathrm{O}_2}} \exp\left(-\frac{E}{RT_b}\right) , \tag{6.37}$$

and

$$b = \frac{\varepsilon c_p (T_b - T_u) \nu'_F \nu'_{\mathrm{O}_2} W_F W_{\mathrm{O}_2}}{\left(Y_{F,b} \nu'_{\mathrm{O}_2} W_{\mathrm{O}_2} + Y_{\mathrm{O}_2,b} \nu'_F W_F\right) Q} , \tag{6.38}$$

a grouping of quantities that will be discussed below. Introducing the expansion (6.30), (6.31) and (6.36) into the non-dimensional temperature equation one obtains to leading order

$$\frac{\mathrm{d}^2 y}{\mathrm{d}\zeta^2} = \Lambda (y + by^2) \exp(-y) . \tag{6.39}$$

Here the first order derivative of the temperature, which was the convective term, has been neglected as being small of order $\mathrm{O}(\varepsilon)$ compared to the second order derivative, the thermal diffusive term. In addition, the burning velocity eigenvalue

$$\Lambda = \varepsilon^2 \mathrm{Da} \tag{6.40}$$

has been introduced. This quantity must be of order $\mathrm{O}(1)$ if the reaction term is to balance the diffusive term in the reaction. This indicates that the Damköhler number must be large of order $\mathrm{O}(\varepsilon^{-2})$.

The boundary conditions of (6.39) must be obtained from matching conditions at the boundary to the preheat zone and towards the burnt gas area region. The latter leads simply to

$$y \to 0 \quad \text{for} \quad \zeta \to \infty \,. \tag{6.41}$$

According to the arguments given above the reaction rate in the preheat zone is exponentially small and can be neglected. This leads to the solution of (6.28) in the preheat zone

$$T^* = \exp x^* \,, \quad x^* < 0 \tag{6.42}$$

where the origin $x^* = 0$ was fixed at the thin reaction zone. Matching between this preheat zone and the reaction zone can be achieved by expanding the preheat zone temperature around $x^* = 0$ as

$$T^* = 1 + x^* \cdot \tag{6.43}$$

and realizing that the solution of (6.39) turns into a linear function as $\zeta \to -\infty$ where the reaction rate term on the r.h.s. vanishes. Therefore

$$y \to c_0 + c_1 \zeta \qquad \text{as} \quad \zeta \to -\infty \,. \tag{6.44}$$

Since the entire flame structure is translationally invariant, the origin of the ζ-coordinate may be shifted by introducing a new coordinate

$$\hat{\zeta} = \zeta + \frac{c_0}{c_1} \tag{6.45}$$

in terms of which (6.44) is $y = c_1 \hat{\zeta}$. Therefore the constant c_0 may be unambiguously set equal to zero.

Matching may formally be performed by introducing an intermediate coordinate

$$x_i = \frac{x}{k(\varepsilon)} = \frac{\varepsilon \zeta}{k(\varepsilon)} \tag{6.46}$$

where $k(\varepsilon) \to 0$ and $k(\varepsilon)/\varepsilon \to \infty$ as $\varepsilon \to 0$. Taking the limit of the difference between the two expansions (6.43) and (6.44) using (6.31) with the intermediate coordinate fixed

$$\lim_{\varepsilon \to 0} [1 + x - (1 - \varepsilon c_1 \zeta)] = \lim_{\varepsilon \to 0} [1 + k(\varepsilon) x_i - (1 - c_1 k(\varepsilon) x_i)] = 0 \tag{6.47}$$

shows that both solutions match to order $\mathrm{O}(k(\varepsilon))$ if

$$c_1 = -1 \,. \tag{6.48}$$

This leads to the second boundary condition for (6.39)

$$y \to -\zeta \qquad \text{for} \quad \zeta \to -\infty \,. \tag{6.49}$$

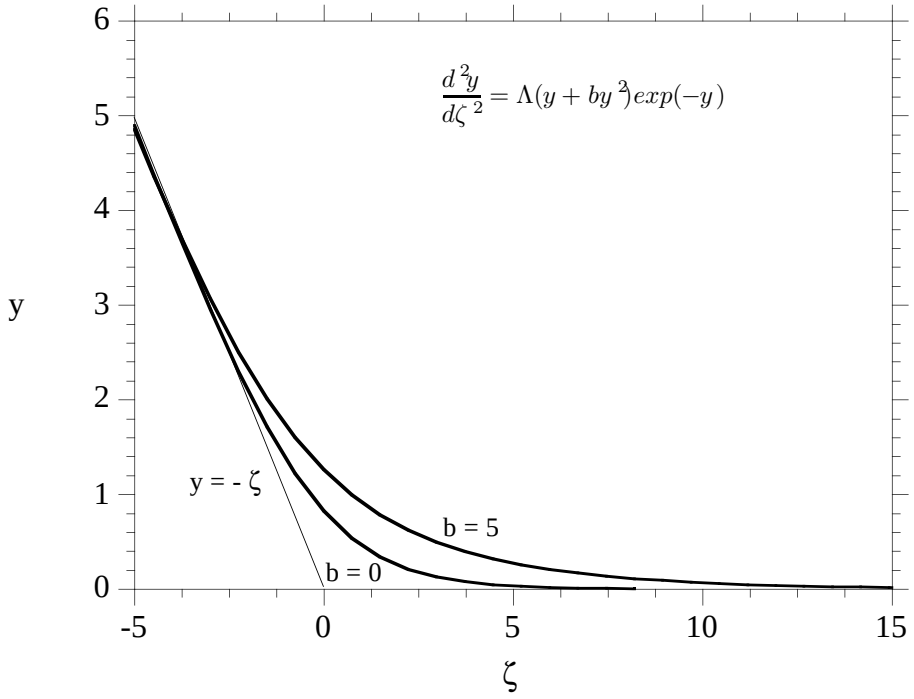

Fig. 6.7: Numerical solutions of (6.39) for $b = 0$ and $b = 5$.

Numerical solutions of (6.39) with (6.41) and (6.49) for $b = 0$ and $b = 5$ are shown in Fig. 6.7.

A first integral of (6.39) can be obtained by introducing the derivative $z = \mathrm{d}y/\mathrm{d}\zeta$ as a new dependent variable and y as the independent variable. Then, since

$$\frac{\mathrm{d}^2y}{\mathrm{d}\zeta^2} = \frac{\mathrm{d}z}{\mathrm{d}\zeta} = \frac{\mathrm{d}y}{\mathrm{d}\zeta}\frac{\mathrm{d}z}{\mathrm{d}y} = z\frac{\mathrm{d}z}{\mathrm{d}y} = \frac{1}{2}\frac{\mathrm{d}z^2}{\mathrm{d}y} \tag{6.50}$$

(6.39) may be written as

$$\frac{\mathrm{d}z^2}{\mathrm{d}y} = 2\Lambda\left(y + by^2\right)\exp\left(-y\right) \tag{6.51}$$

This may be integrated between $\zeta \to -\infty$ where $y \to \infty$, $z \to -1$ and $\zeta \to \infty$ where $y = 0$, $z = 0$ as

$$z^2(\infty) - z^2(-\infty) = 1 = 2\Lambda \int_{-\infty}^{0} (y + by^2)\exp(-y)\mathrm{d}y\,. \tag{6.52}$$

Evaluating the integral with its boundary conditions leads to the following solution for the burning velocity eigenvalue

$$2\Lambda(1 + 2b) = 1\,. \tag{6.53}$$

With (6.40), (6.37) and (6.38) and some algebraic manipulations this may be expressed in terms of physical quantities yielding the following expression for the laminar burning velocity

$$\rho_u s_L = \left(2\frac{B\rho_b\lambda_b R^2 T_b^4}{c_p(T_b - T_u)^2E^2}\exp\left(-\frac{E}{\mathcal{R}T_b}\right)A\right)^{1/2} \tag{6.54}$$

where

$$A = \rho_b \left(\frac{\nu'_F Y_{O_2,b}}{W_{O_2}} + \frac{\nu'_{O_2} Y_{F,b}}{W_F} + 2\,\frac{\nu'_{O_2}\nu'_F c_p \mathcal{R} T_b^2}{QE} \right) . \tag{6.55}$$

For sufficiently lean flames the first term in the quantity A dominates, while for sufficiently rich flames the second one dominates. In both cases the last term is small in the limit $E \to \infty$ which is equivalent to $b = 0$ in (6.39) since in (6.38) the quantity b vanishes for $\varepsilon \to 0$. In that case one obtains the equation

$$\frac{\mathrm{d}^2 y}{\mathrm{d}\zeta^2} = \Lambda y \exp(-y) \tag{6.56}$$

with the burning velocity eigenvalue from (6.53) as

$$\Lambda = 1/2\,. \tag{6.57}$$

It can easily be shown that a first order reaction rate of the form

$$w = B \frac{\rho Y_F}{W_F} \exp\left(-\frac{E}{\mathcal{R} T_b} \right) \tag{6.58}$$

would also lead to (6.56) and the burning velocity is in that case given by (6.54) with $A = \nu'_F$. Similar arguments would apply for rich flames.

In the case of stoichiometric flames both $Y_{F,b}$ and $Y_{O_2,b}$ vanish and b tends to infinity. In this case Λ must be rescaled as

$$\Lambda' = b\Lambda \tag{6.59}$$

and one obtains in the limit $b \to \infty$ instead of (6.39) the following equation

$$\frac{\mathrm{d}^2 y}{\mathrm{d}\zeta^2} = \Lambda' y^2 \exp(-y) \tag{6.60}$$

which leads to the eigenvalue

$$4\,\Lambda' = 4b\Lambda = 1 \tag{6.61}$$

as a limiting expression of (6.53). This corresponds to the case where the last term in (6.55) dominates.

6.4 The Influence of a Lewis Number Nonequal to Unity

We now want to analyze the influence of the Lewis number on the burning velocity eigenvalue. For simplicity we will consider a sufficiently lean flame with the reaction rate expression (6.58). Then, instead of the first of (6.22) we write the balance equation for the fuel mass fraction

$$\rho s_L \frac{\mathrm{d}Y_F}{\mathrm{d}x} = \frac{1}{\mathrm{Le}} \frac{\mathrm{d}}{\mathrm{d}x} \left(\frac{\lambda}{c_p} \frac{\mathrm{d}Y_F}{\mathrm{d}x} \right) - \nu'_F W_F w \tag{6.62}$$

where Le is the Lewis number of the fuel assumed to be constant. Equation (6.62) is now to be solved together with (6.23). Introducing the non-dimensional quantities defined in

(6.25) and (6.26) as before and the normalized fuel mass fraction $Y = Y_F/Y_{F,u}$ one obtains instead of (6.28) the set of equations

$$\begin{aligned} \frac{\mathrm{d}Y}{\mathrm{d}x} &= \frac{1}{\mathrm{Le}}\frac{\mathrm{d}^2Y}{\mathrm{d}x^{*\,2}} - w^* \\ \frac{\mathrm{d}T^*}{\mathrm{d}x^*} &= \frac{\mathrm{d}^2T^*}{\mathrm{d}x^{*\,2}} + w^* \,. \end{aligned} \tag{6.63}$$

Instead of (6.31) we now introduce in the reaction zone the expansions

$$T^* = 1 - \varepsilon z \,, \qquad Y = \varepsilon y \tag{6.64}$$

which leads instead of (6.56) to the system

$$\begin{aligned} \frac{1}{\mathrm{Le}}\frac{\mathrm{d}^2y}{\mathrm{d}\zeta^2} &= \Lambda y \exp(-z) \\ \frac{\mathrm{d}^2z}{\mathrm{d}\zeta^2} &= \Lambda y \exp(-z) \,. \end{aligned} \tag{6.65}$$

In the preheat zone the solution of (6.63) is with $w^* = 0$

$$T^* = \exp x^* \,, \qquad Y = 1 - \exp(\mathrm{Le}\, x^*) \tag{6.66}$$

which leads through matching to the following boundary conditions of (6.65)

$$\begin{aligned} z \to -\zeta \,, \quad y \to -\mathrm{Le}\,\zeta \qquad & \text{for} \quad \zeta \to -\infty \\ z = 0 \quad , \quad y = 0 \qquad\quad & \text{for} \quad \zeta \to +\infty \,. \end{aligned} \tag{6.67}$$

A solution that satisfies (6.65) and the boundary conditions (6.67) is the coupling relation

$$\frac{y}{\mathrm{Le}} = z \,. \tag{6.68}$$

Introducing this into the second of (6.65) leads to the temperature equation of the form

$$\frac{\mathrm{d}^2z}{\mathrm{d}\zeta^2} = \mathrm{Le}\Lambda z \exp(-z) \,. \tag{6.69}$$

A first integration of this equation yields now the burning velocity eigenvalue

$$\Lambda = \frac{1}{2\mathrm{Le}} \tag{6.70}$$

instead of (6.57). Since the burning velocity eigenvalue is inversely proportional to the square of the burning velocity this shows that the burning velocity increases with the square root of the Lewis number.

6.5 Flame Thickness and Flame Time of Laminar Premixed Flames

The laminar burning velocity s_L defines a velocity scale that can be used together with the thermal diffusivity $\lambda/\rho c_p$ to define a length and a time scale. Equation (6.54) may be rewritten as

$$s_L = \left(\frac{\lambda_b}{\rho_u c_p} \frac{1}{t_c} \right)^{1/2} \tag{6.71}$$

where a chemical time scale defined by

$$t_c = \frac{\rho_u c_p (T_b - T_u)^2 E^2}{2B\rho_b R^2 T_b^4 A} \exp\left(\frac{E}{\mathcal{R} T_b} \right) \tag{6.72}$$

is introduced. An expression for the flame thickness may be derived by considering (6.25). When x^* is set equal to unity in (6.25) and the corresponding spatial distance x equal to the flame thickness ℓ_F this leads to the definition

$$\ell_F = \frac{(\lambda/c_p)_{T_{\rm ref}}}{\rho_u s_L} \,. \tag{6.73}$$

Since in the one-step asymptotic model all properties relevant to the reaction rate are to be evaluated at the burnt gas temperature as reference temperature suggest that c_p/λ should also be evaluated at T_b. From this the time required for the flame to traverse its own thickness, called the flame time, may also be derived

$$t_F = \ell_F / s_L \,. \tag{6.74}$$

Comparing (6.71)–(6.73), it is seen that the flame time t_F is equal to t_c for a one-step flame. Therefore, it has the same physical significance as the chemical time.

The flame thickness defined by (6.73) is a measure of the width of the preheat zone of a premixed flame. For real flames the evaluation of the properties at T_b is not realistic. It will be shown in the next lecture that a quantity called the inner layer temperature T^0 is a more suitable as a reference temperature. Typical values of ℓ_F for atmospheric stoichiometric methane-air flames lie around 0.175 mm when $(\lambda/c_p)_{T_{\rm ref}}/\rho_u$ is estimated as $7 \times 10^{-5} \mathrm{m}^2/\mathrm{sec}$ and s_L as 0.4 m/s [6.4]. The corresponding flame time is 0.4375×10^{-3}sec. As the pressure p increases, the density increases linearly with pressure, whereas λ/c_p is independent of pressure for ideal gases. However, the burning velocity also changes with pressure. For hydrocarbon flames, the burning velocity decreases approximately as p^{-n}, where the exponent n is around 0.5 for methane flames. Therefore, the flame thickness varies with pressure as p^{n-1}.

References

[6.1] Mauss, F., Peters, N., Reduced Kinetic Mechanisms for Premixed Methane-Air Flames, in "Reduced Kinetic Mechanisms for Applications in Combustion Systems", Peters, N., and Rogg, B., editors, Lecture Notes in Physics, **m 15**, p. 58–75, Springer Verlag Berlin, 1993.

[6.2] Warnatz, J., Eighteenth Symposium (International) on Combustion, pp. 369 – 384, The Combustion Institute, 1981.

[6.3] Law, C.K., A Compilation of Recent Experimental Data of Premixed Laminar Flames, in Peters, N., and Rogg, B., editors, "Reduced Kinetic Mechanisms for Applications in Combustion Systems", Lecture Notes in Physics, **m 15**, p. 19 – 30, Springer Verlag Berlin, 1993.

[6.4] Kennel, C., Mauss, F., Peters, N., Reduced Kinetic Mechanisms for Premixed Propane-Air Flames, in "Reduced Kinetic Mechanisms for Applications in Combustion Systems", Peters, N., and Rogg, B., editors, Lecture Notes in Physics, **m 15**, p. 121–140, Springer Verlag Berlin, 1993.

[6.5] Metghalchi, M., Keck, J.C., Comb. Flame 38, 143, (1982).

[6.6] Smith, D.B., Taylor, S.C., Williams, A., Burning Velocities in Stretched Flames, Poster P220 presented at the Twenty-Second Symposium (International) on Combustion, 1988.

[6.7] Scholte, T.G., Vaags, P.B., Comb. Flame, 3, 495, (1959).

[6.8] Yamaoka, I. Tsuji, H., Twentieth Symposium (International) on Combustion, p. 1883, The Combustion Institute, 1985.

Lecture 7: Asymptotic Structure for Four-Step Premixed Methane Flames, Lean Flammability Limits

In the preceeding lecture we have developed an asymptotic description of premixed flames based on an assumed one-step reaction. This has provided a basic understanding of the flame structure when a large sensitivity to temperature was built into the model. There is no chemical basis for such a one-step assumption and the results must we regarded with caution when conclusions about dependence of the burning velocity on parameters effecting the chemistry, such as pressure and reactant concentrations, as well as flammability and extinction limits are concerned. While numerical calculations of full and reduced mechanisms are able to predict these flame properties, they contribute little to the understanding of the fundamental parameters that influence flame behaviour. Therefore there is a need to fill the gap between the numerical calculations based on reduced mechanisms with elementary kinetics and asymptotic analysis based on assumed chemistry models. An asymptotic description of stoichiometric methane-air flames [7.1], based on a four-step reduced mechanism derived in lecture 3, shall be presented in this lecture. Since the basic chemical parameters were retained, this mechanism has been quite successfull in describing the dependance of the burning velocity on pressure and preheat temperature. A similar asymptotic analysis as in [7.1] was also carried out for lean methane flames [7.2]. This description may, with some modifications, also serve as a model for other hydrocarbon flames. This will be shown by using analytical approximation [7.3] formulas that are based on the asymptotic description of methane flames for flames of C_2H_6, C_2H_4, C_2H_2 and C_3H_8 in air. Even lean flammability limits that cannot be adressed by the one-step formulation can be predicted by such a description.

7.1 The Four-Step Model for Methane-Air Flames

The four-step model for methane flames derived in Lecture 3 in (3.25) is

$$\begin{array}{lcl} \mathrm{I} & \mathrm{CH_4 + 2H + H_2O} & \rightleftharpoons \quad \mathrm{CO + 4H_2} \\ \mathrm{II} & \mathrm{CO + H_2O} & \rightleftharpoons \quad \mathrm{CO_2 + H_2} \\ \mathrm{III} & \mathrm{H + H + M} & \rightleftharpoons \quad \mathrm{H_2 + M} \\ \mathrm{IV} & \mathrm{O_2 + 3H_2} & \rightleftharpoons \quad \mathrm{2H + 2H_2O\,.} \end{array} \tag{7.1}$$

From the global rates (3.26) based on the elementary scheme given in Table 3.1 we will retain here only the principle rates

$$\begin{aligned} w_{\mathrm{I}} &= w_{11}\,, \quad w_{\mathrm{II}} = w_9 \\ w_{\mathrm{III}} &= w_5\,, \quad w_{\mathrm{IV}} = w_1 \end{aligned} \tag{7.2}$$

which correspond to the elementary reactions

$$\begin{array}{lcl} 11 & \mathrm{CH_4 + H} & \rightarrow \quad \mathrm{CH_3 + H_2} \\ 9 & \mathrm{CO + OH} & \rightleftharpoons \quad \mathrm{CO_2 + H} \\ 5 & \mathrm{H + O_2 + M} & \rightarrow \quad \mathrm{HO_2 + M} \\ 1 & \mathrm{H + O_2} & \rightleftharpoons \quad \mathrm{OH + O\,.} \end{array} \tag{7.3}$$

We neglect the influence of the other reactions here in order to make the algebraic description more tractable.

Since OH and O appear in this formulation as reactants we need to express them in terms of the species in the four-step mechanism by using the partial equilibrium assumption of reactions 2 and 3 in Table 3.1

$$\begin{aligned} [\mathrm{O}] &= \frac{[\mathrm{H}][\mathrm{OH}]}{K_2[\mathrm{H_2}]} \\ [\mathrm{OH}] &= \frac{[\mathrm{H_2O}][\mathrm{H}]}{K_3[\mathrm{H_2}]}\,. \end{aligned} \tag{7.4}$$

This leads to the following reaction rates of the global steps I–IV:

$$\begin{aligned} w_{\mathrm{I}} &= k_{38}[\mathrm{CH_4}][\mathrm{H}] \\ w_{\mathrm{II}} &= \frac{k_{18f}}{K_3}\frac{[\mathrm{H}]}{[\mathrm{H_2}]}\left\{[\mathrm{CO}][\mathrm{H_2O}] - \frac{1}{K_{\mathrm{II}}}[\mathrm{CO_2}][\mathrm{H_2}]\right\} \\ w_{\mathrm{III}} &= k_5[\mathrm{H}][\mathrm{O_2}][\mathrm{M}] \\ w_{\mathrm{IV}} &= k_1\frac{[\mathrm{H}]}{[\mathrm{H_2}]^3}\left\{[\mathrm{O_2}][\mathrm{H_2}]^3 - \frac{1}{K_{\mathrm{IV}}}[\mathrm{H_2}]^2[\mathrm{H_2O}]^2\right\}\,. \end{aligned} \tag{7.5}$$

which is explicit in terms of the concentrations of species appearing in the four-step mechanism.

The equilibrium constants in these rates are given by

$$\begin{aligned} K_3 &= 0.216\exp(7658/T) \\ K_{\mathrm{II}} &= 0.035\exp(3652/T) \\ K_{\mathrm{IV}} &= 1.48\exp(6133/T)\,. \end{aligned} \tag{7.6}$$

We now want to go one step further and assume steady state of the radical H. Adding reaction IV to I and III leads to the three steps

$$\begin{array}{lrcl} \mathrm{I'} & \mathrm{CH_4 + O_2} & = & \mathrm{CO + H_2 + H_2O} \\ \mathrm{II'} & \mathrm{CO + H_2O} & = & \mathrm{CO_2 + H_2} \\ \mathrm{III'} & \mathrm{O_2 + 2H_2} & = & \mathrm{2H_2O} \end{array} \tag{7.7}$$

with the first three rates of (7.5). The concentration of H must now be determined from the steady state equation for H

$$w_{\mathrm{I}} + w_{\mathrm{III}} = w_{\mathrm{IV}}\,. \tag{7.8}$$

This may be written as

$$[\mathrm{H}] = [\mathrm{H_{eq}}]\left(1 - \frac{k_5[\mathrm{M}]}{k_1} - \frac{k_{38}[\mathrm{CH_4}]}{k_1[\mathrm{O_2}]}\right)^{1/2} \tag{7.9}$$

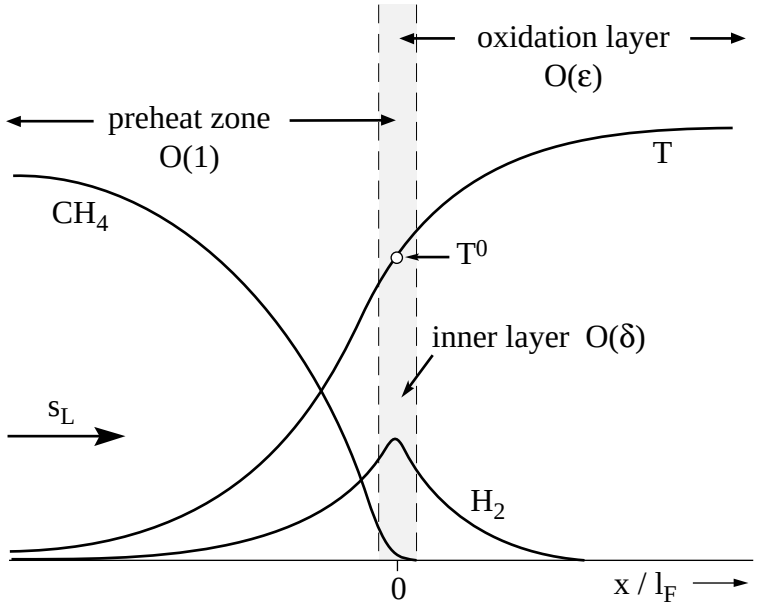

Fig. 7.1: Schematic illustration of the structure of a premixed methane-air flame.

where $[H_{eq}]$ based on partial equilibrium of reaction IV

$$[H_{eq}] = K_{IV}^{1/2} \frac{[O_2]^{1/2}[H_2]^{3/2}}{[H_2O]} . \tag{7.10}$$

Equation (7.9) shows an interesting structure: At temperatures of 1400K and above the second term in the brackets is small and the ratio k_{38}/k_1 is much larger than unity. It follows that $[CH_4]/[O_2]$ must be much smaller than unity, if [H] is to remain real. This will be used to develop an asymptotic description of the inner layer below but also shows that (7.9) cannnot be valid in the preheat zone upstream of the inner layer. The structure of the flame is schematically shown in Fig. 7.1. From (7.9) it follows that [H] vanishes in the preheat zone which is therefore chemically inert.

A further approximation that will reduce the three step mechanism (7.7) effectively to a two-step mechanism is the assumption of partial equilibrium of reaction II. Assuming the concentrations of H_2O and CO_2 to be known this leads to a coupling between CO and H_2 of the form

$$[CO] = \alpha'[H_2] \tag{7.11}$$

where

$$\alpha' = \frac{[CO_2]}{[H_2O]K_{II}(T)} \tag{7.12}$$

In introducing partial equilibrium of reaction II one assumes that the effective rate coefficient k_{18}/K_3 in the second equation of (7.5) tends to infinity while the term in curly brackets tends to zero and w_{II} remains finite. Since w_{II} is indefinite, the rate w_{II} must be eliminated from the balance equations. For the three-step mechanism these are written in

the following operator form

$$\begin{array}{lrcll} \text{Species} & L_i(Y_i) & \equiv & \rho_u s_L \dfrac{\mathrm{d}Y_i}{\mathrm{d}x} - \dfrac{1}{\mathrm{Le}_i}\dfrac{\mathrm{d}}{\mathrm{d}x}\left(\dfrac{\lambda}{c_p}\dfrac{\mathrm{d}Y_i}{\mathrm{d}x}\right) & = & W_i \displaystyle\sum_{k=\mathrm{I}'}^{\mathrm{III}'} \nu_{ik} w_k \\ \text{Temperature} & L_T(T) & \equiv & \rho_u s_L \dfrac{\mathrm{d}T}{\mathrm{d}x} - \dfrac{\mathrm{d}}{\mathrm{d}x}\left(\dfrac{\lambda}{c_p}\dfrac{\mathrm{d}T}{\mathrm{d}x}\right) & = & \dfrac{1}{c_p}\displaystyle\sum_{k=1}^{\mathrm{III}'} Q_k w_k \,. \end{array} \tag{7.13}$$

In terms of the variable $\Gamma_i = Y_i/W_i$ introduced in (2.33) and using the stoichiometric coefficients of the three-step mechanism, the balance equations for the concentrations are

$$\begin{aligned} L_F(\Gamma_F) &= -w_{\mathrm{I}} \\ L_{\mathrm{O}_2}(\Gamma_{\mathrm{O}_2}) &= w_{\mathrm{I}} + w_{\mathrm{III}} \\ L_{\mathrm{H}_2}(\Gamma_{\mathrm{H}_2}) &= w_{\mathrm{I}} + w_{\mathrm{II}} - 2w_{\mathrm{III}} \\ L_{\mathrm{CO}}(\Gamma_{\mathrm{CO}}) &= w_{\mathrm{I}} - w_{\mathrm{II}} \\ L_{\mathrm{H_2O}}(\Gamma_{\mathrm{H_2O}}) &= w_{\mathrm{I}} - w_{\mathrm{II}} + 2w_{\mathrm{III}} \\ L_{\mathrm{CO}_2}(\Gamma_{\mathrm{CO}_2}) &= w_{\mathrm{II}} \,. \end{aligned} \tag{7.14}$$

Here F stands for the fuel CH_4.

The rate w_{II} may be eliminated from (7.14) by combining the balance equations of H_2, $\mathrm{H_2O}$, and CO_2 with that of CO

$$\begin{aligned} L_{\mathrm{H}_2}(\Gamma_{\mathrm{H}_2}) + L_{\mathrm{CO}}(\Gamma_{\mathrm{CO}}) &= 2w_{\mathrm{I}} - 2w_{\mathrm{III}} \\ L_{\mathrm{H_2O}}(\Gamma_{\mathrm{H_2O}}) - L_{\mathrm{CO}}(\Gamma_{\mathrm{CO}}) &= 2w_{\mathrm{III}} \\ L_{\mathrm{CO}_2}(\Gamma_{\mathrm{CO}_2}) + L_{\mathrm{CO}}(\Gamma_{\mathrm{CO}}) &= w_{\mathrm{I}} \,. \end{aligned} \tag{7.15}$$

We will anticipate that in the thin reaction layers to be considered below, the diffusive terms dominate for the same reason as in the thin reaction zone for one-step asymptotics. Therefore we will neglect the convective terms in the operators (7.13) for the thin reaction zones and consider only the diffusive terms. This suggests that the concentrations should be scaled with the Lewis numbers. We introduce the non-dimensional variables

$$\begin{aligned} X_i &= \frac{Y_i W_F}{Y_{Fu} W_i} \,, \quad x_i = \frac{X_i}{\mathrm{Le}_i} \,, \\ T^* &= \frac{T - T_u}{T_b - T_u} \,, \quad x^* = \rho_u s_L \int_0^x \frac{c_p}{\lambda} \mathrm{d}x \,, \\ w_k^* &= \frac{\lambda W_F w_k}{c_p Y_{Fu} (\rho v)_u^2} \,, \quad Q_k^* = \frac{Q_k Y_{Fu}}{c_p (T_b - T_u) W_F} \,, \end{aligned} \tag{7.16}$$

and redefine the parameter α'

$$\alpha = \alpha' \frac{\mathrm{Le}_{\mathrm{H}_2}}{\mathrm{Le}_{\mathrm{CO}}} \,. \tag{7.17}$$

With (7.11) one then obtains the following balance equations of the two-step mechanism (the asterisks will be removed from here on)

$$\begin{aligned}
-\frac{\mathrm{d}^2}{\mathrm{d}x^2}(x_F) &= -w_{\mathrm{I}}\,,\\
-\frac{\mathrm{d}^2}{\mathrm{d}x^2}(x_{\mathrm{O}_2}) &= -w_{\mathrm{I}} - w_{\mathrm{III}}\,,\\
-\frac{\mathrm{d}^2}{\mathrm{d}x^2}(x_{\mathrm{H}_2}) &= \frac{2}{1+\alpha}(w_{\mathrm{I}} - w_{\mathrm{III}})\,,\\
-\frac{\mathrm{d}^2}{\mathrm{d}x^2}(x_{\mathrm{CO}}) &= \frac{2\alpha}{1+\alpha}(w_{\mathrm{I}} - w_{\mathrm{III}})\,,\\
-\frac{\mathrm{d}^2}{\mathrm{d}x^2}(x_{\mathrm{H_2O}}) &= \frac{2\alpha}{1+\alpha}w_{\mathrm{I}} + \frac{2}{1+\alpha}w_{\mathrm{III}}\,,\\
-\frac{\mathrm{d}^2}{\mathrm{d}x^2}(x_{\mathrm{CO}_2}) &= \frac{1-\alpha}{1+\alpha}w_{\mathrm{I}} + \frac{2\alpha}{1+\alpha}w_{\mathrm{III}}\,.
\end{aligned} \tag{7.18}$$

The stoichiometric coefficients are those of the two global reactions

$$\begin{aligned}
&\mathrm{I}'' && \mathrm{CH_4} + \mathrm{O_2} = \frac{2}{1+\alpha}(\mathrm{H_2} + \alpha\mathrm{CO}) + \frac{2\alpha}{1+\alpha}\mathrm{H_2O} + \frac{1-\alpha}{1+\alpha}\mathrm{CO_2}\,,\\
&\mathrm{III}'' && \mathrm{O_2} + \frac{2}{1+\alpha}(\mathrm{H_2} + \alpha\mathrm{CO}) = \frac{2}{1+\alpha}\mathrm{H_2O} + \frac{2\alpha}{1+\alpha}\mathrm{CO_2}\,.
\end{aligned} \tag{7.19}$$

Here the combination $\mathrm{H_2} + \alpha\mathrm{CO}$ appears as an intermediate which is formed in I″ and consumed in III″. The rates of these reactions are still the same as of I and III in the four-step mechanism.

If the balance equations $(7.18)_1$ and $(7.18)_3$ are used to determine x_F and x_{H}, all other concentrations and the temperature can be determined deriving the following coupling equations from (7.18) and the corresponding temperature equation

$$\begin{aligned}
&\frac{\mathrm{d}^2}{\mathrm{d}x^2}[(1+\alpha)x_{\mathrm{H}_2} + 4x_F - 2x_{\mathrm{O}_2}] = 0\,,\\
&\frac{\mathrm{d}^2}{\mathrm{d}x^2}[x_{\mathrm{H}_2} + 2x_F + x_{\mathrm{H_2O}}] = 0\,,\\
&\frac{\mathrm{d}^2}{\mathrm{d}x^2}[x_{\mathrm{H}_2} + x_F + x_{\mathrm{CO}_2}] = 0\,,\\
&\frac{\mathrm{d}^2}{\mathrm{d}x^2}[(q_{\mathrm{H}_2} + \alpha q_{\mathrm{CO}})x_{\mathrm{H}_2} + x_F + T] = 0\,.
\end{aligned} \tag{7.20}$$

Here the reduced heats of reaction are

$$\begin{aligned}
q_{\mathrm{H}_2} &= \frac{1}{2}\frac{Q_{\mathrm{III}}}{Q} = 0.3116\\
q_{\mathrm{CO}} &= \frac{(\frac{1}{2}Q_{\mathrm{III}} + Q_{\mathrm{II}})}{Q} = 0.3479
\end{aligned} \tag{7.21}$$

where Q is the heat of reaction of the global step

$$CH_4 + 2O_2 = CO_2 + 2H_2O\,.$$

In the following we approximate both q_{H_2} and q_{CO} by $q = 0.33$ for simplicity.

7.2 The Asymptotic Structure of Stoichiometric Methane-Air Flames

The flame structure of the two-step mechanism is shown in Fig 7.1 and contains three layers

1. a chemically inert preheat zone of order O(1) upstream,
2. an thin inner layer of order O(δ) in which the fuel is consumed and the intermediates H_2 and CO formed according to the global step I$''$,
3. a thin oxidation layer of order O(ε) downstream where H_2 and CO are oxidized according to the global step III$''$.

At first the inner layer shall be analysed. We will denote quantities at the inner layer with a subscript 0 but the inner layer temperature as T^0. In this layer all concentrations except that of the fuel, which is depleted may be assumed constant to leading order. Introducing (7.9) into the $(7.5)_1$ and neglecting the second term in the brackets of (7.9) this leads to

$$w_{\mathrm{I}} = \mathrm{Da_I} x_F \left(1 - \frac{x_F}{\delta}\right)^{1/2} \tag{7.22}$$

where the Damköhler number of reaction I is

$$\mathrm{Da_I} = \frac{\rho_0^2}{\rho_u^2 s_L^2} \frac{Y_{Fu}}{W_F} \frac{\lambda_0}{c_{p0}} \frac{\left(K_{\mathrm{IV}} X_{O_2} X_{H_2}^3\right)_0^{1/2}}{X_{H_2O}} \mathrm{Le}_F k_{38}(T^0)\,. \tag{7.23}$$

The small parameter δ was defined as

$$\delta = \frac{k_1(T^0) X_{O_2,0}}{k_{38}(T^0)\mathrm{Le}_F} \tag{7.24}$$

It describes the ratio of the rate coefficients of reaction I and II and thereby describes the competition of these two reactions in producing and consuming H-radicals according to the global steps IV and I. Since it happens that the reaction rate k_1 is typically smaller than k_{38}, and since also X_{O_2} in the inner layer is smaller than unity, δ is around 0.1 and sufficiently small for an asymptotic expansion. If δ is small, since w_{I} must be real it follows from the term in brackets in (7.22) that x_F must not exceed the value of δ. Fig 7.1 shows that the fuel is of order O(1) in the preheat zone but decreases rapidly towards the inner layer. In the inner layer x_F is then of order O(δ) and one may introduce the scaling

$$y = \frac{x_F}{\delta} \tag{7.25}$$

and the stretched variable

$$\zeta = \frac{x}{\delta}\,. \tag{7.26}$$

Introducing these into the first equation of (7.18) leads to the differential equation that governs the structure of the inner layer

$$\frac{\mathrm{d}^2 y}{\mathrm{d}\zeta^2} = (\delta^2 \mathrm{Da_I}) y (1-y)^{1/2} \,. \tag{7.27}$$

The downstream boundary condition of this equation is

$$y = 0 \quad \text{as} \quad \zeta \to +\infty \tag{7.28}$$

since reaction I is irreversible. The matching with the preheat zone should, as for the one-step asymptotic problem, provide the second boundary condition. The solution for the fuel concentration in the preheat zone is

$$X_F = 1 - \exp(\mathrm{Le}_F \, x) \tag{7.29}$$

which leads to the expansion $x_F = -x\cdot$ around $x = 0$. It turns out, however, that the inner layer and the preheat zone are separated by an additional thin layer, the radical consumption layer where the steady state approximation for the H-radical breaks down. This layer occurs at $y = 1$, $\zeta = -1$ in terms of the inner layer variables. Since the fuel is not consumed in this radical layer the slope of the fuel concentration is continuous and matching across this layer leads to

$$y = 1 \,, \quad \frac{\mathrm{d}y}{\mathrm{d}\zeta} = -1 \quad \text{at} \quad \zeta = -1 \,. \tag{7.30}$$

With the boundary conditions (7.28) and (7.30) equation (7.27) can be integrated once to obtain the eigenvalue

$$\delta^2 \mathrm{Da_I} = \frac{15}{8} \tag{7.31}$$

With (7.31) one could now determine the burning velocity s_L if the temperature T_0 and all other properties at the inner layer were known. In order to determine these, the structure of the oxidation layer also must be resolved. In the oxidation layer $x_F = 0$ and therefore $w_\mathrm{I} = 0$. The temperature varies only slowly in this layer and since the activation energy of k_5 is small, temperature variations may be neglected. Since most of the chemical activity takes place in the vicinity of the inner layer, all properties shall be evaluated at $x = 0$. Choosing $x_{\mathrm{H_2}}$ as the dependent variable in the oxidation layer and scaling it in terms of a new variable z as

$$x_{\mathrm{H_2}} = \frac{\varepsilon z}{(1+\alpha) q} \tag{7.32}$$

one may use the coupling relations (7.20) to show that the downstream boundary conditions are satisfied by

$$x_{\mathrm{O_2}} = \varepsilon z / 2q \,, \quad T = 1 - \varepsilon z \,.$$

In these expansions ε is the small parameter related to the thickness of the oxidation layer. Introducing (7.32) and (7.33) into the third of (7.5) leads to

$$w_\mathrm{III} = 2q \mathrm{Da_{III}} \varepsilon^3 z^3 \tag{7.33}$$

where the Damköhler number of reaction III is defined

$$\mathrm{Da_{III}} = \frac{\rho_0^2}{\rho_u^2 s_L^2} \frac{Y_{Fu}}{W_F} \frac{\lambda_0}{c_{p0}} \left(\frac{K_{\mathrm{IV}} \mathrm{Le}_{\mathrm{O_2}}^3 \mathrm{Le}_{\mathrm{H_2}}^3}{2^5 (1+\alpha)^3} \right)_0^{1/2} \frac{k_5[\mathrm{M}]}{q^4 X_{\mathrm{HO_2}}} \tag{7.34}$$

The concentration of the third body is reaction 5 may be determined approximately by using the third body efficiencies given in Table 3.1 evaluated at the burnt gas conditions. This leads to

$$[\mathrm{M}] = \frac{1.6p}{\mathcal{R}T}$$

which introduces a pressure dependence of $\mathrm{Da_I}$ and will finally determine the pressure dependence of the burning velocity. Introduction of a stretched coordinate

$$\eta = \frac{2qx}{\varepsilon} \tag{7.35}$$

then leads from the third equation of (7.18) with $w_{\mathrm{I}} = 0$ to the governing equation of the oxidation layer

$$\frac{\mathrm{d}^2 z}{\mathrm{d}\eta^2} = (\varepsilon^4 \mathrm{Da_{III}}) z^3 \,. \tag{7.36}$$

This suggests the definition

$$\varepsilon = \mathrm{Da_{III}^{-1/4}} \,. \tag{7.37}$$

It turns out that for $p \geq 1\,\mathrm{atm}$ ε is smaller than unity but typically larger than δ. Even though ε is not very small, we will consider it as small enough to justify an asymptotic description of the oxidation layer. The downstream boundary condition of (7.36) is

$$z = 0 \quad \text{for} \quad \eta \to \infty \tag{7.38}$$

since reaction III is irreversible. The upstream boundary condition must be determined from jump conditions across the inner layer. Since the fuel is depleted and $\mathrm{H_2}$ is formed in the inner layer following reaction I″, the stoichiometry of this reaction also determines the change of slopes of the $\mathrm{H_2}$ in comparison of those of the fuel. This is written as

$$\left. \frac{\mathrm{d}x_F}{\mathrm{d}x} \right|_{0-} - \left. \frac{\mathrm{d}x_F}{\mathrm{d}x} \right|_{0+} = 1 = -\frac{1+\alpha}{2} \left\{ \left. \frac{\mathrm{d}x_{\mathrm{H_2}}}{\mathrm{d}x} \right|_{0-} - \left. \frac{\mathrm{d}x_{\mathrm{H_2}}}{\mathrm{d}x} \right|_{0+} \right\} \tag{7.39}$$

Since the thickness of the preheat zone is of order O(1) and that of the oxidation layer of order $\mathrm{O}(\varepsilon)$ the upstream slope of the $\mathrm{H_2}$ concentration $(\mathrm{dH_2}/\mathrm{d}x)_{0+}$ can be neglected compared to the downstream slope $(\mathrm{dH_2}/\mathrm{d}x)_{0-}$. It then follows with (7.32) and (7.35) that the upstream boundary condition of (7.36) is

$$\frac{\mathrm{d}z}{\mathrm{d}\eta} = -1 \quad \text{at} \quad \eta = 0 \,. \tag{7.40}$$

Then the solution of (7.36) with (7.37) is

$$z = \frac{2^{1/2}}{2^{1/4} + \eta} \tag{7.41}$$

with

$$z_0 = 2^{1/4} \quad \text{at} \quad \eta = 0\,. \tag{7.42}$$

The form of the solution is plotted in Fig. 7.2 showing a very slow decrease of z towards $\eta \to \infty$. This may explain why in numerically and experimentally obtained concentration and temperature profiles the downstream conditions are approached only very far behind the flame.

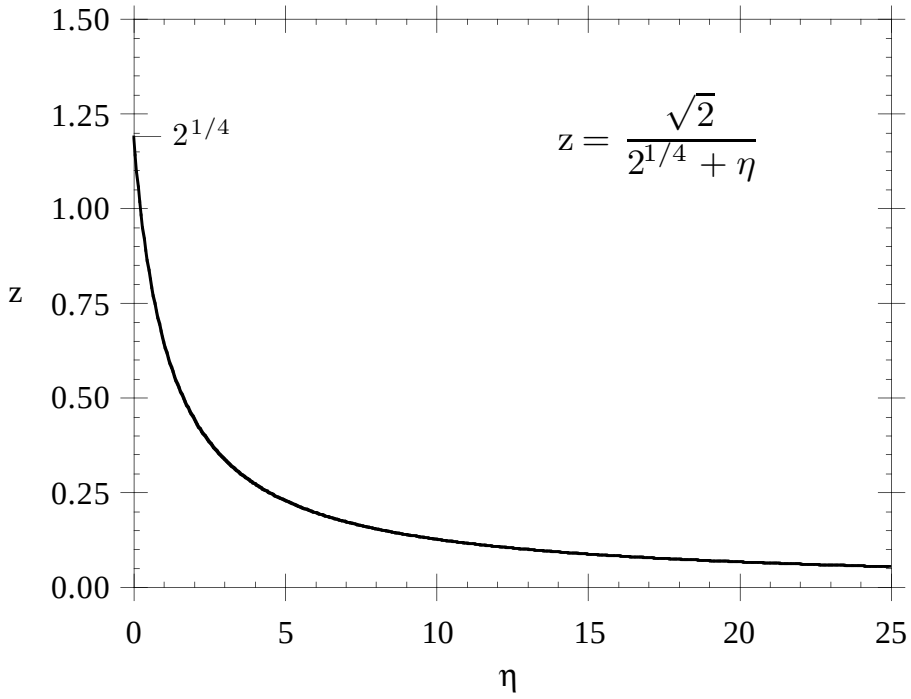

Fig. 7.2: Normalized H_2-profile in the oxidation layer

7.3 An Analytic Expression for the Burning Velocity

The result (7.42) may now be used in (7.32) and (7.33) to determine the quantities required in (7.23) and thereby the burning velocity s_L. Also by dividing (7.23) by (7.35) one can eliminate s_L and obtain a relation of the form

$$\frac{k_1^2(T^0)}{k_{38}(T^0)k_5(T^0)/\mathcal{R}T^0} = 1.5p\,\frac{\mathrm{Le}_F}{\mathrm{Le}_{\mathrm{O}_2}}\,. \tag{7.43}$$

Here the universal gas constant $\mathcal{R}$ must be used as $\mathcal{R} = 82.05\,\mathrm{atm\,cm^3/mol\,K}$ in order to be consistent with the units of the reaction rates and the pressure. Equation (7.43) shows that with the rate coefficients fixed, the inner layer temperature is function of the pressure

only. It does not depend on the preheat temperature, the dilution of the fuel concentration in the unburnt mixture and thereby the adiabatic flame temperature. This is an important property that will be discussed below.

After some algebraic manipulations the expression for the burning velocity reads

$$s_L^2 = \frac{8}{15}\frac{k_1^2}{k_{38}}\frac{1}{q^4 X_{\mathrm{H_2O}}}\frac{Y_{Fu}}{W_F}\frac{\lambda_0}{c_{p0}}\left(\frac{\mathrm{Le}_{\mathrm{O_2}}^5 \mathrm{Le}_{\mathrm{H_2}}^3 K_{\mathrm{IV}}(T^0)}{\mathrm{Le}_F 2^5 (1+\alpha_0)^3}\right)^{1/2}\frac{T_u^2}{T_0^2}\frac{(T_b - T^0)^4}{(T_b - T_u)^4} \tag{7.44}$$

where (7.42) and (7.33) were used to relate ε to the difference between T_b and T_0

$$\varepsilon z_0 = \frac{T_b - T^0}{T_b - T_u}\,. \tag{7.45}$$

The burning velocity calculated from (7.44) and the pressure from (7.43) are plotted in Fig. 7.3 for an undiluted flame with $T_u = 300\,\mathrm{K}$ as a function of T_0 choosing $p = 1\,\mathrm{atm}$ one obtains a laminar burning velocity of 54 cm/sec for stoichiometric methane flames. This value is satisfactory in view of the many approximations that were made and the few kinetic rates that were retained. In fact, it is seen from (7.43) and (7.44) that only the rates of reactions 1, 5, and 11 influence the burning velocity in this approximation.

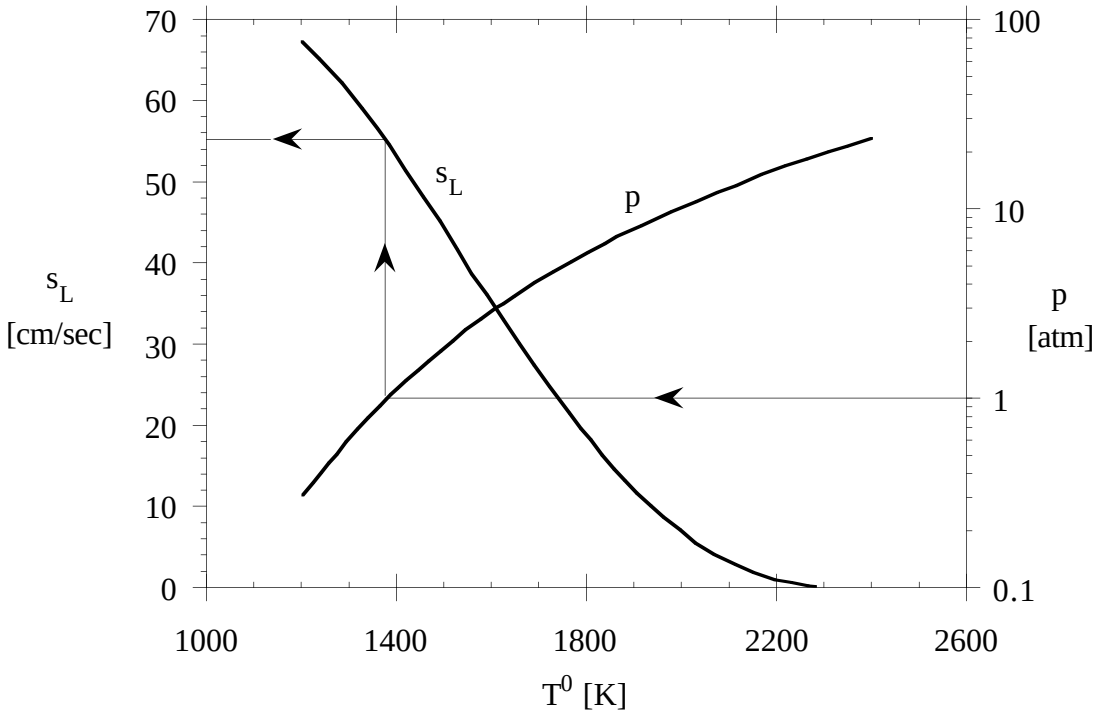

Fig. 7.3: The burning velocity for an undiluted stoichiometric methane-air flame at $T_u = 300\,\mathrm{K}$

A further consequence of (7.44) is that the burning velocity vanishes as T^0 reaches T_b. This is seen in Fig. 7.3 with $T_b = 2320\,\mathrm{K}$ the pressure is larger than approximately 20 atm. Different values of T_b would been obtained for a diluted or preheated flame. The fact that at a fixed pressure T^0 is fixed by the rate of rate coefficients in (7.43) points towards the possibility to explain flammability limits at least in terms of dilution for stoichiometric flames: if the amount of fuel is so low that in the unburnt mixture the corresponding adiabatic flame temperature is lower than T^0, a premixed flame cannot be established.

7.4 Relation to the Activation Energy of the One-step Model

Using the burning velocity expression (6.52) from the preceeding lecture, one may plot the burning velocity in an Arrhenius diagram over $1/T_b$. Then in the limit of a large activation energy the slope in this diagram is given by

$$\frac{\mathrm{d}\ln s_L^2}{\mathrm{d}(1/T_b)} = -\frac{E}{\mathcal{R}} \tag{7.46}$$

or

$$\frac{\mathrm{d}\ln s_L^2}{\mathrm{d}\ln T_b} = \frac{E}{\mathcal{R}T_b} \tag{7.47}$$

Applying this form to (7.44) with T_0 fixed leads to

$$\frac{\mathrm{d}\ln s_L^2}{\mathrm{d}\ln T_b} = \frac{4\,T_b}{T_b - T^0} - \frac{4\,T_b}{T_b - T_u} \tag{7.48}$$

Since the second of the terms is much smaller then the first one obtains with (7.45) when T^0 approaches T_b and ε is small

$$\frac{E}{\mathcal{R}T_b} = \frac{4\,T_b}{T_b - T_u}\frac{1}{\varepsilon z_0} \tag{7.49}$$

Therefore the Zeldovich number introduced in (6.35) may be expressed as

$$\mathrm{Ze} = \frac{E(T_b - T_u)}{\mathcal{R}T_b^2} = \frac{4}{\varepsilon z_0} \tag{7.50}$$

In the one-step model the thickness of the reaction zone was of the order of the inverse of the Zeldovich number. This corresponds for the two-step model for methane flames to the thickness of the oxidation layer. Therefore the oxidation layer seems to play a similar role in hydrocarbon flames as the reaction zone in one-step asymptotics.

Values of the Zeldovich number for lean to stoichiometric methane flames, obtained by asymptotic analysis in [7.2] are shown in Fig. 7.4. The Zeldovich number measures the sensitivity of the burning velocity to perturbations of the maximum temperature. Figure 7.4 shows that this sensitivity increases as the mixture becomes leaner and when

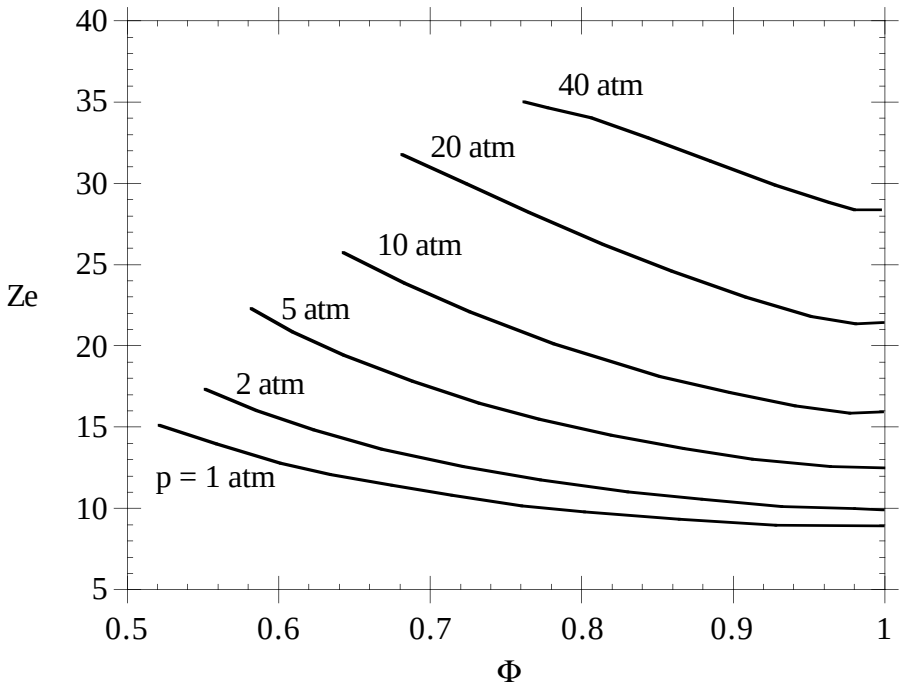

Fig. 7.4: Variation in the value of the effective Zeldovich number with Φ for various values of p at $T_u = 300$ K.

the pressure increases. The flame will then become very sensitive to heat loss and flame stretch effects.

7.5 Analytic Approximations of Burning Velocities for Lean CH_4, C_2H_6, C_2H_4, C_2H_2, and C_3H_8 Flames

The burning velocity expression presented in (7.43) and (7.44) may be generalized by writing an approximation formula for burning velocities as

$$s_L = Y_{Fu}^m \, A(T^0) \, \frac{T_u}{T^0} \left(\frac{T_b - T^0}{T_b - T_u} \right)^n \tag{7.51}$$

and

$$p = P(T^0) \tag{7.52}$$

where the functions $A(T^0)$ and $P(T^0)$ are determined by fitting numerical or experimental data and the values $m = 1/2$ and $n = 2$ would correspond to the previous expressions for premixed methane flames.

Equation (7.52) assumes that the inner layer temperature is a function of pressure only, and it does not depend, for instance, on the equivalence ratio. This is a fairly crude

approximation as may be seen from Fig. 7.5 where inner layer temperatures obtained from asymptotic analysis [7.2] are plotted together with the adiabatic temperatures as a function of the equivalence ratio. If one would replace the curves for the inner layer temperature by a horizontal line, its intersection with the curve for T_b would yield a lower theoretical limit for the lean flammability limit. This will be discussed in the next section.

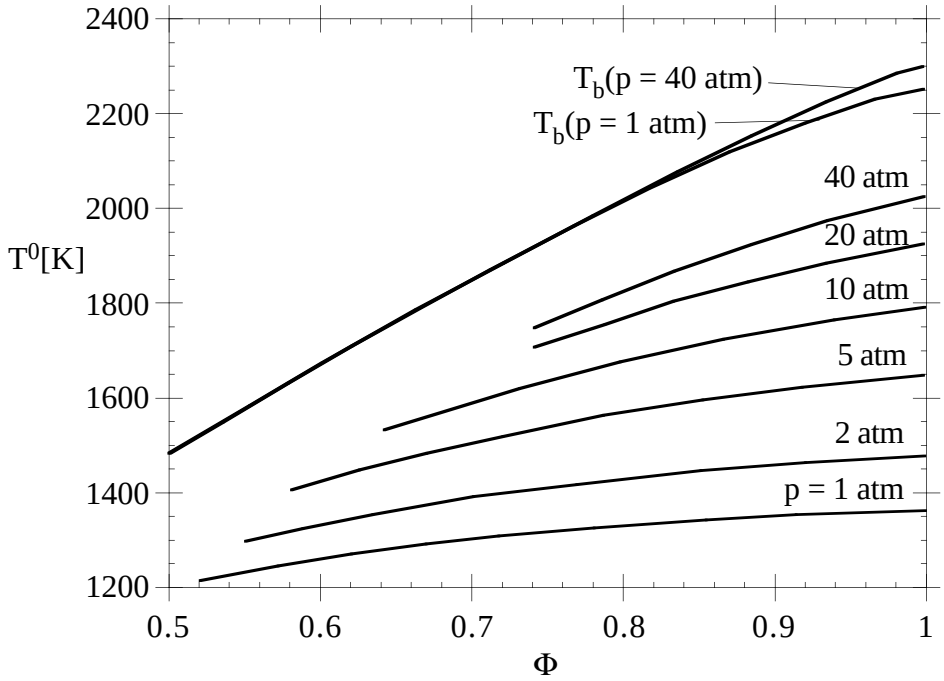

Fig. 7.5: Variation of the adiabatic flame temperature T_b and the temperature at the inner layer T^0 with equivalence ratio Φ for various values at the pressure p, and for $T_u = 300$ K.

If the structure of any other hydrocarbon fuel is similiar to that of methane, these exponents should not differ very much from these numbers. Since $A(T^0)$ and $B(T^0)$ contain essentially the temperature dependence due to rate coefficients, we express them in Arrhenius form

$$A(T^0) = F \exp(-G/T^0) \tag{7.53}$$

$$P(T^0) = B \exp(-E/T^0)\,. \tag{7.54}$$

This concept was tested in [7.3]. The basis of the approximation was a data set of 197, 223, 252, 248, and 215 premixed flames for CH_4, C_2H_6, C_2H_4, C_2H_2 and C_3H_8, respectively in the range between $p = 1$ atm and 40 atm, T_u between 298 K and 800 K, and the fuel-air equivalence ratio between $\Phi = 0.4$ and $\Phi = 1.0$. A nonlinear approximation procedure was employed, yielding the following values for the coefficients:
The approximation was surprisingly the best for C_2H_2, yielding a standard deviation for s_L of 2.3%, followed by C_2H_4 with 3.2%, C_2H_6 and C_3H_8 with 6.2%, and CH_4 with 7.4%.

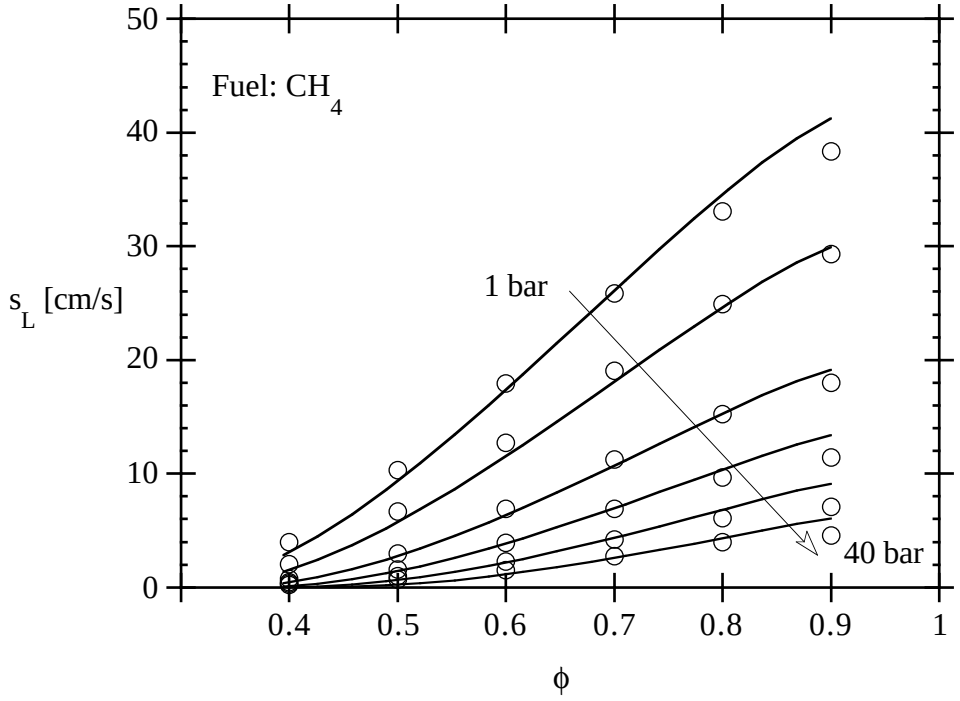

Fig. 7.6: Burning velocity s_L of methane vs. fuel-air-equivalence ratio Φ for various pressures with a fixed unburnt temperature T_u of 298 K (solid lines). The markers denote the values of detailed numerical calculations.

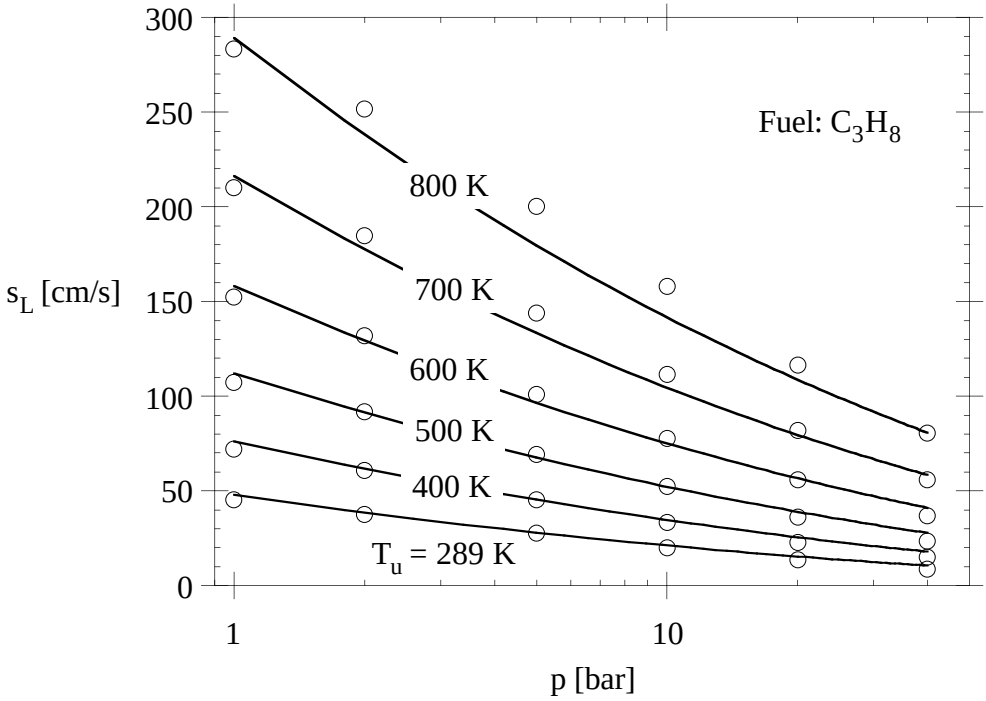

Fig. 7.7: Burning velocity s_L of propane vs. pressure for various unburnt gas temperatures T_u at stoichiometric mixture (solid lines). The markers denote the values of detailed numerical calculations.

Fuel	B [bar]	E [K]	F [cm/s]	G [K]	m	n
CH_4	3.1557e8	23873.0	22.176	-6444.27	0.565175	2.5158
C_2H_2	56834.0	11344.4	37746.6	1032.36	0.907619	2.5874
C_2H_4	3.7036e5	14368.7	9978.9	263.23	0.771333	2.3998
C_2H_6	4.3203e6	18859.0	1900.41	-506.973	0.431345	2.1804
C_3H_8	2.2501e6	17223.5	1274.89	-1324.78	0.582214	2.3970

Table 7.1: Approximation coefficients for the burning velocity.

These deviations may be considered extremely small in view of the fact that such a large range of equivalence ratios, pressures and preheat temperatures has been covered with an approximation formula containing only six coefficients. A closer look at the exponents m and n shows that m is close to 1/2 for CH_4 and C_3H_8, but close to unity for C_2H_2 and C_2H_4, suggesting that the asymptotic model for these flames should differ from the one for CH_4 in some important details. The exponent m lies around 2.5 and thereby sufficiently close to 2 for all fuels.

Burning velocities for methane calculated from (7.51) and (7.52) are shown as a function of equivalence ratio for different pressures at $T_u = 298\,\mathrm{K}$ in Fig. 7.6 and compared with the values obtained from the numerical computations. Generally the largest derivations from the numerical computations occur around $\phi = 1$. The pressure and unburnt temperature variation of s_L at stoichiometric mixture is shown in Fig. 7.7 for propane.

7.6 Lean flammability limits of hydrocarbon flames

Flammability is the ability of a mixture, once it has been ignited, to enable flame propagation without further heat addition. This requires that a sufficient amount of fuel is available to reach a temperature, that, in view of the flame structure as shown in Fig. 7.1 should exceed the inner layer temperature T^0.

Le Chatelier in 1891 was the first to point towards a criterion that relates the flammability limit to the thermodynamic properties of the fuel mixture. In 1898 Le Chatelier and Boudouard investigated experimental data and wrote that "the flammability limit of most hydrocarbons corresponds to a heat of combustion close to 12.5 kcal". This is essentially Le Chatelier's famous "mixing rule". It determines an adiabatic flame temperature and should be valid for mixtures of hydrocarbons with inerts, too.

Equation (7.51) now shows that the burning velocity vanishes if the adiabatic flame temperature is equal to the inner layer temperature. A lower theoretical limit for the lean flammability limit is therefore given by

$$T_b = T^0\,. \tag{7.55}$$

In view of this criterion the adiabatic flame temperature identified by Le Chatelier and Boudouard corresponds to the inner layer temperature and thus describes a chemical rather than a thermodynamic property. In using (7.55) the concept can generalized to

variable preheat temperatures and pressures and compared with experimental data. Many data on flammability limits are given in [7.7]

As the lean flammability limit is approached, the burning velocity drops sharply, but shows a finite value at the limiting point. Egerton and Thabet [7.5] and Powling [7.6] report a value of 5 cm/s at atmospheric pressure using flat-flame burners. Experimental data for the lean flammability limit are always influenced by external disturbances, such as radiative heat loss or flame stretch. Radiation heat loss will be discussed in the next section. We note that flame extinction occurs at a finite value of the burning velocity.

Equation (7.55) may be used to calculate the limiting fuel mass fraction $(Y_{F,u})_{l.l.}$ as a quantity that determines the flammability limit. At the flammability limit it is accurate enough to assume complete combustion and to use (2.9) to determine T_b as a function of $Y_{F,u}$ and T_u. Then, with $T_b = T^0$, one obtains

$$(Y_{F,u})_{l.l.} = \frac{(T^0 - T_u)c_p\nu'_F W_F}{Q_{\text{ref}}} \tag{7.56}$$

This indicates that the limiting fuel mass fraction decreases linearly with increasing T_u.

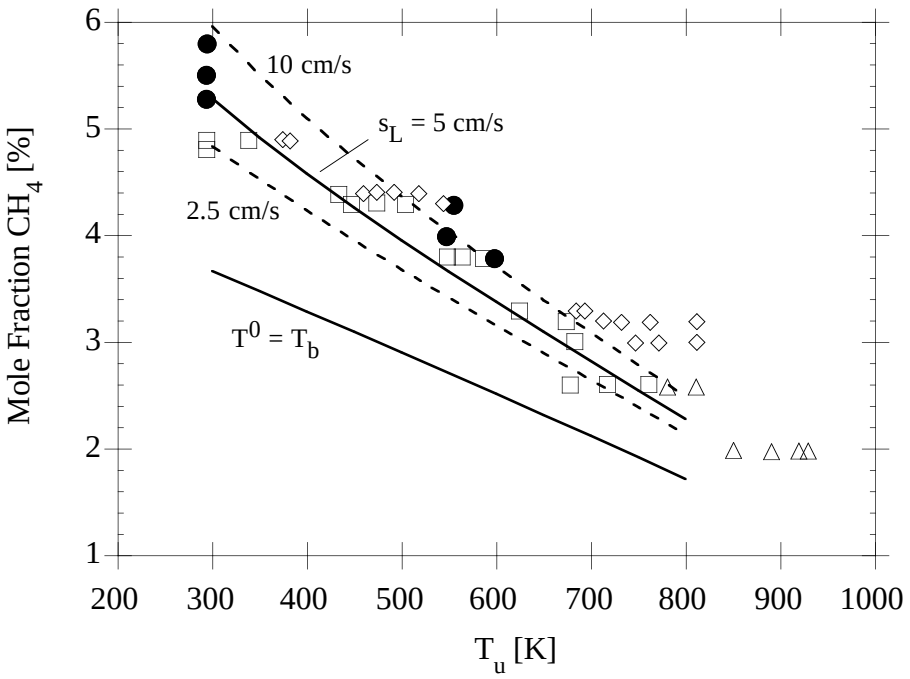

Fig. 7.8: Comparison of experimental data for the lean limit CH_4 mole fraction from [7.7] for different preheat temperatures with the two criteria.

Fig. 7.8 compares the results using (7.56) with recent experimental data obtained by Hustad and Sønju [7.8]. The criterion $T^0 = T_b$ underpredicts the measured values for the lean limit, but shows already the right behavior. The criterion $s_L = 5$ cm/s is in

excellent agreement with the measured values. In this figure we also plotted the curves for $s_L = 2.5$ cm/s and $s_L = 10$ cm/s showing that the present model is not very sensitive to the precise value of the limiting burning velocity.

7.7 Extinction of a Plane Flame by Volumetric Heat Loss

An additional influence that affects the stability of flames is volumetric heat loss. In order to analyse this effect we will compare the one-step model with a large activation energy and unity Lewis number and the four-step model. We will assume that the volumetric heat loss q_R is proportional to the temperature difference $T - T_u$ and write

$$q_R = -\alpha(T - T_u)\,. \tag{7.57}$$

where α is a heat loss coeffizient. The one-dimensional temperature equation for a steady state premixed flame is then written as

$$\rho_u s_L \frac{\mathrm{d}T}{\mathrm{d}x} = \frac{\mathrm{d}}{\mathrm{d}x}\left(\frac{\lambda}{c_p}\frac{\mathrm{d}T}{\mathrm{d}x}\right) + \frac{Q}{c_p}w - \frac{\alpha}{c_p}(T - T_u)\,. \tag{7.58}$$

In terms of the nondimensional quantities defined in (6.25)—(6.27) this may be written (with the asterisks removed)

$$M\frac{\mathrm{d}T}{\mathrm{d}x} = \frac{\mathrm{d}^2T}{\mathrm{d}x^2} + w - \pi T\,. \tag{7.59}$$

Here M is the burning velocity of the plane flame with heat loss normalized by the reference burning velocity $s_{L,\mathrm{ref}}$ of a plane flame without heat loss

$$M = \frac{s_L}{s_{L,\mathrm{ref}}}\,. \tag{7.60}$$

The non-dimensional heat loss parameter is defined

$$\pi = \frac{\lambda\alpha}{\rho_u^2 s_{L,\mathrm{ref}}^2 c_p^2}\,. \tag{7.61}$$

It will be assumed constant with λ evaluated at $T = T_0$. It should be noted here that π increases rapidly as $s_{L,\mathrm{ref}}$ decreases. Therefore heat loss has a strong influence close to the flammability limit when $s_{L,\mathrm{ref}}$ is small.

The structure of a premixed flame with heat loss is shown in Fig. 7.9. We will treat π as a small expansion parameter and expand the temperature as

$$T = T_0(1 + \pi z) \tag{7.62}$$

where T_0 is the leading order temperature for $\pi \to 0$. The reaction term w in (7.58) can be eliminated by coupling it with the equation (6.22) for the fuel mass fraction. In non-dimensional form one then obtains the enthalpy

$$h = T + Y - 1 \tag{7.63}$$

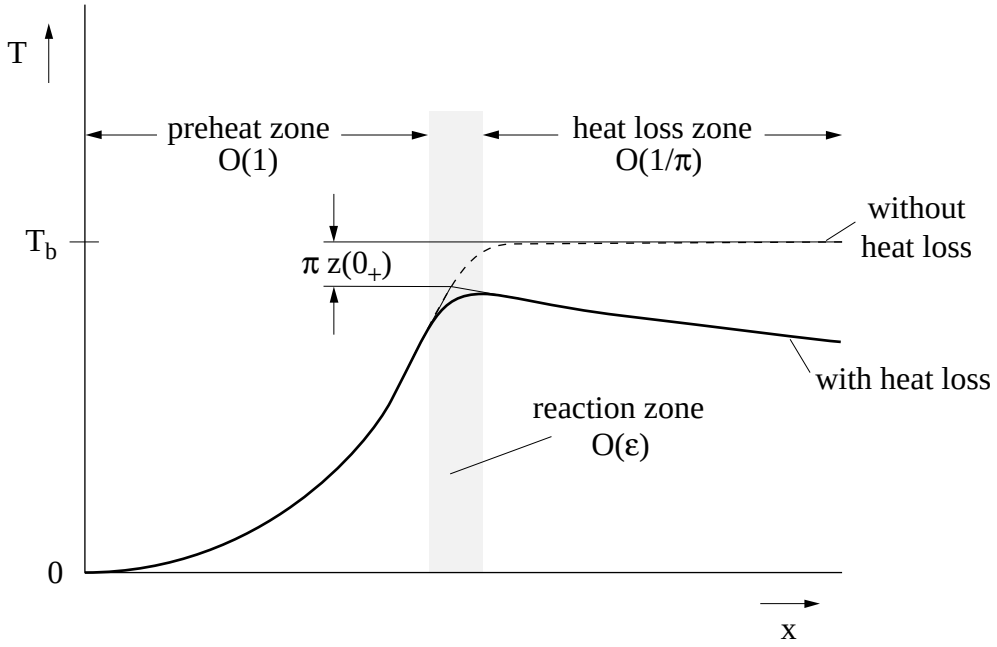

Fig. 7.9: Structure of a premixed flame with heat loss

governed by the equation

$$M\frac{\mathrm{d}h}{\mathrm{d}x} = \frac{\mathrm{d}^2h}{\mathrm{d}x^2} - \pi T\,. \tag{7.64}$$

This equation may be integrated across the thin reaction zone from $x = -\infty$ to $x = 0_+$. This leads to

$$Mh(0_+) = \left.\frac{\mathrm{d}h}{\mathrm{d}x}\right|_{0_+} - \pi \int_{-\infty}^{0_+} T_0 \mathrm{d}x \tag{7.65}$$

since at $x \to -\infty$ the enthalpy and its gradient vanishes. Introducing (7.62) into (7.63) at $x = 0_+$, where $T_0 = 1$ and $Y = 0$ one obtains

$$h(0_+) = \pi z(0_+)\,. \tag{7.66}$$

The integral over the preheat zone in (7.65) may evaluated by integrating the temperature equation (7.59) to leading order

$$M\frac{\mathrm{d}T_0}{\mathrm{d}x} = \frac{\mathrm{d}^2T_0}{\mathrm{d}x^2} \tag{7.67}$$

leading to

$$T_0 = \exp(Mx) \quad \text{for} \quad x < 0\,. \tag{7.68}$$

The downstream enthalpy gradient at the flame front is equal to the downstream temperature gradient since $Y = 0$ for $x \geq 0$. It can be evaluated by realizing that the heat

loss region behind the flame is broad of order $O(\pi^{-1})$. This suggest the introduction of a contracted coordinate

$$\tilde{x} = \pi x \tag{7.69}$$

into the downstream temperature equation

$$M\frac{\mathrm{d}T}{\mathrm{d}\tilde{x}} = \pi\frac{\mathrm{d}^2T}{\mathrm{d}\tilde{x}^2} - T \qquad x > 0\,. \tag{7.70}$$

In the limit $\pi \to 0$ the heat conduction term can now be neglected and with $T_0(0_+) = 1$ one obtains to leading order

$$\left.\frac{\mathrm{d}h}{\mathrm{d}x}\right|_{0_+} = \left.\frac{\mathrm{d}T}{\mathrm{d}x}\right|_{0_+} = -\frac{\pi}{M}\,. \tag{7.71}$$

With (7.66), (7.68) and (7.71) inserted into (7.65) the flame temperature pertubation is

$$z(0_+) = -\frac{2}{M^2}\,. \tag{7.72}$$

Since for a one step flame with a large activation energy the burning velocity depends according to (6.52) on the flame temperature as

$$s_L^2 \sim \exp\left(-\frac{E}{RT_b}\right)\,, \tag{7.73}$$

a perturbation of the temperature at $x = 0_+$ behind the reaction zone will lead in terms of the dimensional temperature to

$$M = \exp\left\{-\frac{E}{2R}\left(\frac{1}{T(0_+)} - \frac{1}{T_0}\right)\right\} \tag{7.74}$$

Using the expansion (7.62) in terms of the non-dimensional temperature one obtains with (6.35)

$$M = \exp\left(\pi\,\mathrm{Ze}\,z(0_+)\right) \tag{7.75}$$

When this is combined with (7.72) one obtains

$$M^2 \ln M^2 = -2\pi\mathrm{Ze}\,. \tag{7.76}$$

A similar analysis may be performed for the four-step asymptotic analysis of methane flames. Then, since with (7.44)

$$s_L^2 \sim (T_b - T^0)^4 \tag{7.77}$$

one obtains with (7.45) and (7.50)

$$M^2 = \frac{\left(T_b - T^0 + T_b\pi z(0_+)\right)^4}{(T_b - T^0)^4} = \left(1 + \frac{\pi\mathrm{Ze}z(0_+)}{4}\right)^4\,, \tag{7.78}$$

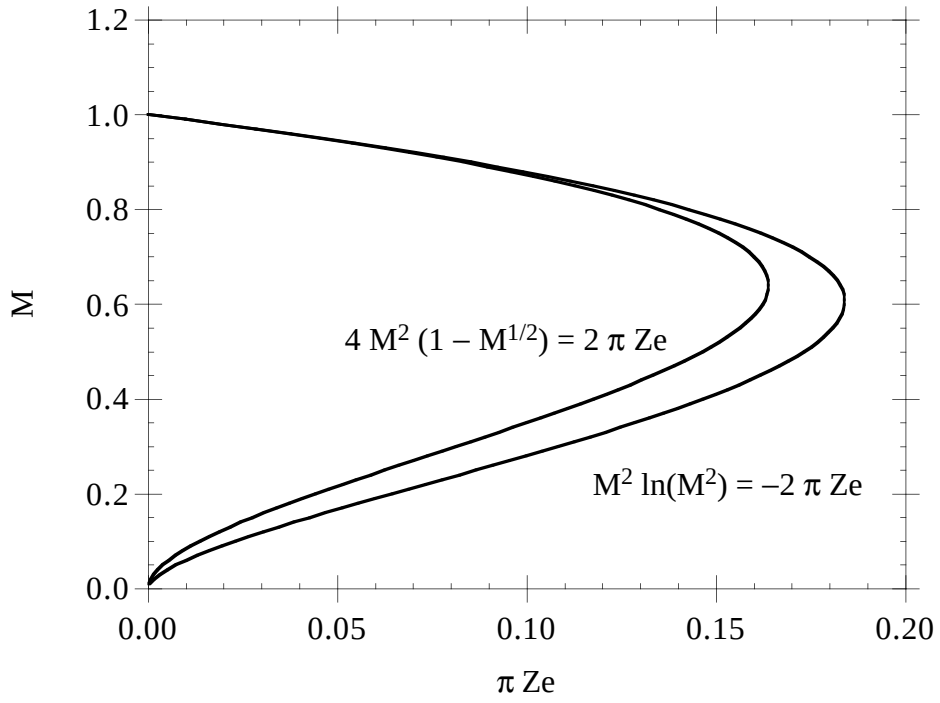

Fig. 7.10: The change of burning velocity and flame extinction due to heat loss for one-step and four-step asymptotics

since $T_b/(T_b - T^0) = 1/(\varepsilon z_0) = \mathrm{Ze}/4$ to leading oeder. If this is now combined with (7.72) one obtains

$$M^2 \left(1 - M^{1/2}\right) = \pi \mathrm{Ze} \tag{7.79}$$

instead of (7.76). Both equations, (7.76) and (7.79), are plotted in Fig. 7.10 showing a qualitatively and even quantitatively very similar behaviour.

Only the upper branch of these curves represents a stable solution. It shows a decrease of the burning velocity as the heat loss parameter π increases. There is a maximum value for the product πZe for each of these curves beyond which no solution exists. At this value heat loss extinguishes the flame. The non-dimensional burning rates at which this happens are very close to each other: $M_{\mathrm{ex}} = 0.61$ for the one step kinetics and $M_{\mathrm{ex}} = 0.64$ for the four-step kinetics. This is surprising because the kinetics for both cases are fundamentally different. This supports the previous conclusion that the one-step large activation energy model is a good approximation for the temperature sensitivity of hydrocarbon flames.

References

[7.1] Peters, N. and Williams, F.A., "Asymptotic Structure of Stoichiometric Methane-Air Flames", Combustion and Flame,**68**, (1987), pp. 185–207.

[7.2] Seshadri, K. and Göttgens, J., "Reduced Kinetic Mechanisms and Asymptotic Approximations for Methane-Air Flames", Smooke, M.D. (Ed.), Lecture Notes in Physics, **384**, pp. 111–136, Springer-Verlag Berlin 1991.

[7.3] Göttgens, J., Mauss, F. and Peters, N., Analytic Approximations of Burning Velocities and Flame Thickness of Lean Hydrogen, Methane, Ethylene, Ethane, Acethylene and Propane Flames, 24^{th} Symposium (International) on Combustion, 1992, to appear.

[7.4] Göttgens, J., Terhoeven, P. and Peters, N., "Calculation of Lean Flammability Limits Based on Analytical Approximations of Burning Velocities", Bul. Soc. Chim. Belg., 101, n° 10, 1992, pp. 885–891.

[7.5] Egerton, A. and Thabet, S.K., Proc. R. Soc. (London) A **211**, p. 455, 1952.

[7.6] Powling, J., "Experimental Methods in Combustion Research", Suruge, J. (Ed.), Pergamon Press London 1961.

[7.7] Coward, H.F., Jones, G.W., U.S. Bur. Min. **503**, 1952

[7.8] Hustad, J.E., Sønju, O.K., Combust. Flame **71** (1988) 283–294

Lecture 8: Laminar Premixed Flames: Flames Shapes and Instabilities

The fundamental property of a premixed flame is its ability to propagate normal to itself with a burning velocity that, to first approximation, depends on thermo-chemical parameters of the premixed gas ahead of the flame only. In a steady flow of premixed gas a premixed flame will propagate against the flow until it stabilizes itself such that locally the flow velocity normal to the flame is equal to burning velocity. We have already discussed that for a Bunsen flame the condition of a constant burning velocity is violated at the top of the flame and that additional influences such as flame curvature must be taken into account. In this chapter we want to calculate flame shapes. We then will consider external influences that locally change the burning velocity and discuss the response of the flame to these disturbances.

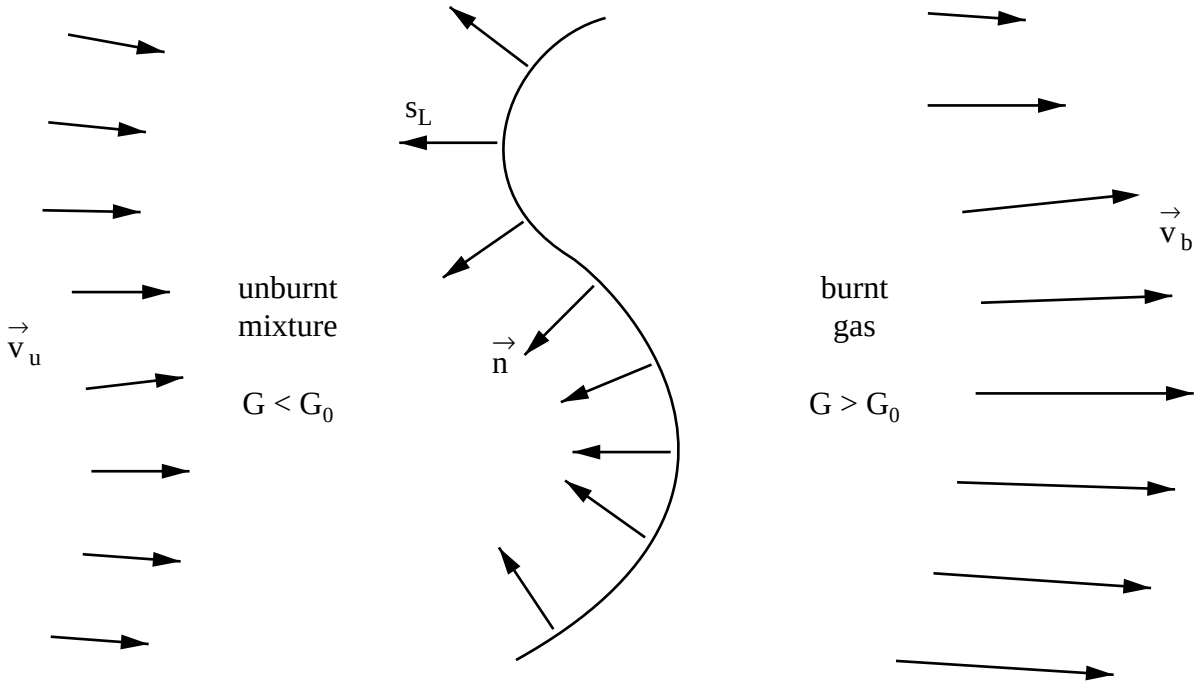

Fig. 8.1: Schematic illustration of a propagating flame with arbitrary shape

8.1 A Field Equation Describing the Flame Position

The kinematic relation (6.8) between the propagation velocity, the flow velocity, and the burning velocity that was derived for spherical flame propagation may be generalized by introducing the vector $\boldsymbol{n}$ normal to the flame and writing

$$\vec{n}\frac{\mathrm{d}\boldsymbol{x}}{\mathrm{d}t}\Big|_f = \boldsymbol{v}\,\boldsymbol{n} + s_L \tag{8.1}$$

where $\boldsymbol{x}_f$ is the vector describing the flame position, $(\mathrm{d}\boldsymbol{x}/\mathrm{d}t)_f$ the flame propagation velocity, and $\boldsymbol{v}$ the velocity vector.
The normal vector points towards the unburnt mixture and is given by

$$\boldsymbol{n} = -\frac{\nabla G}{|\nabla G|}\,. \tag{8.2}$$

where $G(\boldsymbol{x}, t)$ can be identified as a scalar field whose level surfaces

$$G(\boldsymbol{x}, t) = G_0 \tag{8.3}$$

where G_0 is arbitrary, represent the flame surface (conf. Fig 8.1). The flame contour $G(\boldsymbol{x}, t) = G_0$ divides the physical field into two regions where $G > G_0$ is the region of burnt gas and $G < G_0$ that of the unburnt mixture. If one differentiates (8.3) with respect to t at $G = G_0$, such as

$$\frac{\partial G}{\partial t} + \nabla G\,\frac{\partial \boldsymbol{x}}{\partial t}\Big|_{G=G_0} = 0\,, \tag{8.4}$$

one obtains with (8.2)

$$\frac{\partial G}{\partial t} = |\nabla G|\,\vec{n}\frac{\partial \boldsymbol{x}}{\partial t}\Big|_{G=G_0}\,. \tag{8.5}$$

Introducing (8.1) into (8.5) and identifying $(\mathrm{d}\boldsymbol{x}/\mathrm{d}t)_f$ as $(\mathrm{d}\boldsymbol{x}/\mathrm{d}t)_{G=G_0}$ one obtains the field equation

$$\rho\left(\frac{\partial G}{\partial t} + \boldsymbol{v}\,\nabla G\right) = (\rho s_L)\;|\nabla G|\,. \tag{8.6}$$

It will be called G-equation in the following. If the burning velocity s_L is defined with respect to the unburnt mixture, then $\rho = \rho_u$ the flow velocity $\boldsymbol{v}$ in (8.6) is defined as the conditioned velocity field in the unburnt mixture ahead of the flame. For a constant value of s_L the solution of (8.6) is non unique, and cusps will be formed where different parts of the flame intersect. Even an originally smooth ondulated front in a quiescent flow will form cusps and eventually become flatter with time as illustrated in Fig. 8.2. This is called Huygen's principle.

As an example of a closed form solution of the G-equation let us consider the case of a slot burner with a constant exit velocity u for premixed combustion, Fig. 8.3. This is the two-dimensional planar version of the axisymmetric Bunsen burner.

The G-equation takes the form

$$u\frac{\partial G}{\partial x} = s_L\sqrt{\left(\frac{\partial G}{\partial x}\right)^2 + \left(\frac{\partial G}{\partial y}\right)^2}\,. \tag{8.7}$$

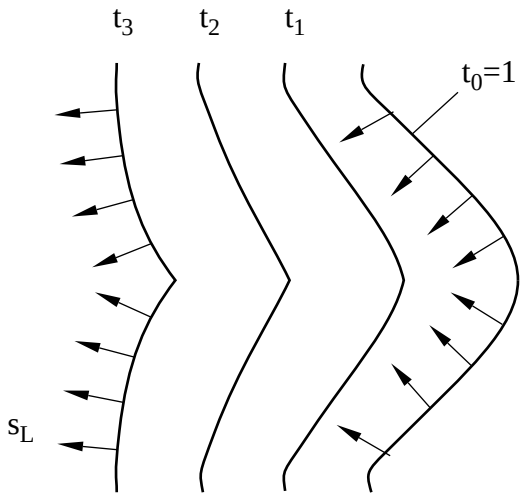

Fig. 8.2: Illustration of Huygens principle in flame propagation with constant s_L

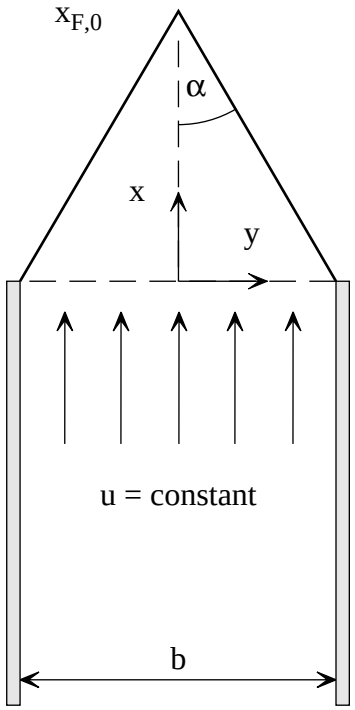

Fig. 8.3: A premixed laminar flame on a slot burner.

With the ansatz

$$G = x + F(y) \tag{8.8}$$

and $G_0 = 0$ one obtains

$$u = s_L \sqrt{1 + \left(\frac{\partial F}{\partial y}\right)^2} \tag{8.9}$$

leading to

$$F = \frac{\left(u^2 - s_L^2\right)^{1/2}}{s_L} |y| + \text{ const}\,. \tag{8.10}$$

As the flame is attached at $x = 0$, $y = \pm b/2$, where $G = 0$, this leads to the solution

$$G = \frac{\left(u^2 - s_L^2\right)^{1/2}}{s_L} \left(|y| - \frac{b}{2}\right) + x\,. \tag{8.11}$$

The flame tip lies with $|y| = 0$, $G = 0$ at

$$x_0 = \frac{b}{2} \frac{\left(u^2 - s_L^2\right)^2}{s_L} \tag{8.12}$$

and the flame angle α is given by

$$\tan\alpha = \frac{b/2}{x_0} = \frac{s_L}{\left(u^2 - s_L^2\right)^{1/2}} \tag{8.13}$$

With $\tan^2\alpha = \sin^2\alpha/(1 - \sin^2\alpha)$ it follows that

$$\sin\alpha = \frac{s_L}{u} \tag{8.13}$$

which is equivalent to (6.6).

This solution shows a cusp at the flame top $x = x_0$, $y = 0$. In order to obtain a rounded flame tip, one has to take modifications of the burning velocity due to flame curvature into account. This leads to the concept of flame stretch.

8.2 Flame stretch

Flame stretch consists of two contributions: One due to flame curvature and another due to flow divergence. It may be showen [8.1], [8.2] that for a one-step large activation energy reaction and with the assumption of constant propaties the burning velocity s_L is modified by these two effects as

$$s_L = s_L^0 - s_L^0\, \mathcal{L}\, \kappa + \mathcal{L}\, \boldsymbol{n} \cdot \nabla\, \boldsymbol{v} \cdot \boldsymbol{n}\,. \tag{8.15}$$

Here s_L^0 is the burning velocity for an unstretched flame and $\mathcal{L}$ is the Markstein length to the presented below. The flame curvature κ is defined as

$$\kappa = \nabla \cdot \boldsymbol{n} = -\nabla \cdot \left(\frac{\nabla G}{|\nabla G|}\right)\,, \tag{8.16}$$

which may be transformed as

$$\kappa = -\frac{\nabla^2 G}{|\nabla G|} + \frac{\nabla |\nabla G| \nabla G}{|\nabla G|^2} = -\frac{\nabla^2 G + \boldsymbol{n} \cdot \nabla |\nabla G|}{|\nabla G|} \,. \tag{8.17}$$

We will explore the influence of the curvature effect by considering the burnout of a spherical pocket of premixed gas by inward flame propagation. For this unsteady process the velocity within the pocket is assumed zero and the G-equation takes with (8.17) the form

$$\frac{\partial G}{\partial t} = s_L^0 \left[\left| \frac{\partial G}{\partial r} \right| + \mathcal{L} \left(\frac{1}{r^2} \frac{\partial}{\partial r} \left(r^2 \frac{\partial G}{\partial r} \right) - \frac{\partial}{\partial r} \left| \frac{\partial G}{\partial r} \right| \right) \right] . \tag{8.18}$$

For the solution of (8.18) the ansatz

$$G = r - r_F(t) \tag{8.19}$$

leads to

$$\frac{\partial r_F}{\partial t} = -s_L^0 \left(1 + \frac{2\mathcal{L}}{r_F} \right) \tag{8.20}$$

where $G = 0$, $r = r_F$ at the flame front has been used. This may be integrated to obtain the time t in term s of $r_F(t)$

$$s_L^0 t = -\left(r_F - r_{F,0} \right) + 2\mathcal{L} \ln \left(\frac{r_F + 2\mathcal{L}}{r_{F,0} + 2\mathcal{L}} \right) \tag{8.21}$$

which is plotted in non-dimensional form in Fig. 8.4. At $t = 0$ the initial flame radius $r_{F,0}$ was taken as $10\mathcal{L}$.

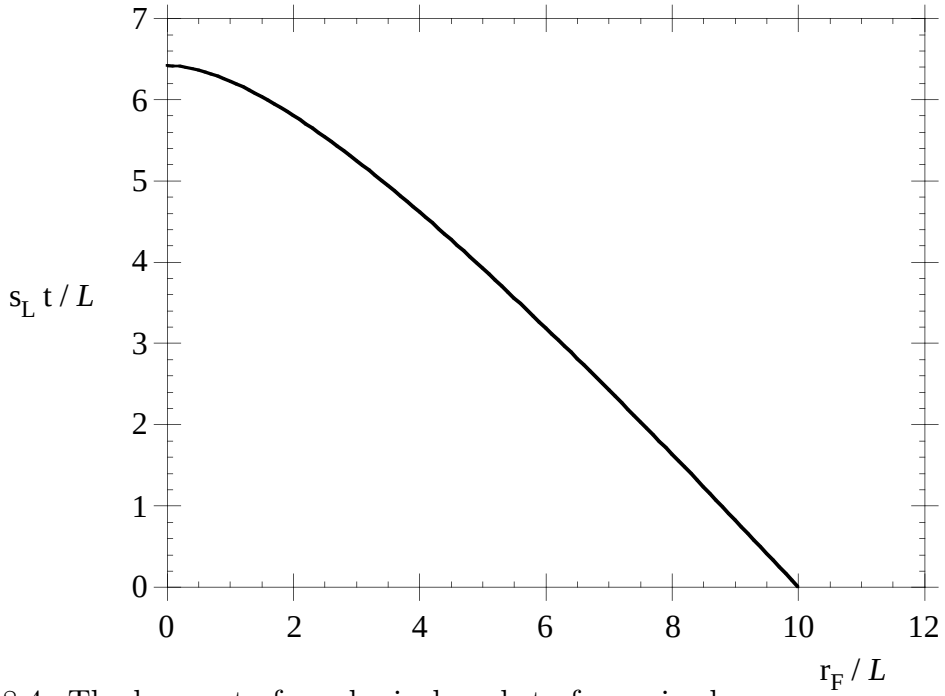

Fig. 8.4: The burnout of a spherical pocket of premixed gas.

It is seen that the burnout accelerates as the pocket becomes smaller and the curvature effect increases.

The Markstein length is a quantity of the order of the flame thickness. For the case of a one-step large activation energy reaction and a constant thermal conductivity λ, dynamic viscosity μ and heat capacity c_p, the ratio of $\mathcal{L}$ to the flame thickness l_F is

$$\frac{\mathcal{L}}{\ell_F} = \frac{1}{\gamma}\ln\frac{1}{1-\gamma} + \frac{\mathrm{Ze}(\mathrm{Le}-1)}{2}\,\frac{(1-\gamma)}{\gamma}\int_0^{\gamma/(1-\gamma)}\frac{\ln(1+x)}{x}\,dx\,. \tag{8.22}$$

This expression was first derived by Clavin and Williams [8.3]. Here $\gamma = (T_b - T_u)/T_b$ where T_b and T_u are the temperatures in the burnt and the unburnt gas, respectively, $\mathrm{Ze} = E(T_b - T_u)/\mathrm{R}T_b^2$ is the Zeldovich number, where E is the activation energy and R the universal gas constant, and $\mathrm{Le} = \lambda/\rho\, c_p\, D$ is the Lewis number of the reactant, assumed constant, where D is the molecular diffusivity. The flame thickness is $\ell_F = \lambda/(\rho\, c_p\, s_L)$. Equation (8.22) was derived with respect to the unburnt mixture. Clavin [8.1] shows that with respect to the burnt gas one obtains a similar but different expression where the factor $(1-\gamma)$ in the nominator of the second term is missing. This increases the influence of Lewis number effects since the term $(1-\gamma)$ is equal to T_u/T_b, which is typically between 0.15 and 0.2 in technical flames. For the four-step asymptotic model for methane presented in lecture 7 the same expression as (8.22) can be derived with the Zeldovich number replaced by $\mathrm{Ze} = 4/\varepsilon z_0$ as in (7.50) [8.4]. Experimental values for the ratio in (8.22) range typically from $\mathcal{L}/\ell_F = 2$ to $\mathcal{L}/\ell_F = 6$ (Searby and Quinard [8.5]). The last term in (8.15), the flame stretch due to flow divergence, will not be discussed here but in the context of turbulent premixed flames, lecture 14.

8.3 Flame Front Instability

As it was discussed in lecture 6 gas expansion in the flame front will lead to a deflection of a stream line that enters the front with an angle. This is shown in Fig. 8.5 where a slightly ondilated flame front in the x-y coordinate system is assumed.

A stream tube with cross-sectional area A_0 and upstream flow velocity $u_{-\infty}$ widens due to flow-divergence ahead of the flame. This divergence effect is generated by the expansion at the front that induces a flow component normal to the flame contour. As the stream lines cross the front they are deflected. At large distances from the front the stream lines are parallel again, but the downstream velocity is $u_\infty = (\rho_u/\rho_b)u_{-\infty}$. At the cross section A_1, where the density is still equal to ρ_u the flow velocity due to continuity and the widening of the stream tube is

$$u_1 = \frac{A}{A_1}u_{-\infty} < u_{-\infty}$$

Since the unperturbed flame propagates with $u_{-\infty} = s_L$ the burning velocity is larger than u_1 and the flame will propagate upstream and thereby enhance the initial pertubation.

In the following we will neglect viscous and gravity effects and treat the flame as a discontinuity in density that propagates normal to itself. While the influence of the

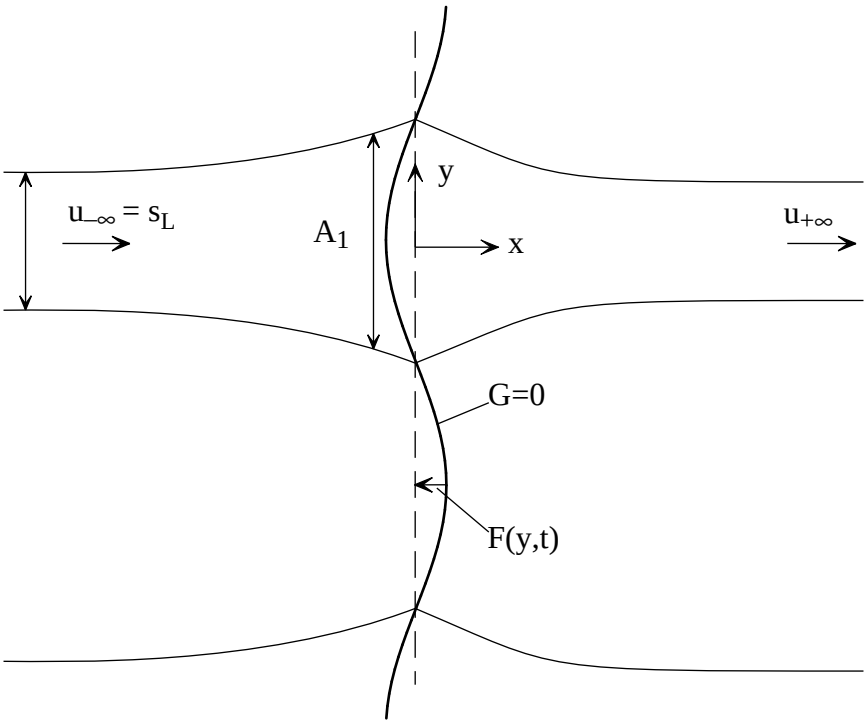

Fig. 8.5: Illustration of the hydro-dynamic instability

flame curvature on the burning velocity is retained, flame stretch due to flow divergence is neglected (see [8.7]). The burning velocity is then given by

$$s_L = s_{L_0}\,(1 + \chi\mathcal{L})\ . \tag{8.23}$$

The velocity components u and v will be normalized with the burning velocity s_{Lu} (defined with respect to the unburnt mixture), the coordinates x and y with the flame thickness ℓ_F and the time with ℓ_F/s_{Lu}. As a reference value for the density we take ρ_u, introduce the density rate $r = \frac{\rho_b}{\rho_u}$ and normalize the pressure with $\rho_u s_{Lu}^2$.

$$\begin{aligned} u^* &= u/s_{Lu}\,, \quad v^* = v/s_{Lu}\,, \quad p^* = \frac{p}{\rho_u s_{Lu}^2}\,, \\ x^* &= x/\ell_F\,, \quad y^* = y/\ell_F\,, \quad t^* = t s_{Lu}/\ell_F\,. \end{aligned} \tag{8.24}$$

The non-dimensional governing equations are then (with the asterisks removed)

$$\begin{aligned} u_x + v_y &= 0 \\ u_t + uu_x + vu_y + \frac{1}{\rho}p_x &= 0 \\ v_t + uv_x + vv_y + \frac{1}{\rho}p_y &= 0 \end{aligned} \tag{8.25}$$

where $\rho_u = 1$ and $\rho_b = r$ in the unburnt and burnt mixture respectively. The G-field is described by

$$G = x - F(y,t)\,. \tag{8.26}$$

With equations (8.2) and (8.5) the normal vector $\vec{n}$ and the normal propagation velocity then are

$$\boldsymbol{n} = \left(\frac{-1}{\sqrt{1+F_y^2}}, \frac{F_y}{\sqrt{1+F_y^2}} \right)\,, \qquad \boldsymbol{n}\frac{\mathrm{d}\boldsymbol{x}}{\mathrm{d}t}\Big|_{G=G_0} = \frac{-F_t}{\sqrt{1+F_y^2}}\,. \tag{8.27}$$

Due to the discontinuity in density at the flame front, the Euler equations (8.25) are only valid on either side of the front, but do not hold across it. Therefore jump conditions for mass and momentum conservation across the discontinuity are introduced (conf. [8.6], p. 13):

$$\begin{aligned} (r-1)\boldsymbol{n}\frac{\mathrm{d}\boldsymbol{x}}{\mathrm{d}t} &= (r\boldsymbol{v}_+ - \boldsymbol{v}_-)\boldsymbol{n} \\ (r\boldsymbol{v}_+ - \boldsymbol{v}_-)\boldsymbol{n}\frac{\mathrm{d}\boldsymbol{x}}{\mathrm{d}t} &= r\boldsymbol{v}_+\boldsymbol{v}_+\boldsymbol{n} + p_+\boldsymbol{n} - \boldsymbol{v}_-\boldsymbol{v}_-\boldsymbol{n} - p_-\boldsymbol{n}\,. \end{aligned} \tag{8.28}$$

Here the subscripts "+" and "−" refer to the burnt and the unburnt gas respectively and denote the properties immediately downstream and upstream of the flame front. In terms of the u and v components the jump conditions are written

$$\begin{aligned} (r-1)F_t &= ru_+ - u_- - F_y(rv_+ - v_-) \\ (ru_+ - u_-)F_t &= ru_+(u_+ - F_y v_+) - u_-(u_- - F_y v_-) + p_+ - p_- \\ (rv_+ - v_-)F_t &= rv_+(u_+ - F_y v_+) - v_-(u_- - F_y v_-) - F_y(p_+ - p_-)\,. \end{aligned} \tag{8.29}$$

With the coordinate transformation:

$$x = \xi + F(\eta,\tau), \quad y = \eta, \quad t = \tau \tag{8.30}$$

we fix the discontinuity at $\xi = 0$. Under the assumption of small perturbations of the front, the unknowns are expanded as

$$\begin{aligned} u &= U + \varepsilon u, \quad v = \varepsilon v \\ p &= P + \varepsilon p, \quad F = \varepsilon f \end{aligned} \tag{8.31}$$

where ε is an asymptotically small parameter. Inserting (8.30) into the jump conditions one obtains to the leading order the steady-state solution

$$\begin{aligned} U_- &= 1, \qquad P_- = 0 \\ U_+ &= 1/r, \quad P_+ = (r-1)/r\,. \end{aligned} \tag{8.32}$$

and to first order

$$\begin{aligned} (r-1)f_\tau &= ru_+ - u_- \\ 0 &= 2(u_+ - u_-) + p_+ - p_- \\ 0 &= v_+ - v_- + \frac{1-r}{r} f_\eta \end{aligned} \tag{8.33}$$

where the leading order mass flux $\dot{m}'' = rU_+ = U_-$ has been set equal to 1. To first order the equations for the perturbed quantities on both sides of the flame front now read

$$\begin{aligned} u_\xi + v_\eta &= 0 \\ u_\tau + Uu_\xi + \frac{1}{\rho}p_\xi &= 0 \\ v_\tau + Uv_\xi + \frac{1}{\rho}p_\eta &= 0 \end{aligned} \tag{8.34}$$

where $\rho = 1$ for $\xi < 0$ (unburnt gas) and $\rho = r$ for $\xi > 0$ (burnt gas) is to be used. To test the solutions for instability, we want them of such structure that the perturbations increase with time, are periodic in the η-direction and vanish for $\xi \to \pm\infty$. Since the system is linear, the solution may be written as

$$\boldsymbol{w} = \begin{pmatrix} u \\ v \\ p \end{pmatrix} = \boldsymbol{w}_0 \exp(\alpha\xi) \exp(\sigma\tau - ik\eta) \tag{8.35}$$

$$\overline{\overline{A}}\ \boldsymbol{w} = 0 \tag{8.36}$$

where σ is the non-dimensional growth rate and k the non-dimensional wave number. Introducing this into (8.32) one obtains a linear system where the matrix $\overline{\overline{A}}$ is given by

$$\overline{\overline{A}} = \begin{pmatrix} \alpha & -ik & 0 \\ \sigma + \alpha U & 0 & \alpha/\rho \\ 0 & \sigma + \alpha U & -ik/\rho \end{pmatrix} . \tag{8.37}$$

The eigenvalues of $\overline{\overline{A}}$ are obtained by setting $\det|A| = 0$. This leads to the characteristic equation

$$\det|A| = \frac{1}{\rho}(k^2 - \alpha^2)(\sigma + \frac{\alpha}{\rho}) = 0\,. \tag{8.38}$$

Here again $U = 1/\rho$, $\rho = r$ for $\xi > 0$ and $\rho = 1$ for $\xi < 0$ were used. There are three solutions of (8.38) for the eigenvalues α_j, where positive values satisfy the upstream ($\xi < 0$) and negative values the downstream ($\xi > 0$) boundary conditions of (8.34). Therefore

$$\begin{aligned} \xi > 0: &\quad \alpha_1 = -r\sigma, \quad \alpha_2 = -k \\ \xi < 0: &\quad \alpha_3 = k\,. \end{aligned} \tag{8.39}$$

The corresponding eigenvectors $w_{0,j}$ are determined by introducing the eigenvalues α_j ($j = 1, 2, 3$) into $\overline{\overline{A}}$ and solving again

$$\overline{\overline{A}}\ \boldsymbol{w}_j = 0\,. \tag{8.40}$$

This leads to

$$
\begin{aligned}
j=1: \quad & w_{0,1} = a \begin{pmatrix} 1 \\ ir\sigma/k \\ 0 \end{pmatrix} \\
j=2: \quad & w_{0,2} = b \begin{pmatrix} 1 \\ i \\ -1+r\sigma/k \end{pmatrix} \\
j=3: \quad & w_{0,3} = c \begin{pmatrix} 1 \\ -i \\ -1-\sigma/k \end{pmatrix} .
\end{aligned}
$$

In terms of the original unknowns u, v and p the solution is now

$$
\begin{aligned}
\xi > 0: \quad & \begin{pmatrix} u \\ v \\ p \end{pmatrix} = \left\{ a \begin{pmatrix} 1 \\ ir\sigma/k \\ 0 \end{pmatrix} e^{-r\sigma\xi} + b \begin{pmatrix} 1 \\ i \\ -1+r\sigma/k \end{pmatrix} e^{-k\xi} \right\} e^{\sigma\tau - ik\eta} \\
\xi < 0: \quad & \begin{pmatrix} u \\ v \\ p \end{pmatrix} = c \begin{pmatrix} 1 \\ -i \\ -1-\sigma/k \end{pmatrix} e^{(k\xi+\sigma\tau-ik\eta)} .
\end{aligned}
\tag{8.41}
$$

For the perturbation $f(\eta,\tau)$ the form

$$
f = \tilde{f} e^{\sigma\tau - ik\eta} \tag{8.42}
$$

will be introduced.
Inserting (8.17), (8.26) and (8.31) into the non-dimensional G-equation

$$
\rho \left(\frac{\partial G}{\partial t} + u\frac{\partial G}{\partial x} + v\frac{\partial G}{\partial y} \right) = \sqrt{\left(\frac{\partial G}{\partial x}\right)^2 + \left(\frac{\partial G}{\partial y}\right)^2}\, \rho s_{L_0} \left(1 + \chi\mathcal{L}\right)
$$

satisfies to leading order (8.32) and $x = 0_-$, $x = 0_+$ respectively and leads to first order to

$$
\begin{aligned}
u_- &= f_\tau - f_{\eta\eta}\mathcal{L} \\
u_+ &= f_\tau - \frac{f_{\eta\eta}}{r}\mathcal{L} .
\end{aligned}
\tag{8.43}
$$

With (8.42) the jump conditions (8.33) can be written as

$$
\begin{aligned}
(r-1)\sigma\tilde{f} &= r(a+b) - c \\
0 &= 2a + b\left(1 + r\frac{\sigma}{k}\right) + c\left(\frac{\sigma}{k} - 1\right) \\
\frac{1-r}{r} k\tilde{f} &= a\frac{\sigma}{k} + b + c
\end{aligned}
\tag{8.44}
$$

and (8.43) then reads

$$\begin{aligned} c &= \sigma\tilde{f} + k^2\mathcal{L} \\ a + b &= \sigma\tilde{f} + \frac{k^2\mathcal{L}}{r}\,. \end{aligned} \tag{8.45}$$

Since equation $(8.44)_1$ is linear dependent from equations $(8.45)_{1,2}$ it is dropped and the equations $(8.44)_{2,3}$ and $(8.45)_{1,2}$ remain for the determination of a, b, c and $\sigma(k)$. Dividing all equations by $k\tilde{f}$ one obtains four equations for $\hat{a} = k\tilde{f}$, $\hat{b} = b/k\tilde{f}$, $\hat{c} = c/k\tilde{f}$ and $\varphi = \frac{\sigma}{k}$. The elimination of the first three unknown yields the equation

$$\varphi^2(1+r) + 2\varphi(1+k\mathcal{L}) + \frac{2k\mathcal{L}}{r} + \frac{r-1}{r} = 0\,. \tag{8.46}$$

The solution may be written in terms of dimensional quantities as

$$\sigma = \frac{s_{L_0}^- k}{1+r}\left\{\sqrt{1 + k^2\mathcal{L}^2 - \frac{2k\mathcal{L}}{r} + \frac{1-r^2}{r}} - (1+k\mathcal{L})\right\} \tag{8.47}$$

Here only the positive root of (8.46) has been taken since it refers to possible solutions with exponential growing amplitudes. (8.47) is the dispersion relation which shows that the perturbation f grows exponentially in time only for a certain wavenumber range $0 < k < k^*$ with $k^* = \frac{r-1}{2\mathcal{L}}$.

For perturbations at wavenumbers $k > k^*$ a plane flame of infinitively small thickness, described as a discontinuity in density, velocity and pressure is unconditionally stable. This is due to the influence of the front curvature on the burning velocity. As one would expect on the basis of simple thermal theories of flame propagation, the burning velocity increases when the flame front is concave and decreases when it is convex towards the unburnt gas, so that initial perturbations are smoothened.

However, hydronamic and curvature effects are not the only influencing factors for flame front stability. Flame stretch due to flow divergence, gravity (in a downward propagating flame) and the thermo-diffusive effect with a Lewis number larger unity are stabilizing effects. A more detailed discussion of these phenomena may be found in [8.1] and [8.6].

Exercise 8.3.1

Under the assumption of a constant burning velocity $s_L = s_{L_0}$ the linear stability analysis leads to the following dispersion relation

$$\sigma = \frac{s_{L_0}^- k}{r+1}\left\{\sqrt{1 + \frac{1-r^2}{r}} - 1\right\}\,. \tag{8.48}$$

Validate this expression by inserting $\mathcal{L} = 0$ in (8.47). What is the physical meaning of this result? What effect has the front curvature on the flame front stability?

Solution:

The dispersion relation for constant burning velocity $s_L = s_{L_0}$, (8.48), shows that the perturbation f grows exponentially in time for all wavenumbers. The growth rate σ is proportional to the wavenumber k and always positive since the density rate r is less than unity. This means that a plane flame front with constant burning velocity is unstable to any perturbation. The front curvature has a stabilizing effect on the flame front stability. As it is shown in 8.3, the linear stability analysis for a burning velocity with the curvature effect retained leads to instability of the front only for the wavenumber range $0 < k < k^* = \frac{r-1}{2\mathcal{L}}$, whereas the front is stable to all perturbations with $k > k^*$.

8.4 Extinction of a Plane Flame by Volumetric Heat Loss

An additional influence that affects the stability of flames is volumetric heat loss. In order to analyse this effect we will consider for simplicity a one-step model with a large activation energy and unity Lewis number and the four-step model derived in lecture 7 where α is a heat loss coeffizient. For thin gas radiation it may be related to radiative emission and (8.49) may be interpreted as a lincarized version of radiativ heat exchange. We will assume that the volumetric heat loss is proportional to the temperature difference $T - T_u$ and write

$$q_R = -\alpha(T - T_u)\,. \tag{8.48}$$

The one-dimensional temperature equation for a steady state premixed flame is then written as

$$\rho_u s_L \frac{\mathrm{d}T}{\mathrm{d}x} = \frac{\mathrm{d}}{\mathrm{d}x}\left(\frac{\lambda}{c_p}\frac{\mathrm{d}T}{\mathrm{d}x}\right) + \frac{Q}{c_p}w - \frac{\alpha}{c_p}(T - T_u)\,. \tag{8.49}$$

In terms of the nondimensional quantities defined in (6.25)—(6.27) this may be written (with the asterisks removed)

$$M\frac{\mathrm{d}T}{\mathrm{d}x} = \frac{\mathrm{d}^2T}{\mathrm{d}x^2} + w - \pi T\,. \tag{8.50}$$

Here M is the burning velocity of the plane flame with heat loss normalized by the reference burning velocity $s_{L,\mathrm{ref}}$ of a plane flame without heat loss

$$M = \frac{s_L}{s_{L,\mathrm{ref}}}\,. \tag{8.51}$$

The non-dimensional heat loss parameter is defined

$$\pi = \frac{\lambda\alpha}{\rho_u^2 s_{L,\mathrm{ref}}^2 c_p^2}\,. \tag{8.52}$$

It will be assumed constant with λ evaluated at $T = T_0$. It should be noted here that π increases rapidly as $s_{L,\mathrm{ref}}$ decreases. Therefore heat loss has a strong influence close to the flammability limit when $s_{L,\mathrm{ref}}$ is small.

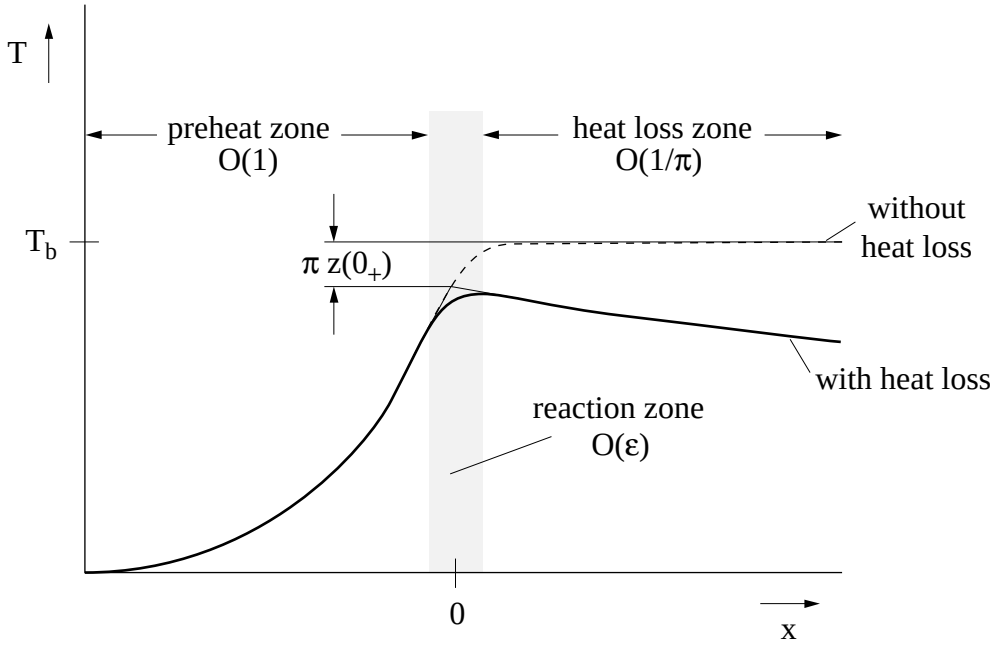

Fig. 8.6: Structure of a premixed flame with heat loss

The structure of a premixed flame with heat loss is shown in Fig. 8.6. We will treat π as a small expansion parameter and expand the temperature as

$$T = T_0(1 + \pi z) \tag{8.53}$$

where T_0 is the leading order temperature. The reaction term w in (8.49) can be eliminated by coupling it with the equation (6.22) for the fuel mass fraction. In non-dimensional form one then obtains the enthalpy

$$h = T + Y - 1 \tag{8.54}$$

governed by the equation

$$M\frac{\mathrm{d}h}{\mathrm{d}x} = \frac{\mathrm{d}^2h}{\mathrm{d}x^2} - \pi T\,. \tag{8.55}$$

This equation may be integrated across the thin reaction zone from $x = -\infty$ to $x = 0_+$. This leads to

$$Mh(0_+) = \left.\frac{\mathrm{d}h}{\mathrm{d}x}\right|_{0_+} - \pi \int_{-\infty}^{0_+} T_0 \mathrm{d}x \tag{8.56}$$

since at $x \to -\infty$ the enthalpy and its gradient vanishes. Introducing (8.53) into (8.54) at $x = 0_+$, where $T_0 = 1$ and $Y = 0$ one obtains

$$h(0_+) = \pi z(0_+)\,. \tag{8.57}$$

The integral over the preheat zone in (8.56) may evaluated by integrating the temperature equation (8.50) to lesding order

$$M\frac{\mathrm{d}T_0}{\mathrm{d}x} = \frac{\mathrm{d}^2T_0}{\mathrm{d}x^2} \tag{8.58}$$

leading to

$$T_0 = \exp(Mx) \quad \text{for} \quad x < 0\,. \tag{8.59}$$

The downstream enthalpy gradient at the flame front is equal to the downstream temperature gradient since $Y = 0$ for $x \geq 0$. It can be evaluated by realizing that the heat loss region behind the flame is broad of order $\mathrm{O}(\pi^{-1})$. This suggest the introduction of a contracted coordinate

$$\tilde{x} = \pi x \tag{8.60}$$

into the downstream temperature equation

$$M\frac{\mathrm{d}T}{\mathrm{d}\tilde{x}} = \pi\frac{\mathrm{d}^2T}{\mathrm{d}\tilde{x}^2} - T \qquad x > 0\,. \tag{8.61}$$

In the limit $\pi \to 0$ the heat conduction term can now be neglected and with $T_0(0_+) = 1$ one obtains to leading order

$$\left.\frac{\mathrm{d}h}{\mathrm{d}x}\right|_{0_+} = \left.\frac{\mathrm{d}T}{\mathrm{d}x}\right|_{0_+} = -\frac{\pi}{M}\,. \tag{8.62}$$

With (8.57), (8.59) and (8.62) inserted into (8.56) the flame temperature pertubation is

$$z(0_+) = -\frac{2}{M^2}\,, \tag{8.63}$$

since for a one step flame with a large activation energy the burning velocity depends according to (6.52) on the flame temperature as

$$s_L^2 \sim \exp\left(-\frac{E}{RT_b}\right)\,. \tag{8.64}$$

A temperature pertubation of the form (8.53) will lead to

$$M = \exp\left(\pi\,\mathrm{Ze}\,z(0_+)\right) \tag{8.65}$$

When this is combined with (8.63) one obtains

$$M^2\ln M^2 = -2\pi\mathrm{Ze}\,. \tag{8.66}$$

A similar analysis may be performed for the four-step asymptotic analysis of methane flames. Then, since with (7.44)

$$s_L^2 \sim (T_b - T^0)^4 \tag{8.67}$$

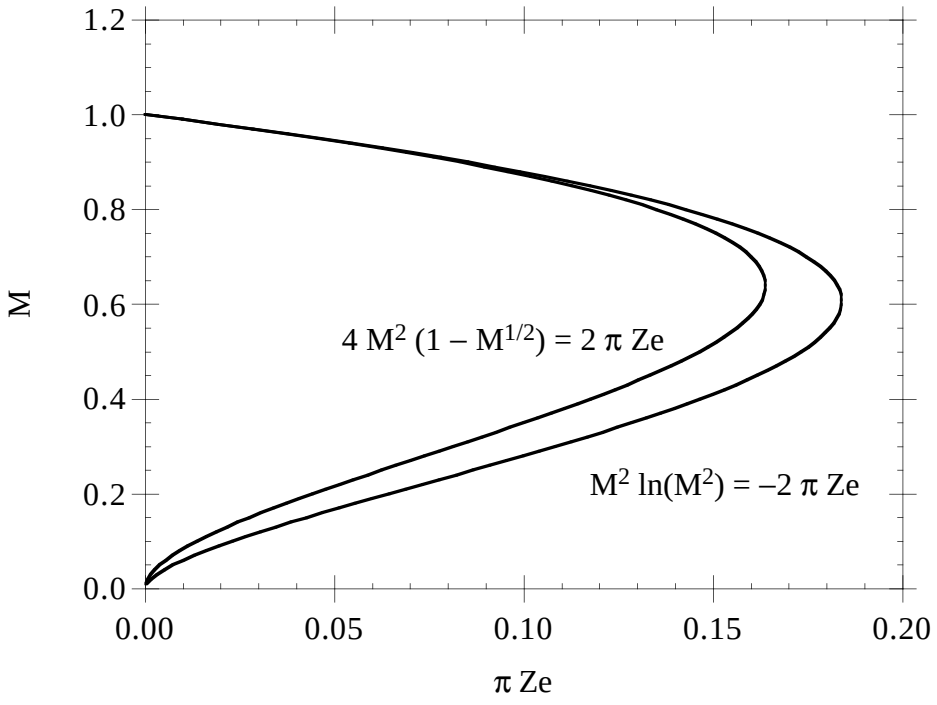

Fig. 8.7: The change of burning velocity and flame extinction due to heat loss for one-step and four-step asymptotics

one obtains with (7.45) and (7.50)

$$M^2 = \frac{\left(T_b - T^0 + T_b \pi z(0_+)\right)^4}{(T_b - T^0)^4} = \left(1 + \frac{\pi \mathrm{Ze} z(0_+)}{4}\right)^4 , \tag{8.68}$$

since $T_b/(T_b - T^0) = 1/(\varepsilon z_0) = \mathrm{Ze}/4$ to leading oeder. If this is now combined with (8.64) one obtains

$$4M^2 \left(1 - M^{1/2}\right) = 2\pi \mathrm{Ze} \tag{8.69}$$

instead of (8.66). Both equations, (8.66) and (8.69), are plotted in Fig. 8.7 showing a qualitatively and even quantitatively very similar behaviour.

Only the upper branch of these curves represents a stable solution. It shows a decrease of the burning velocity as the heat loss parameter π increases. There is a maximum value for the product πZe for each of these curves beyond which no solution exists. At this value heat loss extinguishes the flame. The non-dimensional burning rates at which this happens are very close to each other: $M_{\mathrm{ex}} = 0.61$ for the one step kinetics and $M_{\mathrm{ex}} = 0.64$ for the four-step kinetics. This is surprising because the kinetics for both cases are fundamentally different. This supports again, as it was already pointed out for the Markstein length, that the one-step large activation energy model is a good approximation for predicting the response of hydrocarbon flames to external pertubations.

References

[8.1] Clavin, P., Dynamic behaviour of premixed flame fronts in laminar and turbulent flows, Progr. Energy Combust. Sci. **11** (1985), pp. 1–59.

[8.2] Matalon, M.,Matkowsky, B.J., Flames as gasdynamics discontinuities, J. Fluid Mech. **124** (1982), pp. 239–259.

[8.3] Clavin, P., Williams, F.A., Effects of molecular diffusion and thermal expansion on the structure and dynamics of premixed flames in turbulent flows of large scale and low intensity, J. Fluid Mech. **116** (1982), pp. 251–282.

[8.4] Rogg, B., Peters, N., Comb. Flame **79** (1990), pp 402–420

[8.5] Searby, G., Quinard, J., Direct and Indirect Measurements of Markstein Numbers of Premixed Flames, Comb. Flame **82** (1990), pp 298–311

[8.6] Williams, F.A., "Combustion Theory", Second Edition, The Benjamin Cummings Publishing Co. Menlo Park Ca. 1985.

[8.7] Markstein, G.H., "Experimental and Theoretical Studies of Flame Front Stability", J. Aeronautical Sciences, March (1951), pp. 199-209.

Lecture 9: Laminar Diffusion Flames: Flame Structure

In this lecture we will consider systems where fuel and oxidizer enter separately into the combustion chamber initially non-premixed. Mixing then takes place by convection and diffusion. Only where fuel and oxidizer are mixed on the molecular level, chemical reactions can occur. This is why flames in non-premixed combustion are called diffusion flames. A classical example of a diffusion flame is a candle flame shown in Fig. 9.1.

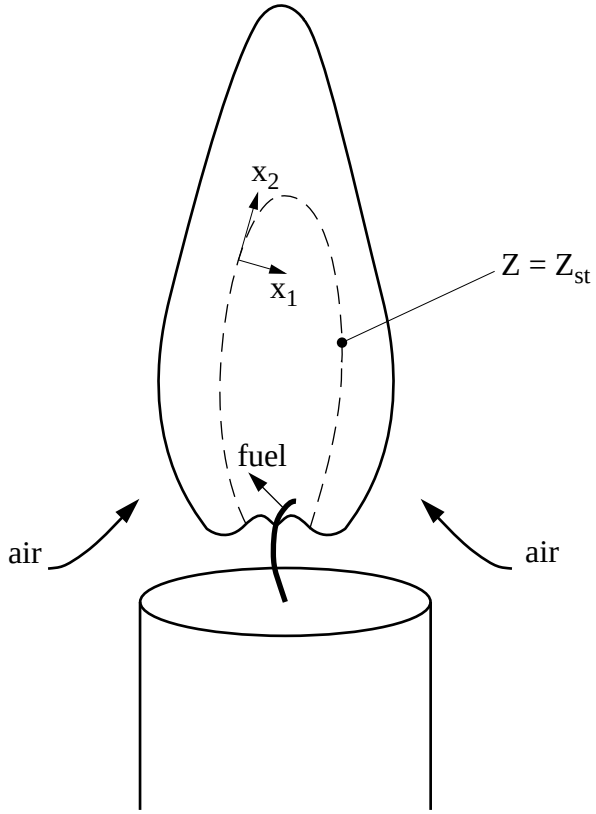

Fig. 9.1: The candle flame as the classical example of a laminar diffusion flame

Its structure is similar to that shown in the introduction, except that the flow entraining the air into the flame is driven by buoyancy rather than by forced convection as in a jet flame. The paraffin of the candle first melts due to radiative heat from the flame to the candle, mounts by capillary forces into the wick where it then evaporates to become paraffin vapor, a gaseous fuel.

In this lecture we will focus on the structure of the combustion zones in a diffusion flame. These are best described by an asymptotic expansion for very fast chemistry starting from the limit of complete combustion. To leading order one obtains the adiabatic flame

temperature which is a function of mixture fraction only as already shown in lecture 1. The asymptotic expansion around this limit will then describe the influence of finite rate chemistry. If the expansion takes the temperature sensitivity of the chemistry into account diffusion flame quenching can also be described. The quenching mechanism is similar to that described for the continuously stirred reactor in lecture 4. It will be shown that by introducing the mixture fraction as an independent coordinate for all reacting scalars, a universal coordinate transformation leads in the limit of sufficiently fast chemistry to a one-dimensional problem for the reaction zone. This is the basis of the flamelet formulation for non-premixed combustion.

9.1 Flamelet Structure of a Diffusion Flame

Under the condition that equal diffusivities of chemical species and temperature can be assumed (an assumption that is good for hydrocarbon flames but much less realistic for hydrogen flames), all Lewis numbers

$$\mathrm{Le}_i = \lambda / \left(c_p \rho D_i\right) = 1 \quad (i = 1, 2, ..., n) \tag{9.1}$$

are unity, and a common diffusion coefficient $D = \lambda/(\rho c_p)$ can be introduced. The balance equation for Z, (5.51), and the temperature T, (5.39), are in cartesian coordinates

$$\rho \frac{\partial Z}{\partial t} + \rho v_\alpha \frac{\partial Z}{\partial x_\alpha} - \frac{\partial}{\partial x_\alpha}\left(\rho D \frac{\partial Z}{\partial x_\alpha}\right) = 0\,, \tag{9.2}$$

$$\rho \frac{\partial T}{\partial t} + \rho v_\alpha \frac{\partial T}{\partial x_\alpha} - \frac{\partial}{\partial x_\alpha}\left(\rho D \frac{\partial T}{\partial x_\alpha}\right) = \sum_{k=1}^{r} \frac{Q_k}{c_p} w_k + \frac{q_R}{c_p} + \frac{1}{c_p}\frac{\partial p}{\partial t}\,. \tag{9.3}$$

Here the low Mach number limit that leads to zero spatial pressure gradients has been employed, but the temporal pressure change $\partial p/\partial t$ has been retained. The heat capacity c_p is assumed constant for simplicity. The equations (5.40) for the mass fractions of the species could also have been written down and can be analyzed in a similar way as the temperature equation. They are omitted here for brevity. Equation (9.2) does not contain a chemical source term, since Z represents the chemical elements originally contained in the fuel, and elements are conserved during combustion. We assume the mixture fraction Z to be given in the flow field as a function of space and time by solution of (9.2) as shown schematically in Fig. 5.2. Then the surface of the stoichiometric mixture can be determined from

$$Z(x_\alpha, t) = Z_{\mathrm{st}}\,.$$

Combustion occurs in a thin layer in the vicinity of this surface if the local mixture fraction gradient is sufficiently high. Let us locally introduce an orthogonal coordinate system x_1, x_2, x_3, t attached to the surface of a stoichiometric mixture as as shown in Fig. 9.1, where x_1 points normal to the surface $Z(x_\alpha, t) = Z_{\mathrm{st}}$ and x_2 and x_3 lie within the surface. We replace the coordinate x_1 by the mixture fraction Z and x_2, x_3 and t by $Z_2 = x_2$, $Z_3 = x_3$ and $t = \tau$. This is a coordinate transformation of the Crocco type. (Crocco expressed the temperature in a flat-plate boundary layer as functions of another dependent variable, the

velocity.) Here the temperature T, and similarly the mass fractions, will be expressed as a function of the mixture fraction Z. By definition, the new coordinate Z is locally normal to the surface of the stoichiometric mixture. With the transformation rules

$$\begin{aligned} \frac{\partial}{\partial t} &= \frac{\partial}{\partial \tau} + \frac{\partial Z}{\partial t}\frac{\partial}{\partial Z}\,, \\ \frac{\partial}{\partial x_k} &= \frac{\partial}{\partial Z_k} + \frac{\partial Z}{\partial x_k}\frac{\partial}{\partial Z} \quad (k=2,3)\,, \\ \frac{\partial}{\partial x_1} &= \frac{\partial Z}{\partial x_1}\frac{\partial}{\partial Z} \end{aligned} \tag{9.4}$$

we obtain the temperature equation in the form

$$\begin{aligned} &\rho\left(\frac{\partial T}{\partial \tau} + v_2\frac{\partial T}{\partial Z_2} + v_3\frac{\partial T}{\partial Z_3}\right) - \frac{\partial(\rho D)}{\partial x_2}\frac{\partial T}{\partial Z_2} - \frac{\partial(\rho D)}{\partial x_3}\frac{\partial T}{\partial Z_3} \\ &- \rho D\left[\left(\frac{\partial Z}{\partial x_\alpha}\right)^2\frac{\partial^2 T}{\partial Z^2} + 2\frac{\partial Z}{\partial x_2}\frac{\partial^2 T}{\partial Z \partial Z_2} + 2\frac{\partial Z}{\partial x_3}\frac{\partial^2 T}{\partial Z \partial Z_3} + \frac{\partial^2 T}{\partial Z_2^2} + \frac{\partial^2 T}{\partial Z_3^2}\right] \\ &= \sum_{k=1}^{r}\frac{Q_k}{c_p}w_k + \frac{q_R}{c_p} + \frac{1}{c_p}\frac{\partial p}{\partial t}\,. \end{aligned} \tag{9.5}$$

If the flamelet is thin in the Z direction, an order-of-magnitude analysis similar to that for a boundary layer shows that the second derivative with respect to Z is the dominating term on the left-hand side of (9.5). This term must balance the terms on the right-hand side. All other terms containing spatial derivatives in x_2 and x_3 directions can be neglected to leading order. This is equivalent to the assumption that the temperature derivatives normal to the flame surface are much smaller than those in tangential direction. The term containing the time derivative in (9.5) is important only if very rapid changes, such as extinction, occur. Formally, this can be shown by introducing the stretched coordinate ξ and the fast time scale σ

$$\xi = (Z - Z_{\mathrm{st}})/\varepsilon\,, \quad \sigma = \tau/\varepsilon^2 \tag{9.6}$$

where ε is a small parameter, the inverse of a large Damköhler number or a large activation energy, for example, representing the width of the reaction zone.

If the time derivative term is retained, the flamelet structure is to leading order described by the one-dimensional time-dependent temperature equation

$$\rho\frac{\partial T}{\partial t} - \rho\frac{\chi}{2}\frac{\partial^2 T}{\partial Z^2} = \sum_{k=1}^{r}\frac{Q_k}{c_p}w_k + \frac{q_R}{c_p}\,. \tag{9.7}$$

Similar equations may be derived for the mass fractions. In Eq.(9.7)

$$\chi = 2D\left(\frac{\partial Z}{\partial x_\alpha}\right)^2 \tag{9.8}$$

is the instantaneous scalar dissipation rate. It has the dimension 1/s and may be interpreted as the inverse of a characteristic diffusion time. It may depend on t and Z and acts as a prescribed parameter in (9.7), representing the flow and the mixture field. As a result of the transformation, it implicitly incorporates the influence of convection and diffusion normal to the surface of the stoichiometric mixture. In the limit $\chi \to 0$, equations for the homogeneous reactor, analyzed in lecture 4, are obtained.

The neglection of all spatial derivatives tangential to the flame front is formally only valid in the thin reactionzone around $Z = Z_{\mathrm{st}}$. This is shown in [9.1]. There are, however, a number of typical flow configurations where (9.7) is valid in the entire Z-space. As example, we will analyze here the unsteady reacting mixing layer and the counterflow diffusion flame.

9.2 The Unsteady Mixing Layer

We consider the instationary interdiffusion of fuel and oxidizer in a quiescent flow field. The continuity equation then yields $\partial\rho/\partial t = 0$. The mixture fraction and the temperature are governed by the equations

$$\rho\frac{\partial Z}{\partial t} = \frac{\partial}{\partial y}\left(\rho D\frac{\partial Z}{\partial y}\right) \tag{9.9}$$

$$\rho\frac{\partial T}{\partial t} = \frac{\partial}{\partial y}\left(\rho D\frac{\partial T}{\partial y}\right) + \sum_{k=1}^{r}\frac{Q_k}{c_p}w_k + \frac{q_R}{c_p} + \frac{1}{c_p}\frac{\partial p}{\partial t} \tag{9.10}$$

with the initial and boundary conditions

$$\begin{aligned} t = 0: \quad & Z = 1\,, \quad T = T_1 \quad \text{for } y < 0, \quad Z = 0\,, \quad T = T_2 \quad \text{for } y > 0, \\ t > 0: \quad & Z = 1\,, \quad T = T_1 \quad \text{for } x \to -\infty, \quad Z = 0\,, \quad T = T_2 \quad \text{for } y \to +\infty. \end{aligned}$$

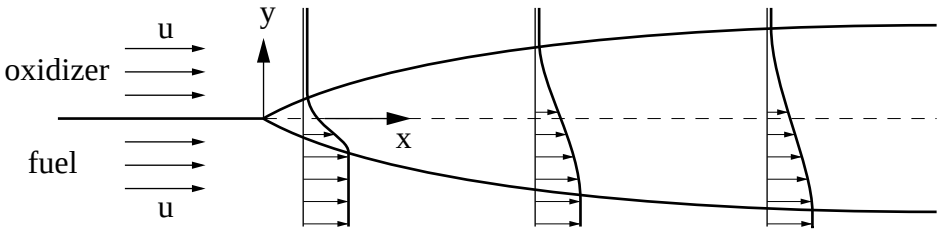

Fig. 9.2: The mixture fraction profile in the flow behind a splitter plate

Here t denotes the time and y the spatial coordinate. For a steady two-dimensional flow behind a splitter plate, shown in Fig. 9.2, which is of the boundary layer type, where the velocity u in x-direction depends only on x and the normal velocity v is zero, t may represent a transformed axial coordinate

$$t = \int_0^x u^{-1}(x)\,\mathrm{d}x\,. \tag{9.11}$$

Introducing the Chapman-Rubesin parameter

$$C = \frac{\rho^2 D}{(\rho^2 D)_0} \tag{9.12}$$

where the subscript 0 denotes the initial state for $y > 0$, for example, one obtains in terms of the similarity coordinate

$$\eta = \frac{1}{2}\left(D_0 t\right)^{-1/2} \int_0^y \frac{\rho}{\rho_0} \mathrm{d}y\,, \quad \tau = t \tag{9.13}$$

the equations

$$t\frac{\partial Z}{\partial t} - \frac{1}{2}\eta\frac{\partial Z}{\partial \eta} = \frac{\partial}{\partial \eta}\left(C\frac{\partial Z}{\partial \eta}\right) \tag{9.14}$$

$$t\frac{\partial T}{\partial t} - \frac{1}{2}\eta\frac{\partial T}{\partial \eta} = \frac{\partial}{\partial \eta}\left(C\frac{\partial T}{\partial \eta}\right) + \frac{t}{\rho c_p}\left(\sum_{k=1}^{r} Q_k w_k + q_R + \frac{\partial p}{\partial t}\right) \tag{9.15}$$

The mixture fraction equation has a steady state solution which, for the special case $C = 1$ is

$$Z = \frac{1}{2}\,\mathrm{erfc}\left(\eta\right) \tag{9.16}$$

where erfc is the complementary error function. If one now transforms (9.15) again by replacing the similarity coordinate η by Z one obtains

$$t\frac{\partial T}{\partial t} + \frac{\partial T}{\partial Z}\left[\frac{\partial Z}{\partial t} - \frac{1}{2}\eta\frac{\partial Z}{\partial \eta} - \frac{\partial}{\partial \eta}\left(C\frac{\partial Z}{\partial \eta}\right)\right] = C\frac{\partial^2 Z}{\partial \eta^2}\frac{\partial^2 T}{\partial Z^2} + \frac{t}{\rho c_p}\left(\sum_{k=1}^{r} Q_k w_k + q_R + \frac{\partial p}{\partial t}\right). \tag{9.17}$$

Since the term in square brackets is equal to (9.14) and therefore vanishes, (9.17) is identical to (9.7) if one reintroduces the transformation (9.13). Therefor the flamelet transformation is exact for the unsteady mixing layer and the steady two-dimensional flow behind a splitter plate. The scalar dissipation rate may be calculated using (9.16) as

$$\chi = \frac{1}{2\pi t}\exp\left(-2\eta^2(Z)\right)\,, \tag{9.18}$$

where for $C = 1$ the inverse of (9.16) can be used to express η in terms of Z

$$\eta(Z) = \mathrm{erfc}^{-1}\left(2Z\right)\,. \tag{9.19}$$

Here erfc^{-1} is the inverse (not the reciprocal) of the complementary error function. For small values of Z (large positive values of η) the complementary error function may be replaced by $\pi^{-1/2}\eta^{-1}\exp\left(-\eta^2\right)$ such that χ can be expressed as

$$\chi = 2Z^2\left[\mathrm{erfc}^{-1}(2Z)\right]/t\,, \tag{9.20}$$

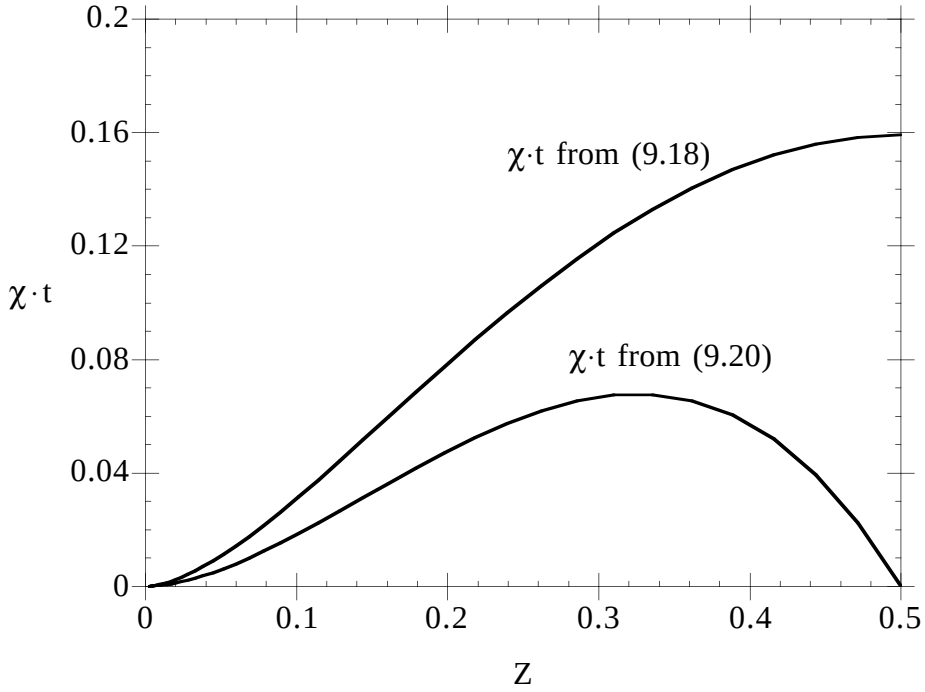

Fig. 9.3: Variation of the normalized scalar dissipation χt with Z in the insteady mixing layer and the two-dimensional flow behind a splitter plate.

showing that it varies as Z^2 for small values of Z. The variation of $\chi \cdot t$ with Z is shown for the two expressions (9.18) with (9.19) and (9.20) in Fig. 9.3.

9.3 The Planar Counterflow Diffusion Flame

Counterflow diffusion flames are very often used experimentally because they represent an essentially one-dimension diffusion flame structures. Fig. 9.6 below shows two typical cases where counterflow flames have been established between an oxidizer stream from above and a fuel stream from below. The latter may either be a gaseous fuel or an evaporating liquid fuel. If one assumes that the flow velocities of both streams are sufficiently large and sufficiently removed from the stagnation plane, the flame is embedded between two potential flows, one coming from the oxidizer and one from the fuel side. Prescribing the potential flow velocity gradient in the oxidizer stream by $a = -\partial v_\infty / \partial y$, the velocities and the mixture fraction are there

$$y \to \infty : \quad v_\infty = -ay\,, \quad u_\infty = ax\,, \quad Z = 0\,. \tag{9.21}$$

Equal stagnation point pressure for both streams requires that the velocities in the fuel stream are

$$y \to -\infty : \quad v_{-\infty} = -\sqrt{\rho_\infty / \rho_{-\infty}}\, ay\,, \quad u_{-\infty} = \sqrt{\rho_\infty / \rho_{-\infty}}\, ax\,, \quad Z = 1\,. \tag{9.22}$$

The equations for continuity, momentum and mixture fraction are given by

$$\frac{\partial(\rho u)}{\partial x} + \frac{\partial(\rho v)}{\partial y} = 0\,, \tag{9.23}$$

$$\rho\left(u\frac{\partial u}{\partial x} + v\frac{\partial u}{\partial y}\right) = -\frac{\partial p}{\partial x} + \frac{\partial}{\partial y}\left(\mu\frac{\partial u}{\partial y}\right)\,, \tag{9.24}$$

$$\rho\left(u\frac{\partial Z}{\partial x} + v\frac{\partial Z}{\partial y}\right) = \frac{\partial}{\partial y}\left(\rho D\frac{\partial Z}{\partial y}\right)\,. \tag{9.25}$$

Introducing the similarity transformation

$$\eta = \left(\frac{a}{(\rho\mu)_\infty}\right)^{1/2}\int_o^y \rho \mathrm{d}y\,, \quad \xi = x \tag{9.26}$$

one obtains the system of ordinary differential equations

$$f = \int_0^\eta f'\mathrm{d}\eta \tag{9.27}$$

$$\frac{\partial}{\partial\eta}\left(C\frac{\partial f'}{\partial\eta}\right) + f\frac{\partial f'}{\partial\eta} + \frac{\rho_\infty}{\rho} - f'^2 = 0 \tag{9.28}$$

$$\frac{\partial}{\partial\eta}\left(\frac{C}{\mathrm{Sc}}\frac{\partial Z}{\partial\eta}\right) + f\frac{\partial Z}{\partial\eta} = 0 \tag{9.29}$$

in terms of the nondimensional stream function

$$f = -\frac{\rho v}{\left((\rho\mu)_\infty\, a\right)^{1/2}} \tag{9.30}$$

and the normalized tangential velocity

$$f' = \frac{u}{ax}\,. \tag{9.31}$$

Furthermore the Chapman-Rubesin parameter C and the Schmidt number Sc are defined

$$C = \frac{\rho\mu}{(\rho\mu)_\infty}\,, \quad \mathrm{Sc} = \frac{\mu}{\rho D}\,. \tag{9.32}$$

The boundary equations are

$$\begin{aligned} \eta = +\infty &: \quad f' = 1\,, \quad Z = 0 \\ \eta = -\infty &: \quad f' = \rho_\infty/\rho_{-\infty}\,, \quad Z = 1\,. \end{aligned} \tag{9.33}$$

An integral of the Z-equation is obtained as

$$Z = \frac{1}{2}\frac{I(\infty) - I(\eta)}{I(\infty)} \tag{9.34}$$

where the integral $I(\eta)$ is defined as

$$I(\eta) = \int_o^\eta \frac{\mathrm{Sc}}{C} \exp\left\{ -\int_0^\eta f\mathrm{Sc}/C \mathrm{d}\eta \right\} \mathrm{d}\eta\,. \tag{9.35}$$

For constant properties ($\rho = \rho_\infty$, $C = 1$) $f = \eta$ satisfies (9.28) and

$$Z = \frac{1}{2}\,\mathrm{erfc}\left(\eta/\sqrt{2}\right)\,. \tag{9.36}$$

The instantaneous scalar dissipation rate is here

$$\chi = 2D\left(\frac{\partial Z}{\partial y}\right)^2 = 2\left(\frac{C}{\mathrm{Sc}}\right) a \left(\frac{\partial Z}{\partial \eta}\right)^2 \tag{9.37}$$

where Eqs. (9.26) and (9.32) have been used. When the scalar dissipation rate is evaluated with the assumptions that led to (9.36) one obtains

$$\chi = \frac{a}{\pi}\exp\left[-\eta^2(Z)\right] = \frac{a}{\pi}\exp\left(-2\left[\mathrm{erfc}^{-1}(2Z)\right]^2\right) \tag{9.38}$$

where $\eta(Z)$ is obtained as inverse of (9.36). For small Z one obtains with l'Hospital's rule

$$\frac{\mathrm{d}Z}{\mathrm{d}\eta} = -\frac{1}{2}\frac{\mathrm{d}I}{\mathrm{d}\eta}\frac{1}{I(\infty)} = \frac{-\mathrm{d}I/\mathrm{d}\eta}{I(\infty) - I(\eta)}\,Z = -\frac{\mathrm{Sc}}{C} f Z\,. \tag{9.39}$$

Therefore, in terms of the velocity gradient a the scalar dissipation rate becomes

$$\chi = 2a f^2 Z^2 (\mathrm{Sc}/C) \tag{9.40}$$

showing that χ increases as Z^2 for small Z. Assuming again $f = \eta$ as well as $C/\mathrm{Sc} = 1$ one obtains

$$\chi = 4aZ^2\left[\mathrm{erfc}^{-1}(2Z^2)\right] \tag{9.41}$$

The scalar dissipation rate in (9.38) and in (9.41) has the same Z-dependence as for the unsteady mixing layer and the two-dimensional flow behind a splitter plate. This points towards common features for these two flow configurations as far as the scalar structure is concerned. Fig. 9.3 is therefore also valid for counterflow diffusion flames if one replaces the time t by $(2a)^{-1}$.

9.4 Steady State Combustion and Quenching of Diffusion Flames with One-Step Chemistry

If the unsteady term is neglected, (9.7) is an ordinary differential equation that describes the structure of a steady state flamelet normal to the surface of stoichiometric mixture. It can be solved for general reaction rates either numerically or by asymptotic analysis. In the following we will express the chemistry by a one-step reaction with a large activation energy, assume constant pressure and the heat loss term q_R to be negligible. We will analyze the upper branch of the S-shaped curve shown in Fig. 9.4. This curve is equivalent to that previously discussed in Fig. 4.8 for $E = 10$. We will introduce an asymptotic analysis for large Damköhler numbers and large activation energies. In the limit of large Damköhler numbers which corresponds to complete combustion the chemical reaction is confined to an infinitely thin sheet around $Z = Z_{\rm st}$. Assuming constant c_p the temperature and the fuel, oxidizer, and product mass fraction profiles are piecewise linear functions of Z. These are shown in Figs. 1.??? and 1.???. The temperature profile is given by (2.13) with (2.14). This is called the Burke-Schumann solution. The coupling relations (6.24) yield the corresponding profiles for Y_F and $Y_{\rm O_2}$:
lean mixture, $Z \le Z_{\rm st}$:

$$T(Z) = T_u(Z) + \frac{QY_{F,1}}{c_p \nu'_F W_F} Z\,, \quad Y_F = 0\,, Y_{\rm O_2} = Y_{\rm O_2,2}\left(1 - \frac{Z}{Z_{\rm st}}\right)\,, \tag{9.42}$$

rich mixture, $Z \ge Z_{\rm st}$:

$$T(Z) = T_u(Z) + \frac{QY_{\rm O_2,2}}{c_p \nu'_{\rm O_2} W_{\rm O_2}}(1 - Z)\,, \quad Y_{\rm O_2} = 0\,, Y_F = Y_{F,1}\left(\frac{Z - Z_{\rm st}}{1 - Z_{\rm st}}\right) \tag{9.43}$$

where

$$T_u(Z) = T_2 + Z(T_1 - T_2)\,. \tag{9.44}$$

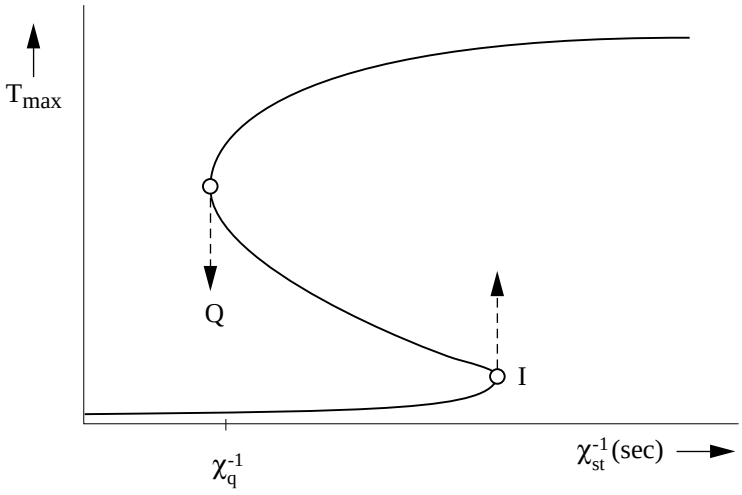

Fig. 9.4: The S-shaped curve showing the maximum temperature in a diffusion flame as a function of the inverse of the scalar dissipation rate at stoichiometric mixture.

The mass fractions of product species may be written similarly. We define the reaction rate as in (6.20) to show that (9.7) is able to describe diffusion flame quenching. For simplicity we will assume $T_1 = T_2 = T_u$. Then, for one reaction with

$$\frac{Q}{c_p} = \frac{(T_{\rm st} - T_u)\,\nu'_F W_F}{Y_{F,1} Z_{\rm st}} \tag{9.45}$$

(9.7) is written as

$$\frac{{\rm d}^2 T}{{\rm d}Z^2} = -\frac{2B\nu'_F \rho\,(T_{\rm st} - T_u)}{\chi Y_{F,1} Z_{\rm st} W_{\rm O_2}} Y_F Y_{\rm O_2} \exp\left(-\frac{E}{{\rm R}T}\right) . \tag{9.46}$$

The temperature and the fuel and oxygen mass fraction are expanded around $Z_{\rm st}$ as

$$\begin{aligned} T &= T_{\rm st} - \varepsilon\,(T_{\rm st} - T_u)\,y \\ Y_F &= Y_{F,1}\varepsilon\,(Z_{\rm st} + \xi) \\ Y_{\rm O_2} &= Y_{\rm O_2,2}\varepsilon\,((1 - Z_{\rm st}) - \xi) \end{aligned} \tag{9.47}$$

where ε is a small parameter to be defined during the analyses. The exponential term in the reaction rate may be expanded as

$$\exp\left(-\frac{E}{\mathcal{R}T}\right) = \exp\left(-\frac{E}{\mathcal{R}T_{\rm st}}\right) \exp({\rm Ze}\,\varepsilon y) \tag{9.48}$$

where the Zeldovich number is defined as

$${\rm Ze} = \frac{E\,(T_{\rm st} - T_u)}{\mathcal{R}T_{\rm st}^2} . \tag{9.49}$$

If all other quantities in (9.46) are expanded around their value at the stoichiometric flame temperature one obtains

$$\frac{{\rm d}^2 y}{{\rm d}\xi^2} = 2\,{\rm Da}\,\varepsilon^3\,(Z_{\rm st} y + \xi)\,((1 - Z_{\rm st})y - \xi)\exp(-{\rm Ze}\,\varepsilon y) \tag{9.50}$$

where

$${\rm Da} = \frac{B\rho_{\rm st}\nu'_{\rm O_2} Y_{F,1}}{\chi_{\rm st} W_F (1 - Z_{\rm st})} \exp\left(-\frac{E}{\mathcal{R}T}\right) \tag{9.51}$$

is the Damköhler number.

The differential equation (9.50) is cast into the same form as the one that governs Liñán's diffusion flame regime [9.3] by using the further transformation

$$\begin{aligned} z &= 2y(1 - Z_{\rm st})Z_{\rm st} - \gamma\xi \\ \gamma &= 2Z_{\rm st} - 1 \\ \beta &= {\rm Ze}\Big/\,[2Z_{\rm st}\,(1 - Z_{\rm st})] \end{aligned} \tag{9.52}$$

to yield

$$\frac{\mathrm{d}^2 z}{\mathrm{d}\xi^2} = \mathrm{Da}\,\varepsilon^3 (z^2 - \xi^2) \exp\left[-\beta\varepsilon(z + \gamma\xi)\right] . \tag{9.53}$$

There are evidently two ways to define the expansion parameter ε, either by setting $\beta\varepsilon = 1$ or by setting $\mathrm{Da}\,\varepsilon^3 = 1$. The first one would be called a large activation energy expansion and the second one a large Damköhler number expansion. Both formulations are interrelated if we introduce the distinguished limit where the rescaled Damköhler number

$$\delta = \mathrm{Da}/\beta^3 \tag{9.54}$$

is assumed to be of order one. Thus a definite relation between the Damköhler number and the activation energy is assumed as ε goes to zero. We set

$$\varepsilon = \mathrm{Da}^{-1/3} = \delta^{-1/3}/\beta \tag{9.55}$$

to obtain Liñán's equation for the diffusion flame regime

$$\frac{\mathrm{d}^2 z}{\mathrm{d}\xi^2} = (z^2 - \xi^2) \exp[-\delta^{-1/3}(z + \gamma\xi)] . \tag{9.56}$$

The boundary conditions are obtained by matching to the outer flow solution

$$\begin{aligned} \frac{\mathrm{d}z}{\mathrm{d}\xi} &= 1 \qquad \text{for} \quad \xi \to \infty , \\ \frac{\mathrm{d}z}{\mathrm{d}\xi} &= -1 \qquad \text{for} \quad \xi \to -\infty . \end{aligned} \tag{9.57}$$

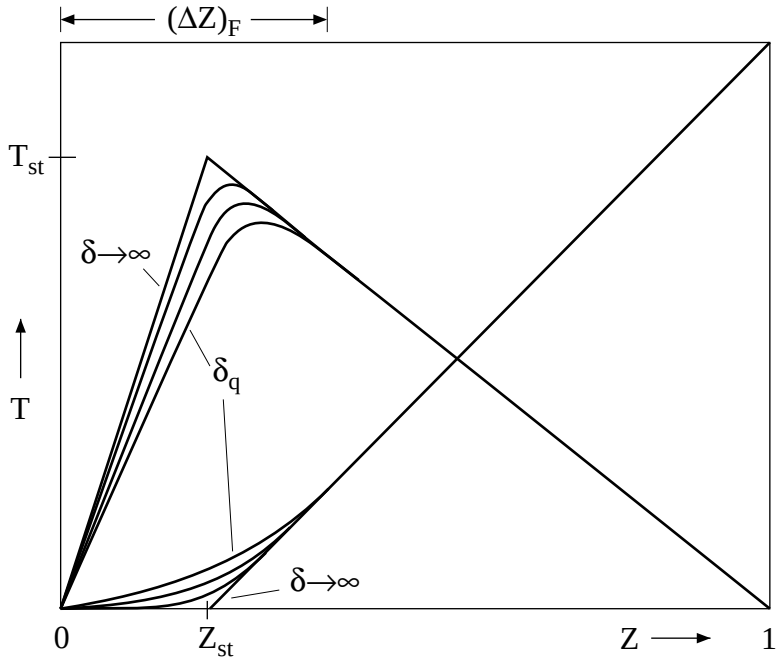

Fig. 9.5: Temperature and fuel mass fraction profiles over mixture fraction for diffusion flamelet at increasing Damköhler numbers.

The essential property of this equation, as compared to the large Damköhler number limit ($\delta \to \infty$) is that the exponential term remains, since δ was assumed to be finite. This allows extinction to occur if the parameter δ decreases below a critical value δ_q. Liñán gives an approximation of δ_q in terms of $|\gamma|$. For small values of $Z_{\rm st}$ extinction occurs at the transition to the premixed-flame regime [9.3]. He obtains

$$\delta_q = e(1 - |\gamma|)\,. \tag{9.58}$$

Characteristic profiles for the temperature over Z are schematically shown in Fig. 9.5 with δ as a parameter. There is a limiting profile $T_q(Z)$ corresponding to δ_q. Any solution below this profile is unstable, and the flamelet would be extinguished.

The extinction condition $\delta = \delta_y$ defines with (9.54) and (9.51) a maximum dissipation rate χ_q at the surface of stoichiometric mixture for a flamelet to be burning, namely

$$\chi_q = \frac{8B\rho_{\rm st}\nu'_{\rm O_2}Y_{F,1}Z_{\rm st}^3(1-Z_{\rm st})^2}{W_F\delta_q {\rm Ze}^3}\exp\left(-\frac{E}{\mathcal{R}T_{\rm st}}\right)\,. \tag{9.59}$$

We may interpret $\chi_{\rm st}$ as the inverse of a characteristic diffusion time. If $\chi_{\rm st}$ is large, heat will be conducted to both sides of the flamelet at a rate that is not balanced by the heat production due to chemical reaction. Thus the maximum temperature will decrease until the flamelet is quenched at a value of $\chi_{\rm st} = \chi_q$. This is shown in Fig. 9.4. Burning of the flamelet corresponds to the upper branch of the S-shaped curve. If $\chi_{\rm st}$ is increased, the curve is traversed to the left until χ_q is reached, beyond which value only the lower, nonreacting branch exists. Thus at $\chi_{\rm st} = \chi_q$ the quenching of the diffusion flamelet occurs.

The transition from the point Q to the lower state corresponds to the unsteady transition. Auto-ignition, which would correspond to an unsteady transition from the point I to the upper curve, is unlikely to occur in open diffusion flames, since the required very large residence times (very small values of $\chi_{\rm st}$) are not reached. An example for auto-ignition in non-premixed systems is the combustion in a Diesel engine. Here interdiffusion of the fuel from the Diesel spray with the surrounding hot air leads to continuously decreasing mixture fraction gradients and therefore to decreasing scalar dissipation rates. This corresponds to a shift on the lower branch of the S-shaped curve up to the point I where ignition occurs.

9.5 Time and Length Scales in Diffusion Flames

We will define the chemical time scale at extinction as

$$t_c = Z_{\rm st}^2(1-Z_{\rm st})^2/\chi_q\,. \tag{9.60}$$

This definition is motivated by expression (9.59) for χ_q. By comparing this with the time scale of a premixed flame with the same chemical source term one obtains

$$t_c = \frac{\delta_q\,(\rho\lambda/c_p)_{\rm st}}{2\,(\rho_u s_L)_{\rm st}^2} \tag{9.61}$$

where $(\rho_u s_L)_{\rm st}$ has been calculated using (6.54) and (6.55) for a stoichiometric premixed flame. This indicates that there is a fundamental relation between a premixed flame and a diffusion flame at extinction: In a diffusion flame at extinction the heat conduction out of the reaction zone towards the lean and the rich side just balances the heat generation by the reaction. In a premixed flame the heat conduction towards the outburnt mixture is such that it balances the heat generation by the reaction for a particular burning velocity. These two processes are equivalent. A diffusion flame, however, can exist at lower scalar dissipation rates and therefore at lower characteristic flow times. The flow time in a premixed flow is fixed by the burning velocity, which is an eigenvalue of the problem. Therefore combustion in diffusion flame offers an additional degree of freedom: that of choosing the ratio of the convective to the reactive time, represented by the Damköhler number defined in (9.51) as long as $\chi_{\rm st}$ is smaller than χ_q. This makes non-premixed combustion to be better controllable and diffusion flames more stable. It is also one of the reasons why combustion in Diesel engines which operate in the non-premixed regime is more robust and less fuel quality dependent than that in spark ignition engines where fuel and air are premixed before ignition.

Equations (9.60) and (9.38) may now be used to calculate chemical time scales for diffusion flames. The inverse complementary error function $\mathrm{erfc}^{-1}(2Z_{\rm st})$ is 1.13 for methane-air flames with $Z_{\rm st} = 0.055$ and 1.34 for H_2-air flames with $Z_{\rm st} = 0.0284$. Extinction of the H_2-air diffusion flame occurs at a strain rate $a_q = 14260/\mathrm{s}$ and that of the CH_4-air flame at 420/s. This leads to $t_c = 0.64 \cdot 10^{-5}\mathrm{s}$ for hydrogen-air/diffusion flames and to $t_c = 0.29 \cdot 10^{-3}\mathrm{s}$ for methane-air/diffusion flames. The latter estimate is of the same order of magnitude as t_c for stoichiometric premixed methane flames. Comparing the velocity gradient at extinction for premixed methane-air flames of $a_q = 2275/\mathrm{s}$, given in lecture 6, with the value above, one realizes that, while the extinction time scales in premixed methane-air diffusion flames are comparable, the velocity gradients a_q for extinction are larger by a factor of 7 for premixed flames. This indicates that, in terms of the imposed strain rate, a diffusion flame extinguishes more easily than a premixed flame. Physically, this is due to the fact that the inner structure of a diffusion flame looses heat to both sides, the lean and the rich, while a premixed flame looses heat only to the preheat zone.

In diffusion flames, in contrast to premixed flames, there is no velocity scale, such as the burning velocity, by which a characteristic length scale such as the premixed flame thickness l_F could be defined. There is, however, the velocity gradient a, the inverse of which may be interpreted as a flow time.

Based on this flow time one may define an appropriate diffusive length scale. Dimensional analysis leads to a diffusive flame thickness

$$l_F = \sqrt{\frac{D_{\rm ref}}{a}}\,. \tag{9.62}$$

Here the diffusion coefficient D should be evaluated at a suitable reference condition, conveniently chosen at stoichiometric mixture. Assuming a one-dimensional mixture fraction profile in y-direction as for the insteady mixing layer the flame thickness in mixture fraction space may be defined

$$(\Delta Z)_F = \left(\frac{\partial Z}{\partial y}\right)_F l_F\,. \tag{9.63}$$

Here $(\partial Z/\partial y)_F$ is the mixture fraction gradient normal to the flamelet. This flamelet thickness contains the reaction zone and the surrounding diffusive layers. Equation (9.63) leads with (9.62) and (9.8) to

$$(\Delta Z)_F = \sqrt{\frac{\chi_{\rm ref}}{2a}} \tag{9.64}$$

where $\chi_{\rm ref}$ represents the scalar dissipation rate at the reference condition. If $\chi_r ef$ is evaluated at $Z_{\rm st}$ and (9.41) is used, it is seen that $(\Delta Z)_F$ is of the order of $2Z_{\rm st}$ if $Z_{\rm st}$ is small. With an estimate $(\Delta Z)_F = 2Z_{\rm st}$ the flame thickness would cover the reaction zone and the surrounding diffusive layers in a plot of the flamelet structure in mixture fraction space. This is shown schematically in Fig. 9.5.

9.6 Numerical Calculation of Counterflow Diffusion Flames with general boundary conditions

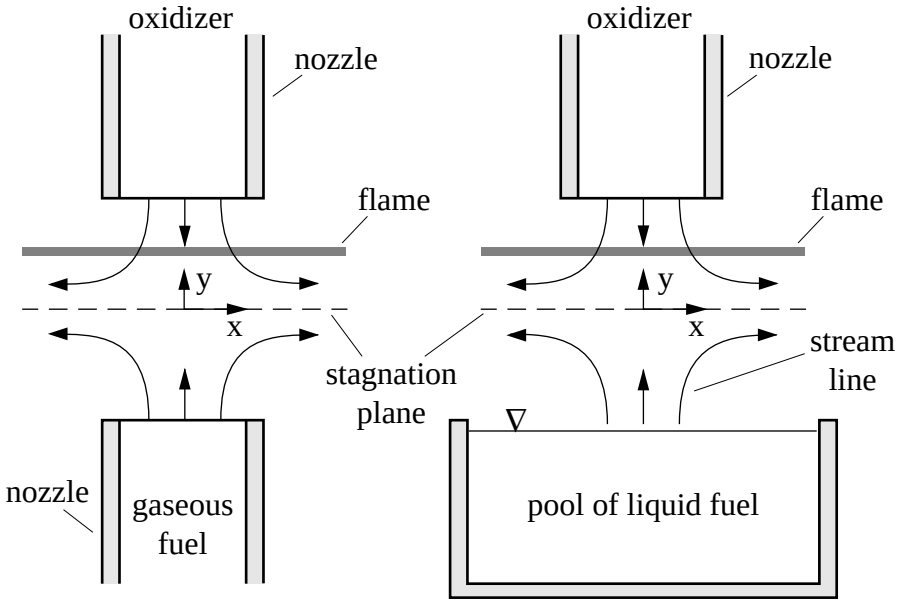

Fig. 9.6: A schematic illustration of the experimental configuration for counterflow flames for gaseous and liquid fuels.

We now consider planar or axi-symmetric counterflow configurations for general boundary conditions and chemical mechanisms. Two configurations are shown in Fig. 9.6 for gaseous and liquid fuels. As for the planar counterflow flame there exists a similarity solution valid in the vicinity of the stagnation line which results in a set of one-dimensional equations. Here we will not introduce a non-dimensional similarity coordinate as in (9.26) but use the y-coordinate directly. Rather than prescribing the velocity u by (9.31) we introduce $u = Gx$ where G replaces af'. Then one obtains the following governing equations:

Continuity

$$\frac{\partial(\rho v)}{\partial y} + (j+1)\rho G = 0\,, \tag{9.65}$$

Momentum

$$\rho v \frac{\mathrm{d}G}{\mathrm{d}y} = -\rho G^2 + P' + \frac{\mathrm{d}}{\mathrm{d}y}\left(\mu \frac{\mathrm{d}G}{\mathrm{d}y}\right) = 0\,, \tag{9.66}$$

Species

$$\rho v \frac{\mathrm{d}Y_i}{\mathrm{d}y} = \frac{\mathrm{d}j_i}{\mathrm{d}y} + \dot{m}_i \quad (i = 1, 2, ..., n)\,, \tag{9.67}$$

Energy

$$\rho v c_p \frac{\mathrm{d}T}{\mathrm{d}y} = \frac{\mathrm{d}}{\mathrm{d}y}\left(\lambda \frac{\mathrm{d}T}{\mathrm{d}y}\right) - \sum_{i=1}^{n} h_i m_i - \sum_{i=1}^{n} c_{pi} j_i \frac{\mathrm{d}T}{\mathrm{d}y}\,, \tag{9.68}$$

Mixture fraction

$$\rho v \frac{\mathrm{d}Z}{\mathrm{d}y} = \frac{\mathrm{d}}{\mathrm{d}y}\left(\frac{\lambda}{c_p}\frac{\mathrm{d}Z}{\mathrm{d}y}\right)\,. \tag{9.69}$$

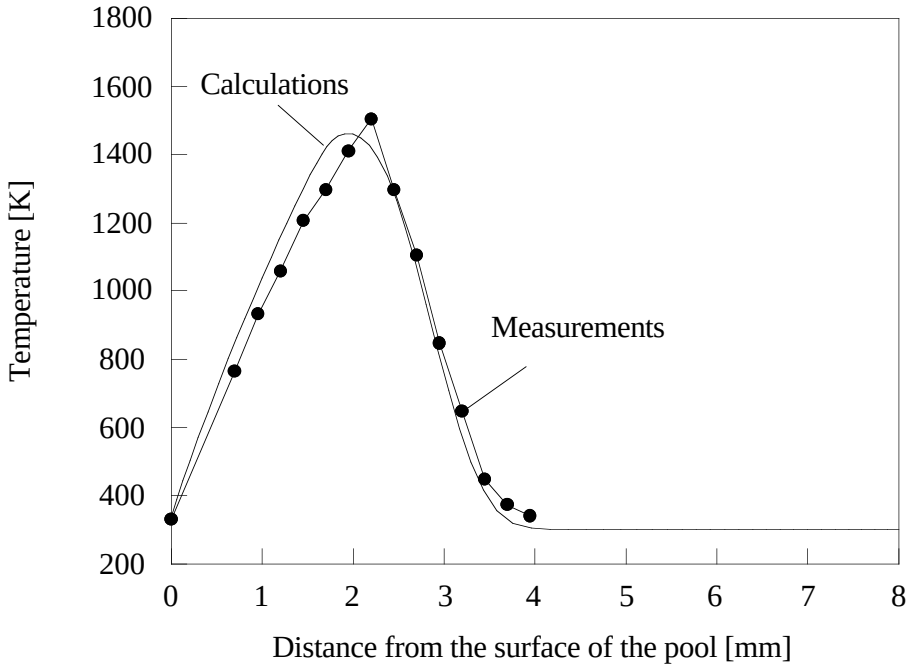

Fig. 9.7: Comparison between the measured (line through points) and calculated temperature profile (From the paper by C. M. Müller, J. Y. Chen and K. Seshadri in [9.4]).

Here $j = 0$ applies for the planar and $j = 1$ for axi-symmetric configuration. The parameter P' represents the axial pressure gradient and is defined for the counterflow flame considered in paragraph 9.3 as

$$P' = \rho_\infty a^2\,, \tag{9.70}$$

where $a = (\partial u/\partial x)_\infty$ is the velocity gradient and $u_\infty = ax$ the tangential velocity in the oxidizer stream. The parameter a represents the strain rate and is prescribed for a counterflow between two potential flows considered above. If, however, the oxidizer or the

gaseous fuel flow issues from a burner sufficiently close to the flame the boundary condition $u = 0$ must be imposed at the burner and the velocity gradient must be calculated as an eigenvalue of the solution. As an example, for the counterflow flame over a liquid pool, the boundary conditions at the exit of the oxidizer duct located at $y = L$ can be written as

$$\begin{aligned} &\rho v = \rho_e v_e \,; \\ &G = 0 \,, \quad Y_{\mathrm{O}_2} = Y_{\mathrm{O}_2 e} \,; \\ &Y_i = 0 \quad (i \neq \mathrm{O}_2, \mathrm{N}_2) \,; \\ &Z = 0 \,; \quad T = T_e \,. \end{aligned} \tag{9.71}$$

Subscript e denotes conditions at the exit of the oxidizer duct. At the surface of the liquid pool located at $y = 0$, the value of the tangential component of the flow velocity is presumed to be zero (no slip) and the appropriate interface balance conditions can be written as

$$\begin{aligned} G &= 0 \,, \\ \rho_w v_w Y_{iw} + j_{iw} &= 0 \quad (i \neq F) \,, \\ \rho_w v_w (1 - Y_{Fw}) - j_{Fw} &= 0 \,, \\ \rho_w v_w (1 - Z_w) + \left[\frac{\lambda}{c_p} \frac{\mathrm{d}Z}{\mathrm{d}y} \right]_w &= 0 \,, \\ \left[\lambda \frac{\mathrm{d}T}{\mathrm{d}y} \right]_w - \rho_w v_w h_L &= 0 \,, \\ T &= T_w \,, \end{aligned} \tag{9.72}$$

where h_L is the latent heat of vaporization of the fuel, which is presumed to be known. Subscript F and w refer to the fuel and conditions on the gas side of the liquid-gas interface respectively. For simplicity the surface temperature T_w is presumed to be equal to the boiling point of methanol. The mass burning rate of the liquid fuel $\rho_w v_w$ is an unknown and will be determined as a part of the solution.

A number of diffusion flames have been calculated numerically with full and reduced mechanisms in [9.4]. As an example the temperature profile over a liquid pool of methanol is shown in Fig. 9.7.

9.7 Diffusion Flames Structure of Methane-Air Flames

The one-step model with a large activation energy is able to predict important features such as extinction, but for small values of Z_{st} it predicts the leakage of fuel through the reaction zone. This was schematically shown in Fig. 9.5. Experiments of methane flames, on the contrary, show leakage of oxygen rather than of fuel through the reaction zone. A numerical calculation with the four-step reduced mechanism

$$\begin{aligned} \mathrm{CH_4} + 2\mathrm{H} + \mathrm{H_2O} &= \mathrm{CO} + 4\mathrm{H_2} \\ \mathrm{CO} + \mathrm{H_2O} &= \mathrm{CO_2} + \mathrm{H_2} \\ \mathrm{H} + \mathrm{H} + \mathrm{M} &= \mathrm{H_2} + \mathrm{M} \\ \mathrm{O_2} + 3\mathrm{H_2} &= 2\mathrm{H} + 2\mathrm{H_2O} \end{aligned}$$

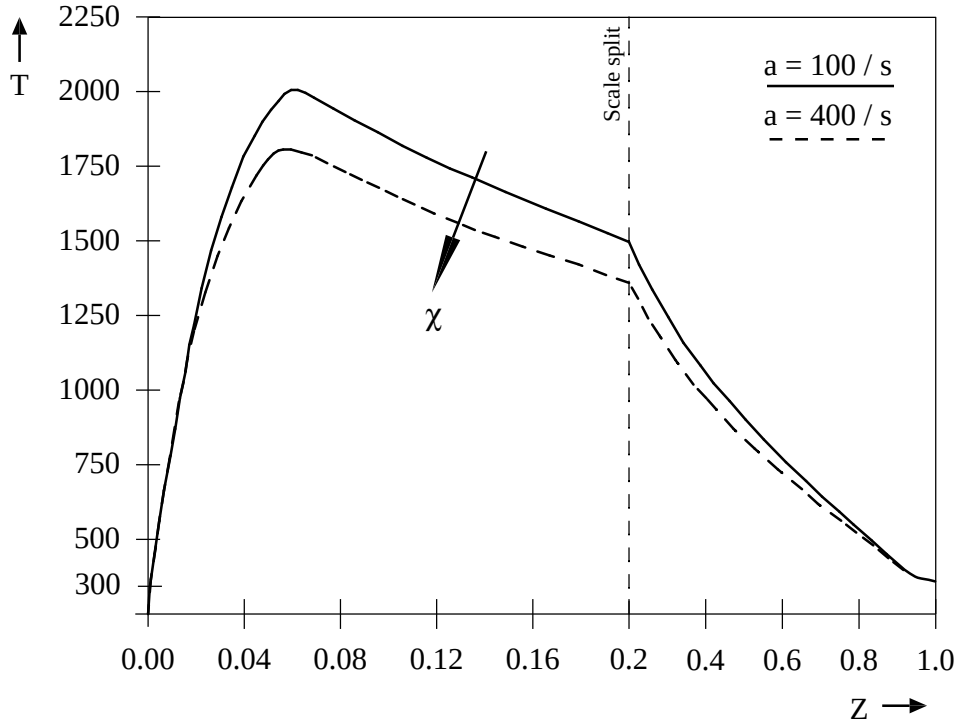

Fig. 9.8: Temperature profiles of methane-air diffusion flames for $a = 100/\text{s}$ and $a = 400/\text{s}$ as a function of mixture fraction.

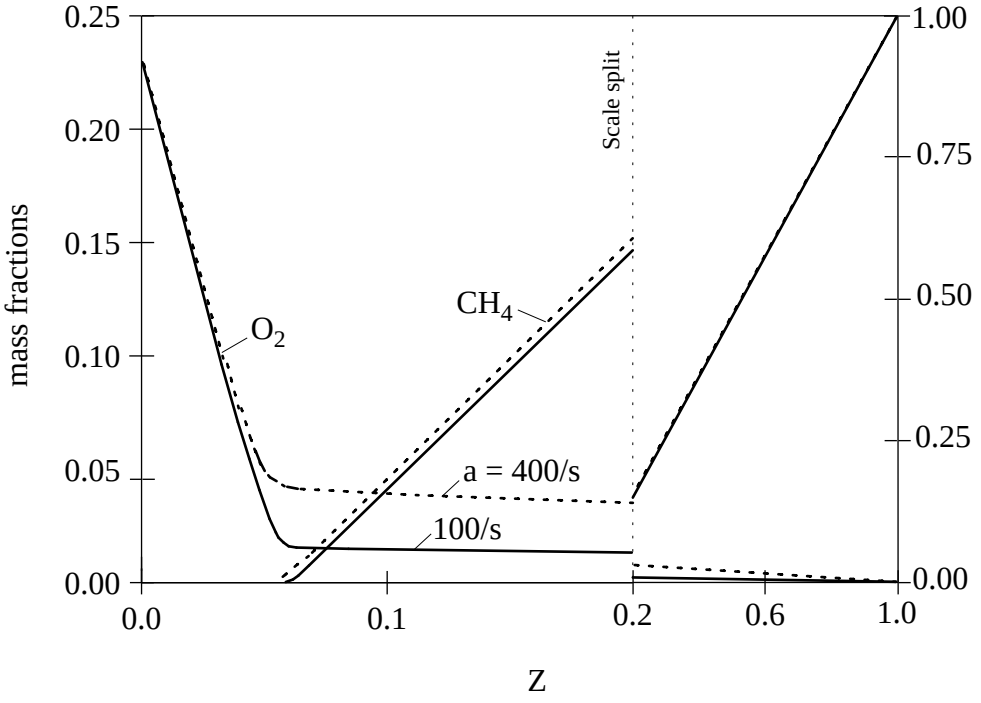

Fig. 9.9: Fuel and oxygen mass fractions for $a = 100/\text{s}$ and $a = 400/\text{s}$ as a function of mixture fraction.

has been performed [9.5] for the counter-flow diffusion flame in the stagnation region of a porous cylinder. This flow configuration, initially used by Tsuji and Yamaoka [9.6], will be presented in the next lecture in Fig. 10.1.

Temperature and fuel and oxygen mass fractions profiles are plotted in Fig. 9.8 and 9.9 for the strain rates of $a = 100/\text{s}$ and $a = 400/\text{s}$ as a function of mixture fraction. The second value of the strain rate corresponds to a condition close to extinction. It is seen that the temperature in the reaction zone decreases and the oxygen leakage increases as extinction is approached.

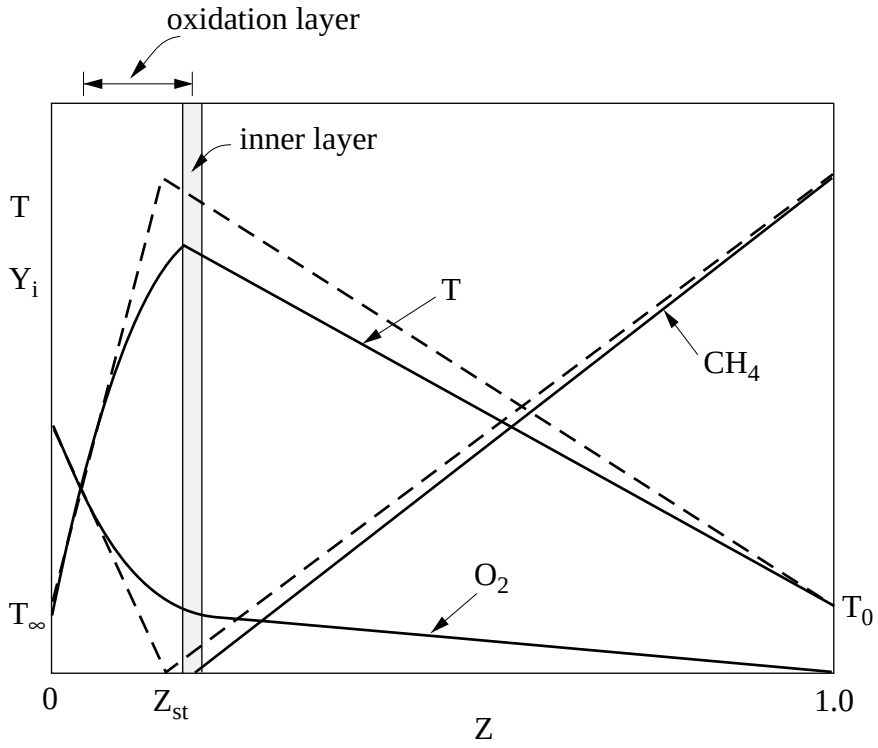

Fig. 9.10: Illustration of the asymptotic structure of the methane-air diffusion flame based on the reduced four-step mechanism [9.7]. The dotted line is the Burke-Schumann solution.

An asymptotic analysis [9.7] based on the four-step model shows a close correspondence between the different layers identified in the premixed methane flame in lecture 7 and those in the diffusion flame. The structure obtained from the asymptotic analysis is schematically shown in Fig. 9.10. The outer structure of the diffusion flame is the classical Burke-Schumann structure governed by the overall one-step reaction $CH_4 + 2O_2 \rightarrow CO_2 + 2H_2O$, with the flame sheet positioned at $Z = Z_{\text{st}}$. The inner structure consists of a thin $H_2 - CO$ oxidation layer of thickness $O(\varepsilon)$ toward the lean side and a thin inner layer of thickness $O(\delta)$ slightly toward the rich side of $Z = Z_{\text{st}}$. Beyond this layer the rich side is chemically inert because all radicals are consumed by the fuel. The comparison of the diffusion flame structure with that of a premixed flame shows that the rich part of the diffusion flame corresponds to the upstream preheat zone of the premixed flame while its lean part corresponds to the downstream oxidation layer.

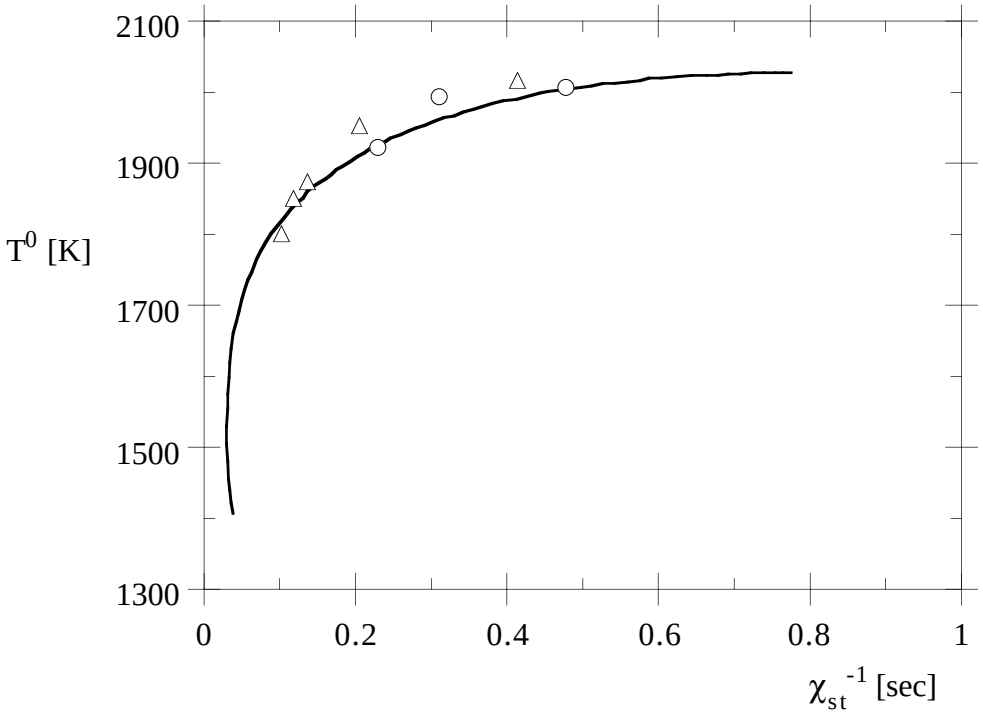

Fig. 9.11: Inner flame temperature T^0 plotted as a function of χ_{st}^{-1}. $\triangle$, numerical calculations using the four-step mechanism [9.5]; $\bigcirc$ experimental data quoted in [9.7].

The maximum temperature which corresponds to the inner layer temperature of the asymptotic structure, is shown in Fig. 9.11 as a function of the inverse of the scalar dissipation rate. This plot corresponds to the upper branch of the S-shaped curve shown in Fig. 9.4. The calculations agree well with numerical [9.5] and experimental [9.8] data and also show the vertical slope of T^0 versus $\chi_{\rm st}^1$ which corresponds to extinction.

References

[9.1] Peters, N., Combustion, Science and Technology **30**, pp. 1–17, 1983.

[9.2] Peters, N., Progress in Energy and Combustion Science, **10**, pp. 319–339, 1984.

[9.3] Liñán, A., Acta Astronautica, **1**, p. 1007, 1974.

[9.4] Peters, N. and Rogg B. (Eds), Reduced Kinetic Mechanisms for Applications in Combustion Systems, to appear 1993.

[9.5] Peters, N., and Kee, R.J., Combustion and Flame, **68**, pp. 17–29, 1987.

[9.6] Tsuji, H., and Yamaoka, I., 13$^{\rm th}$ Symposium (International) on Combustion, p. 723, The Combustion Institute 1971.

[9.7] Seshadri, K. and Peters, N., Combustion and Flame, **73**, pp. 23–44, 1988.

[9.8] Smooke, M.D., Puri, I.K., and Seshadri, K., 21$^{\rm st}$ Symposium (International) on Combustion, pp. 1783–1792, The Combustion Institute 1986.

Lecture 10: Laminar Diffusion Flames:

Different Flame Geometries and Single Droplet Burning

In this lecture we want to present solutions for the velocities and the mixture fraction fields for some typical laminar flame configurations. Based on the assumption chemistry we will then be able to calculate the flame contour defined by the condition $Z(x_\alpha, t) = Z_{\rm st}$. We will for simplicity always assume the Lewis number to be equal to unity and the heat capacity to be constant. The first case to be considered is the flame stagnation point boundary layer, which is similar to the counterflow flow of the previous chapter but with different boundary conditions. We then will investigate a laminar plane jet diffusion flame and determine its flame length. The third example will include the effect of buoyancy in a vertical plane diffusion flame. Finally we will also calculate the combustion of a single droplet surrounded by a diffusion flame.

10.1 Diffusion Flames in a Stagnation Point Boundary Layer: The Tsuji Flame

Let us consider the flame configuration shown in Fig. 10.1. Gaseous fuel from a sinter metal tube is injected into the surrounding air which flows vertically upwards. Below the tube a stagnation point is formed. This burner is known as the Tsuji burner [10.1]. If the Reynolds number based on the cylinder radius and the free stream velocity is large, the flow field may be split into an inviscous outer flow and a boundary layer close to the surface. The potential flow solution for the flow around a cylinder then yields at the stagnation point the velocity gradient

$$a = \frac{2v_\infty}{R} \tag{10.1}$$

where v_∞ is the velocity very far from the cylinder. The free-stream velocities at the edge of the boundary layer are

$$u_e = ax, \quad v_e = -ay\,. \tag{10.2}$$

If the boundary layer thickness δ, which is proportional to the viscous length

$$\ell_\nu = \sqrt{\frac{\nu_e}{a}}\,, \tag{10.3}$$

where ν_e is the kinematic viscosity at the edge of the boundary layer, is small compared to the cylinder radius, the curvature of the cylinder surface may be neglected and the boundary may be treated as two-dimensional in a cartesian coordinate system.

The equations describing the boundary layer flow are the

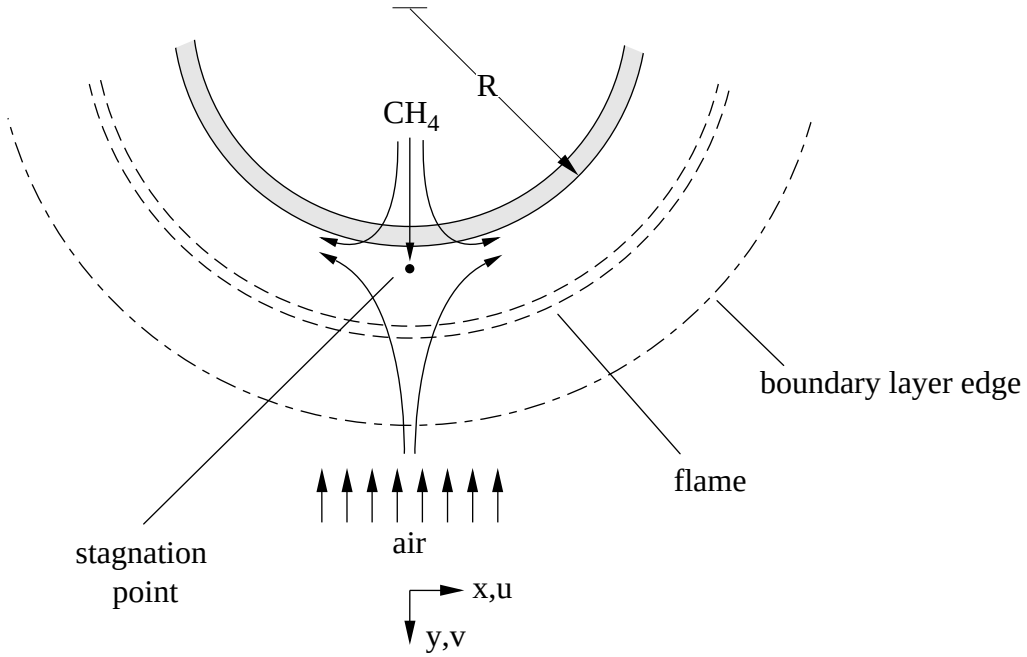

Fig. 10.1: Schematic diagram of a stagnation point diffusion flame in front of a porous cylinder

Continuity

$$\frac{\partial(\rho u)}{\partial x} + \frac{\partial(\rho v)}{\partial y} = 0\,, \tag{10.4}$$

Momentum

$$\rho u \frac{\partial u}{\partial x} + \rho v \frac{\partial u}{\partial y} = \left.\frac{\mathrm{d}p}{\mathrm{d}x}\right|_e + \frac{\partial}{\partial y}\left(\rho\nu \frac{\partial u}{\partial y}\right)\,, \tag{10.5}$$

Mixture fraction

$$\rho u \frac{\partial Z}{\partial x} + \rho v \frac{\partial Z}{\partial y} = \frac{\partial}{\partial y}\left(\rho D \frac{\partial Z}{\partial y}\right)\,. \tag{10.6}$$

The pressure gradient at the boundary layer edge is obtained from Bernoulli's equation

$$\rho_e u_e \frac{\mathrm{d}u_e}{\mathrm{d}x} = -\left.\frac{\mathrm{d}p}{\mathrm{d}x}\right|_e = -\rho_e a^2 x\,. \tag{10.7}$$

The boundary conditions are

$$u = 0\,, \quad \dot{m}_w = (\rho v)_w\,, \quad (\rho D)_w \left.\frac{\partial Z}{\partial y}\right|_w = m_w(Z_w - 1) \quad \text{at} \quad y = 0\,, \tag{10.8}$$

and

$$u = ax\,, \quad Z = 0 \quad \text{at} \quad y \to \infty\,. \tag{10.9}$$

Here $u = 0$ is the non-slip condition at the surface. The mass flow rate $\dot{m}_w$ of fuel issuing through the porous metal into the boundary layer is imposed. The boundary condition for the mixture fraction equation represents the integrated mixture fraction balance at the surface of the porous metal by assuming that the mixture fraction gradient within the metal is zero. Introducing the similarity variable

$$\eta = \left(\frac{a}{\nu_e}\right)^{1/2} \int_0^y \frac{\rho}{\rho_e}\, dy \tag{10.10}$$

The continuity equation is satisfied by introducing the stream function ψ such that

$$\begin{aligned} \rho u &= \frac{\partial \psi}{\partial \eta}\,, \\ \rho v &= -\frac{\partial \psi}{\partial x} \end{aligned} \tag{10.11}$$

A non-dimensional stream function $f(\eta)$, that depends on the similarity variable η only, is then defined as

$$f(\eta) = \frac{\psi}{\rho_e x \sqrt{a\nu_e}} \tag{10.12}$$

such that the velocities are

$$u = ax\frac{\partial f}{\partial \eta}\,, \quad v = -\frac{\rho_e}{\rho}(a\nu_e)^{1/2} f(\eta) \tag{10.13}$$

one obtains the similarity equations

$$-f\frac{\mathrm{d}^2 f}{\mathrm{d}\eta^2} = \left[\frac{\rho_e}{\rho} - \left(\frac{\mathrm{d}f}{\mathrm{d}\eta}\right)^2\right] \frac{\mathrm{d}}{\mathrm{d}\eta}\left(C\frac{\mathrm{d}^2 f}{\mathrm{d}\eta^2}\right) \tag{10.14}$$

$$-f\frac{\mathrm{d}Z}{\mathrm{d}\eta} = \frac{\mathrm{d}}{\mathrm{d}\eta}\left(\frac{C}{\mathrm{Sc}}\frac{\mathrm{d}Z}{\mathrm{d}\eta}\right) \tag{10.15}$$

Here $\mathrm{Sc} = \nu/D$ is the Schmidt number and C is the Chapman-Rubesin parameter

$$C = \frac{\rho^2 \nu}{\rho_e^2 \nu_e}\,. \tag{10.16}$$

Since ν changes as with temperature as $T^{1.7}$ and ρ as T^{-1}, this quantity changes less than the viscosity itself in a flow with strong heat release. The boundary conditions for the similar solution are

$$f_w = -\frac{(\rho v)_w}{(\rho_e^2 a \nu_e)^{1/2}}\,, \quad f' = 0\,, \frac{C}{\mathrm{Sc}}\frac{\mathrm{d}Z}{\mathrm{d}\eta}\bigg|_w = f_w(1 - Z) \quad \text{at} \quad \eta = 0 \tag{10.17}$$

$$f'(\infty) = 1 \quad \text{for} \quad \eta \to \infty \,. \tag{10.18}$$

The mixture fraction equation may be transformed into

$$\frac{\mathrm{d}}{\mathrm{d}\eta}\left[\ln\left(\frac{C}{\mathrm{Sc}}\frac{\mathrm{d}Z}{\mathrm{d}\eta}\right)\right] = -\frac{f\mathrm{Sc}}{C} \tag{10.19}$$

which can formally be solved as

$$Z = \frac{f_w[I(\eta) - I(\infty)]}{1 - f_w I(\infty)} \tag{10.20}$$

where

$$I(\eta) = \int_0^\eta \frac{\mathrm{Sc}}{C} \exp\left(-\int_0^\eta \frac{f\mathrm{Sc}}{C} d\eta\right) d\eta \,. \tag{10.21}$$

The mixture fraction at the surface is given by

$$Z_w = \frac{-f_w I(\infty)}{1 - f_w I(\infty)} \,. \tag{10.22}$$

This indicates that the mixture fraction varies between $Z = 0$ and $Z = Z_w$ rather than between 0 and 1. The boundary condition for the fuel and oxidizer fractions satisfy the Burke-Schumann solution at Z_w , as may easily be shown. The boundary condition for the temperature at the surface is to be imposed at $Z = Z_w$.

If the mass flow rate at the surface is increased and f_w takes large negativ values, the mixture fraction at the surface tends towards unity. This is the limit of a counter-flow diffusion flame detached from the surface.

Equations (10.14) and (10.15) have been solved numerically using the Burke-Schuhmann solution for combustion of methane in air (1.67)–(1.68) with $Z_{\mathrm{st}} = 0.055$, $T_u = 300\,\mathrm{K}$, and $T_{\mathrm{st}} = 2263$ K. The profiles of u/ax, v, T, Z, ρ/ρ_e, and C are shown in Figures 10.2 a–c.

10.2 The Plane Jet Diffusion Flame on a Slot Burner

For non-premixed combustion a jet flame is the most common flow configuration. Fuel that issues from a nozzle mixes with the surrounding air by convection and diffusion to form a mixture fraction field as already shown in Fig. 5.2 in Lecture 5. Usually the jet velocity is so large that the jet becomes turbulent and turbulent mixing determines the mixture fraction field. This will be considered for a round jet in lecture 13. Here we want to derive a similarity solution for a laminar plane jet issuing from a slot burner. Such a configuration exists in house-hold appliances for hold water supply. In order to obtain a similarity solution buoyancy must be neglected (We will consider the effect of buoyancy separately in the next section). Here we want to extend the classical solution [10.2] for a constant density plane jet to non-constant density jet flames. The stream line pattern and the velocity profiles are shown in Fig. 10.3. The jet issues from a small slot within

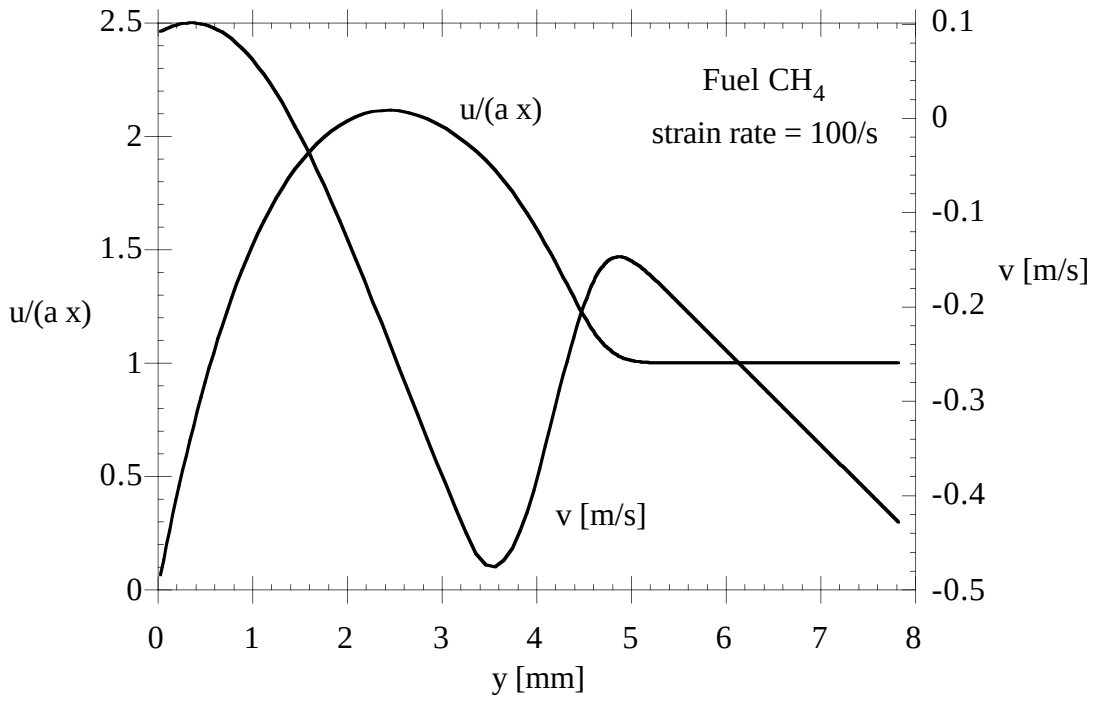

Fig. 10.2a: Velocity profiles for the Tsuji geometry

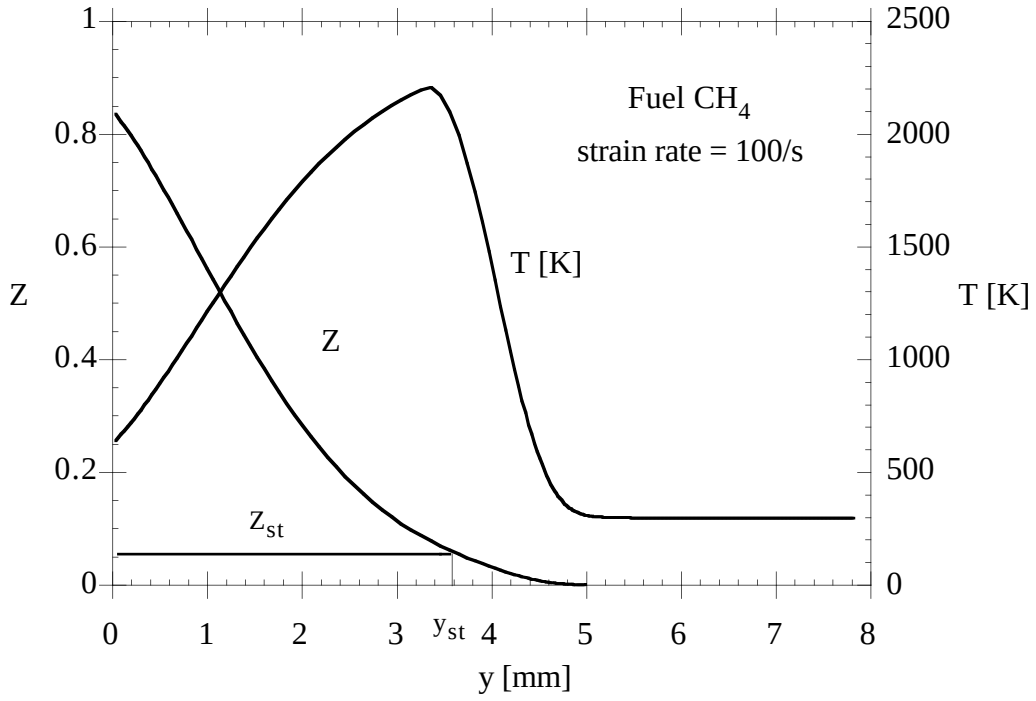

Fig. 10.2b: Mixture fraction and Temperature profiles for the Tsuji geometry

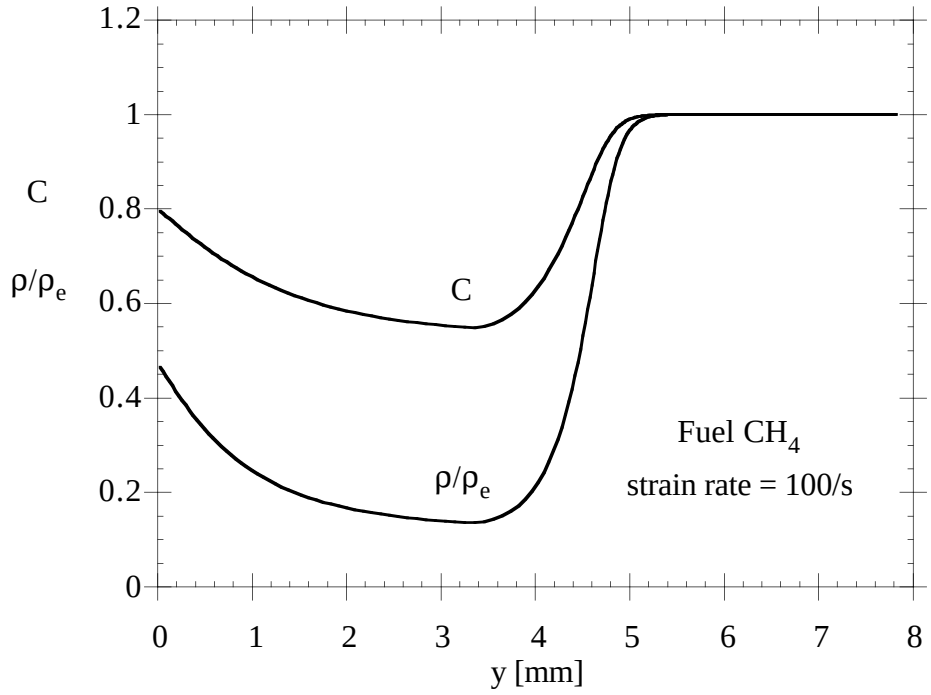

Fig. 10.2c: Chapman-Rubesin parameter and temperature profiles for the Tsuji geometry

a wall and by viscosity entraines the surrounding fluid. Thereby the velocity profile and the maximum velocity decreases. The boundary layer that would develop on the wall will be neglected for simplicity. Then the entrained fluid enters into the jet from the normal direction.

We assume the boundary layer assumptions to be valid and the pressure to be constant. We denote with x the coordinate in jet axis and with y the coordinate normal to it. The corresponding velocity components are denoted by u and v. The boundary layer equations are

Continuity

$$\frac{\partial(\rho u)}{\partial x} + \frac{\partial \rho v}{\partial y} = 0\,, \tag{10.23}$$

Momentum

$$\rho u \frac{\partial u}{\partial x} + \rho v \frac{\partial u}{\partial y} = \frac{\partial}{\partial y}\left(\rho \nu \frac{\partial u}{\partial y}\right)\,, \tag{10.24}$$

Mixture Fraction

$$\rho u \frac{\partial Z}{\partial x} + \rho v \frac{\partial Z}{\partial y} = \frac{\partial}{\partial y}\left(\rho D \frac{\partial Z}{\partial y}\right)\,. \tag{10.25}$$

The momentum equation may be combined with the continuity equation and integrated

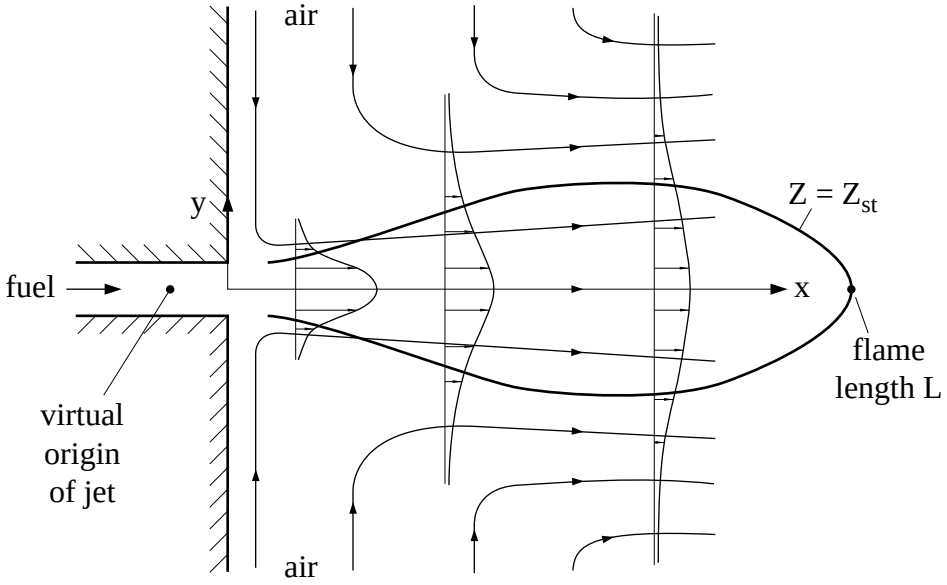

Fig. 10.3: A laminar plane jet diffusion flame

from $y = 0$ to $y \to \infty$

$$\frac{\partial}{\partial x} \int_0^\infty \rho u^2 \, dy + \Big[\rho u v\Big]_0^\infty = \left[\rho \nu \frac{\partial u}{\partial y}\right]_0^\infty . \tag{10.26}$$

With the boundary conditions $u = 0$ and $\partial u/\partial y = 0$ at $y = \infty$ (conf. Fig. 10.3) and $v = 0$ and $du/dy = 0$ at $y = 0$ due to symmetry, the last two terms in (10.26) are zero. It follows that the first integral denoting the jet momentum is independent of x and therefore constant, equal to the momentum at $x = 0$. Assuming a constant exit velocity across the orifice with the half-width b the jet momentum is

$$\int_0^\infty \rho u^2 \, dy = \rho_0 u_0^2 b \tag{10.27}$$

where ρ_0 is the density of the fuel stream. The continuity equation is satisfied by the stream function ψ defined by

$$\rho u = \frac{\partial \psi}{\partial y} , \quad \rho v = -\frac{\partial \psi}{\partial x} . \tag{10.28}$$

We now want to eliminate the x-dependence and introduce a similarity variable of the form $\eta \sim y/x^m$. Requiring that the stream function is of the form $\psi \sim x^m f(\eta)$ we need two conditions to determine n and m. These are the momentum balance (10.27) and the balance between the convective and diffusive terms in (10.24). This leads to $m = 1/3$ and

$n = 2/3$. The approprimate length and velocity scales for a momentum driven viscous jet are

$$\begin{aligned} l_\nu &= \nu_0/u_0 \\ u_\nu &= u_0 \end{aligned} \tag{10.29}$$

where ν_0 is the kinematic viscosity of the fuel stream. The similarity coordinates ζ and η and the non-dimensional stream function $f(\eta)$ may now be written

$$\eta = \frac{1}{3\, l_\nu^{1/3} \zeta^{2/3}} \int_0^y \frac{\rho}{\rho_0} dy = \frac{1}{3} \left(\frac{u_0}{\nu_0 \zeta^2} \right)^{1/3} \int_0^y \frac{\rho}{\rho_0} dy \tag{10.30}$$

$$\zeta = x + a\,,$$

$$f(\eta) = \frac{\psi}{\rho_0 \zeta^{1/3} u_\nu l_\nu^{2/3}} = \frac{\psi}{\rho_0 (\nu_0^2 u_0 \zeta)^{1/3}}\,. \tag{10.31}$$

Here a is the distance between $x = 0$ and the apparent origin of the jet. This leads with (10.28) to the velocities

$$\begin{aligned} u &= \frac{1}{3} \left(\frac{u_0^2 \nu_0}{\zeta} \right)^{1/3} f'(\eta) \\ \rho v &= -\frac{\rho_0}{3} \left(\frac{\nu_0^2 u_0}{\zeta^2} \right)^{1/3} (f - 2\eta f')\,. \end{aligned} \tag{10.32}$$

Here the prime denotes differentiation with respect to η.

A general transformation rule from the x, y to $\eta = \eta(x, y)$, $\zeta = x + a$ coordinate system is

$$\begin{aligned} \frac{\partial}{\partial x} &= \frac{\partial \zeta}{\partial x} \frac{\partial}{\partial \zeta} + \frac{\partial \eta}{\partial x} \frac{\partial}{\partial \eta} \\ \frac{\partial}{\partial y} &= \frac{\partial \eta}{\partial y} \frac{\partial}{\partial \eta}\,. \end{aligned} \tag{10.33}$$

When this is introduced into the convective term of (10.24) one obtains with (10.30) and (10.31)

$$\rho u \frac{\partial u}{\partial x} + \rho v \frac{\partial u}{\partial y} = \frac{\partial \eta}{\partial y} \left(\frac{\partial \psi}{\partial \eta} \frac{\partial u}{\partial \zeta} - \frac{\partial \psi}{\partial \zeta} \frac{\partial u}{\partial \eta} \right) = -\frac{1}{9} \frac{\rho_0 \nu_0 u_0}{\zeta} \frac{\partial \eta}{\partial y} (f'^2 + f f'')\,. \tag{10.34}$$

For the diffusive term it follows

$$\frac{\partial}{\partial y} \left(\rho \nu \frac{\partial u}{\partial y} \right) = \frac{1}{9} \frac{\rho_0 \nu_0 u_0}{\zeta} \frac{\partial \eta}{\partial y} \frac{\partial}{\partial \eta} \left(C \frac{\partial f'}{\partial \eta} \right) \tag{10.35}$$

where C is again the Chapman-Rubesin parameter

$$C = \frac{\rho^2 \nu}{\rho_0^2 \nu_0}\,. \tag{10.36}$$

Combinig these leads to the equation for the non-dimensional stream function

$$f'^2 + ff'' + (Cf'')' = 0 \tag{10.37}$$

with the boundary conditions

$$\begin{aligned} f = 0\,, \quad f'' = 0 \quad &\text{for} \quad \eta = 0 \\ f' = 0 \qquad\quad &\text{for} \quad \eta \to \infty\,. \end{aligned} \tag{10.38}$$

This equation may be integrated once to yield

$$ff' + Cf'' = 0\,. \tag{10.39}$$

This equation remains the same when f divided by and η is multiplied by a constant γ. For simplicity we assume $C = 1$ and integrate again by introducing $F = f/2\gamma$ and $\xi = \gamma\eta$

$$F' + F^2 = 1 \tag{10.40}$$

where the constant of integration has been set equal to unity. A further integration yields

$$\xi = \int_0^F \frac{dF}{1 - F^2} = \frac{1}{2} \ln \frac{1 + F}{1 - F}\,. \tag{10.41}$$

The solution may then be written

$$F = \tanh \xi = \frac{1 - \exp(-2\xi)}{1 + \exp(-2\xi)}\,. \tag{10.42}$$

The constant γ is to be evaluated by using the momentum integral (10.27). With

$$\begin{aligned} f' &= 2\gamma^2 \frac{\partial F}{\partial \xi} = 2\gamma^2 (1 - \tanh^2 \xi) \\ u &= \frac{2}{3}\gamma^2 \left(\frac{u_0^2 \nu_0}{\zeta} \right)^{1/3} (1 - \tanh^2 \xi) \end{aligned} \tag{10.43}$$

This is written as

$$\frac{4}{3}\gamma^3 \rho_0 u_0 \nu_0 \int_0^\infty (1 - \tanh^2 \xi)^2 \, d\xi = \rho_0 u_0^2 b \tag{10.44}$$

where the integral with (10.41) and (10.42)

$$\int_0^\infty (1 - \tanh^2 \xi)^2 d\xi = \int_0^1 (1 - F^2) dF = \frac{2}{3}$$

This leads to

$$\gamma^3 = \frac{9}{8}\frac{u_0 b}{\nu_0} = \frac{9}{8}\mathrm{Re}_0 \tag{10.45}$$

where Re_0 is the jet exit Reynolds number. The equation for the mixture fraction may similarly be transformed by introducing the ansatz

$$Z = \alpha \left(\frac{\nu_0}{u_0 \zeta}\right)^{1/3} \omega \tag{10.46}$$

with a jet unknown coeffizient α, into (10.34) and (10.35) with u replaced by Z. One then obtains

$$f'\omega + f\omega' + \left(\frac{C}{\mathrm{Sc}}\omega'\right)' = 0 \tag{10.47}$$

where Sc is the Schmidt number ν/D. This also may be integrated once to

$$f\omega + \frac{C}{\mathrm{Sc}}\omega' = 0 \tag{10.48}$$

Combing this with (10.39) one finds a coupling between ω and f' as

$$\frac{\mathrm{d}\ln f'}{\mathrm{d}\eta} = \frac{1}{\mathrm{Sc}}\frac{\mathrm{d}\ln \omega}{\mathrm{d}\eta} \tag{10.49}$$

which may be integrated for constant Sc as

$$\omega = (f')^{\mathrm{Sc}} \tag{10.50}$$

For $C = 1$ this leads to

$$Z = \alpha \left(2\gamma^2\right)^{\mathrm{Sc}} \left(\frac{\nu_0}{u_0 \zeta}\right)^{1/3} [1 - \tanh^2(\gamma\eta)]^{\mathrm{Sc}}\,. \tag{10.51}$$

By integrating the mixture fraction equation (10.25) in a similar way as the momentum equation one finds that the integrated mass flow rate must be independent of x

$$\int_0^\infty \rho u Z \, dy = \rho_0 u_0 b\,. \tag{10.52}$$

If (10.45) and (10.51) are introduced this leads to

$$\alpha \left(2\gamma^2\right)^{\mathrm{Sc}} \int_0^1 (1 - F^2)^{\mathrm{Sc}} \, dF = \frac{4}{9}\gamma^2$$

from which the coeffizient α in (10.46) can be determined . For $\mathrm{Sc} = 1$ one obtains $\alpha = 1/3$. In this case the mixture fraction field is proportional to the velocity field

$$Z = \frac{u}{u_0}\,. \tag{10.53}$$

Equation (10.51) may be used to determine the flame length L of the plane jet diffusion flame. By setting $Z = Z_{\mathrm{st}}$ and $\eta = 0$ in (10.51) one obtains for $L = x$

$$L + a = \left(\frac{\alpha\left(2\gamma^2\right)^{\mathrm{Sc}}}{Z_{\mathrm{st}}}\right)^3 \frac{\nu_0}{u_0} = \frac{\alpha^3}{Z_{\mathrm{st}}^3}\left(\frac{9}{\sqrt{8}}\mathrm{Re}_0\right)^{2\mathrm{Sc}} \frac{\nu_0}{u_0}\,, \tag{10.54}$$

where (10.45) has been used. Since Z_{st} is typically small this leads to large values of L in terms of the diffusive length scale ν_0/u_0. The distance a of the virtual jet origin from the exit plane is small compared to L and may therefore be neglected.

10.3 A Buoyancy Driven Planar Diffusion Flame Above a Vertical Splitter Plate

Since many laminar diffusion flames, for instance the candle flame, are largely influenced by buoyancy, we want to consider a buoyancy driven flame in, however, an idealized situation for which again a similarity solution can be obtained. Fig. 10.4 shows a symmetric two-dimensional flame sheet above a splitter plate, called the "infinite candle" [10.3] because the fuel and oxidizer are assumed ininitely large extending to $y \to -\infty$ and $y \to +\infty$, respectively, and from $z = -\infty$ to $z = +\infty$.

We assume that the flame sheet is infinitely thin of the Burke-Schumann type and that the boundary layer approximation is valid. Then the governing equations outside the flame sheet are

Continuity

$$\frac{\partial \rho w}{\partial z} + \frac{\partial \rho v}{\partial y} = 0 \tag{10.55}$$

Momentum in z-direction

$$\rho w\frac{\partial w}{\partial z} + \rho v\frac{\partial w}{\partial y} = \frac{\partial}{\partial y}\left(\rho\nu\frac{\partial w}{\partial y}\right) + (\rho_u - \rho)g \tag{10.56}$$

Temperature

$$\rho w\frac{\partial T}{\partial z} + \rho v\frac{\partial T}{\partial y} = \frac{\partial}{\partial y}\left(\frac{\rho\nu}{\mathrm{Pr}}\frac{\partial T}{\partial y}\right) + \frac{Q}{c_p}w\,. \tag{10.57}$$

Since the chemistry is assumed infinitely fast, the reaction rate w appearing in the temperature equation may be replaced by a δ-function at the flame surface. Here $\mathrm{Pr} = \rho\nu c_p/\lambda$ is the Prandtl number. In order to obtain a symmetric solution we assume equal density and temperature in the unburnt fuel and oxidizer far from the splitter plate. Then the

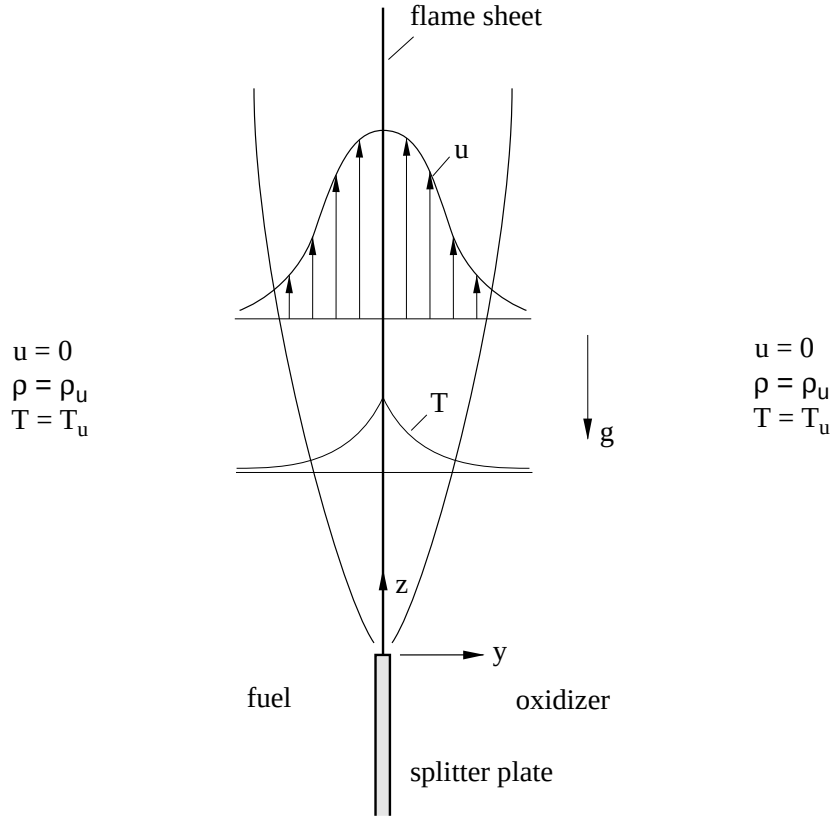

Fig. 10.4: The symmetric infinite candle

flame surface lies at $y = 0$. The boundary conditions for the chemically inert flow outside of the flame surface are

$$\begin{aligned} T = T_{\rm st}\,, \quad v = 0\,, \quad \frac{\partial w}{\partial y} = 0 \quad \text{for} \quad y = 0 \\ \rho = \rho_u\,, \quad T = T_u\,, \quad w = 0 \quad \text{for} \quad y \to \pm\infty\,. \end{aligned} \tag{10.58}$$

Introducing a stream function ψ, defined by

$$\rho w = \frac{\partial \psi}{\partial y}\,, \quad \rho v = -\frac{\partial \psi}{\partial z} \tag{10.59}$$

the continuity equation is satisfied. Characteristic length and velocity scales for buoyancy driven flames are

$$\begin{aligned} l_g &= \left(\frac{\nu_{\rm st}^2 \rho_{\rm st}}{g(\rho_u - \rho_{\rm st})} \right)^{1/3} \\ u_g &= \left(\frac{g \nu_{\rm st} (\rho_u - \rho_{\rm st})}{\rho_{\rm st}} \right)^{1/3} \end{aligned} \tag{10.60}$$

We now introduce the parameter $\sigma = \rho_u/\rho_{\rm st} = T_{\rm st}/T_u$ and the similarity coordinate

$$\eta = \frac{1}{l_g^{3/4} z^{1/4}} \int_0^y \frac{\rho}{\rho_{\rm st}}\, dy = \left[\frac{g(\sigma-1)}{\nu_{\rm st}^2 z}\right]^{1/4} \int_0^y \frac{\rho}{\rho_{\rm st}}\, dy \tag{10.61}$$

A non-dimensional stream function may be defined

$$F(\eta) = \frac{\psi}{\rho_{\rm st} z^{3/4}} \frac{1}{l_g^{1/4} u_g} = \frac{\psi}{\rho_{\rm st}[\nu_{\rm st}^2 g z^3 (\sigma-1)]^{1/4}} \tag{10.62}$$

which is only a function of η. Then it is seen with (10.59) that the velocity w

$$w = [zg(\sigma-1)]^{1/2} \frac{\partial F}{\partial \eta} \tag{10.63}$$

increases with the square root of z. Introducing the similarity transformation one obtains for the convective terms in (10.56)

$$\rho w \frac{\partial w}{\partial z} + \rho v \frac{\partial w}{\partial y} = \frac{\partial \eta}{\partial y}\left(\frac{\partial \psi}{\partial \eta}\frac{\partial w}{\partial z} - \frac{\partial \psi}{\partial z}\frac{\partial w}{\partial \eta}\right) = \rho_{\rm st}[\nu_{\rm st}^2 g^3 (\sigma-1)^3 z]^{1/4} \frac{\partial \eta}{\partial y}\left[\frac{F'^2}{2} - \frac{3}{4} F F''\right]. \tag{10.64}$$

The diffusive term takes the form

$$\frac{\partial}{\partial y}\left(\rho\nu \frac{\partial w}{\partial y}\right) = \rho_{\rm st}[\nu_{\rm st}^2 g^3 (\sigma-1)^3 z]^{1/4} \frac{\partial \eta}{\partial y}\frac{\partial}{\partial \eta}\left(C \frac{\partial^2 F}{\partial \eta^2}\right). \tag{10.65}$$

With these one obtains the momentum equation

$$(CF'')' + \frac{3}{4} F F'' - \frac{1}{2} F'^2 + H = 0 \tag{10.66}$$

Here C is the Chapmann-Rubesin parameter $C = (\rho^2\nu)/(\rho_{\rm st}^2 \nu_{\rm st})$ and H the density ratio

$$H = \frac{\rho_u - \rho}{\rho(\sigma-1)}. \tag{10.67}$$

The ideal gas law shows that $\rho_u/\rho = T/T_u$ and H may be expressed for constant pressure and mean molecular weight as a temperature ratio

$$H = \frac{T - T_u}{T_{\rm st} - T_u} \tag{10.68}$$

With the assumption that the temperature is a function of η only one obtains the temperature equation as

$$\left(\frac{C}{\rm Pr} H'\right)' + \frac{3}{4} F H' = 0. \tag{10.67}$$

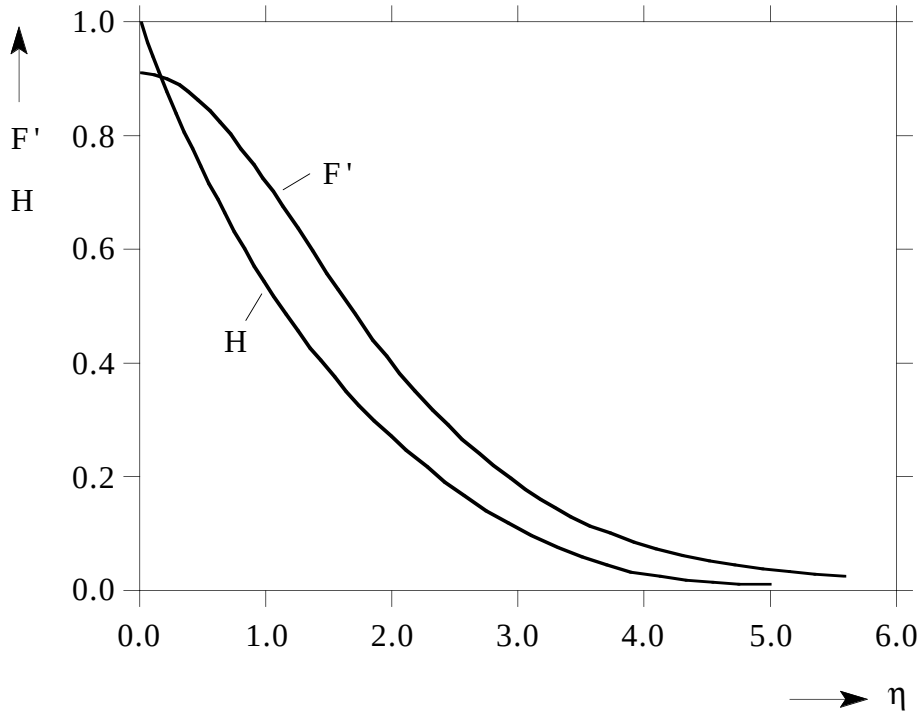

Fig. 10.5: The velocity and temperature functions defined by similarity solution.

The boundary conditions for (10.65) and (10.67) are

$$\begin{aligned} F = 0\,, \quad F'' = 0\,, \quad H = 1 \quad &\text{at} \quad \eta = 0 \\ F' = 0\,, \quad H = 0 \quad &\text{at} \quad \eta \to \infty\,. \end{aligned} \tag{10.68}$$

The solution for F' and H was calculated numerically for $C = 1$, $\mathrm{Pr} = 0.75$ and is plotted in Fig 10.5. There is a buoyancy induced maximum of the velocity profile at the flame surface. The similarity solution is valid above the splitter plate for $z \gg l_g$. For $\nu_{\mathrm{st}} \approx 3.4 \cdot 10^{-4} \mathrm{m}^2/\mathrm{sec}$ and a density ratio $\rho_u/\rho_{\mathrm{st}} \approx 6$ the characteristic length and velocity scales are

$$l_g = 1.3 \text{ mm} \quad \text{and} \quad u_g = 0.24 \text{ m/sec}$$

If an imposed forced convective velocity that is larger than this estimate, the flow field is influenced by both, forced convection and buoyancy. Similarly, buoyancy becomes important in a convection dominated flame like the one considered before, when the convective flow velocity is smaller than u_g.

10.4 Single droplet combustion

In many practical applications fuel liquid fuel is injected into the combustion chamber resulting in a fuel spray. By the combined action of aerodynamical shear, strain, and surface tension the liquid spray will decompose into a large number of single droplets of different diameters. The fuel will then evaporate and a non-homogeneous fuel air mixture will be formed in the flow field surrounding the droplets. When the spray is ignited, the droplets will burn either as a cloud surrounded by a enveloping flame or as single droplets, each being surrounded by its own diffusion flame. The former will the case if the fuel air mixture between different droplets is fuel rich such that the surface of stoichiometric mixture will surround the droplet cloud. We will consider here the latter case, where the surface of stoichiometric mixture surrounds the single droplet. We will furthermore consider very small droplets which follow the flow very closely and assume that the velocity difference between the droplet and the surrounding fuel is zero. Therefore we may consider the case of a spherically symmetric droplet in a quiescent surrounding. We assume the evaporation and combustion process as quasi-steady and can therefore use the steady state equations

Continuity

$$\frac{\mathrm{d}}{\mathrm{d}r}\left(r^2\rho v\right) = 0 \tag{10.69}$$

Mixture fraction

$$\rho v\frac{\mathrm{d}Z}{\mathrm{d}r} = \frac{1}{r^2}\frac{\mathrm{d}}{\mathrm{d}r}\left(r^2\rho D\frac{\partial Z}{\partial r}\right) \tag{10.70}$$

Temperature

$$\rho v\frac{\mathrm{d}T}{\mathrm{d}r} = \frac{1}{r^2}\frac{\mathrm{d}}{\mathrm{d}r}\left(r^2\frac{\lambda}{c_p}\frac{\partial T}{\partial r}\right) + \frac{Q}{c_p}w \tag{10.71}$$

In these equations r is the radial coordinate, and v is the flow velocity in radial direction. Here again a unity Lewis number leading to $\lambda = \rho c_p D$ and a one step reaction with fast chemistry will be assumed. The reaction rate w is then a δ-function at the flame surface located at $Z = Z_{\mathrm{st}}$. The expected temperature and mixture fraction profiles are schematically shown in Fig. 10.6. The boundary conditions for (10.69)–(10.71) at the droplet surface $r = R$ are obtained by integrating the balance equations once across $r = R$.

Since temperature and concentration gradients within the droplet are assumed negligible, the convective flux through the surface equals the diffusive flux in the gas phase at the droplet surface. The convective heat flux through the boundary involves a change of enthalpy, namely the enthalpy of evaporation h_L. Therefore

$$r = R: \quad \lambda\frac{\mathrm{d}T}{\mathrm{d}r}\bigg|_R = (\rho v)_R\, h_L\,. \tag{10.72}$$

Here $(\rho v)_R$ is the convective mass flux through the surface. The mixture fraction of the convective flux involves the difference between the mixture fraction within the droplet, which is unity by definition, and that in the gas phase at the droplet surface, where

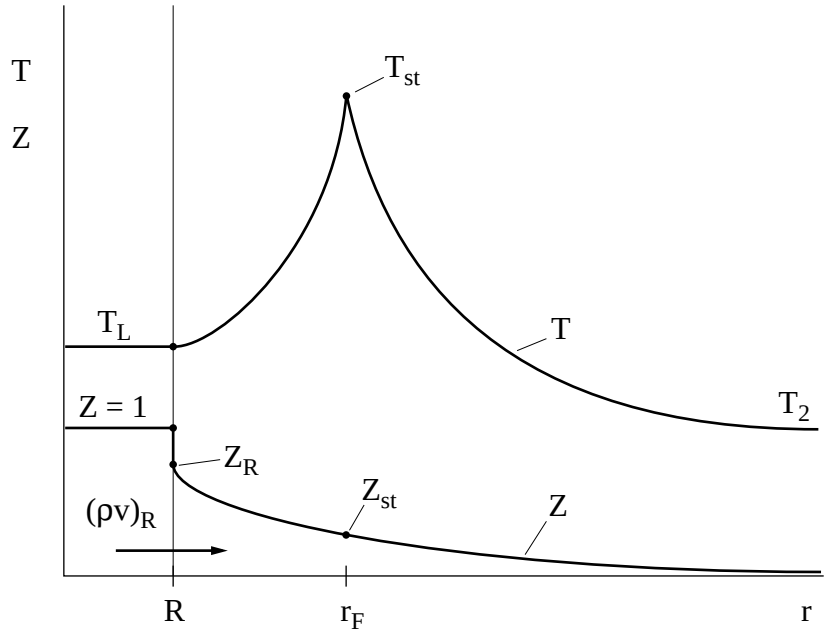

Fig. 10.6: Temperature and mixture fraction profiles at the surface and in the surroundings of a burning spherical droplet.

$Z = Z_R$. This leads to

$$r = R: \quad \rho D \frac{\mathrm{d}Z}{\mathrm{d}r}\bigg|_R = (\rho v)_R (Z_R - 1)\,. \tag{10.73}$$

The changes of temperature and mixture fraction at the surface are also shown in Fig. 10.6. The boundary conditions in the surrounding air are

$$r \to \infty: \quad T = T_2\,, \quad Z = 0 \tag{10.74}$$

In addition, we assume that the temperature T_L at the droplet surface is equal to the boiling temperature of the liquid

$$T = T_L\,. \tag{10.75}$$

Then the temperature equation must satisfy three boundary conditions. This leads to an eigenvalue problem for the mass burning rate

$$\dot{m} = 4\pi R^2 (\rho v)_R \tag{10.76}$$

of the droplet which thereby can be determined. Integration of the continuity equation leads to

$$\rho v r^2 = R^2\,(\rho v)_R \tag{10.77}$$

We will now introduce the nondimensional coordinate

$$\eta = \int_r^\infty \frac{v}{D} \exp(-\zeta) \mathrm{d}r \tag{10.78}$$

where

$$\zeta = \int_r^\infty \frac{v}{D} \mathrm{d}r = \frac{\dot{m}}{4\pi} \int_r^\infty (\rho D r^2)^{-1} \mathrm{d}r \,. \tag{10.79}$$

Between η and ζ there is the relation

$$\frac{\mathrm{d}\eta}{\mathrm{d}\zeta} = \frac{\mathrm{d}\eta/\mathrm{d}r}{\mathrm{d}\zeta/\mathrm{d}r} = \exp(-\zeta) \tag{10.80}$$

This may be integrated with the boundary conditions at $r \to \infty$: $\zeta = 0$, $\eta = 0$ to yield

$$\eta = 1 - \exp(-\zeta) \tag{10.81}$$

and at $r = R$

$$\eta_R = 1 - \exp(-\zeta_R) \,. \tag{10.82}$$

Transformation of (10.70)–(10.71) with their boundary conditions leads to

$$\frac{\mathrm{d}^2 Z}{\mathrm{d}\eta^2} = 0 \tag{10.83}$$

$$\begin{aligned} &\eta = \eta_R : \quad (\eta_R - 1) \frac{\mathrm{d}Z}{\mathrm{d}\eta} = Z_R - 1 \\ &\eta \to 0 : \quad Z = 0 \end{aligned} \tag{10.84}$$

$$\rho D \left(\frac{\mathrm{d}\eta}{\mathrm{d}r} \right)^2 \frac{\mathrm{d}^2 T}{\mathrm{d}\eta^2} = -\frac{Q}{c_p} w \tag{10.85}$$

$$\begin{aligned} &\eta = \eta_R : \quad (\eta - 1) \frac{\mathrm{d}T}{\mathrm{d}\eta} = \frac{h_L}{c_p} \,, \quad T_2 = T_L \\ &\eta \to 0 : \quad T = T_2 \end{aligned} \tag{10.86}$$

The solution of the mixture fraction equation with its boundary condition is readily seen to be

$$Z = \eta \,. \tag{10.87}$$

If this is introduced into the temperature equation and the scalar dissipation rate for the present problem is defined as

$$\chi = 2D \left(\frac{\mathrm{d}Z}{\mathrm{d}r} \right)^2 = 2D \left(\frac{\mathrm{d}\eta}{\mathrm{d}r} \right)^2 \tag{10.88}$$

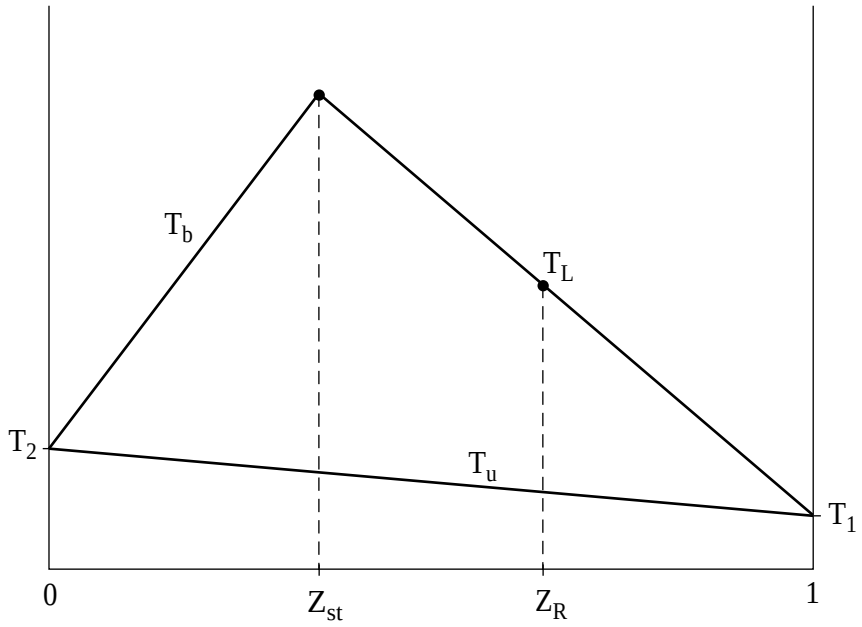

Fig. 10.7: ???

one obtains

$$\rho \frac{\chi}{2} \frac{\mathrm{d}^2 T}{\mathrm{d}Z^2} = -\frac{Q}{c_p} w \tag{10.89}$$

which reduces to (9.7) if the steady state, negligible heat loss, and one-step chemistry was assumed. We therefore find that the one-dimensional droplet combustion problem satisfies the laminar flamelet assumptions exactly.

Here we want to consider the Burke-Schumann-solution (1.67). Then, in the fuel rich region between $r = R$ and $r = r_F$ (conf. Fig. 10.6) we have

$$T(Z) = T_2 + Z(T_1 - T_2) + \frac{QY_{\mathrm{O}_2,2}}{c_p \nu'_{\mathrm{O}_2} W_{\mathrm{O}_2}} (1 - Z) \tag{10.90}$$

Here T_1 is by definition the temperature at $Z = 1$, which does not exist in the present problem. We know, however, from the boundary conditions (10.86) the slope and the value at $Z = Z_R$ where

$$T_L = T_2 + Z_R(T_1 - T_2) + \frac{QY_{\mathrm{O}_2,2}}{c_p \nu'_{\mathrm{O}_2} W_{\mathrm{O}_2}} (1 - Z_R)\,. \tag{10.91}$$

Introducing (10.90) and(10.91) into the first of (10.86) one obtains

$$T_1 = T_L - \frac{h_L}{c_p}\,. \tag{10.92}$$

This is a hypothetical temperature corresponding to the fuel if one considers the droplet as a point source of gaseous fuel. The heat of vaporisation then decreases the temperature of the liquid fuel by the amount h_L/c_p. It should be used in flamelet calculations if one wishes to calculate flamelet profiles in the range $0 < Z < 1$ rather than $0 < Z < Z_R$. The boundary condition (10.86) may also be used with (10.90) and (10.82) to calculate the non-dimensional mass burning rate

$$\zeta_R = \ln\left(1 + \frac{c_p(T_2 - T_L) + Y_{\mathrm{O}_2,2} Q/\nu'_{\mathrm{O}_2} W_{\mathrm{O}_2}}{h_L}\right). \tag{10.93}$$

From this, the mass burning rate may be determined using (10.79). We will introduce radially averaged properties $\overline{\rho D}$ defined by

$$\left(\overline{\rho D}\right)^{-1} = R \int_R^\infty \frac{\mathrm{d}r}{\rho D r^2} \tag{10.94}$$

to obtain

$$\dot{m} = 4\pi\, \overline{\rho D}\, R\, \zeta_R\,. \tag{10.95}$$

Now it is possible to determine the time needed to burn a droplet with initial radius R_0 at time $t = 0$. The droplet mass is $m = 4\pi\, \rho_L\, R^3/3$, where ρ_L is the density of the liquid. Its negative time rate of change equals the mass loss due to the mass burning rate

$$\frac{\mathrm{d}m}{\mathrm{d}t} = 4\pi\, \rho_L\, R^2\, \frac{\mathrm{d}R}{\mathrm{d}t} = -\dot{m}\,. \tag{10.96}$$

Introducing (10.95) and assuming $\overline{\rho D}$ independent of time one obtains by separation of variables

$$\mathrm{d}t = -\frac{\rho_L}{\zeta_R\, \overline{\rho D}}\, R\, \mathrm{d}R\,, \quad t \cong R_0^2 - R^2\,. \tag{10.97}$$

Integrating from $R = R_0$ to $R = 0$ one obtains the burnout time

$$t = \frac{\rho_L}{8\zeta_R\, \overline{\rho D}}\, \mathrm{d}^2 \tag{10.98}$$

where $\mathrm{d} = 2R_0$ is the initial droplet diameter. This is called the d^2-law of droplet combustion and shown in Fig. 10.8. It represents a very good first approximation for the droplet combustion time and has often be confirmed by experiments.

Finally, we want to calculate the radial position of the surrounding flame. Evaluating (10.81) for $Z = Z_{\mathrm{st}} = \eta_{\mathrm{st}}$ one obtains

$$1 - Z_{\mathrm{st}} = \exp(-\zeta_{\mathrm{st}}) \tag{10.99}$$

where with (10.77) and (10.79)

$$\zeta_{\mathrm{st}} = \frac{\dot{m}}{4\pi\, \overline{\rho D}\, \nu_{\mathrm{st}}}\,. \tag{10.100}$$

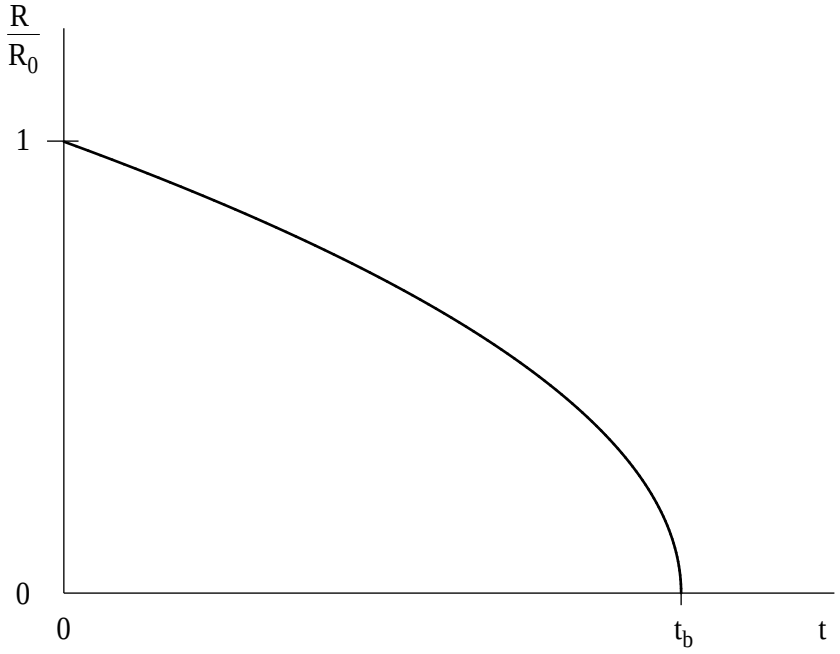

Fig. 10.8: ???

Here $\overline{\rho D}$ is defined as in (10.94) but averaging by an integration from $\nu_{\rm st}$ to ∞ rather than from R to ∞. If both are assumed equal one may use (10.95) to determine the flame radius as

$$\frac{r_{\rm st}}{R} = \frac{\zeta_R}{\ln[1/(1-Z_{\rm st})]}\,. \tag{10.101}$$

For sufficiently small values of $Z_{\rm st}$ the denominator of (10.101) may be approximated by $Z_{\rm st}$ itself showing that ratio $r_{\rm st}/R$ may take quite large values.

Problem 10.1:

Determine the non-dimensional mass burning rate and $r_{\rm st}/R$ for a Diesel fuel where $h_L/c_p = 160$ K, $T_L = 560$ K, $T_2 = 800$ K and $T_{\rm st} - T_u(Z_{\rm st}) = 2000$ K, $Z_{\rm st} = 0.036$.

Solution

Using the Burke-Schumann solution the non-dimensional mass burning rate may be written as

$$\zeta_R = \ln\left[1 + \frac{T_2 - T_L + (T_{\rm st} - T_u(Z_{\rm st}))/(1-Z_{\rm st})}{h_L/c_p}\right] = 2.74\,.$$

The ratio of the flame radius to the droplet radius is then

$$\frac{r_{\rm st}}{R} \approx 75\,.$$

Problem 10.2:

Compare the evaporation rate for the same droplet as in problem 10.1 to that of the mass burning rate.

Solution

The non-dimensional evaporation rate of a droplet may be obtained in a similar way as (10.93). It follows from (10.93) in the limit $Q = 0$, therefore

$$\zeta_R = \ln\left(1 + \frac{T_2 - T_L}{h_L/c_p}\right) = 0.916$$

The combustion rate is approximately three times faster than the evaporation rate.

References

[10.1] Tsuji

[10.2] Schlichting, H., Boundary Layer Theory, 4th ed., McGraw-Hill New York 1960.

[10.3] Buckmaster, J. and Peters, N., 21st Symposium (International) on Combustion, pp. 1829–1836, The Combustion Institute 1986.

Lecture 11: Turbulent Combustion: Introduction and Overview

A major factor in the progress of understanding turbulent combustion is the identification of different regimes defined by different time and length scale ratios. From a technical point of view the interaction between turbulence and chemistry may be classified by two criteria: premixed or non-premixed combustion, slow or fast chemistry. The first criterion is relevant with respect to applications: combustion in large furnaces and gas turbines as well as reactive flows in chemical industry are essentially non-premixed while combustion in spark ignition engines or in household burners occurs in the premixed regime. Slow chemistry is not very often of practical interest: there are a few situations like formation and destruction of pollutants in post-flame regions where chemistry is slow compared to convection and diffusion. On the other hand, reacting flows with fast chemistry occur in nearly all the applications mentioned above. The reason is simple: for combustion to be stable and complete, it must be rapid and therefore the chemical time scales must be sufficiently short under all circumstances. Therefore engines are designed such that only at limit conditions, i.e. at very high engine speeds, turbulent time scales may become comparable to chemical time scales.

11.1 Semi-empirical Models of Turbulence

A classical way to describe turbulent flows is to split all the components of velocity and also scalar quantities like the temperature and mass fractions measured at a point $\underline{x}$ into a mean (denoted by an overbar) and a fluctuation such as

$$u(\underline{x},t) = \bar{u}(\underline{x},t) + u'(\underline{x},t), \quad \text{where} \quad \bar{u'} = 0 \tag{11.1}$$

If the flow is stationary on the average, a time average defines the mean

$$\bar{u}(\underline{x}) = \lim_{\Delta t \to \infty} \left\{ \frac{1}{\Delta t} \int_{t}^{t+\Delta t} u(\underline{x},t)\mathrm{d}t \right\}. \tag{11.2}$$

For general, including instationary flows an ensemble average may be defined

$$\bar{u}(\underline{x},t) = \lim_{n \to \infty} \left\{ \sum_{k=1}^{n} u_k(\underline{x},t)/n \right\}, \tag{11.3}$$

where $u_k(\underline{x},t)$ are instantaneous values measured, for instances at the same time during a repeated measuring cycle. For flows with large density changes like in combustion it is often convenient to introduce a density weighted average $\tilde{u}$, called Favre average, defined by

$$u(\underline{x},t) = \tilde{u}(\underline{x},t) + u''(\underline{x},t) \quad \text{with} \quad \overline{\rho u''} = 0 \tag{11.4}$$

Multiplying (11.4) by the density ρ and time averaging yields

$$\tilde{u} = \overline{\rho u}/\bar{\rho} \tag{11.5}$$

Furthermore the relation between the conventional mean and the Favre mean average is obtained from

$$\overline{\rho u} = \overline{(\bar{\rho} + \rho')(\bar{u} + u')} = \bar{\rho}\bar{u} + \overline{\rho' u'} \tag{11.6}$$

but $\overline{\rho u} = \bar{\rho}+\tilde{u}$ showing that a correlation between velocity and density fluctuations appears in the conventional averaging of the product ρu, but does not appear in Favre averaging. This is a considerable advantage, when the averaging is applied to the balance equations of momentum, energy and chemical species, where the convective terms are dominant in high Reynolds number flows. Since they contain the product of the dependent variable with the density, they are treated very simply by Favre averaging. Difficulties arising in the viscous and diffusive transport are of lower importances since these terms are usually neglected as compared to turbulent diffusion.
In Favre-averaged form the balance equations are written:

Continuity

$$\frac{\partial \bar{\rho}}{\partial t} + \frac{\partial(\bar{\rho}\tilde{v}_\alpha)}{\partial x_\alpha} = 0 \tag{11.7}$$

Momentum

$$\bar{\rho}\frac{\partial \tilde{v}_\beta}{\partial t} + \bar{\rho}\tilde{v}_\alpha \frac{\partial \tilde{u}_\beta}{\partial x_\alpha} = -\frac{\partial \bar{p}}{\partial x_\beta} + \frac{\partial \bar{\tau}_{\alpha\beta}}{\partial x_\alpha} - \frac{\partial}{\partial x_\alpha}\left(\bar{\rho}\,\widetilde{v''_\alpha v''_\beta}\right) + \bar{\rho} g_\beta \tag{11.8}$$

Here the mean viscous stress is often neglected compared to the Reynolds stress term $\bar{\rho}\,\overline{v''_\alpha v''_\beta}$. Introducing a gradient transport hypothesis, this may be modelled as Reynolds stress

$$\bar{\rho}\,\widetilde{v''_\alpha v''_\beta} = \begin{cases} -\bar{\rho}\nu_t\,[2\dfrac{\partial \tilde{v}_\alpha}{\partial x_\beta} - \dfrac{2}{3}\dfrac{\partial \tilde{v}_\gamma}{\partial x_\gamma}] + \dfrac{2}{3}\bar{\rho}\,\tilde{k}\,, & \alpha = \beta \\ -\bar{\rho}\nu_t\,[\dfrac{\partial \tilde{v}_\alpha}{\partial x_\beta} + \dfrac{\partial \tilde{v}_\beta}{\partial x_\alpha}]\,, & \alpha \neq \beta \end{cases} \tag{11.9}$$

where a turbulent viscosity ν_t is introduced

$$\nu_t = c_D\,\frac{\tilde{k}^2}{\tilde{\varepsilon}}\,, \qquad c_D \approx 0.09 \tag{11.10}$$

The scalar quantities $\tilde{k}$ and $\tilde{\varepsilon}$ denote the Favre averaged turbulent kinetic energy and its dissipation. They may be calculated from modelled equations:

Turbulent kinetic energy $\tilde{k} = \frac{1}{2}\widetilde{v''^2_\beta}$

$$\bar{\rho}\frac{\partial \tilde{k}}{\partial t} + \bar{\rho}\tilde{v}_\alpha \frac{\partial \tilde{k}}{\partial x_\alpha} = \frac{\partial}{\partial x_\alpha}\left(\nu_t \frac{\partial \tilde{k}}{\partial x_\alpha}\right) - \bar{\rho}\widetilde{v''_\alpha v''_\beta}\frac{\partial \tilde{u}_\alpha}{\partial x_\beta} - \rho\tilde{\varepsilon} \tag{11.11}$$

Turbulent dissipation

$$\bar{\rho}\frac{\partial \tilde{\varepsilon}}{\partial t} + \rho\tilde{v}_\alpha \frac{\partial \tilde{\varepsilon}}{\partial x_\alpha} = \frac{\partial}{\partial x_\alpha}\left(\frac{\nu_t}{\sigma_\varepsilon}\frac{\partial \tilde{\varepsilon}}{\partial x_\alpha}\right)\frac{\tilde{\varepsilon}}{\tilde{k}}\left(-c_{\varepsilon 1}\bar{\rho}\,\widetilde{v''_\alpha v''_\beta}\,\frac{\partial \tilde{u}_\alpha}{\partial x_\beta} - c_{\varepsilon 2}\rho\frac{\tilde{\varepsilon}}{\tilde{k}}\right) \tag{11.12}$$

In the standard k-ε model the constants $\sigma_\varepsilon \approx 1.3$, $c_{\varepsilon 1} \approx 1.44$, $c_{\varepsilon 2} \approx 1.9$ are used.

In non-premixed combustion modelled equations for the mixture fraction and its variance are also needed. These are
Mixture fraction

$$\bar{\rho}\frac{\partial \tilde{Z}}{\partial t} + \bar{\rho}\tilde{v}_\alpha \frac{\partial \tilde{Z}}{\partial x_\alpha} = \frac{\partial}{\partial x_\alpha}\Big(\bar{\rho}\,\frac{\nu_t}{\mathrm{Sc}}\,\frac{\partial \tilde{Z}}{\partial x_\alpha}\Big) \tag{11.13}$$

Mixture fraction variance

$$\bar{\rho}\frac{\partial \widetilde{Z''^2}}{\partial t} + \bar{\rho}\tilde{v}_\alpha \frac{\partial \widetilde{Z''^2}}{\partial x_\alpha} = \frac{\partial}{\partial x_\alpha}\Big(\bar{\rho}\,\frac{\nu_t}{\mathrm{Sc}}\,\frac{\partial \widetilde{Z''^2}}{\partial x_\alpha}\Big) + 2\bar{\rho}\frac{\nu_t}{\mathrm{Sc}}\Big(\frac{\partial \tilde{Z}}{\partial x_\alpha}\Big)^2 - \bar{\rho}\tilde{\chi} \tag{11.14}$$

Here the mean scalar dissipation is modelled as

$$\tilde{\chi} = c_\chi \frac{\tilde{\varepsilon}}{\tilde{k}} \widetilde{Z''^2}. \tag{11.15}$$

Value s for the turbulent Schmidt number Sc and c_χ are typically $\mathrm{Sc} \approx 0.7$ and $c_\chi \approx 2.0$.

11.2 Turbulent Length, Time, and Velocity Scales

A given turbulent flow field may locally be characterized by the root-mean-square velocity fluctuation v' and the turbulent macroscale ℓ, yielding a turbulent time scale $\tau = \ell/v'$. If conventionally averaged values of the turbulent kinetic energy and its dissipation are used, one may relate v' and ℓ to k and ε, where k is the turbulent kinetic energy and ε its dissipation by

$$v' = (2k/3)^{1/2}, \quad \ell = v'^3/\varepsilon. \tag{11.16}$$

The turbulent time is then

$$\tau = \frac{k}{\varepsilon}. \tag{11.17}$$

In terms of the kinematic viscosity ν and ε the Kolmogorov length, time and velocity scales are

$$\eta = \left(\frac{\nu^3}{\varepsilon}\right)^{1/4}, \quad t_\eta = \left(\frac{\nu}{\varepsilon}\right)^{1/2}, \quad v_\eta = (\nu\varepsilon)^{1/4}. \tag{11.18}$$

Furthermore, for non-premixed combustion, the non-homogeneous mixture field must be considered. Fluctuations of the mixture fraction, to be defined below, are characterized by

$$Z' = \sqrt{\widetilde{Z''^2}}, \tag{11.19}$$

where $\widetilde{Z''^2}$ is the Favre averaged mixture fraction variance.

The Taylor length scale λ as an intermediate scale between the integral and the Kolmogorov scale is defined by replacing the average gradient in the definition of the dissipation by u'/λ. This leads to the definition

$$\varepsilon = \nu\,\overline{\Big(\frac{\partial u_\alpha}{\partial x_\beta}\Big)^2} = 15\nu\frac{v'^2}{\lambda^2} \tag{11.20}$$

Here the factor 15 originates from considerations for isotropic homogeneous turbulence. Using (11.18) it is seen that

$$\lambda = (15\nu\, v'^2/\varepsilon)^{1/2} \sim v' t_\eta \tag{11.21}$$

is proportional to the product of the turnover velocity of the large eddies and the Kolmogorov time. Therefore λ may be interpreted as the distance that a large eddy convects a Kolmogorov eddy during its turnover time t_η.

11.3 Eddy Sizes and Turnover Times in the Inertial Range

According to Kolmogorov's 1941 theory on the universal range of turbulence, there is a transfer from the energy containing eddies of characteristic size of the integral length scale ℓ to smaller and smaller eddies. The energy tranfer per unit turnover time of the large eddies is equal to the dissipation of energy at the dissipation scale η. Therefore

$$\varepsilon = \frac{v'^2}{\tau} = \frac{v'^3}{\ell}. \tag{11.22}$$

We may define a discrete sequence of eddies within the inertial range by defining

$$\ell_n = \frac{\ell}{a^n} \geq \eta, \quad n = 1, 2, ... \tag{11.23}$$

where a is an arbitrary number $a > 1$. Since the energy transfer ε is constant within the inertial range, dimensional analysis relates the turnover time τ_n and the velocity difference v_n across the eddy ℓ_n to ε as

$$\varepsilon = \frac{v_n^2}{t_n} = \frac{v_n^3}{\ell_n} \tag{11.24}$$

This relation includes the integral scales and also holds for the dissipation scales

$$\varepsilon = \frac{v_\eta^2}{t_\eta} = \frac{v_\eta^3}{\eta} \tag{11.25}$$

11.4 Regimes in Turbulent Combustion

Premixed Turbulent Combustion

For scaling purposes it is useful to define a reference viscosity ν_{ref} as the product of the laminar burning velocity and the flame thickness

$$\nu_{\text{ref}} = s_L\, \ell_F \tag{11.26}$$

Then, we may define the turbulent Reynolds number

$$\text{Re}_\ell = v'\ell / s_L \ell_F \tag{11.27}$$

the turbulent Damköhler number

$$\mathrm{Da}_\ell = \tau/t_F = s_L\ell/v'\ell_F \tag{11.28}$$

and the turbulent Karlovitz number

$$\mathrm{Ka} = \mathrm{Da}_\eta^{-1} = t_F/t_\eta = \ell_F^2/\eta^2 = v_\eta^2/s_L^2. \tag{11.29}$$

The Karlovitz number is therefore equal to the inverse of a Damköhler number defined with the Kolmogorov time scale rather than with the integral time scale. These definitions can be used to derive the following relations between the ratios v'/s_L and ℓ/ℓ_F in terms of the three nondimensional numbers Re, Da, and Ka as

$$\begin{aligned} v'/s_L &= \mathrm{Re}(\ell/\ell_F)^{-1} \\ &= \mathrm{Da}^{-1}(\ell/\ell_F) \\ &= \mathrm{Ka}^{2/3}(\ell/\ell_F)^{1/3} \end{aligned} \tag{11.30}$$

In the following we will discuss Borghi's diagramm Fig. 11.1 for premixed combustion (conf. [11.1]) and plot the logarithm of v'/s_L over the logarithm of ℓ/ℓ_F. In this diagramm, the lines $\mathrm{Re} = 1$, $\mathrm{Da} = 1$, and $\mathrm{Ka} = 1$ represent boundaries between the different regimes of premixed turbulent combustion. Another boundary of interest is the line $s_L = 1$, which separates the wrinkled and corrugated flamelets.

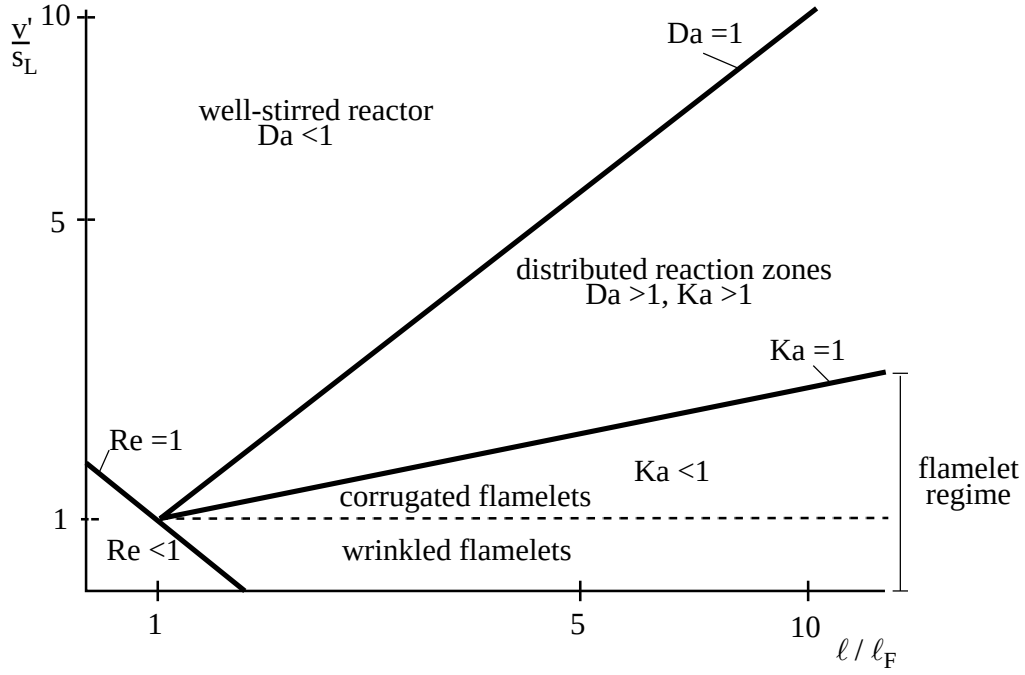

Fig. 11.1: Phase diagram showing different regimes in premixed turbulent combustion

The regime of laminar flames (Re < 1) in the lower-left corner of the diagramm is not of interest in the present context. Among the remaining four regimes, the wrinkled and corrugated flames belong to the flamelet regime, which is characterized by the inequalities Re > 1 (turbulence), Da > 1 (fast chemistry), and Ka < 1 (sufficiently weak flame stretch). Considering the boundary to the distributed reaction regime given by Ka $= 1$, this boundary represents the condition that the flame thickness is equal to the Kolmogorov scale (the Klimov-Williams criterion). However, in addition, since viscosity as a molecular transport process relates Kolmogorov velocity, length, and time scales to each other in the same way as the velocity, length, and time scales are related for flame propagation. The flame time is equal to the Kolmogorov time and the burning velocity is equal to the Kolmogorov velocity. This was used in (11.29).

The disrupted flamelet regime is characterized by Re > 1, Da > 1, and Ka > 1, the last inequality indicating that flame stretch is strong and that the smallest eddies can enter into the flame structure since $\eta < \ell_F$, thereby broadening the flame structure. The smaller eddies produce the largest strain rates and may lead to local extinction of the flamelet. Finally, the well-stirred reactor regime on the upper left of the diagramm is characterized by Re $> 1, \mathrm{Ka} > 1$, but Da < 1, indicating that the chemistry is slow compared with turbulence.

We will now enter into a more detailed discussion of the various regimes. The flamelet regime is subdivided into the regimes of wrinkled, corrugated, and disrupted flamelets. In the wrinkled flamelet regime, where $v' < s_L$, since v' may be interpreted as the turnover velocity of the large eddies, it follows that even those eddies cannot convolute the flame front enough to form multiply connected reaction sheets. Flame propagation is dominating and flame displacement by s_L is faster than displacement by turbulence with v' in this regime.

The regime of corrugated flamelets is much more difficult to analyze analytically or numerically. In view of (11.29), we have with Ka < 1

$$v' \geq s_L \geq v_\eta \tag{11.31}$$

within this regime. Since the velocity of large eddies is larger than the burning velocity, these eddies will push the flame front around, causing a substantial convolution. Conversely, the smallest eddies, having a turnover velocity less than the burning velocity, will not wrinkle the flame front.

To determine the size of the eddy that interacts locally with the flame front, set the turnover velocity v_n in (11.24) equal to the burning velocity s_L. This determines the Gibson scale

$$\ell_G = s_L^3/\varepsilon \tag{11.32}$$

The Gibson scale is the size of the burnt pockets that move into the unburnt mixture. These pockets try to grow there due to the advance of the flame front normal to itself, but are reduced in size again by newly arriving eddies of size ℓ_G. Therefore, there is an equilibrium mechanism for the formation of burnt pockets, while unburnt pockets that penetrate into the burnt gas will be consumed by the flame advancement. It is worth noting that ℓ_G increases with s_L if the turbulence properties are kept constant. At sufficiently

low turbulence levels, the mean thickness of a turbulent flame should be influenced by this mechanism and, therefore, also increase with s_L. Using (11.22), one may also write (11.32) in the form

$$\ell_G/\ell_t = (s_L/v')^3 \tag{11.33}$$

An illustration of the kinematics of the interaction between a premixed flame and a turbulent flowfield may be found in Fig. 9 of Ref. [11.3]. In this numerical study, the characteristic integral length scale ℓ was kept constant, while the turbulence intensity was increased, showing corrugations of smaller and smaller size.

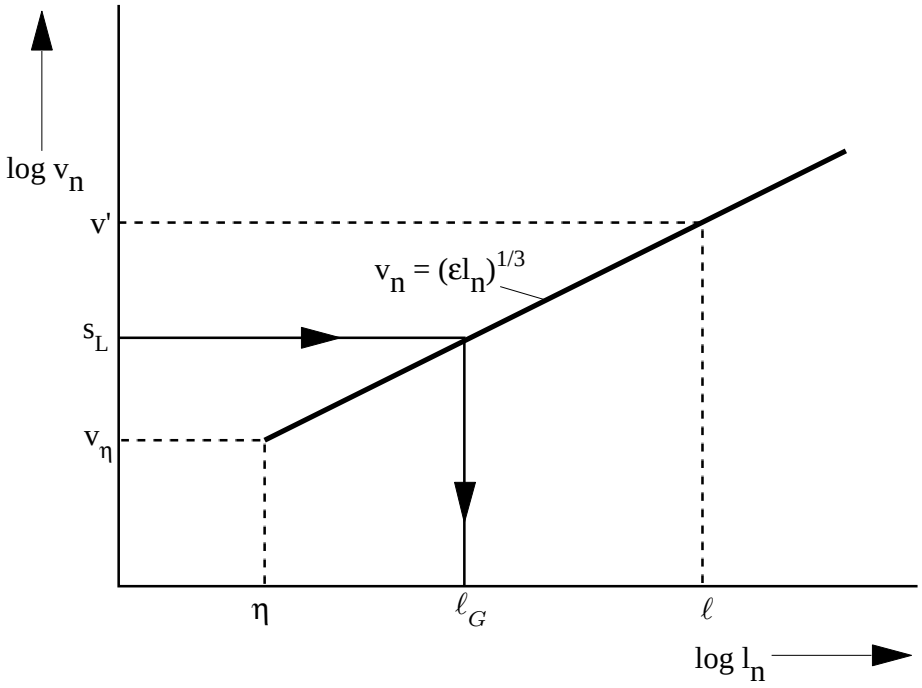

Fig. 11.2: Graphical illustration of the Gibson scale ℓ_G within the inertial range.

For engines, it also may be argued that the integral length scale is constant and depends only on the geometrical dimensions of the combustion chamber, while the turbulence intensity increases linearly with engine speed.

A graphical derivation of the Gibson scale L_G within the inertial range is shown in Fig. 11.2. Here the logarithm of the velocity v_n is plotted over the logarithm of the length scale according to (11.24). If one enters on the vertical axis with the burning velocity s_L equal to v_n into the diagramm, one obtains ℓ_G as the corresponding length scale on the horizontal axis. This diagramm also illustrates the limiting values of ℓ_G: If the burning velocity is equal to v', ℓ_G is equal to the integral length scale ℓ. This case corresponds to the borderline between corrugated and wrinkled flamelets in Fig. 11.1. Conversely, if s_L is equal to the Kolmogorov velocity v_η, ℓ_G is equal to η. This corresponds to the line Ka = 1 in Fig. 11.1. Therefore, ℓ_G may vary between η and ℓ in the corrugated flamelet regime. The next regime of interest in Fig. 11.1 is the regime of disrupted flamelets. As

noted earlier, the small eddies can enter into the flamelet structure and even destroy it, since $\eta < \ell_F$ in this regime. Therefore, the notion of a burning velocity as a relevant velocity scale has no meaning in this regime. Another scale, however, the chemical time scale t_c, remains still meaningful since reactions occur independently of flame propagation. In addition, since there is an inner reaction zone smaller than the flame thickness, the quenching of this inner zone by flame stretch is the important physical process. From the physical point of view, the quench time t_q is the more relevant time scale but, at least for stoichiometric methane flames, the preceding has shown that $t_q \approx t_F$, the latter being equal to t_c. Then, by setting $t_q = t_n$ in (11.24), one obtains the quench scale [11.3]

$$\ell_q = (\varepsilon t_q^3)^{1/2} \tag{11.34}$$

This scale may be interpreted as the size of the largest eddy within the inertial range that is still able to quench a thin reaction zone. Smaller eddies up to ℓ_q induce a larger stretch and, thus, will quench the thin reaction layers within the flowfield more readily and, thereby, try to homogenize the scalar field locally over a distance up to ℓ_q. Therefore, ℓ_q may be interpreted as a correlation length for the reactive scalar field or, in physical terms, as the size of a localized well-stirred reactor. This justifies the characterization of this regime as the distributed reaction zone regime. It has also been characterized by Williams as the regime of broken reaction zones, which gives a clear picture of physical process described earlier.

In the distributed reaction zone regime, the Damköhler number, which is based on the integral time scale t_t and the chemical time scale $t_c = t_F$, is large. At the order of these scales, chemistry is fast, and thin reaction zones may be generated locally. These zones are quenched by flame stretch such that an equilibrium mechanism exists between the generation and the destruction of thin reaction zones over a region of thickness ℓ_q.

Again, the derivation of ℓ_q is illustrated in a diagramm in Fig. 11.3, showing (11.24) in a log-log plot of t_n over ℓ_n. If one enters the time axis at $t_q = t_n$, the quench scale ℓ_q on the length scale axis is obtained. It should be noted that all eddies having a size between η and ℓ_q have larger stretch than ℓ_q and, therefore, are able to quench thin reaction zones locally. If t_q is equal to the Kolmogorov time t_η, Fig. 11.3 shows that ℓ_q is equal to the Kolmogorov scale η. In this case, setting $t_q = t_F$, one obtains $\ell_q = \ell_F$ at the border between the disrupted flamelet regime and the corrugated flamelet regime. Similarly, from Fig. 11.3, if the quench time t_q is equal to the integral time τ, the quench scale is equal to the integral length scale. This would correspond to Da = 1 in Fig. 11.1 and delineates the borderline between the disrupted flamelet regime and the well-stirred reactor regime.

As a final remark related to the disrupted flamelet regime, it may be noted that turbulence in real systems is not homogeneous and ε is not a local constant but has a distribution. This refinement of Kolmogorov's theory has lead to the notion of intermittency, or "spottiness", of the activity of turbulence in a flow field. This may have important consequences on the physical appearance of turbulent flames at sufficiently large Reynolds numbers. One may expect that the flame front shows manifestations of local quenching events as well as of regions where corrugated flamelets appear. The regimes discussed earlier may well overlap each other in an experimentally observed turbulent flame.

In the well-stirred reactor regime, chemistry is slow, as noted earlier. Now all eddies up to ℓ can quench the flame structure, since Da ≤ 1. Turbulence homogenizes the scalar

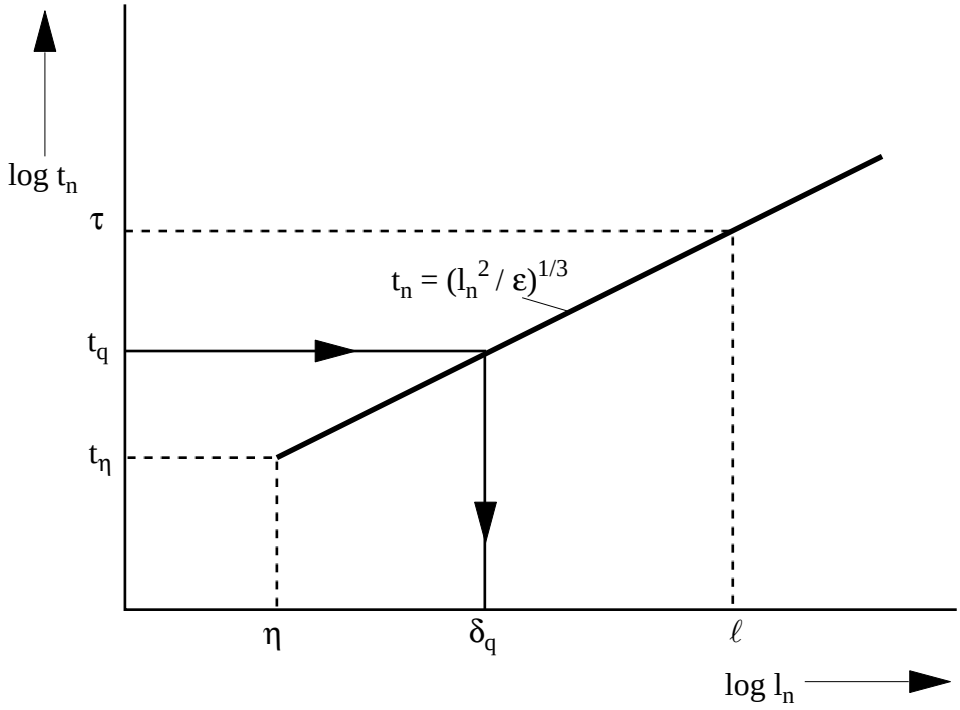

Fig. 11.3: Graphical illustration of the quench scale δ_q within the inertial range.

field by rapid mixing, leaving the slow chemistry to be the rate-determining process. No specific interaction between turbulence and combustion can occur in this regime, and no specific interaction scale is to be defined.

Non-Premixed Turbulent Combustion

In order to construct a phase diagram for non-premixed turbulent combustion, it is necessary to identify the relevant quantities that influence the flame structure. In a non-homogeneous mixture field the reaction zone is attached to the high temperature region close to stoichiometric mixture and is advected and diffused with the mixture field. Differently from premixed combustion, there is no burning velocity, which would move it relative to its previous position. There is a time scale, the chemical reaction time, but since there is no physically meaningful velocity scale there is no meaningful length scale such as the flame thickness for diffusion flames. Therefore the velocity fluctuation v' defined in (11.16) is not the relevant parameter in defining regimes in non-premixed turbulent combustion. Since the mixture field fixes the flame position, mixture fraction fluctuations Z' defined in (11.19) are responsible for corrugations of the flame surface. These fluctuations should be considered in defining different regimes in turbulent diffusion flames.

In a non-homogeneous turbulent mixture field mean reaction rates are large where the mean mixture fraction corresponds to the stoichiometric value. Now consider fluctuations

around that mean value. For small mixture fraction variances, which may be due either to intense mixing or to partial premixing, a situation arises where reactions are sufficiently fast everywhere and the reaction zones are connected. Combustion in such a situation corresponds to partially premixed rather than to non-premixed combustion. If, on the other hand, mixture fraction fluctuations are sufficiently large, diffusion flame structures are separated. Therefore a criterion must be derived, that distinguishes between the partially premixed and the separated flamelet regimes. This criterion will be based on the flame thickness in mixture fraction space $(\Delta Z)_F$. If mixture fraction fluctuations are larger than $(\Delta Z)_F$ one has separated flamelets, otherwise connected reaction zones. In the limit of very large Damköhler numbers, when the flamelet structure approaches local equilibrium, the distinction between separated and connected zones becomes irrelevant, since there is chemical equilibrium everywhere.

The second criterion, based on time scales, should as in premixed combustion, consider the ratio of the Kolmogorov to the chemical time. The Kolmogorov time $t_\eta = (\nu/\tilde{\varepsilon})^{1/2}$ is the turnover time of the smallest eddies and therefore the shortest characteristic time of turbulence. If combustion is fast with respect to this time scale, it may be considered as quasi-steady and the diffusion flamelet concept is valid. If however, the Kolmogorov time is of the same order or shorter than the chemical time, the flamelet regime breaks down and regions of intense mixing and reaction will appear. As in premixed combustion, we will call this regime the distributed reaction zones regime (conf. [11.4]).

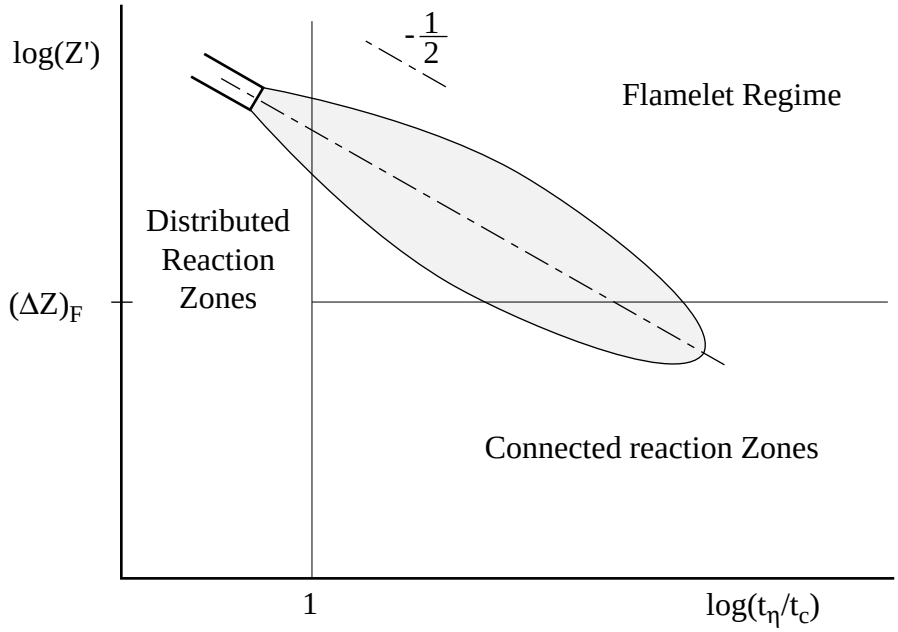

Fig. 11.4: Regimes in non-premixed turbulent combustion

Figure 11.4 shows the three regimes of non-premixed turbulent combustion in a phase

diagram in terms of the mixture fraction fluctuation and the time scale ratio. Local conditions of a non-premixed turbulent jet diffusion flame would range from the distributed reaction zone regime close to the nozzle into the flamelet regime further downstream. Close to the flame tip where typically $Z' \approx 0.3\tilde{Z} = 0.3Z_{st} < (\Delta Z)_F$ it enters into the connected reaction zones regime. Since Z' decreases as x^{-1} and the characteristic times of turbulence increase as x^2 in a jet flame, where x is the distance from the nozzle local conditions follow a line with slope $-1/2$ in the double-logarithmic plot in Fig. 11.4.

References

[11.1] Peters, N., Twenty-first Symp. (Int.) on Combustion, p. 1231–1256, The Combustion Institute, 1986.

[11.2] Ashurst, Wm.T., Barr, P.K., Combust. Sci. Technol. **34** (1983) p. 227.

[11.3] Peters, N., in "Turbulent Reactive Flows", (R. Borghi, S.N.B. Murthy, Eds.) Lecture Notes in Engineering **40**, pp. 242–256, Springer-Verlag, 1989.

[11.4] Peters, N., in "Numerical Approaches to Combustion Modeling", (E.S. Oran, J.A. Boris, Eds.) Pogr. Astronautics Aeronautics **135**, pp. 155–182, AIAA 1991.

Lecture 12: Laminar Flamelet Models for Non-Premixed Turbulent Combustion

12.1. Introduction

The flamelet concept for non-premixed combustion has been presented in previous reviews [12.1], [11.1] , as a non-equilibrium version of the classical Burke-Schumann limit. It approaches this limit asymptotically in the limit of a one-step reaction with a large Damköhler number. The scalar dissipation rate was in lecture 9 identified as a characteristic quantity to describe the departure from the large Damköhler number limit. An asymptotic analysis of the flamelet structure for quasi-steady unity Lewis number flames suggests that, to leading order, the scalar dissipation rate should account for non-equilibrium effects caused by both, convection and diffusion. It follows, from the same reasoning, that rapid unsteady changes, large local differences between convection and diffusion time scales, flamelet curvature, strong variations of the scalar dissipation within the flamelet structure and effects caused by non-unity Lewis numbers and multi-step chemistry require a more detailled analysis. It also may happen that, if any of these effects are too strong, they must be included into the leading order analysis and thereby add to the complexity of the parametric description.

The transition from the point Q to the lower state corresponds to the unsteady transition. Auto-ignition, which would correspond to an unsteady transition from the point I to the upper curve, is unlikely to occur in open diffusion flames, since the required very large residence times (very small values of χ_{st}) are not reached.

An example for auto-ignition in non-premixed systems is combustion in a Diesel engine. Here interdiffusion of the fuel from the Diesel spray with the surrounding hot air leads to continuously decreasing mixture fraction grradients and therefore to decreasing mixture fraction gradients and therefore to decreasing scalar dissipation rates. This corresponds to a shift on the lower branch of the S-shaped curve up to the point I of ignition.

12.2 Diffusion Flamelets in Turbulent Combustion

The flamelet concept views a turbulent diffusion flame as an ensemble of laminar diffusion flamelets. Once the flamelet structure has been resolved as a function of prescribed parameters and is available in form of a flamelet library, all scalars are known functions of these parameters. The main advantage of the flamelet concept is the fact that chemical time and length scales need not be resolved in calculating the turbulent flame. In turbulent non-premixed combustion it has become common practise to use Favre (density weighted) averaged equations. In addition to the continuity and momentum equations, and equations describing turbulence quantities like $\widetilde{k}$ and $\widetilde{\varepsilon}$ and thereby the turbulent length and time scales, we need the balance equations for the mixture fraction (11.13) and the mixture fraction variance (11.14).

In previous presentations [12.1] the enthalpy has been related to the mixture fraction by (5.54). For a general formulation, however, it is preferable to modify this analysis by including the enthalpy as a additional variable

$$\begin{aligned}\overline{\rho}\,\frac{\partial\widetilde{h}}{\partial t}+\overline{\rho}\,\widetilde{v_\alpha}\,\frac{\partial\widetilde{h}}{\partial x_\alpha}&=\frac{\partial}{\partial x_\alpha}\left(\overline{\rho}\,\frac{\nu_t}{\mathrm{Pr}}\,\frac{\partial\tilde{h}}{\partial x_\alpha}\right)\\&+\frac{\partial\overline{p}}{\partial t}+\widetilde{u}\,\frac{\partial\overline{p}}{\partial x_\alpha}+\widetilde{u''_\alpha}\,\frac{\partial\overline{p}}{\partial x_\alpha}+\overline{u''_\alpha}\,\frac{\partial\overline{p'}}{\partial x_\alpha}-\overline{q_R}\,.\end{aligned}\tag{12.1}$$

Here Pr is a turbulent Prandtl number. The terms containing the mean spatial pressure gradient and its fluctuations must be retained if gasdynamic effects are to be described. These terms may be neglected in the limit of zero Mach number, when fast acoustic waves are rapidly homogenizing the pressure field. The term describing temporal mean pressure changes $\partial\overline{p}/\partial t$ is important in internal combustion engines operating under non-premixed conditions, such as the Diesel engine. Finally the mean volumetric heat loss term must be retained if radiative heat exchange focusses influence on the local enthalpy balance. This may well be the case in large furnaces where it influences the prediction of NO_x formation which is very sensitive to temperature.

By substracting from $\widetilde{h}$ the part that is due to mixing and related to the mean mixture fraction, one may define an enthalpy defect

$$(\widetilde{\triangle h})=\widetilde{h}-h_2-\widetilde{Z}\,(h_2-h_1)\tag{12.2}$$

which is caused by heat loss and pressure gradient effects. This enthalpy defect will lower the enthalpy, which is locally available. It therefore represents an additional parameter imposed on the flamelet.

No equation for enthalpy fluctuations has been written here. Fluctuations of the enthalpy are mainly due to mixture fraction fluctuations and are described by those. Additional effects due to non-unity Lewis numbers, fluctuations of pressure and volumetric heat losses are difficult to quantify and will be neglected here.

In Eqs. (12.6), (12.7) and (12.8) diffusive terms containing molecular diffusivities have been neglected as small compared to the turbulent transport terms in the large Reynolds number limit. Diffusive effects have only be retained in the mean scalar dissipation $\widetilde{\chi}$ which is modelled by (11.15).

We assume that profiles of any reactive scalar of interest are available from a flamelet library. Parameters of the library are the mixture fraction coordinate Z, the enthalpy, and the strain rate a, the latter representing the inverse of the flow. Conceptually, one could define partially premixed flamelets [12.2], [12.3] by moving the boundary conditions towards the reaction zone while keeping the strain rate constant and therefore the scalar dissipation rate in the combustion zone fixed. At the new boundary conditions burnt gas partially mixed with fuel or oxidizer are imposed. If the boundary conditions are moved inwards on the fuel side, only, the profiles in the reaction zone and even the extinction strain rate are not expected to change much in the case of hydrogen or hydrocarbon combustion in air. This is due to the fact that Z_{st} is small in these cases and that heat loss is predominant

towards the oxidizer side. In the turbulent flow, however, the corresponding reduction in mixture fraction variation accross the flamelet, expressed in terms of mixture fraction fluctuations would decrease the mean scalar dissipation rate. Equation (11.15) may, in fact, be interpreted as representing two effects: the influence of time scale represented by $\widetilde{\varepsilon}/\widetilde{k}$ and the influence of scalar fluctuations. Chemistry, however, responds to a change of strain rate only, not to the change of mixture fraction fluctuations as long as these do not enter into the reaction zone. We therefore propose to use the strain rate a imposed on the flamelet as the appropriate time scale for the flamelet library. Its mean should be proportional to the inverse of the turbulent time scale

$$\overline{a} = c_1 \frac{\widetilde{\varepsilon}}{\widetilde{k}}. \tag{12.3}$$

The constant c_1 can be estimated by equating production and dissipation in the turbulent energy equation. With (11.9)–(11.11) one then obtains for boundary layer flows $\overline{a} = \partial\widetilde{u}/\partial y$ and $c_1 = c_D^{-1/2} = 3.33$. Using the relation between χ and a, (9.32) and taking its turbulent mean, one may define the corresponding mean scalar dissipation rate acting upon the flamelets as

$$\overline{\chi}_F = 2\overline{a}\,(\triangle Z)_F^2 = 8c_1 \frac{\widetilde{\varepsilon}}{\widetilde{k}} Z_{\rm st}^2\,, \tag{12.4}$$

where $(\triangle Z)_F = 2Z_{\rm st}$ has been used. When this expression is compared to Eq. (12.18) it is seen that it corresponds to a fixed mixture fraction fluctuation, namely the flame thickness in mixture fraction space.

12.3. Mean Values and Variances of Scalars in a Turbulent Flow Field

Local conditions of the turbulent scalar field are characterized by the mean mixture fraction $\widetilde{Z}(x_\alpha, t)$, its variance $\widetilde{Z''^2}(x_\alpha, t)$, the mean strain rate $\overline{a}(x_\alpha, t) = \widetilde{\varepsilon}(x_\alpha, t)/\widetilde{k}(x_\alpha, t)$ and the mean enthalpy defect $\widetilde{(\Delta h)}(x_\alpha, t)$. The parameters determining the structure of a steady state flamelet to be used locally are then $a = \bar{a}$ and the enthalpy defect $(\triangle h) = \widetilde{(\triangle h)}$. In order to calculate a flamelet with the desired enthalpy defect, it is neceessary to vary the heat loss term q_R, keeping the strain rate and, if present, $\partial p/\partial t$ fixed or simply lowering the available enthalpy. This will lead to lower mean temperatures and will alter the heat exchange and extinction condition.

Fluctuations of the mixture fraction are taken into account by introducing a pre-assumed probability density function (pdf). A generally accepted form for the mixture fraction pdf is the beta function pdf

$$\widetilde{P}(Z) = Z^{\alpha-1}\,(1-Z)^{\beta-1}\,\frac{\Gamma(\gamma)}{\Gamma(\alpha)\,\Gamma(\beta)} \tag{12.5}$$

where

$$\begin{aligned} \gamma &= \frac{\widetilde{Z}(1-\widetilde{Z})}{\widetilde{Z''^2}} - 1 \\ \alpha &= \widetilde{Z}\,\gamma\,, \quad \beta = (1-\widetilde{Z})\,\gamma\,. \end{aligned} \tag{12.6}$$

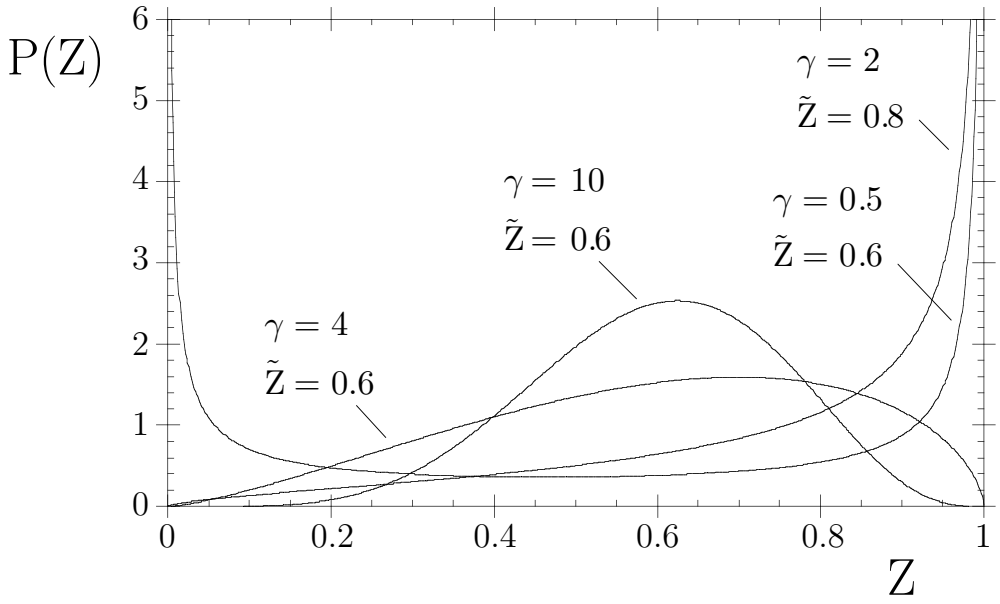

Fig. 12.1: Shapes of the beta-function distribution

Shapes of the beta function for various parameters are shown in Fig. 12.1. For small variances, i.e. large values of $\widetilde{Z''^2}$, it approaches a Gaussian.

Equations for the mean and the variance of the temperature T or the mass fractions Y_i are then

$$\begin{aligned}
\tilde{T}(x_\alpha, t) &= \int_0^1 T(Z)\, \tilde{P}(Z)\, dZ \\
\widetilde{Y_i}(x_\alpha, t) &= \int_0^1 Y_i(Z)\, \tilde{P}(Z)\, dZ \\
\widetilde{T''^2}(x_\alpha, t) &= \int_0^1 (T(Z) - \tilde{T})^2\, \tilde{P}(Z)\, dZ \\
\widetilde{Y_i''^2}(x_\alpha, t) &= \int_0^1 (Y_i(Z) - \tilde{Y}_i)^2\, \tilde{P}(Z)\, dZ.
\end{aligned} \tag{12.7}$$

For the solution of the modelled equations, the mean density $\overline{\rho}$ is needed. As an initial guess, ρ may be approximated by the Burke-Schumann solution which is independent of strain rate and relating the enthalpy to the mixture fraction. Using the definition of the Favre mean pdf $\tilde{P} = \rho P/\overline{\rho}$ one obtains for the mean density

$$\frac{1}{\overline{\rho}} = \int_0^1 \frac{1}{\rho(Z)}\, \widetilde{P}(Z)\, dZ\,. \tag{12.8}$$

12.4 Experimental Data Showing Non-Equilibrium Effects in Jet Diffusion Flames

While the flame length may be calculated on the basis of the mixture fraction field only, more details on scalars are needed if one wants to determine chemical effects and pollutant formation in jet flames. Chemical extinction effects leading to lift-off were already considered in Chapter 12. Here we want to discuss as an example data taken locally in a jet flame. They were obtained by Raman-scattering and laser-induced fluorescence in diluted hydrogen-air diffusion flames by Barlow et al. [12.4]. The fuel stream consisted of a mixture of 78 mole % H_2, 22 mole % argon, the nozzle inner diameter d was 5.2 mm and the co-flow air velocity was 9.2 m/s. The resulting flame length was approximately $L = 60\,d$. Two cases of nozzle exit velocities were analysed but only the case B, $u_0 = 150$m/s will be considered here.

The stable species H_2, O_2, N_2, and H_2O were measured using Raman-scattering with light from a flash-lamp pumped dye laser. In addition quantitative OH radical concentrations from LIF measurements were obtained by using the instantaneous local Raman data to calculate quenching corrections for each laser shot. The correction factor was close to unity for stoichiometric and moderately lean conditions but increased rapidly for very lean and moderately rich mixtures. The temperature was calculated for each laser shot by adding number densities of the major species and using the perfect gas law for this atmospheric pressure flame. The mixture fraction was calculated similarly from the stable species concentrations. An ensemble of one-point, one-time Raman-scattering measurements of major species and temperature are plotted over mixture fraction in Fig. 12.2. They were taken at $s/d = 30$, $r/d = 2$ in the case B flame. Also shown are calculations based on the assumption of chemical equilibrium.

The over-all agreement between the experimental data and the equilibrium solution is quite good. This is often observed for hydrogen flames where the chemistry is very fast. On the contrary, hydrocarbon flames at high strain rates are likely to exhibit local quenching effects and non-equilibrium effects due to slow conversion of CO to CO_2. Fig. 12.3 shows temperature profiles versus mixture fraction calculated for counter flow diffusion flames at different strain rates. These flamelet profiles display a characteristic decrease of the maximum temperature with increasing strain rates as shown schematically by the upper branch of the S-shaped curve in Fig. 12.2.

The strain rates vary here between $a = 100$/s which is close to chemical equilibrium and $a = 1000$/s. For comparison, the mean strain rate in the jet flame, defined here as $\bar{a} = u(s)/b(s)$ may be estimated as $\bar{a} = 12.15$/s at $s/d = 30$ based on (13.17).

Data of OH-concentrations are shown in Fig. 12.4. They are to be compared to flamelet calculations in Fig. 12.5 for the different strain rates mentioned before. It is evident from Fig. 12.4 that the local OH-concentrations exceed those of the equilibrium profile by a factor 2 to 3. The flamelet calculations show an increase of the maximum values by a factor of 3 already at the low strain rates $a = 100$/s and $a = 1000$/s, while the OH-profile over mixture fraction decreases and broadens for the maximum value $a = 10000$/s. This value is close to extinction for the diluted flamelet considered here.

It should be mentioned that also Monte-Carlo simulations to solve a pdf-transport

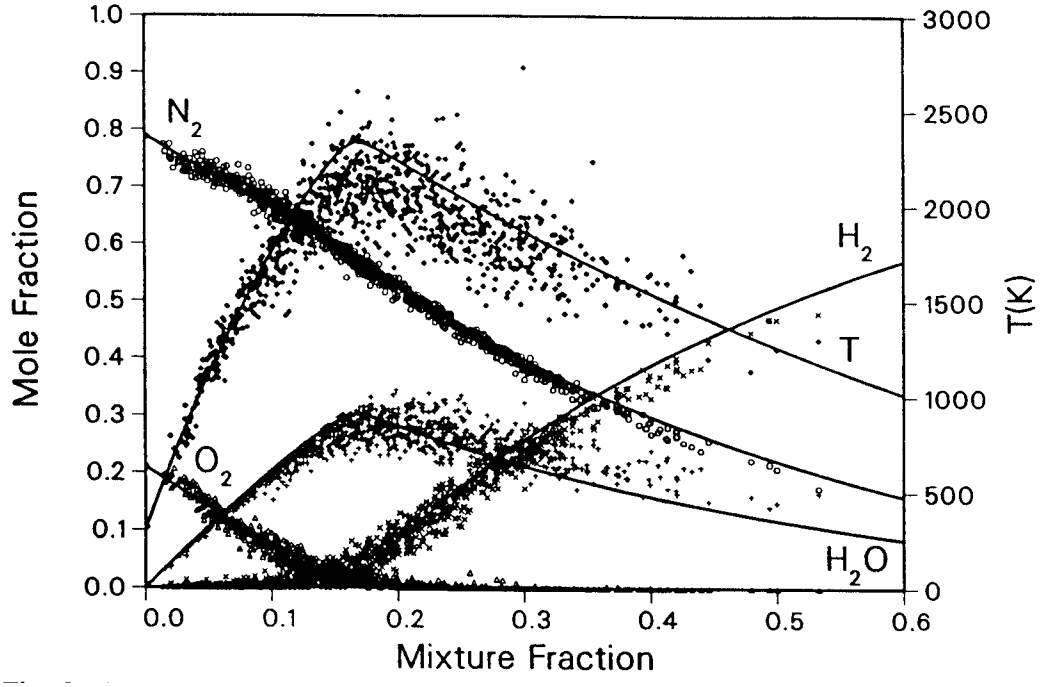

Fig. 12.2: Ensemble of Raman scattering measurements of major species concentrations and temperatures at $s/d = 30, r/D = 2$. The solid curves show equilibrium conditions.

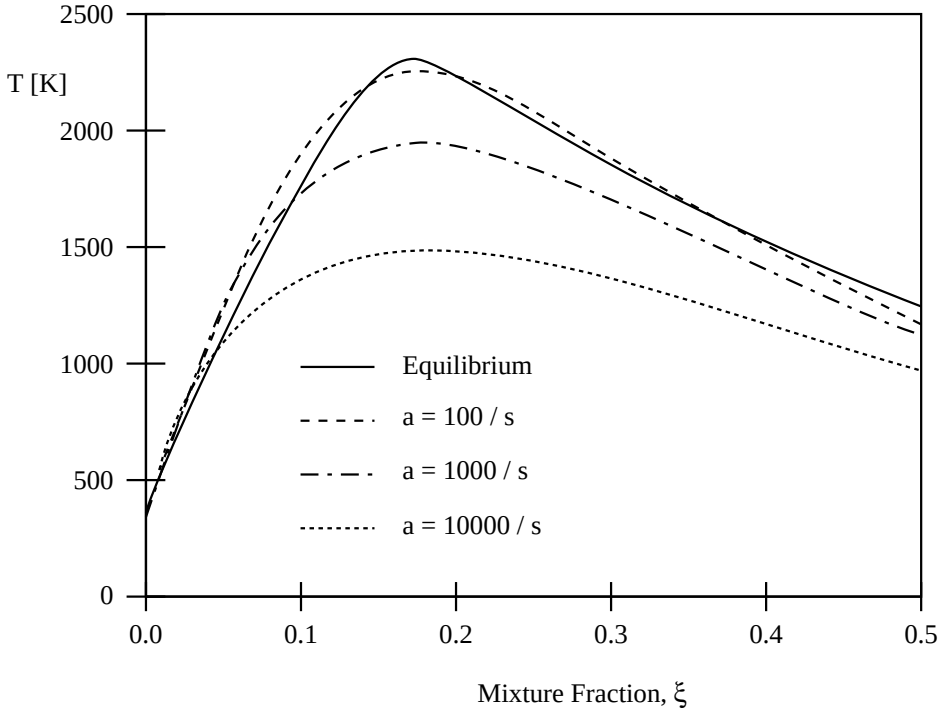

Fig. 12.3: Temperature profiles from flamelet calculations at different strain rates.

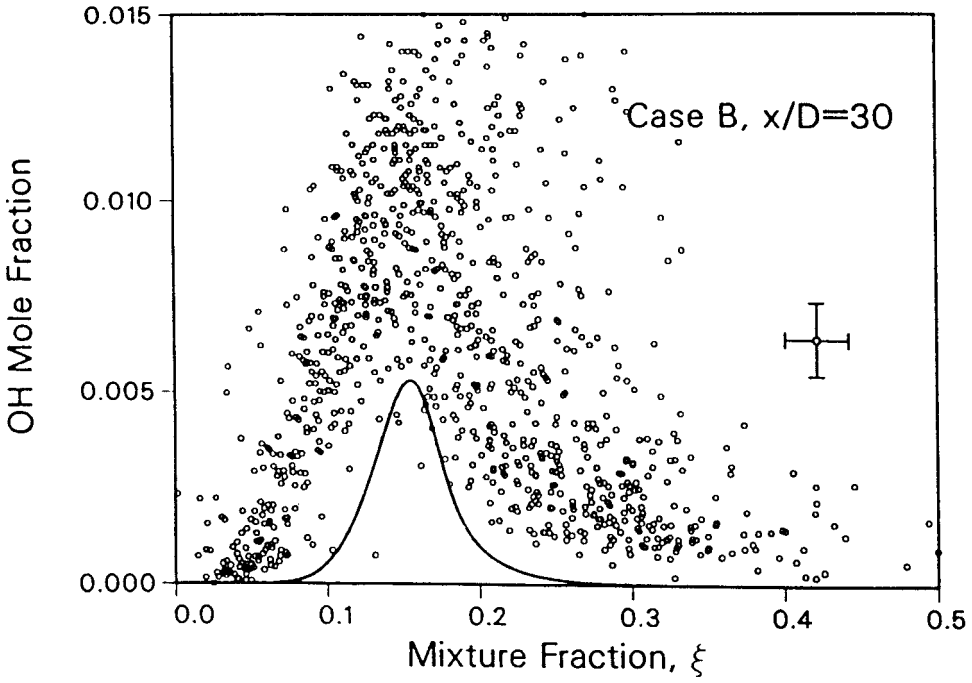

Fig. 12.4: Ensemble of LIF measurements of OH concentrations at $s/d = 30, r/D = 2$. The solid curve shows equilibrium solution.

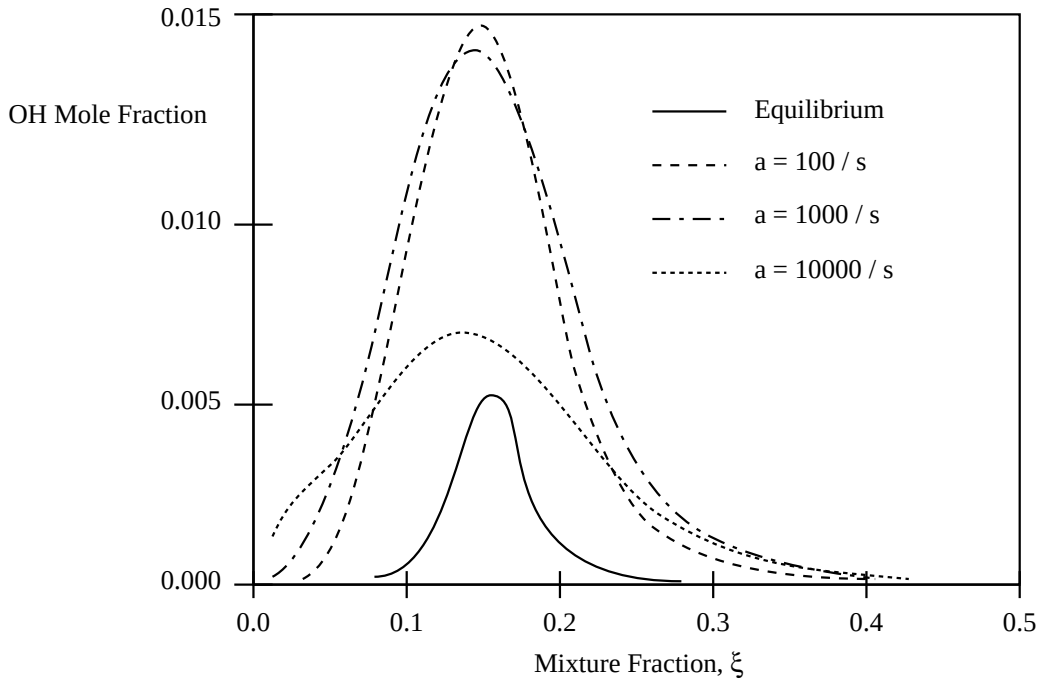

Fig. 12.5: OH mole fractions from flamelet calculations at different strain rates.

equation were performed of this experimental configuration. Since the prediction of chemically reacting flows by pdf-transport equations suffers from limitations of the turbulent mixing model, we will not discuss these results here.

In summary, it may be concluded that one-point, one-time experimental data for hydrogen flames when plotted as a function of mixture fraction, show qualitatively similar tendencies as flamelet profiles. Non-equilibrium effects are evident in both cases and lead to an increase of radical concentrations and a decrease of temperatures. This will be of importance for the discussion on NO_x formation in turbulent diffusion flames.

12.5. Application to Lifted Jet Diffusion Flames

If the nozzle exit velocity of the fuel in a jet diffusion flame exceeds a characteristic value, the flame is abruptly detached from the nozzle. It now acquires a new configuration of stabilization in which combustion begins a number of nozzle diameters downstream. The liftoff height is the centerline distance from the nozzle to the plane of flame stabilization. A further increase in the exit velocity increases the liftoff height without significantly modifying the turbulent flame length. The flame height will be calculated in the next paragraph.

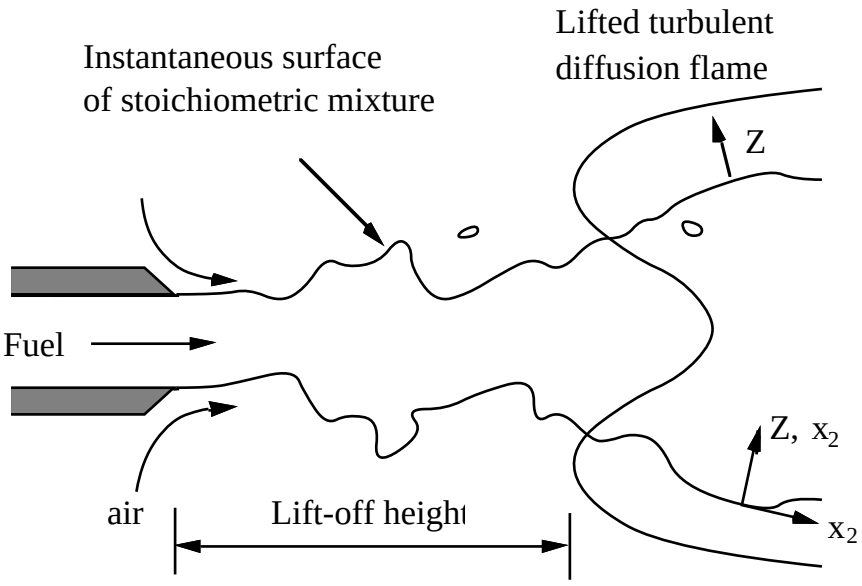

Fig. 12.6: Schematic presentation of a lifted jet diffusion flame

The liftoff-height was identified in the past [12.5] as the position where too many flamelets are quenched, so that flame propagation from the bulk of the turbulent flame towards the nozzle cannot proceed. This flame propagation would preferably take place along the instantaneous surface of stoichiometric mixture. It has been noted above that the scalar dissipation rate at quenching corresponds to the inverse of flame time of a premixed flame. Therefore flame propagation along the surface of stoichiometric mixture should also scale with χ_q^{-1} as the characteristic laminar time scale.

Lift-off should therefore occur, where the mean turbulent scalar dissipation rate is equal to χ_q

$$\overline{\chi}_F = \chi_q. \tag{12.9}$$

Here, different from previous formulations, where $\tilde{\chi}$, Eq. (11.15), was used, we take $\overline{\chi}_F$ from Eq. (12.4) which does not decrease with $\widetilde{Z''^2}$. Eq. (12.9) is in view of Eq. (9.32) also equivalent to equating the turbulent strain rate to the strain rate of the diffusion flamelet at quenching

$$c_1 \frac{\tilde{\varepsilon}}{\tilde{k}} = a_q. \tag{12.10}$$

This new formulation has been used to re-analyse liftoff data of methane flames obtained by Donnerhack and Peters [12.6] for different dilutions. In Fig. 12.7 non-dimensional stabilization heights of undiluted methane flames are plotted as a function of the nozzle exit velocity u_0 for different nozzle diameters. Similar data were obtained for methane in diluted air. The scalar dissipation rate at quenching χ_q taken from laminar flamelet measurements was multiplied with d/u_0 to obtain χ_q^*. These data are plotted as a function of H/d and are compared in Fig. 12.8 with

$$\chi_F^* = \frac{\overline{\chi}_F d}{u_0} = 2c_1 \left(\frac{\tilde{\varepsilon}}{\tilde{k}}\right)_{\tilde{Z}=Z_{st}} (\triangle Z)_F^2 \frac{d}{u_0}, \tag{12.11}$$

the non-dimensional turbulent dissipation rate at $\tilde{Z} = Z_{st}$, where $(\triangle Z)_F = 2Z_{st}$ and where $(\tilde{\varepsilon}/\tilde{k})$ was calculated using a $\tilde{k}$-$\tilde{\varepsilon}$ turbulence model for a methane jet where it was evaluated at $\tilde{Z} = Z_{st}$. The slope of the curve follows the experimental data for the different dilutions quite well while the previous formulation, denoted by

$$\chi_{st}^* = \frac{\tilde{\chi}_{st} d}{u_0} = c_\chi \left(\frac{\tilde{\varepsilon}}{\tilde{k}} \widetilde{Z''^2}\right)_{\tilde{Z}=Z_{st}} \frac{d}{u_0}, \tag{12.12}$$

does not. This gives some support for using (12.9) rather than equating the mean scalar dissipation rate $\tilde{\chi}$ with χ_q in diffusion flamelet modeling for jet flames.

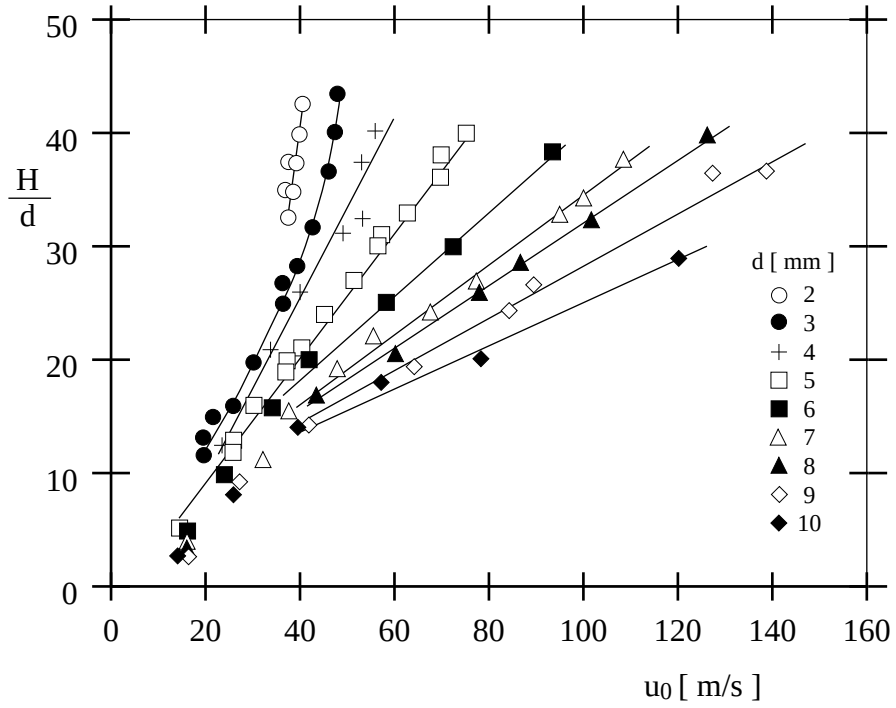

Fig. 12.7: Non-dimensional liftoff heights for methane-air flames

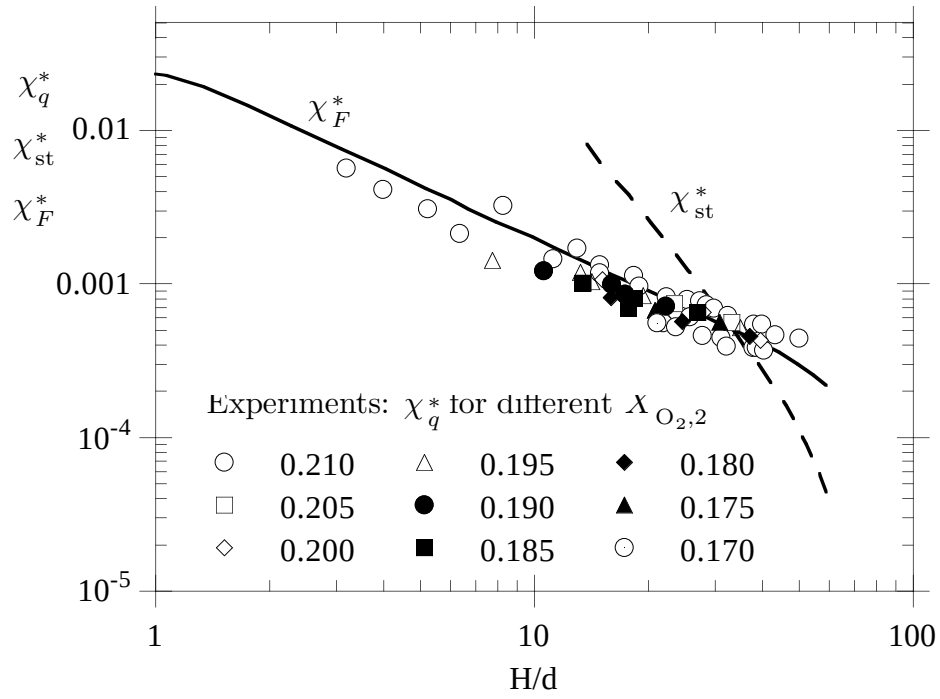

Fig. 12.8: Lifted flames: Different non-dimensional scalar dissipation formulations as a function of the non dimensional liftoff height. Experimental data for different dilutions, where $X_{O_{2,2}}$is the mole fraction of O_2 in the oxidizer stream.

References

[12.1] Peters, N., Progress in Energy and Combustion Science, **10** (1984) 319.

[12.2] Rogg, B., Behrendt, F., Warnatz, J., 21st Symposium (Int.) on Combustion, P. 1533–1541, 1986.

[12.3] Seshadri, K., Puri, I., Peters, N., Combustion and Flame, **61** (1985) 251–260.

[12.4] Barlow, R.S., Dibble, R.W., Chen, J.Y., Lucht, R.P., Combust. Flame, **82** (1990) 235.

[12.5] Peters, N., Williams, F.A., AAIA J. **21** (1983) 423–429.

[12.6] Donnerhack, S., Peters, N., Combust. Sci. Technol. **41** (1984) 101–108.

Lecture 13: Turbulent Diffusion Flames: Experiments and Modeling Aspects

Introduction

Turbulent diffusion flames owe their name to the rate determining mechanism that controls the combustion in many applications: namely diffusion. In technical furnaces, but also in gas turbine combustion chambers fuel and oxidizer are injected seperately. Mixing then occurs by turbulent and eventually molecular diffusion. Only when fuel and oxidizer are mixed at the molecular scales, combustion can take place.
In many applications the fuel is issued as a turbulent jet, with or without swirl. To provide an understanding of the basic properties of jet diffusion flames, we will consider here at first the easiest case, the round jet flame into still air with or without buoyancy, for which we can obtain approximate analytical solutions. We want to determine the flame length of jet diffusion flames. We consider a fuel jet issuing from a round nozzle with diameter d and exit velocity u_0 into a surrounding air stream which may have a constant co-flow velocity of $u_\infty < u_0$. The indices 0 and ∞ denote conditions at the nozzle and in the ambient air, respectively. When buoyancy is included we restrict the analysis to a vertical jet without co-flow. The flame length is then defined as the distance from the nozzle on the centerline of the flame where the mean mixture fraction is equal to the stoichiometric value Z_{st}.

13.1 Non-buoyant Turbulent Jet Diffusion Flames into Still Air

The flow configuration and the flame contour of a vertical jet diffusion flame is shown in Fig. 13.1.

With the previous assumptions this leads to a two-dimensional axi-symmetric problem governed by equations (11.7), (11.8), and (11.13) written in the following form:

$$\frac{\partial}{\partial s}\left(\bar{\rho}\tilde{u}r\right) + \frac{\partial}{\partial r}\left(\bar{\rho}\tilde{v}r\right) = 0 \tag{13.1}$$

Momentum in s-direction:

$$\bar{\rho}\tilde{u}r\frac{\partial\tilde{u}}{\partial s} + \bar{\rho}\tilde{v}r\frac{\partial\tilde{u}}{\partial r} = \frac{\partial}{\partial r}\left(\bar{\rho}\nu_t r\frac{\partial\tilde{u}}{\partial r}\right) + r\left(\rho_\infty - \bar{\rho}\right)g \tag{13.2}$$

$$\bar{\rho}\tilde{u}r\frac{\partial\tilde{Z}}{\partial s} + \bar{\rho}\tilde{v}r\frac{\partial\tilde{Z}}{\partial r} = \frac{\partial}{\partial r}\left(\frac{\bar{\rho}\nu_t r}{\sigma_Z}\frac{\partial\tilde{Z}}{\partial r}\right) \tag{13.3}$$

Here we have introduced the boundary layer assumption and neglected the viscous stress as compared to the Reynolds stress component which was modelled as

$$-\bar{\rho}\widetilde{u''v''} = \bar{\rho}\nu_t\frac{\partial\tilde{u}}{\partial v}\,. \tag{13.4}$$

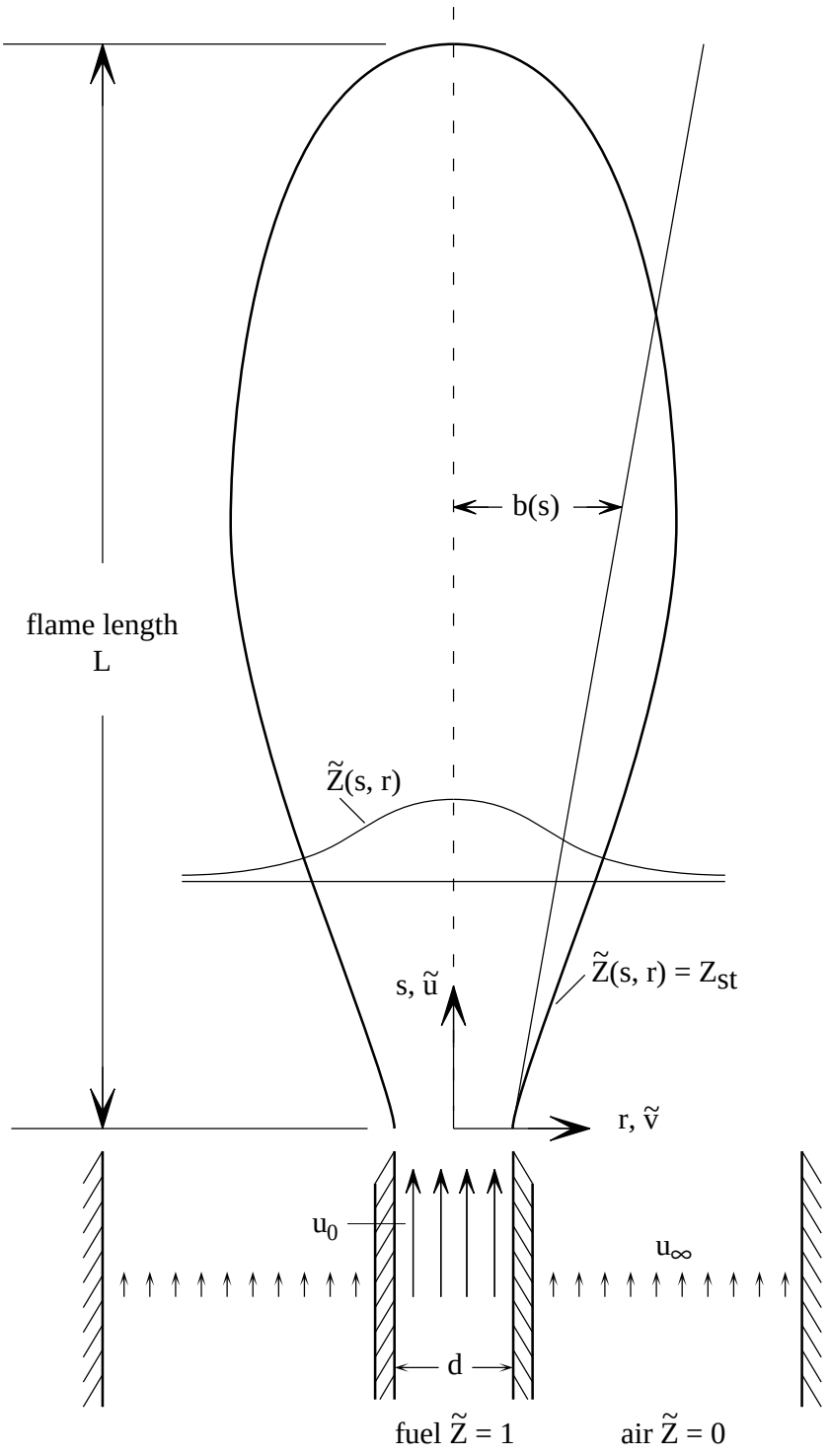

Fig. 13.1: Schematic representation of a vertical jet flame with co-flowing air

In addition, we have used the relation for the static pressure in the surrounding air

$$\frac{\partial p}{\partial s} = g\bar{\rho}_\infty \,. \tag{13.5}$$

For the case of a non-buoyant jet into still air this system of equations may be solved approximately by introducing a similarity transformation (Peters and Donnerhack, [13.1])

$$\eta = \frac{\bar{r}}{\zeta} \;,\; \bar{r}^2 = 2\int_0^r \frac{\bar{\rho}}{\rho_\infty} r\, dr \;,\; \zeta = s + s_0 \,, \tag{13.6}$$

which contains a density transformation leading to the density weighted radial coordinate $\bar{r}$. The new axial coordinate ζ starts from the virtual origin of the jet located at $s = -s_0$. The basic assumption introduced here is that the Chapman-Rubesin parameter

$$C = \frac{\bar{\rho}^2 \nu_t r^2}{\rho_\infty^2 \nu_{tr} \bar{r}^2} = \frac{\left(\rho_0 \rho_{\rm st}\right)^{1/2}}{\rho_\infty} \tag{13.7}$$

is a constant in the entire jet. Here the eddy viscosity ν_{tr} is that of a jet with constant density. It is adjusted to fit experimental data leading to (conf. Schlichting, [11.1])

$$\nu_{tr} = \frac{u_0 d}{70} \,. \tag{13.8}$$

The second equality in (13.7) was derived by adjusting flame length data (conf. below). The axial velocity profile is then given by

$$\frac{\tilde{u}}{u_0} = \frac{6.56\, d}{s + s_0} \left(\frac{\rho_0}{\rho_{\rm st}}\right)^{1/2} \left(1 + \frac{(\gamma\eta)^2}{4}\right)^{-2} \tag{13.9}$$

where the jet spreading parameter is

$$\gamma = 15.1 \left(\frac{\rho_\infty}{\rho_{\rm st}}\right)^{1/2} \,. \tag{13.10}$$

The mixture fraction profile is

$$\tilde{Z} = \frac{2.19\,(1 + 2\sigma_Z)\, d}{s + s_0} \left(\frac{\rho_0}{\rho_{\rm st}}\right)^{1/2} \left(1 + \frac{\gamma\eta^2}{4}\right)^{-2\sigma_Z} \,. \tag{13.11}$$

Choosing the turbulent Prandtl number σ_Z as 0.71 and C as in (13.7) where $\rho_{\rm st}$ is the density at the stoichiometric mixture, one obtains for the flame length by setting $L = s$ at $r = 0$ and $\tilde{Z} = Z_{\rm st}$,

$$\frac{L + s_0}{d} = \frac{5.3}{Z_{\rm st}} \left(\frac{\rho_0}{\rho_{\rm st}}\right)^{1/2} \tag{13.12}$$

which corresponds to the experimental data of Hawthorne, Weddel, and Hottel [13.2]. The distance of the virtual origin from $s = 0$ may be estimated by setting $\tilde{u} = u_0$ at $s = 0$, $r = 0$ in (13.9) so that

$$s_0 = 6.56\, d \left(\frac{\rho_0}{\rho_{\mathrm{st}}} \right)^{1/2} . \tag{13.13}$$

Since at the stoichiometric mixture the molecular weight is approximately that of nitrogen, the density ratio $\rho_0/\rho_{\mathrm{st}}$ may be estimated as

$$\frac{\rho_0}{\rho_{\mathrm{st}}} = \frac{W_0}{W_{\mathrm{N_2}}} \frac{T_{\mathrm{st}}}{T_0} . \tag{13.14}$$

This takes for methane and with the estimate $T_{\mathrm{st}} \sim 2000\,\mathrm{K}$ the value $\rho_0/\rho_{\mathrm{st}} = 3.8$. The flame length may then be calculated with $Z_{\mathrm{st}} = 0.055$ as $L = 200\, d$.

13.2 Turbulent Jet Diffusion Flames with Co-flowing Air and Vertical Flames with Buoyancy Effects

For flames with co-flow and with buoyancy effects a closed form solution of the governing equations cannot be derived. Here we seek an estimate by replacing the velocity and mixture fraction profile by top hat profiles (Peters, Göttgens, [13.3])

$$\tilde{u}, \tilde{Z} = \begin{cases} \hat{u}, \hat{Z} & \text{for } r \le b(s) \\ 0 & \text{for } r > b(s) \end{cases} \tag{13.15}$$

where $b(s)$ is the half-width of the jet (conf. Fig. 13.1). If the profiles are known, $b(s)$, $\hat{u}(s)$, and $\hat{Z}(s)$ can be obtained from the area averages

$$\begin{aligned} \rho_\infty \hat{u}^2 b^2 &= 2 \int_0^\infty \bar{\rho} \tilde{u}^2 r \, dr \\ \rho_\infty \hat{u} b^2 &= 2 \int_0^\infty \bar{\rho} \tilde{u} r \, dr \\ \rho_\infty \hat{Z} b^2 &= 2 \int_0^\infty \bar{\rho} \tilde{Z} r \, dr . \end{aligned} \tag{13.16}$$

This leads for the non-buoyant jet flame into still air to

$$\begin{aligned} \frac{\hat{u}}{u_0} = \hat{Z} &= 2.19 \frac{d}{s + s_0} \left(\frac{\rho_0}{\rho_{\mathrm{st}}} \right)^{1/2} \\ b(s) &= 0.23\, s \left(\frac{\rho_{\mathrm{st}}}{\rho_\infty} \right)^{1/2} . \end{aligned} \tag{13.17}$$

For the more general cases of a jet flame with co-flow or a vertical flame with buoyancy we may integrate (13.1)–(13.2) over r from $r = 0$ to $r = \infty$ to obtain an integrated form of the continuity and momentum equation

$$\begin{aligned} \frac{\mathrm{d}}{\mathrm{d}s} \left[\hat{u} b^2 \right] + 2 \lim_{r \to \infty} (\tilde{v} r) &= 0 \\ \frac{\mathrm{d}}{\mathrm{d}s} \left[\hat{u}^2 b^2 \right] - u_\infty \frac{\mathrm{d}}{\mathrm{d}s} \left[\hat{u} b^2 \right] &= 2g \int_0^r \left(1 - \frac{\bar{\rho}}{\rho_\infty} \right) r \, dr \end{aligned} \tag{13.18}$$

Here the first two definitions of (13.16) have been used. The integrated continuity equation has been introduced into the momentum equation to replace the integral over the second convective term.

Similarly, the integrated mixture fraction equation may be written

$$\frac{\mathrm{d}}{\mathrm{d}s}\left[\hat{u}\hat{Z}b^2\right] = 0\,. \tag{13.19}$$

Applying the initial condition $\hat{Z} = 1$ at the nozzle, where $b = d/2$ and $\bar{\rho} = \rho_0 =$ constant such that the right-hand side of $(13.16)_3$ is $\rho_0 u_0 d^2/4$, the integrated form of (13.19) is

$$\hat{u}\hat{Z}b^2 = \frac{d^2}{4}\frac{\rho_0}{\rho_\infty}u_0\,. \tag{13.20}$$

This allows the effective exit diameter to be defined as

$$d_{\mathrm{eff}} = d\left(\frac{\rho_0}{\rho_\infty}\right)^{1/2}\,. \tag{13.21}$$

For a non-buoyant jet flame $(13.18)_2$ can be integrated analytically with respect to s

$$\hat{u}\left(\hat{u} - u_\infty\right)b^2 = \frac{d^2}{4}\frac{\rho_0}{\rho_\infty}u_0\left(u_0 - u_\infty\right)\,. \tag{13.22}$$

In the following we relate all velocities to the jet exit velocity and all lengths to the effective diameter. Then, with $u^* = \hat{u}/u_0$, $u^*_\infty = u_\infty/u_0$, $b^* = b/d_{\mathrm{eff}}$, the velocity u^* may be written in terms of b^* as

$$u^* = \frac{1}{2}u^*_\infty + \frac{1}{2}\left({u^*}^2_\infty + \frac{1 - u^*_\infty}{{b^*}^2}\right)^{1/2}\,. \tag{13.23}$$

The next step is to evaluate the half-width $b(s)$. Following Schlichting [11.1], chapter 24, we note that the spreading of free shear flows is due to velocity fluctuations normal to the main axis. The substantial change is proportional to

$$\frac{Db}{Dt} \sim v'\,. \tag{13.24}$$

Relating v' to the mixing length l and the velocity gradient $d\tilde{u}/dr$, the latter being proportional to $\left(u_{\max} - u_{\min}\right)/b$, where b is again proportional to the mixing length, we can write

$$\frac{Db}{Dt} \sim \left(u_{\max} - u_{\min}\right)\,. \tag{13.25}$$

Replacing for a stationary flow Db/Dt by $\hat{u}\,db/ds$ and $u_{\max} - u_{\min}$ by $\hat{u} - u_\infty$, we obtain the relation

$$\hat{u}\frac{\mathrm{d}b}{\mathrm{d}s} = \beta\left(\hat{u} - u_\infty\right)\,, \tag{13.26}$$

where β is a proportionality constant. For a non-buoyant flame without co-flow it follows from $(13.17)_2$ that $\beta = 0.23\,(\rho_{\rm st}/\rho_\infty)^{1/2}$. For the general case, combining (13.23) and (13.26), with $s^* = s/d_{\rm eff}$, one obtains

$$\left[u^*_\infty + \left({u^*}^2_\infty + \frac{1-u^*_\infty}{{b^*}^2}\right)^{1/2}\right]^2 {b^*}^2 \frac{{\rm d}b^*}{{\rm d}s^*} = \beta\,(1-u^*_\infty)\ . \tag{13.27}$$

This may be written in terms of $y = b^* u^*_\infty/\,(1-u^*_\infty)^{1/2}$ as

$$\int_0^y \left(y + \sqrt{y^2+1}\right)^2 dy = \frac{\beta u^*_\infty}{(1-u^*_\infty)^{1/2}} \int_0^s ds^*\,. \tag{13.28}$$

Integration yields

$$y + \frac{2}{3}\left(\left(y^2+1\right)^{3/2} - 1\right) + \frac{2}{3}y^3 = \frac{\beta u^*_\infty}{(1-u^*_\infty)^{1/2}} s^*\,. \tag{13.29}$$

For small values of u^*_∞ the variable y is small, and the left-hand side of (13.28) may be expanded to second order as $y + y^2$ such that the half-width develops as

$$b = \beta s - \frac{u_\infty}{u_0}\beta^2 \frac{s^2}{d_{\rm eff}}\,, \tag{13.30}$$

showing linear spreading $b = \beta s$ for small values of s, but slower spreading for large s, since the velocity difference $\hat{u} - u_\infty$ as the driving force for the spreading is diminishing.

The flame length is defined by the location where $\tilde{Z}$ on the centerline is equal to $Z_{\rm st}$. The area-averaged value $\hat{Z}$ is smaller than the centerline value, as $\hat{u}$ is smaller than the centerline velocity. Therefore, rather than using $Z_{\rm st}$ we use $\hat{Z} = Z_{\rm st}/\alpha_1$, where α_1 is a correction factor for the mixing over the jet area. In order to determine the value of α_1 we consider again a jet into still air. From (13.17) we obtain

$$\frac{L+s_0}{d} = 2.19\,\alpha_1 \frac{1}{Z_{\rm st}} \left(\frac{\rho_0}{\rho_{\rm st}}\right)^{1/2}\,, \tag{13.31}$$

which is identical to (13.12), if α_1 is set equal to 2.42. We adopt this value in the following. (13.20)–(13.22) and (13.29) can be used to evaluate the flame length for non-buoyant flames with co-flowing air.

13.3 Effects of Buoyancy on Vertical Flames

Buoyancy becomes important in flames due to the density differences that combustion generates. The density decreases from ρ_0 at the nozzle to $\rho_{\rm st}$ at the flame length. The integral on the r.h.s. of (13.18) may be approximated by

$$2\int_0^\infty \left(1-\frac{\bar\rho}{\rho_\infty}\right) r\,dr = b^2\alpha_2\left(1-\frac{\rho_{\rm st}}{\rho_\infty}\right), \tag{13.32}$$

where α_2 is an empirical coefficient that takes the variable density into account. Introducing a modified Froude number

$$\mathrm{Fr}^* = \frac{u_0^2}{g d_{\rm eff}}\frac{\rho_\infty}{\alpha_2\left(\rho_\infty-\rho_{\rm st}\right)} = \mathrm{Fr}\sqrt{\frac{\rho_0}{\rho_\infty}}\frac{\rho_\infty}{\alpha_2\left(\rho_\infty-\rho_{\rm st}\right)}, \tag{13.33}$$

where $\mathrm{Fr}=u_0^2/gd$, we may replace (13.18) for $u_\infty=0$ by

$$\frac{\mathrm{d}}{\mathrm{d}s^*}\left[u^{*2}b^{*2}\right] = \frac{b^{*2}}{\mathrm{Fr}^*}. \tag{13.34}$$

With $b=\beta s$ this leads to

$$\frac{\mathrm{d}u^{*2}}{\mathrm{d}b^*} + \frac{2u^{*2}}{b^*} = \frac{1}{\beta\mathrm{Fr}^*}, \tag{13.35}$$

which is a linear first-order differential equation for u^{*2} and may therefore be solved analytically. One obtains

$$u^{*2} = \frac{c_0}{b^{*2}} + \frac{b^*}{3\beta\mathrm{Fr}^*}, \quad c_0 = \frac{1}{4} - \frac{1}{24\beta\mathrm{Fr}^*}, \tag{13.36}$$

with the initial condition $u^*=1/2$. The first term describes the momentum-dominated part of the vertical flame which reduces to $u^*=1/(2b^*)$ for large Froude numbers. The second term, which increases with b^*, describes the influence of buoyancy. Using only this term the flame length L is obtained with $4u^*\hat Z b^{*2}=1$ from (13.20) and $\hat Z = Z_{\rm st}/\alpha_1$ as

$$\frac{L}{d_{\rm eff}} = \frac{1}{\beta}\left(\frac{3\beta\alpha_1^2}{16Z_{\rm st}^2}\mathrm{Fr}^*\right)^{1/5}, \tag{13.37}$$

This shows the 1/5-exponential dependence of the flame length on the Froude number. A comparison with experimental data reported in Sønju and Hustad [13.4] allows determination of the yet unknown empirical constant α_2 as $\alpha_2=1$. A general equation for the flame length is obtained by combining (13.20) and (13.35) as

$$\left(\frac{3}{4}\beta\mathrm{Fr}^*-\frac{1}{8}\right)\left(\frac{\beta L}{d_{\rm eff}}\right)^2 + \left(\frac{\beta L}{d_{\rm eff}}\right)^5 = \frac{3\beta\alpha_1^2}{16Z_{\rm st}^2}\mathrm{Fr}^*, \tag{13.38}$$

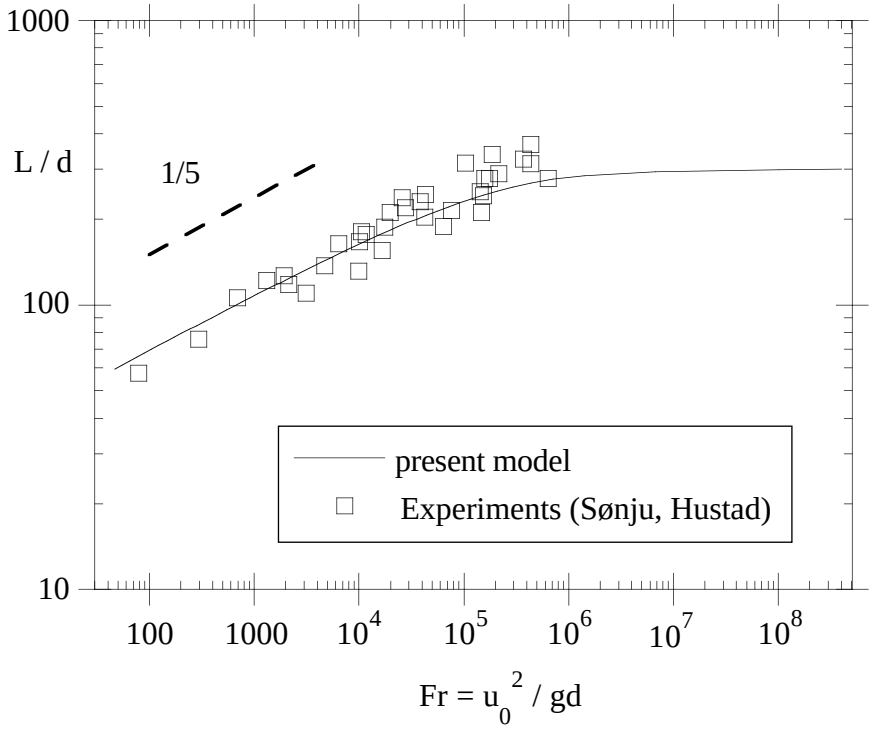

Fig. 13.2: Dimensionless flame length, L/d, versus Froude number, Fr, for propane and comparison with experimental data of Sønju and Hustad [13.4]

which reduces for sufficiently large values of L to (13.37) and for large Froude numbers to the momentum-dominated flame described by (13.12). Equation (13.38) has been evaluated for propane with $\rho_{\mathrm{st}}/\rho_\infty \approx T_\infty/T_{\mathrm{st}}$ and compared with experimental data in Fig. 13.2.

The buoyancy-dominated regime is valid for Froude numbers $\mathrm{Fr} < 10^5$ showing a 0.2-slope in this range, whereas the Froude number independent solution is approached for $\mathrm{Fr} > 10^6$. For lower Froude numbers there is excellent agreement between the predictions of (13.38) and the experimental data.

13.4 Nitric Oxide Formation in Turbulent Jet Diffusion Flames

One of the major pollutants formed in furnaces and many other combustion devices is NO which is easily oxidized to NO_2. The sum of NO and NO_2 is often called NO_x. Here we want to estimate the formation of NO in turbulent jet diffusion using some of the approximations introduced above. It has been recognized that there are essentially two paths that lead to NO formation in flames: The thermal NO formed through the Zeldovich mechanism, and the "prompt NO" mechnism wherein hydrocarbon fragments attack bimolecular nitrogen, producing atomic nitrogen, cyanides, and amines, which subsequently oxidize to nitric oxide. Which one of these mechanisms predominates depends mainly on the flame temperature. Prompt NO is not very sensitive to temperature, it contributes between ten to thirty ppm to the total NO production in hydrocarbon flames, while thermal NO may contribute up to several hundred ppm. It is clear that the high NO levels that occur in practical systems can only be reduced by reducing thermal NO formation. We will therefore consider the thermal NO production only. The subsquent analysis follows Peters and Donnerhack [13.1]. Since in the Zeldovich mechanism

$$\mathrm{O} + \mathrm{N_2} \rightarrow \mathrm{NO} + \mathrm{N} \qquad (N1)$$

$$\mathrm{N} + \mathrm{O_2} \rightarrow \mathrm{NO} + \mathrm{O} \qquad (N2)$$

the intermediate N-radical may be assumed in steady state, the rate of formation of NO is determined by taking the first reaction twice

$$\dot{w}_{\mathrm{NO}} = 2K_{N1}(T)[\mathrm{N_2}][\mathrm{O}] \tag{13.39}$$

For an order of magnitude analysis we will assume that the O-radical is in partial equilibrium with O_2. Using the equilibrium constant for O_2-dissociation, [O] may be related to $[O_2]$ at 1 atm by

$$\frac{[\mathrm{O}]}{[\mathrm{O_2}]^{1/2}} = 4.1 \exp\left(-\frac{29150}{T}\right) \left(\mathrm{mol/cm^3}\right)^{1/2} \tag{13.40}$$

With the rate $K_{N1} = 7 \cdot 10^{13} \exp$ (-37750/T) one obtains

$$S_{\mathrm{NO}} \equiv \frac{\dot{w}_{\mathrm{NO}}}{\rho} = B_{\mathrm{NO}} M_{\mathrm{NO}} \frac{Y_{\mathrm{N_2}}}{M_{\mathrm{N_2}}} \left(\frac{\rho Y_{\mathrm{O_2}}}{M_{\mathrm{O_2}}}\right)^{1/2} \exp\left(-\frac{E_{\mathrm{NO}}}{T}\right) \tag{13.41}$$

$$B_{\mathrm{NO}} = 5.74 \cdot 10^1 4(\mathrm{cm^3/mol})^{1/2}/s, \quad E_{\mathrm{NO}} = 66900\mathrm{K}$$

It will be assumed that the combustion reactions are locally in chemically equilibrium and that the only kinetically controlled process is the production of NO. Then, since the temperature and concentrations are a function of the mixture fraction the local NO production rate is a function of mixture fraction only. The turbulent mean production rate is then

$$\bar{\dot{w}}_{\mathrm{NO}} = \bar{\rho}\hat{S} = \bar{\rho} \int_0^1 S_{\mathrm{NO}}(Z)\tilde{P}(Z)\, dZ \tag{13.42}$$

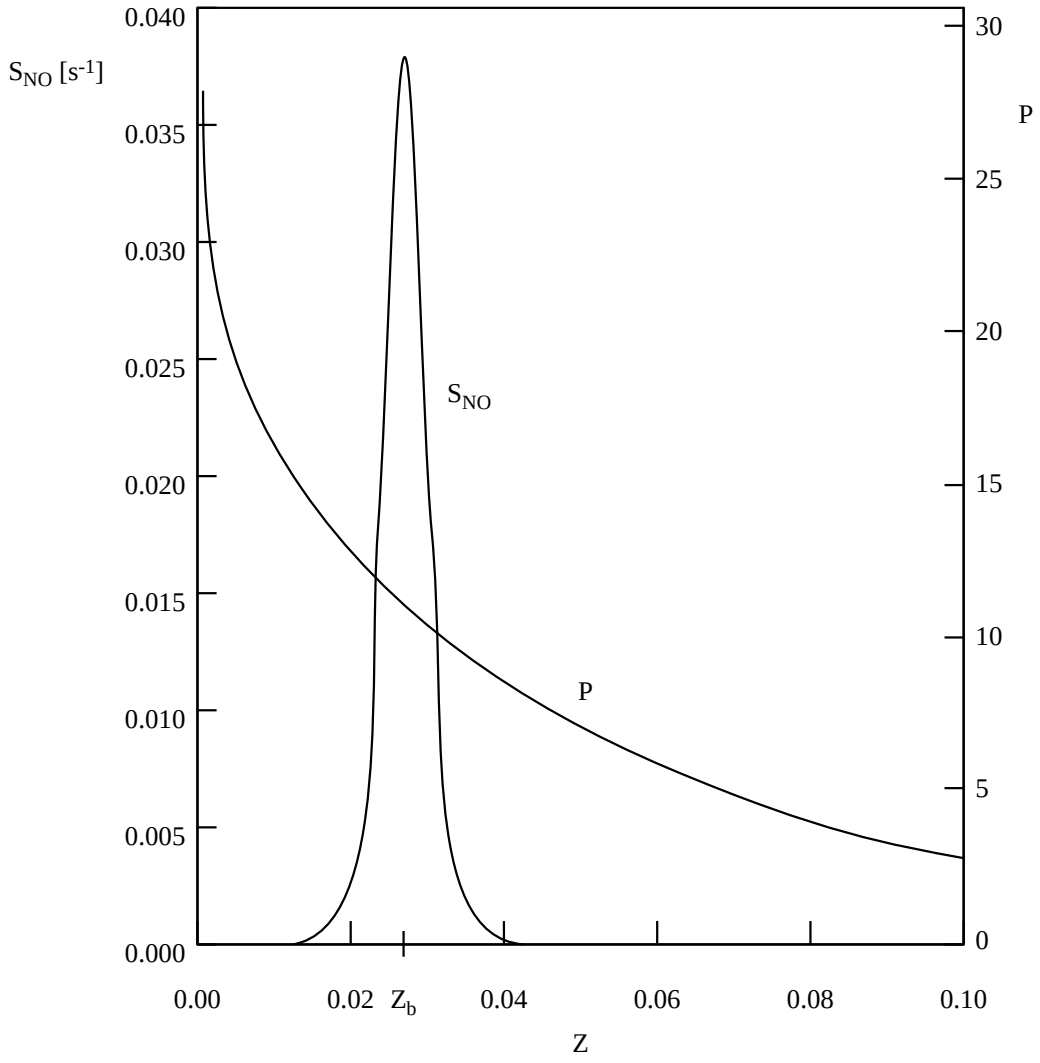

Fig. 13.3: NO-reaction rate and pdf for a hydrogen-air mixture.

where $\tilde{P}(Z)$ is the Favre pdf of Z. In Fig. 13.3 $S_{\rm NO}(Z)$ and $\tilde{P}(Z)$ are plotted as a function of Z for a hydrogen-air flame.

The production rate $S_{\rm NO}(Z)$ has a very sharp peak at the mixture fraction Z_b which corresponds to the maximum temperature T_b. Since T_b occurs close to the stoichiometric mixture fraction one may assume $Z_b \approx Z_{\rm st}$. The asymptotic analysis in Peters and Donnerhack [13.1] shows that $S_{\rm NO}$ may be replaced by a Gaussian with a small width of order ε defined by

$$\varepsilon = \frac{T_b}{Z_b}\left(-\frac{2}{E_{\rm NO}\left(d^2T/dZ^2\right)_b}\right)^{1/2} . \tag{13.43}$$

This indicates that the width of $S_{\rm NO}$ is small for a large activation energy $E_{\rm NO}$, provided that the temperature profile in mixture fraction space drops sufficiently rapidly towards both sides around the maximum value. The latter is parameterized by the second derivative of the temperature profile $\left(d^2T/dZ^2\right)_b$. If, on the other hand, $\tilde{P}(Z)$ does not change too much in the vicinity of Z_b, it may be replaced by $\tilde{P}(Z_b)$ and the integral may be expressed as

$$\overline{\dot{w}_{\rm NO}} = \bar{\rho}\tilde{P}(Z_b)\int_0^1 S_{\rm NO}(Z)\ dZ\ , \tag{13.44}$$

which was evaluated as

$$\dot{w}_{\rm NO} = \bar{\rho}\ S_{\rm NO}(Z_b)\ \tilde{P}(Z_b)\ \varepsilon\ Z_b\ \pi^{1/2} \tag{13.45}$$

The total NO-production rate $G_{\rm NO}$ in a jet diffusion flame is the integral over the entire flame volume

$$\begin{aligned} G_{\rm NO} &= 2\pi\ \int_0^L\int_0^\infty \overline{\dot{w}_{\rm NO}}\ r\ dr\ ds \\ &= 2\pi\rho_\infty\ \int_{s_0}^L \zeta^2\ \int_0^\infty \tilde{S}_{\rm NO}(\eta)\ \eta\ d\eta\ d\zeta \end{aligned} \tag{13.46}$$

where (13.6) was used. With (13.11) the integral over η may be expressed as

$$\int_0^\infty\ \tilde{S}_{\rm NO}\ \eta\ d\eta = \frac{S_{\rm NO}(Z_b)\varepsilon\pi^{1/2}(\zeta/L)^{-1/2\sigma_Z}}{\sigma_Z\gamma^2}\ {\rm H}(\tilde{Z},\widetilde{Z''^2}) \tag{13.47}$$

where the function ${\rm H}(\tilde{Z},\widetilde{Z''^2})$ represents an integral over $\tilde{P}(Z_b)$. In the limit of small variances $\widetilde{Z''^2}$ the function H approaches unity. It remains of that order of magnitude for typical values of $\widetilde{Z''^2}$ and may therefore be replaced by the constant value ${\rm H} = 1$ for simplicity. Then (13.46) may be evaluated in the limit $s_0 \to 0$ as

$${\rm G_{NO}} = \frac{4\pi^{3/2}\ \rho_\infty\ {\rm S_{NO}}(Z_b)\varepsilon L^3}{(6\sigma_Z - 1)\gamma^2} = 0.03\ \rho_{\rm st}{\rm S_{NO}}(Z_b)\varepsilon L^3 \tag{13.48}$$

This shows that the NO-production rate is proportional to the cube of the flame length, since the flame width scales with the flame length.

We now want to estimate the NO-production of buoyant jet diffusion flames of propane in air by using (13.48) to calculate the emission index E refered to NO_2 in g NO_2/ kg fuel defined as

$${\rm E_{NO_2}} = \frac{W_{\rm NO_2}}{W_{\rm NO}}\frac{\rm G_{NO_2}}{\rm G_0}\ 10^3$$

where ${\rm G_0} = \pi\rho_0 d^2 u_0/4$ is the fuel mass flow rate from the jet nozzle and $w_{\rm NO_2}$ and $w_{\rm NO}$ are the molecular weights of NO_2 and NO. For propane ${\rm S_{NO}}(Z_b)\cdot 10^3$ are 10.8/s and $\varepsilon = 0.109$ according to Peters and Donnerhack and L may be calculated from (13.37) as

$$\frac{L}{d} = 22\ {\rm Fr}^{1/5}\ .$$

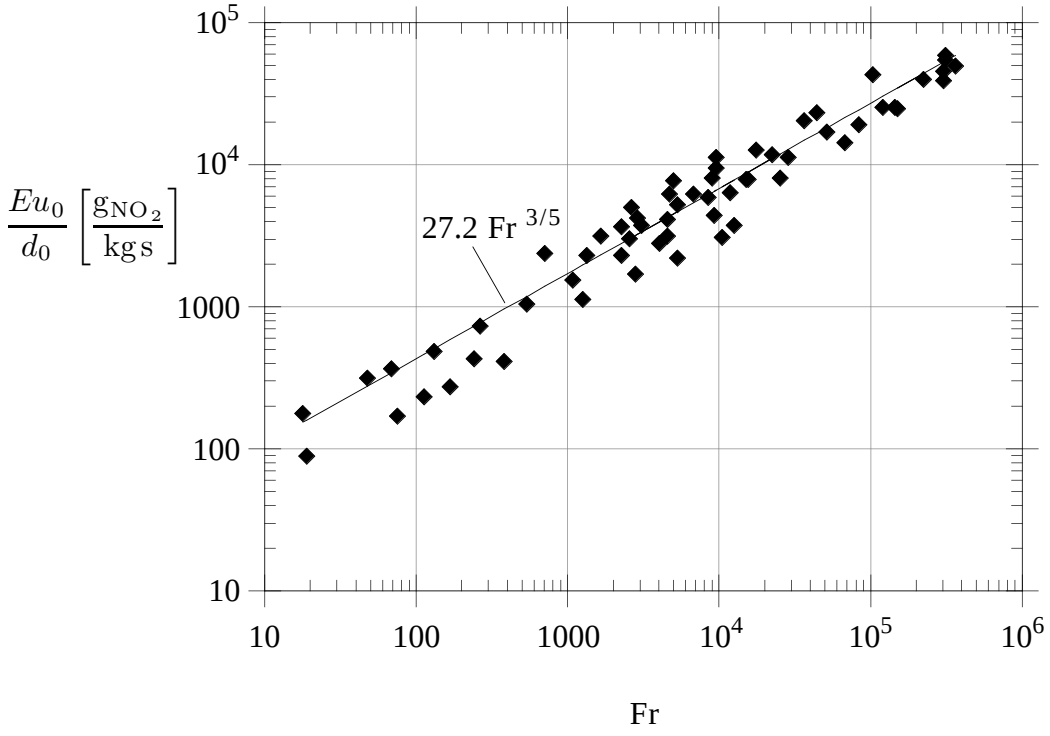

Fig. 13.4: Emission Index versus Froude number for buoyant jet diffusion flames of propane in air. Experimental data from [13.5]

This leads for E u_0/d with $\rho_0/\rho_{st} = 3/20$ to

$$\text{E } u_0/d = 27.2 \text{ Fr}^{3/5} \left[\frac{\text{g NO}_2}{\text{kg fuel sec}}\right]$$

This value overestimates somewhat the data taken from Røkke et al. [13.5] shown in Fig. 13.4.
This may have several reasons:

1. The assumption of local chemical equilibrium overestimates the temperature but underestimates the O-radical concentration in the calculation of $S_{NO}(Z_b)$. These effects tend to compensate each other for small strain rates, as may be estimated from Figs. 13.4 and 13.6, if one assumes a similar non-equilibrium increase for O as for OH. For large strain rates, however, the temperature decrease in (13.39) dominates, leading to lower values of S_{NO}.
2. Radiative heat loss which is most effective at the maximum temperature will decrease the temperature and thereby the thermal S_{NO}.
3. Prompt NO, which is not taken into account here, will decrease the total NO-production. Its contribution was estimated in Røkke et al. [13.5] to be of the order of 30% for the buoyant jet flames considered here.

References

[13.1] Peters, N., Donnerhack, S., 18th Symp. (Int.) on Combustion 33–42, The Combustion Institute 1981.

[13.2] Schlichting, H., Grenzschichttheorie, p.690, Braun, 1965.

[13.3] Sønju, O.K., Hustad, J., Prog. Astronaut. Aeronaut. **95** (1984) 320.

[13.4] Røkke, N.A., Hustad, J.E., Sønju, O.K., Williams, F.A., 24th Symposium (International) on Combustion, 1992, to appear.

Lecture 14. Laminar Flamelet Models for Premixed Turbulent Combustion

At first sight, premixed combustion would appear easier to analyse than non-premixed combustion, since mixture fraction variations do not need to be considered. The flamelet concept for premixed combustion is, however, not yet as well developed. For non-premixed combustion it was derived from first principles by a local coordinate transformation to the governing equations. Then, by considering an equation for the mixture fraction, which fixes the instantaneous location of the flamelets around $Z(\boldsymbol{x},t) = Z_{\rm st}$ in the turbulent flow the chemical source terms could be removed from the calculations of the turbulent flow and mixture field. A similar approach for premixed combustion would also require an equation that describes the location of the flamelets but does not contain the chemical source terms per se. This equation should also be derived from first principles and would have to be modelled in a similar way as the mixture fraction equation. It is the field equation for the scalar $G(x,t)$ that has been derived in Lecture 8. When strain and curvature is included it reads

$$\rho\frac{\mathrm{D}G}{\mathrm{D}t} = (\rho s_L^\circ)\,|\nabla G| - \underbrace{(\rho\mathcal{D}_\mathcal{L})\,\kappa|\nabla G|}_{\text{flame curvature}} + \underbrace{(\rho\mathcal{L})\,\boldsymbol{n}\cdot\nabla\boldsymbol{v}\cdot\boldsymbol{n}|\nabla G|}_{\text{flame stretch}} \tag{14.1}$$

where the curvature κ is defined

$$\kappa = \nabla\cdot\boldsymbol{n} = \nabla\cdot\left(-\frac{\nabla G}{|\nabla G|}\right)\,. \tag{14.2}$$

The iso-scalar level surface $G(\boldsymbol{x},t) = G_0$ represents the instanteneous flame location. This is shown schematically in Fig. 14.1.

14.1 Derivation of a Field Equation for the Mean Flame Location and its Variance

As noted earlier, it is necessary to specify (14.1) consistently in terms either of unburnt mixture properties or of burnt gas properties. It is convenient to choose unburnt gas quantities and then $\rho = \rho_u, s_L^\circ$ is the burning velocity in terms of these properties and $\mathcal{L}$ is the corresponding Markstein length. Because the flame is asymptotically thin compared with flow field length scales it appears as a discontinuity across which density suddenly changes from ρ_u to ρ_b. From the point of view of (14.1) we need be interested only in the flame position defined by $G(\boldsymbol{x},t) = G_0$, and in the flow immediately upstream of it, i.e. $G(\boldsymbol{x},t) - G_0, = O_-$ where $\rho = \rho_u$, that is, a constant density nonreacting flow.

It follows that ρ may be cancelled from (14.1). Mean and fluctuating components of G are then Reynolds rather than Favre averages and we write

$$G(\boldsymbol{x},t) = \bar{G}(\boldsymbol{x}) + G'(\boldsymbol{x},t)\,.$$

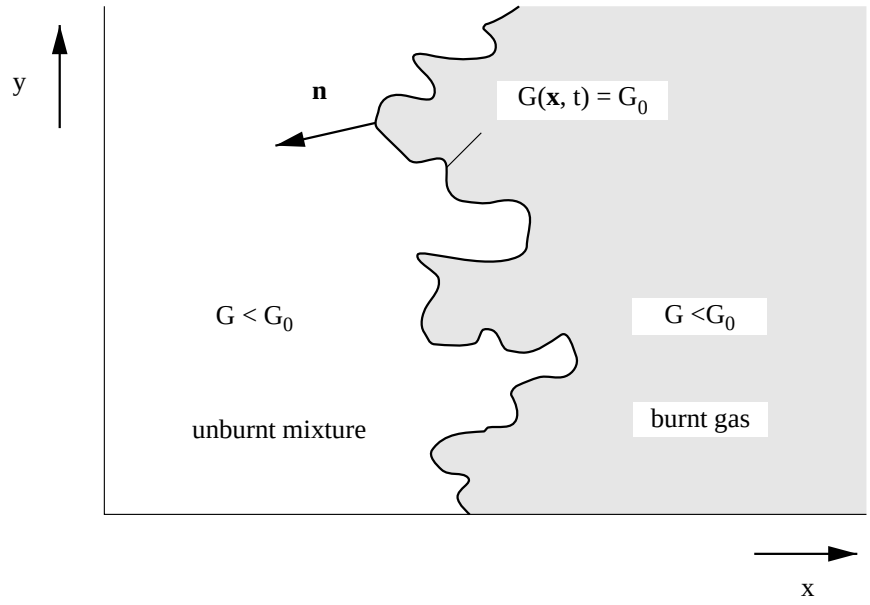

Fig. 14.1 Burnt and unburnt gas regions separated by a thin flame surface at $G(\boldsymbol{x}, t) = G_0$

Note that the mean value $\bar{G}$ will in general include contributions from the burnt gas where $G(\boldsymbol{x}, t) > G_0$ so $\rho = \rho_b$ rather than ρ_u. However, values of G simply represent levels of displacement from the flame surface at $G(\boldsymbol{x}, t) = G_0$. The velocity $\boldsymbol{v}$ in (14.1) is the velocity in the unburnt gas ahead of the flame. That is, the component in direction x_α is

$$v_\alpha(\boldsymbol{x}, t) = \bar{v}_{\alpha u}(\boldsymbol{x}, t) + v'_{\alpha u}(\boldsymbol{x}, t); \quad G(\boldsymbol{x}, t) - G_0 = 0_- \tag{14.3}$$

where as usual subscript u denotes unburnt reactants. The velocity field in the burnt gas downstream of the flame does not enter the equation and does not contribute to the mean.

In the following the modulus of ∇G will be denoted by

$$\sigma \equiv |\nabla G| = \left[(\nabla G)^2\right]^{1/2} . \tag{14.4}$$

The mean of (14.1) is then

$$\frac{\partial \bar{G}}{\partial t} + \overline{v_{\alpha u}} \frac{\partial \bar{G}}{\partial x_\alpha} + \frac{\partial}{\partial x_\alpha} \left(\overline{v'_{\alpha u} G'}\right) = \overline{s_L^\circ \sigma} - \overline{\mathcal{D}_\mathcal{L} \kappa |\nabla G|} + \mathcal{L}\, \overline{\boldsymbol{n} \cdot \nabla \boldsymbol{v}_u \cdot \boldsymbol{n} |\nabla G|} \tag{14.5}$$

where, in view of (14.4), $\bar{\sigma}$ is not equal to $|\nabla \bar{G}|$.

The equation for the variance is obtained by multiplying the equation for the fluctuation G' by $2G'$ and averaging

$$\frac{\partial \overline{G'^2}}{\partial t} + \overline{v_{\alpha u}} \frac{\partial \overline{G'^2}}{\partial x_\alpha} = -\frac{\partial}{\partial x_\alpha} \left(\overline{v'_{\alpha u} G'^2}\right) - 2\, \overline{v'_{\alpha u} G'} \frac{\partial \bar{G}}{\partial x_\alpha} - \bar{\omega} - \overline{\chi_\mathcal{L}} - \bar{\Sigma}_\mathcal{L} . \tag{14.6}$$

Here the first term on the r.h.s. denotes the turbulent transport of the scalar variance and the second its production by turbulent fluctuations. The last three terms are specific for the present problem and are defined [8.1] as

Kinematic Restoration

$$\bar{\omega} = -2\overline{s_L^\circ G'\sigma'} \tag{14.7}$$

Scalar Dissipation

$$\overline{\chi}_{\mathcal{L}} = -2\ \overline{\mathcal{D}_{\mathcal{L}} G' \left(\kappa |\nabla G|\right)'} \tag{14.8}$$

Scalar-Strain Co-Variance

$$\bar{\Sigma}_{\mathcal{L}} = 2\ \overline{\mathcal{L} G' \left(\boldsymbol{n}\cdot\nabla \boldsymbol{v}_u \cdot \boldsymbol{n} |\nabla G|\right)'}\,. \tag{14.9}$$

The kinematic restoration represents the co-variance of the scalar fluctuation with the first source term in (14.1). This co-variance is expected to be negative. It accounts for the smoothing of the scalar field and thereby of the flame surface by laminar flame propagation. Scalar fluctuations produced by turbulence are reduced or restored by this kinematic effect, which is most effective at the Gibson length scale L_G. Since L_G represents the cut-off scale of the inertial range for the G-equation, the kinematic restoration will play a dominating role in removing scalar fluctuations.

The scalar dissipation incorporates the co-variance between G' and fluctuations of the curvature. It is called scalar dissipation since it contains the diffusivity. It is therefore expected to be positive and the co-variance negative. It can be shown to be most effective at a Corrsin length scale

$$L_C = \left(D_{\mathcal{L}}^3/\varepsilon\right)^{1/4} = L_G^{1/4}\mathcal{L}^{3/4} \tag{14.10}$$

based on the Markstein diffusivity $\mathcal{D}_{\mathcal{L}}$. Finally, the scalar-strain co-variance accounts for the reduction of scalar variance due to strain. As the straining motion of the turbulent flow field acts on flame surface preferentially by stretching it (rather than by compressing it), this term smooths the flame front further and thereby reduces the remaining scalar fluctuations. It is therefore expected to be positive and the co-variance negative. It is most effective at the Markstein length $\mathcal{L}$.

14.2 Closure of the Mean Field Equations in the Limit $v'/s_L^\circ \to \infty$

Closure of (14.5) and (14.6) is proposed following [8.1] and [8.2]. Time and length scales of the velocity field are obtained from $\bar{k}-\bar{\varepsilon}$ equations as $\bar{k}/\bar{\varepsilon}$ and $\bar{k}^{3/2}/\bar{\varepsilon}$, respectively; strictly these should be conditional quantities in the unburned gas. For homogeneous isotropic turbulence two point-scalar correlations have been considered and a spectral closure has been introduced which shows that the kinematic restoration in the variance (14.6) can be modelled in the limit $v'/s_L^\circ \to \infty$ as

$$\bar{\omega} = c_\omega \frac{\bar{\varepsilon}}{\bar{k}} \overline{G'^2} \tag{14.11}$$

where c_ω is assumed to be a constant of order unity. It has been estimated as 1.62 (cf. [8.1]), but for finite values of s_L°/v' it depends weakly on s_L°/v' and on the ratio $\mathcal{L}/L_G$. Since the scalar dissipation and the scalar-strain co-variance are effective at scales lower than the Gibson scale, a spectral theory based on dimensional analysis cannot provide definite equations for these quantities.

We will refer to direct simulations by Ashurst [8.3] below. Furthermore, dimensional analysis in the limit $v'/s_L^\circ \to \infty$ suggests that the main source term in (14.5) should be independent of s_L° and should be modelled as

$$\overline{s_L^\circ \sigma} = a_1 \left(\bar{\omega} \frac{\bar{\varepsilon}}{\bar{k}} \right)^{1/2} . \tag{14.12}$$

It is consistent with standard arguments in turbulence modelling to consider the limit where production equals the sum of the kinematic restoration, scalar dissipation, and the scalar strain terms in the variance equation (14.6). Such arguments lead to Prandtl's mixing length theory in turbulent shear flows and to the eddy break-up limit, where the mean reaction rate is proportional to the scalar dissipation rate, in progress variable descriptions of premixed turbulent combustion. Assuming a gradient flux approximation in the production term

$$-\overline{v'_{\alpha u} G'} = D_T \frac{\partial \bar{G}}{\partial x_\alpha} \tag{14.13}$$

where the turbulent diffusivity is

$$D_T = c_1 \bar{k}^2 / \bar{\varepsilon} \tag{14.14}$$

and c_1 is a constant, this limit yields

$$2 D_T |\nabla \bar{G}|^2 = \bar{\omega} + \overline{\chi_{\mathcal{L}}} + \overline{\Sigma_{\mathcal{L}}} \, . \tag{14.15}$$

Let us at first consider the limit $\mathcal{L} \to 0$ so that the last two terms in (14.15) can be neglected. Then from (14.14) and (14.15) we obtain

$$\bar{\omega} = 2 c_1 \bar{k}^2 |\nabla \bar{G}|^2 / \bar{\varepsilon} \, . \tag{14.16}$$

Substituting this, together with (14.12) into (14.5) we find in the limit $v'/s_L^\circ \to \infty$

$$\begin{aligned} &\frac{\partial \bar{G}}{\partial t} + \overline{v_{\alpha u}} \frac{\partial \bar{G}}{\partial x_\alpha} + \frac{\partial}{\partial x_\alpha} \left(\overline{v'_{\alpha u} G'} \right) = \\ &\qquad a_1 (3 c_1)^{1/2} v' |\nabla \bar{G}| - \overline{\mathcal{D}_{\mathcal{L}} \kappa |\nabla G|} + \mathcal{L} \overline{\underline{n} \cdot \nabla \underline{v}_u \cdot \underline{n} |\nabla G|} \, . \end{aligned} \tag{14.17}$$

The first term on the right-hand side of (14.17) is exactly analogous to that in (14.1) except that s_L° is replaced by a constant times the turbulence intensity v'. In a homogeneous turbulent flow field the mean contour of a turbulent premixed flame could then be calculated in a similar way as a laminar flame with the laminar burning velocity replaced by v'. This is consistent with renormalisation arguments (Yakhot, [8.4]). Since the field equation (14.1) is a Hamilton-Jacobi equation with a parabolic curvature term, its turbulent counterpart, again following renormalisation arguments, should have the same character in order to be consistent with the boundary and initial conditions. This suggests that the terms in (14.17), which represent turbulent transport and Markstein diffusion, should be combined and modelled as a curvature term

$$-\frac{\partial}{\partial x_\alpha} (\overline{v'_{\alpha u} G'}) \; - \; \overline{\mathcal{D}_{\mathcal{L}} \kappa |\nabla G|} = - \; D_{T,\bar{G}} \bar{\kappa} |\nabla \bar{G}| \, . \tag{14.18}$$

Here $\bar{\kappa}$ is the mean curvature defined as in (14.2) but with $\bar{G}$ instead of G. The diffusion coefficient $D_{T,\bar{G}}$ should be of the order of D_T defined in (14.13).

14.3 Results of Recent Direct Numerical Simulations of the *G*-Equation

Recently, Ashurst [8.3] has re-analysed numerical results obtained from a numerical simulation of (14.1) on a $32\times32\times32$ mesh. These simulations are based on the constant density three-dimensional Navier-Stokes equations, where the large-scale strain rate was adjusted to achieve constant energy turbulence. These simulations were performed for small values of v'/s_L° equal to 0.5, 1.0, 2.0 and 4.0 and are therefore complementary to the spectral modelling results in the limit of $v'/s_L^\circ \to \infty$ considered above. The turbulence intensity was unity by definition and the dissipation, based on the length scale of the box and a normalized viscosity of 0.002, was $\varepsilon = 1.88$. Using (11.16) this leads to an integral length scale of 0.2. The Markstein length based on unit length of the box was varied between 0.05, 0.025 and 0.0125. The results show an increase of $\bar{\omega}$ and $\bar{\chi}_{\mathcal{L}}/D_{\mathcal{L}}$ with $\overline{G'^2}$ essentially independent of the Markstein length. Also, the scalar-strain correlation $\bar{\Sigma}_{\mathcal{L}}$ was found to be very small and shows no correlation with $\overline{G'^2}$ or $\mathcal{L}$. This leads to the scaling of the source terms in (14.6) as

$$\bar{\omega} + \bar{\chi}_{\mathcal{L}} + \overline{\Sigma_{\mathcal{L}}} = c_\omega \frac{\bar{\varepsilon}}{\bar{k}} \overline{G'^2} \left(1 + \alpha \frac{s_L^\circ \mathcal{L}}{\nu}\right) \tag{14.19}$$

where c_ω was found as $c_\omega = 1.2$ and $\alpha = 0.2$. For the source terms in (14.5) it was found that $\overline{s_L^\circ \sigma}$ increases approximately as

$$\overline{s_L^\circ \sigma} = s_L^\circ + 0.8\,(s_L^\circ v')^{1/2} \quad . \tag{14.20}$$

Also, the mean curvature term $\overline{\mathcal{D}_{\mathcal{L}} \kappa |\nabla G|}$ is very small for all values of v'/S_L^o and $\mathcal{L}$. This is consistent with an analysis (Bray and Cant, [8.5]) of direct numerical simulations of premixed turbulent combustion which show the mean flamelet curvature to be zero. Finally, the correlation $\boldsymbol{n} \cdot \boldsymbol{x}_u \cdot \boldsymbol{n} |\nabla G|$ in the last term of (14.5), representing the effect of strain in the mean equation is always negative. When this term, divided by the first source term $\overline{s_L^\circ \sigma}$ is plotted in Fig. 14.2 over v'/s_L° for the different values of the Markstein length it is seen that the ratio is linear in v'/s_L° and independent of $\mathcal{L}$.

This gives rise to the scaling

$$\overline{s_L^\circ \sigma} + \mathcal{L} \overline{\boldsymbol{n} \cdot \nabla \boldsymbol{x}_u \cdot \boldsymbol{n} |\nabla G|} = \left[s_L^\circ + b_2\,(s_L^\circ v')^{1/2}\right] \left(1 - b_3 \frac{\mathcal{L}}{\ell_t} \frac{v'}{s_L^\circ}\right) \tag{14.21}$$

where $b_2 = 0.8$ and $b_3 = 1.4$ were obtained based on these numerical simulations.

If the scaling relations obtained from the direct numerical simulations covering the range of small v'/s_L° are combined with the results from the turbulence modelling in the limit of large v'/s_L°, one obtains finally

$$\frac{D\bar{G}}{Dt} = \left[s_L^\circ + b_2\,(s_L^\circ v')^{1/2} + b_1 v'\right] \left(1 - b_3 \frac{\mathcal{L}}{\ell_t} \frac{v'}{s_L^\circ}\right) |\nabla \bar{G}| - D_{T,\bar{G}} \bar{\kappa} |\nabla \bar{G}| \tag{14.22}$$

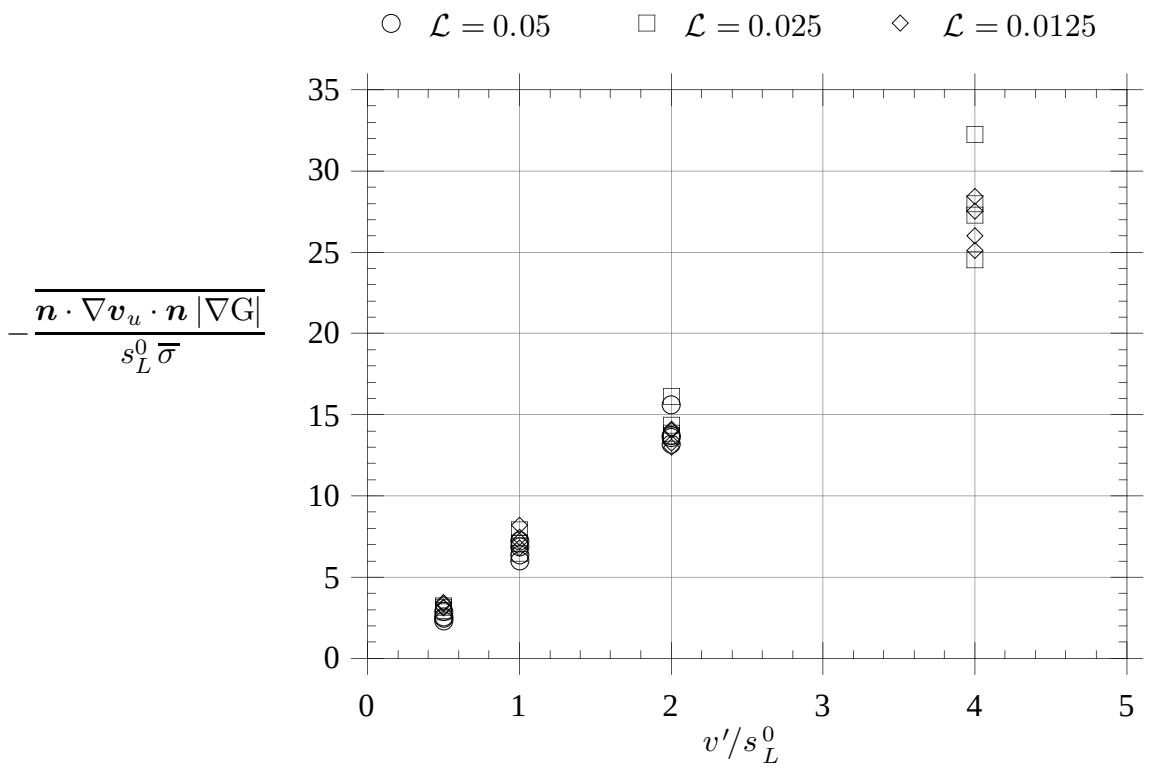

Fig.14.2 Results of numerical simulation of the strain rate term

where $b_1 = a_1\,(3c_1)^{1/2}$ should be of order unity.

If (14.15) together with (14.19) instead of (14.16) had been used, it would follow that b_1 decreases with an increasing Markstein length. In addition b_1 may well depend on the density ratio ρ_u/ρ_b due to gas expansion effects and possibly on the pressure gradient across the flame.

One may solve (14.22) for a plane steady turbulent flame normal to the x-direction. The solution $\bar{G} = x$ then leads to a turbulent burning velocity given by

$$s_T = \left[s_L^\circ + b_2\,(s_L^\circ v')^{1/2} + b_1 v'\right]\left(1 - b_3 \frac{\mathcal{L}}{\ell_t}\,\frac{v'}{s_L^\circ}\right) \tag{14.23}$$

In a graph of s_T/s_L° plotted against v'/s_L° comparison with previous correlations by Bray [8.6] and Gülder [8.7] is shown in Fig. 14.3 for $\ell_F/\ell = 0.02$ and assuming $\mathcal{L}/\ell_F = 4.0$ such that $\mathcal{L}/\ell = 0.08$.

According to (14.18) and (14.22) the $\bar{G}$ field is unaffected by turbulent diffusion in the absence of curvature of the turbulent flame brush, i.e. when $\bar{\kappa} = 0$. Some preliminary experimental evidence from a turbulent Bunsen flame (Armstrong, [8.8]) supports this conclusion. Armstrong reports simultaneous two dimensional image measurements of velocity by particle image velocimetry and of wrinkled flame location by Mie scattering from the added seed particles. His data from this flame whose mean shape is essentially without curvature in the plane of the measurements, clearly resolves the countergradient turbulent diffusion of the progress variable (Bray et al. [8.9]). However within the accuracy of the

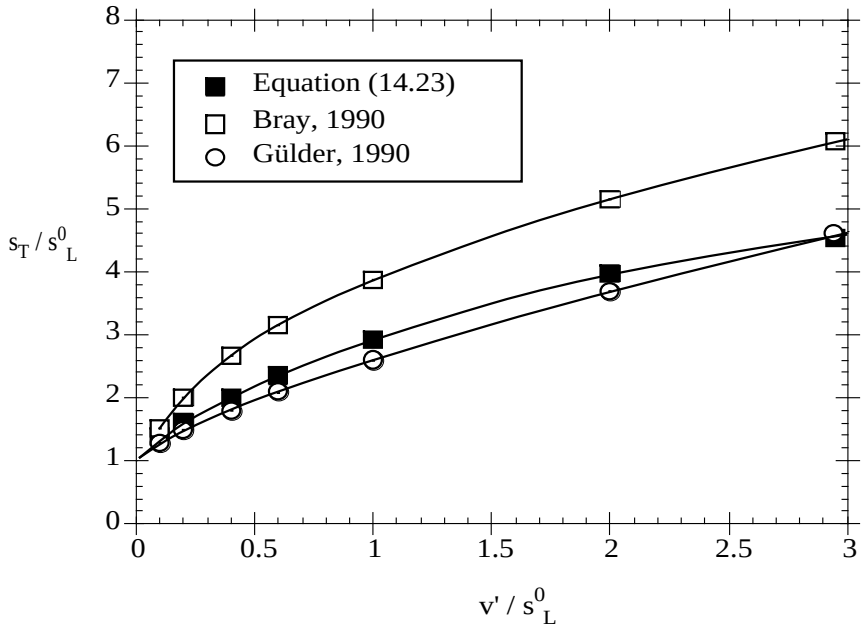

Fig.14.3 Comparison of different correlations for the ratio of the turbulent and the laminar burning velocity as a function of v'/s_L° for $\ell_F/\ell = 0.02$

experiments the turbulent fluxes $\overline{G'u'_u}$ across the flame and $\overline{G'v'_u}$ along the flame are both zero.

14.4 Taylor Microscale of G Field

We can gain some insight into the physical meaning of these closure expressions by using them to calculate a characteristic length scale of the scalar field. The analysis in [8.1] and [8.2] assumes a homogeneous isotropic field. We can then define a Taylor microscale λ_G for the G field in analogy to (11.20) to represent the inverse of the average gradient of the G field by

$$\overline{\left(\frac{\partial G}{\partial x_\alpha}\right)^2} = \frac{\overline{G'2}}{\lambda_G^2} \tag{14.24}$$

Now (14.12) models the left-hand side of this expression leading to

$$\overline{\left(\frac{\partial G}{\partial x_\alpha}\right)^2} \approx \bar{\sigma}^2 = \frac{a_1^2}{s_L^2}\bar{\omega}\ \frac{\bar{\varepsilon}}{\bar{k}} \tag{14.25}$$

while (14.11) relates $\overline{G'^{\,2}}$ to $\bar{\omega}$ and $\bar{\varepsilon}/\bar{k}$. From using (11.17) for the integral length scale of the turbulence we find that

$$\frac{\lambda_G}{\ell_t} \;=\; c_L \frac{s_L^\circ}{v'} \tag{14.26}$$

where $c_L = 3/(2a_1c_dc_\omega)^{\,1/2}$ is a constant.

Because (14.24) defines the root-mean-square gradient of G, we see that $2\lambda_G$ is the mean distance between excursions of G from its mean value which, in turn, is the mean

separation between one flamelet and the next. This separation is inversively proportional to the mean number of flamelet crossings per unit distance and scales with the length scale $\hat{L}_y$ proposed by Bray [8.6]. It may be shown that

$$\lambda_G \;=\; \hat{L}_y \,. \tag{14.27}$$

If this is substituted into (14.26) we recover the expression proposed by Bray [8.6] for the length $\hat{L}_y$.

14.5 Relationship to Bray-Moss-Libby Model

The model proposed originally by Bray, Moss, and Libby [8.9] is based on a progress variable c where $c = 0$ represents the unburnt mixture and $c = 1$ the fully burnt mixture. The pdf of c is written

$$P(c, \boldsymbol{x}) = \alpha(\boldsymbol{x})\delta(c) + \beta(\boldsymbol{x})\delta(1-c) + \gamma(\boldsymbol{x}) f(c, \boldsymbol{x}) \tag{14.28}$$

where α, β, and γ are the probabilities of finding unburnt, fully burnt and burning mixture, respectively, at station $\boldsymbol{x}$, δ is the Dirac delta function and $f(c, \boldsymbol{x})$ is the pdf of the burning mode. In the flamelet regime the limit $\gamma \to 0$ leads to a two-delta function description of the pdf with

$$\alpha(\boldsymbol{x}) + \beta(\boldsymbol{x}) = 1 \tag{14.29}$$

and the Reynolds mean progress variable

$$\bar{c} = \int_0^1 c \; P(c, \boldsymbol{x}) \; dc = \beta(\boldsymbol{x}) \,. \tag{14.30}$$

In the thin flamelet limit the progress variable c of BML is

$$c = \mathrm{H}\,(G - G_0) \;= \begin{cases} 0 & \text{for } G < G_0 \\ 1 & \text{for } G > G_0 \end{cases} \tag{14.31}$$

where H is the Heaviside function. Then

$$\bar{c}(\boldsymbol{x}) = \int_{-\infty}^{\infty} c P(G; \boldsymbol{x}) \; dG \;=\; \int_{G_0}^{\infty} P(G; \boldsymbol{x}) \; dG \,. \tag{14.32}$$

Here we have introduced the pdf $P(G; \boldsymbol{x})$. For a planar turbulent flame we may consider the thin wrinkled flame shown in Fig. 14.4 whose mean position lies in the plane $x = 0$. It is then possible to define $G(\boldsymbol{x}, t)$ such that

$$G(\boldsymbol{x}, t) - G_0 = x + F(y, z, t) \tag{14.33}$$

where $F(y, z, t)$ is the displacement of the flame surface from its mean position towards the unburnt gas. Then $G - G_0$ is simply the x-distance between the flame and the given

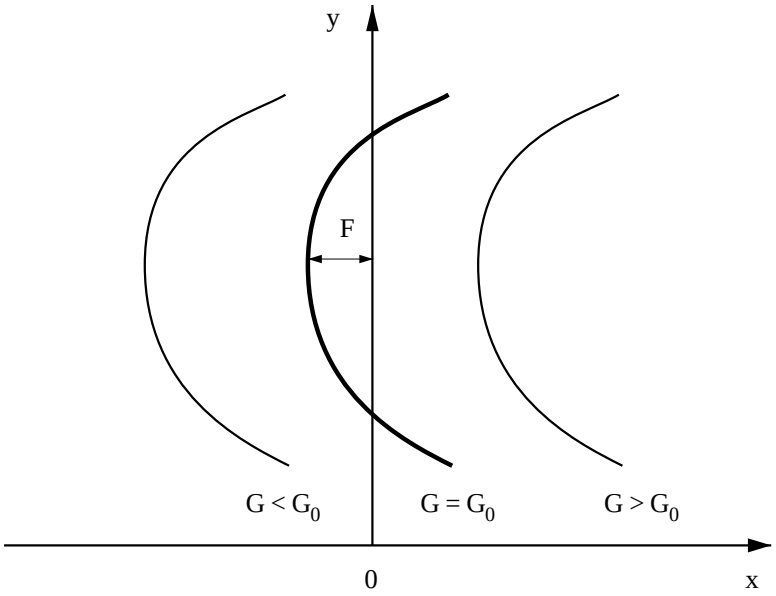

Fig.14.4 Relationship between the flame displacement $F(y,z,t)$ and the scalar field variable $G(\boldsymbol{x})$. The flame is represented by the surface $G(\boldsymbol{x}) = G_0$.

level surface. More generally $G - G_0$ defines a localised spatial coordinate at the flame surface.

For a planar turbulent flame the pdf of the spatial displacement F of the flamelet from its mean position is typically a nearly Gaussian function; see for example the experiments of Armstrong [8.8]. Since the flame front is fixed at $G = G_0$ in this case the pdf of the displacement corresponds to the conditional pdf $P(G_0;\boldsymbol{x})$. Furthermore, for the planar turbulent flame brush we may write $\bar{G}(\boldsymbol{x}) - G_0 = x$ and from translational invariance of the mean turbulent flame it follows that the pdf of $G - \bar{G}$ is independent of $\boldsymbol{x}$, leading to

$$P(G;\boldsymbol{x}) = P(G-\bar{G}) = P(G - G_0 - x) = P(F)\ . \tag{14.34}$$

Therefore $P(G-\bar{G})$ at fixed x has the same form as the pdf of the displacement $P(G_0;\boldsymbol{x}) = P(-x)$.

Other mean properties are evaluated similarly. For example, the mean of the density which is defined in the thin flamelet limit as $\rho = \rho_u + c(\rho_b - \rho_u)$ is calculated as

$$\begin{aligned} \bar{\rho}(\boldsymbol{x}) &= \int_{-\infty}^{\infty} \rho\ P(G;\boldsymbol{x})\ dG \\ &= \int_{-\infty}^{\infty} \left[\rho_u + H\left(G - G_0\right)\left(\rho_b - \rho_u\right)\right]\ P(G;\boldsymbol{x})\ dG \\ &= \rho_u + \bar{c}(\boldsymbol{x})\left[\rho_b - \rho_u\right] \end{aligned} \tag{14.35}$$

In order to proceed further we need an expression for $P(G;\boldsymbol{x})$ which may be obtained in the form of a pdf transport equation (O'Brien, [8.10]). For this purpose assume s_L to

be a constant, equal to s_L°, and consider (14.1) for $\mathcal{L} \to 0$ for a planar turbulent flame in a random field. Let $\mathcal{P}\left(\hat{G};\boldsymbol{x}\right)$ be the "fine grained density" whose ensemble average is the pdf $P(\hat{G};\boldsymbol{x})$ where $\hat{G}$ is the independent variable corresponding to $G(\boldsymbol{x},t)$. Then by analogy with [8.10] we write

$$0 = \frac{\partial \mathcal{P}}{\partial t} + \boldsymbol{v}\cdot\nabla\mathcal{P} + s_L^\circ \frac{\partial}{\partial \hat{G}} \ [< |\nabla G|_G > \mathcal{P}] \tag{14.36}$$

where $< |\nabla G|_G >$ is the conditional ensemble average of $|\nabla G|$. Since G_0 is arbitrary, level surfaces $G(\boldsymbol{x},t) = G_0$ are statistically independent and the conditioning is unnecessary here. Introducing the model

$$< \boldsymbol{v}\cdot\nabla\mathcal{P} > = \ \bar{\boldsymbol{v}}\cdot\nabla P \tag{14.37}$$

we obtain

$$\frac{\partial P}{\partial t} \ + \ \bar{\boldsymbol{v}}\cdot\nabla P \ = \ -s_L^\circ \frac{\partial}{\partial \hat{G}} [< |\nabla G| > P] \ . \tag{14.38}$$

An equation for $\bar{c}(\boldsymbol{x})$ may now be derived from (14.38). Define $\hat{c} = \mathrm{H}(\hat{G} - G) = 0$ for $\hat{G} < G_0$ and $\hat{c} = 1$ for $\hat{G} > G_0$. Multiply (14.38) by $\hat{c}$ and integrate from $\hat{G} = \ -\infty$ to $\hat{G} = \infty$. Noting that $\partial\hat{c}/\partial\hat{G} \ = \ \delta(G - G_0)$ we obtain

$$\begin{aligned} \frac{\partial \bar{c}}{\partial t} + \bar{\boldsymbol{v}}_u\cdot\nabla\bar{c} = \ & s_L^\circ \int_{-\infty}^{\infty} \delta(G - G_0) < |\nabla G| > P(G) \ dG \\ = \ & s_L^\circ < |\nabla G| \ > P(G_0;\boldsymbol{x}) \ . \end{aligned} \tag{14.39}$$

A transport equation for the instanteneous progress variable, when it is interpreted as a product concentration, for instance may be written as

$$\frac{\partial}{\partial t}(\rho c) + \frac{\partial}{\partial x_\alpha}(\rho v_\alpha c) = \frac{\partial}{\partial x_\alpha}\left(\rho D \frac{\partial c}{\partial x_\alpha}\right) + \dot{\omega} \ . \tag{14.40}$$

Here $\dot{\omega}$ is interpreted as a chemical source term. Straightforward averaging of the instantaneous transport equation for $1 - c(\boldsymbol{x},t)$, neglecting molecular transport terms, yields

$$\frac{\partial}{\partial t}\overline{\rho(1-c)} \ + \ \frac{\partial}{\partial x_\alpha}\overline{\rho v_\alpha (1-c)} \ = \ - \ \bar{\dot{\omega}} \ . \tag{14.41}$$

Using the joint pdf of Equation (14.28) together with (14.31) we find that

$$\begin{aligned} \overline{\rho(1-c)} = \ & (1-\bar{c})\rho_u \\ \overline{\rho v_\alpha (1-c)} = \ & (1-\bar{c})\rho_u \ \bar{v}_{\alpha u} \end{aligned} \tag{14.42}$$

so that the equation for $\bar{c}$ becomes

$$\frac{\partial \bar{c}}{\partial t} + \bar{\boldsymbol{v}}_u\cdot\nabla\bar{c} \ = \ \bar{\dot{\omega}}/\rho_u \ . \tag{14.43}$$

Note that in this form, in terms of the conditional velocity $\bar{\boldsymbol{v}}_u$, no turbulent transport flux appears in (14.43). Comparing this equation with (14.39) we find that the mean chemical source term for $\bar{c}$ is

$$\bar{\omega} \;=\; \rho_u s_L^\circ < |\nabla G| \; > P\left(G_0; \boldsymbol{x}\right) . \tag{14.44}$$

This expression is readily interpreted. The ensemble average $< |\nabla G| \; >$ corresponds to $\bar{\sigma}$ in (14.5). For the case of a planar steady flame with $\bar{G} - G_0 = x$ it is a constant which may be interpreted as the flame surface per unit volume and in the limit $\mathcal{L} \rightarrow 0$ considered here the solution of (14.5) leads to

$$s_T = s_L^\circ < |\nabla G| \; > \tag{14.45}$$

The displacement pdf $P(G_0; \boldsymbol{x})$ in (14.44), on the other hand, represents the spatial variation of the source term in (14.43).

Finally, the expressions derived above will be used to estimate the shape of the pdf $P(G; \boldsymbol{x})$. We again consider the case of a planar turbulent flame brush for which Equation (14.39) may be written

$$\frac{\mathrm{D}\bar{c}}{\mathrm{D}x} = K_1 P(G_0; \boldsymbol{x}) \tag{14.46}$$

where $K_1 = s_L^\circ < |\nabla G| \; > / s_T$.

Integrating (14.46) from $x = -\infty$ where $\bar{c} = 0$ to $x = +\infty$ where $\bar{c} = 1$ with the condition

$$\int_{-\infty}^{\infty} P(G_0; \boldsymbol{x}) dx \;=\; 1 \tag{14.47}$$

leads to the requirement that $K_1 = 1$ as anticipated by (14.45).
We assume

$$P(G_0; \boldsymbol{x}) \;=\; a \; \bar{c}(x) \left[1 - \bar{c}(x)\right] \tag{14.48}$$

from which it follows that

$$\frac{\mathrm{d}\bar{c}}{\mathrm{d}x} \;=\; a\bar{c}(1 - \bar{c}) \; . \tag{14.49}$$

Integrating and imposing the boundary condition that $\bar{c} = 1/2$ where $x = 0$ it is readily found that

$$\bar{c}(x) \;=\; \frac{1}{1 + e^{-ax}} \; . \tag{14.50}$$

Equation (14.48) then becomes

$$P(G_0; \boldsymbol{x}) \;=\; \frac{a \; e^{-ax}}{\left(1 + e^{-ax}\right)^2} \;=\; \frac{a}{\left(2 + c^{ax} + e^{-ax}\right)} \; . \tag{14.51}$$

The flame brush thickness may be defined as twice the variance of the pdf of the spatial displacement for a plane turbulent flame

$$\ell_{F,t}^2 = 4 \int_{-\infty}^{+\infty} F^2 P(F) \, dF \tag{14.52}$$

With Equation (14.34) this is equivalent to

$$\ell_{F,t}^2 = 4 \int_{-\infty}^{+\infty} G'^2 P(G;\boldsymbol{x})\, dG = 4\,\overline{G'^2}\ . \tag{14.53}$$

For a plane flame with general orientation in physical space a more general definition may be

$$\ell_{F,t} \ = \ 2\frac{\sqrt{\overline{G'^2}}}{|\nabla G|}\ . \tag{14.54}$$

which reduces to the previous one for the plane turbulent flame travelling in x-direction where $G \ = \ x + G_0$. In that case $\overline{G'^2}$ is independent of x and (14.6) reduces with (14.13) to (14.15). With (14.19) and (14.14) and $\overline{G'^2}$ may then be calculated as

$$\overline{G'^2} \ = \ \frac{2}{c_\omega}\frac{c_1 \bar{k}^3}{\bar{\varepsilon}^2} \ \left(1 + \alpha \frac{s_L^\circ \mathcal{L}}{\nu}\right)^{-1}\ . \tag{14.55}$$

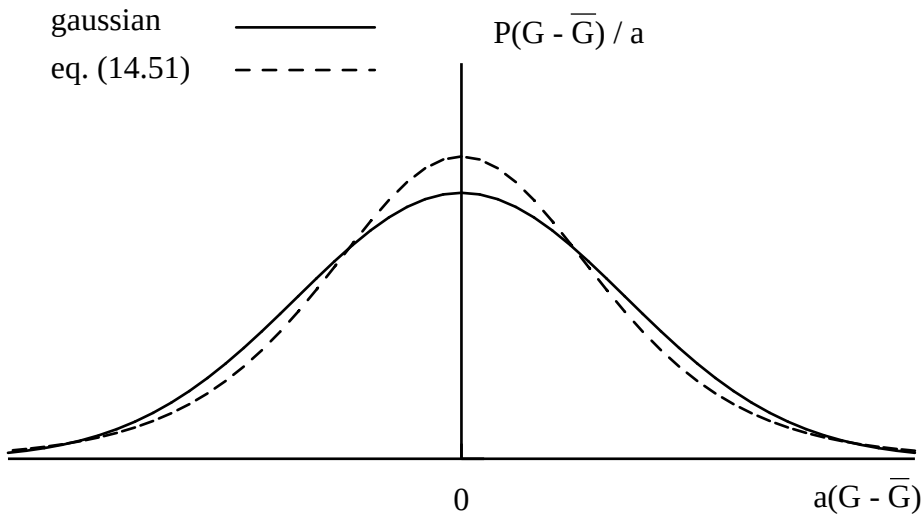

Fig. 14.5: The probability density function $P(G - \bar{G})$

Introducing (11.16) this leads to

$$\ell_{F,t} \ = \ c_2 \ell_t \left(\left(1 + \alpha \frac{s_L^\circ \mathcal{L}}{\nu}\right)\right)^{-1/2} \tag{14.52}$$

where $c_2 = \left(27 c_1 / c_w c_d^2\right)^{1/2}$. This shows that the flame brush thickness is proportional to the integral length scale but should decrease with increasing values of the Markstein length, which increases with Lewis number. This corresponds to a reduction of the flame surface

due to the smoothing effect of flame curvature, which has been observed experimentally by Wu et al. [8.11].

In view of the fact, noted earlier, that $P(G-\bar{G})$ is independent of x, we may now write Equation (14.51) as

$$P(G-\bar{G}) \;=\; \frac{a\exp\left(+a(G-\bar{G})\right)}{\left[1+\exp\left(+a(G-\bar{G})\right)\right]^2} \tag{14.53}$$

at any location in the flame. Fig. 14.5 shows this function to be symmetric and to have a shape similar to that of a Gaussian. Evaluating the second moment according to Equation (14.53) relates $\ell_{F,t}$ to a as

$$\ell_{F,t} \;=\; 2\left(\overline{G'^2}\right)^{1/2} \;=\; \frac{2\pi}{a\sqrt{3}} \tag{14.54}$$

Use of Equations (14.32) also allows us to obtain $\bar{c}$ explicitly in terms of $\bar{G}-G_0$ as

$$\bar{c} = \int_{G_0}^{\infty} P\left(G-\bar{G}\right)\,dG = \frac{1}{1+\exp\left[-a(\bar{G}-G_0)\right]} \tag{14.55}$$

which will be recognised as a restatement of (14.50) with x replaced by $\bar{G}-G_0$. Fig. 14.6 illustrates properties of the planar flame solution.

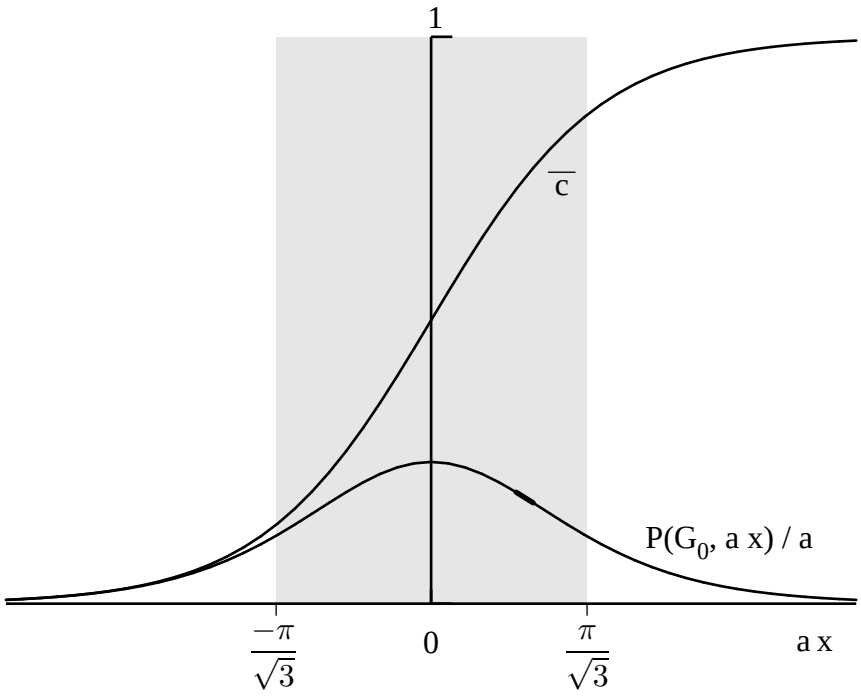

Fig. 14.6: Properties of the planar flame brush

As for non-premixed flamelets a flamelet library may be constructed by plotting all scalars that have been calculated for laminar premixed flames over $G - G_0 = x$. Due to translational invariance the origin $x = 0$ may be chosen appropriately. Such a library of unstrained premixed flamelets can be used to calculate the mean and the variance of any scalar Y available in the library according to

$$\begin{aligned} \bar{Y} &= \int_{-\infty}^{+\infty} Y P(G)\, dG \\ \overline{Y''^2} &= \int_{-\infty}^{+\infty} \left(Y - \bar{Y}\right)^2 P(G)\, dG \end{aligned} \tag{14.56}$$

This procedure can also be extended to strained premixed flamelets in a similar way as for non-premixed combustion.

References

[14.1] Peters, N., "A spectral closure for premixed turbulent combustion in the flamelet regime", J. Fluid Mech., to appear 1992.

[14.2] Wirth, M. and Peters, N., Turbulent premixed combustion: "A flamelet formulation and spectral analysis in theory and IC-engine experiments", 24$^{\text{th}}$ Symposium (International) on Combustion, The Combustion Institute, to appear 1992.

[14.3] Ashurst, W.T., Personal communication calculations as in "Geometry of Premixed Flames in Three-Dimensional Turbulence", Center for Turbulence Research, Proceedings of the Summer Program 1990.

[14.4] Yakhot, V., "Propagation Velocity of premixed turbulent flames", Combust. Sci. Technol. **60**, pp. 191–214, 1988.

[14.5] Bray, K.N.C. and Cant, R.S., Proc. Royal Soc. Lond. A **434**, pp. 217–240, 1990.

[14.6] Bray, K.N.C., "Studies of the Turbulent Burning Velocity", Proc. R. Soc. London A **431**, pp. 315–335, 1990.

[14.7] Gülder, Ö.L., "Turbulent Premixed Flame Propagation Models for Different Combustion Regimes", 23$^{\text{rd}}$ Symposium (International) on Combustion, The Combustion Institute, pp. 743–750 , 1990.

[14.8] Armstrong, N., "Planar Flowfield Measurements in Premixed Turbulent Combustion", PhD thesis, University of Cambridge, 1992.

[14.9] Bray, K.N.C., Libby, P.A., Masuya, G. and Moss, J.B., Combust. Sci. Techn. **25** , p. 127, 1981.

[14.10] O'Brien, E.E., in: Turbulent Recting Flows, Libby, P.A. and Williams, F.A. (Eds.), pp. 195–218, Springer-Verlag 1980.

[14.11] Wu, M.-S., Kwon, S., Driscoll, J.F. and Faeth, G.M., "Preferential Diffusion Effects on the Surface Structure of Turbulent Premixed Hydrogen/Air Flames", Combust. Sci. Technol., **78**, pp. 69–96, 1991.

Lecture 15. Turbulent Burning Velocities: Experiments and Correlation of Data

The turbulent burning velocity s_T introduced in (14.23) may be defined in analogy to the laminar burning velocity as the speed of advancement of the turbulent flame relative to the flow. Focussing on the turbulent burning velocity alone, however, leaves many other important aspects aside. It assumes that the interaction between turbulence and combustion is determined by local properties of the flow and that this interaction is locally in a steady state.

15.1 Experiments in Premixed Turbulent Combustion

An Idealized Normal Flame

Consider a steady turbulent flow with constant mean velocity $\bar{v}$ and uniform turbulence properties characterized by the turbulent intensity

$$v' = (2/3\bar{k})^{1/2} \tag{15.1}$$

and the integral length scale

$$\ell = c_d \, v'^3/\varepsilon \ . \tag{15.2}$$

Then a plane turbulent flame should propagate in opposite direction to the flow. A steady flame is obtained if the turbulent burning velocity is equal to the turbulent flow velocity

$$s_T = \bar{v} \tag{15.3}$$

This is the basis of the turbulent burning velocity formula (14.23) in lecture 14. This formula also shows how the burning velocity should depend on laminar kinetic parameters such as the laminar burning velocity, the laminar flame thickness or the Markstein length due to the effect of the flame stretch. Other parameters like the density ratio or heat loss are not even accounted for in this formula.

An idealized normal flame as shown in Fig. 15.1 has not yet been realized experimentally. Due to inhomogeneities in the turbulent flow and a very dynamic response of the flame thereon, a plane turbulent flame can only be established when additional measures are taken to stabilize it. These will be discussed below, when flames in a divergent or swirling flow are discussed.

The definition of a turbulent burning velocity goes back to Damköhler [15.1] who also introduced the concept of an instanteneous wrinkled turbulent flame surface, which for constant turbulence and combustion properties should have reached statistically a steady state. He equated the mass flux $\dot{m}$ of unburnt gas with the laminar burning velocity s_L through the turbulent flame surface area F_T to the mass flux through the cross sectional area F with the turbulent burning velocity s_T (conf. Fig. 15.1)

$$\dot{m} = \rho_u \ s_L \ F_T = \rho_u \ s_T \ F \ . \tag{15.4}$$

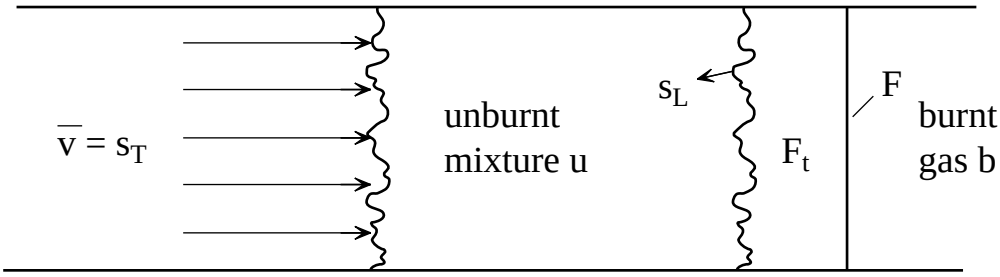

Fig. 15.1: An idealized normal premixed flame in a duct with constant flow velocity

This leads to

$$\frac{s_T}{s_L} = \frac{F_T}{F} \tag{15.5}$$

Using the geometrical analogy with a Bunsen flame, Damköhler assumed that the area increase of the wrinkled flame surface area relative to the cross sectional area is proportional to the increase of flow velocity over the laminar burning velocity

$$\frac{F_T}{F} = \frac{s_L + v'}{s_L} \ . \tag{15.6}$$

Here v' is the velocity increase which finally is identified as the turbulence intensity v'. Combining (15.5) and (15.6) leads to

$$\frac{s_T}{s_L} = 1 + \frac{v'}{s_L} \tag{15.7}$$

or in the limit $v' \gg s_L$

$$s_T \sim v' \tag{15.8}$$

which is Damköhler's result. It states that the turbulent burning velocity should be independent of any laminar velocity, length and time scale of combustion. Therefore chemistry should not affect the process of turbulent flame propagation. This is inconsistent with experimental data which show a dependence of s_T/s_L on fuel composition, turbulent and laminar length scales and in general a non-linear dependence on the ratio v'/s_L. Therefore a generalisation of (15.7) has been proposed

$$\frac{s_T}{s_L} = 1 + c \left(\frac{v'}{s_L} \right)^n \tag{15.9}$$

where n is called the "bending exponent" and c is a fuel dependent parameter which contains influences of the length scale ratio and/or the turbulent Reynolds number. Experimentally derived values of n typically vary between $n = 0.5$ and $n = 1.0$ and c between

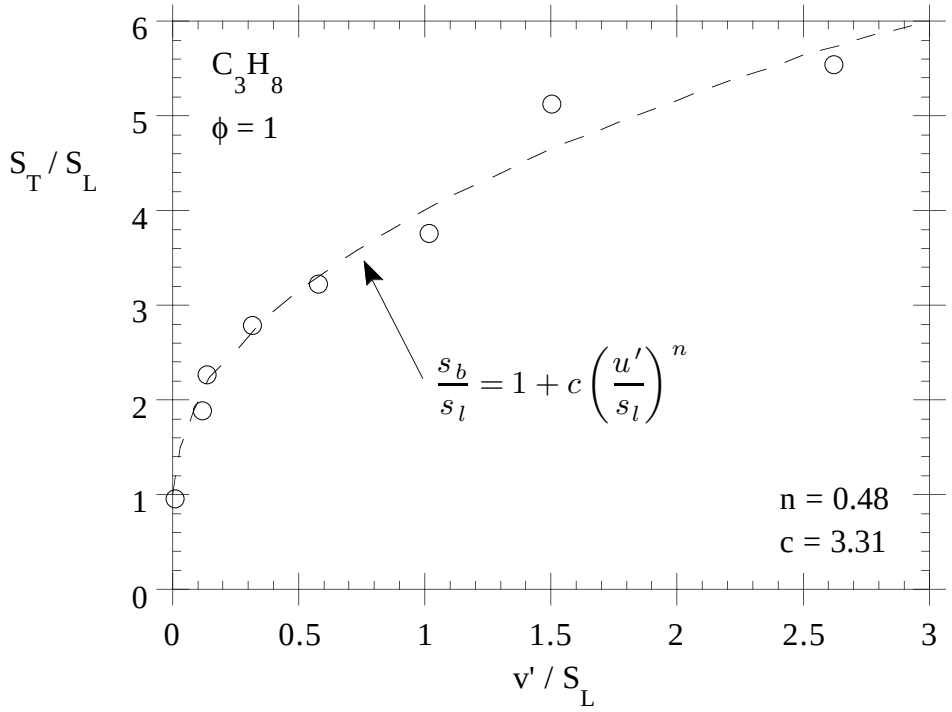

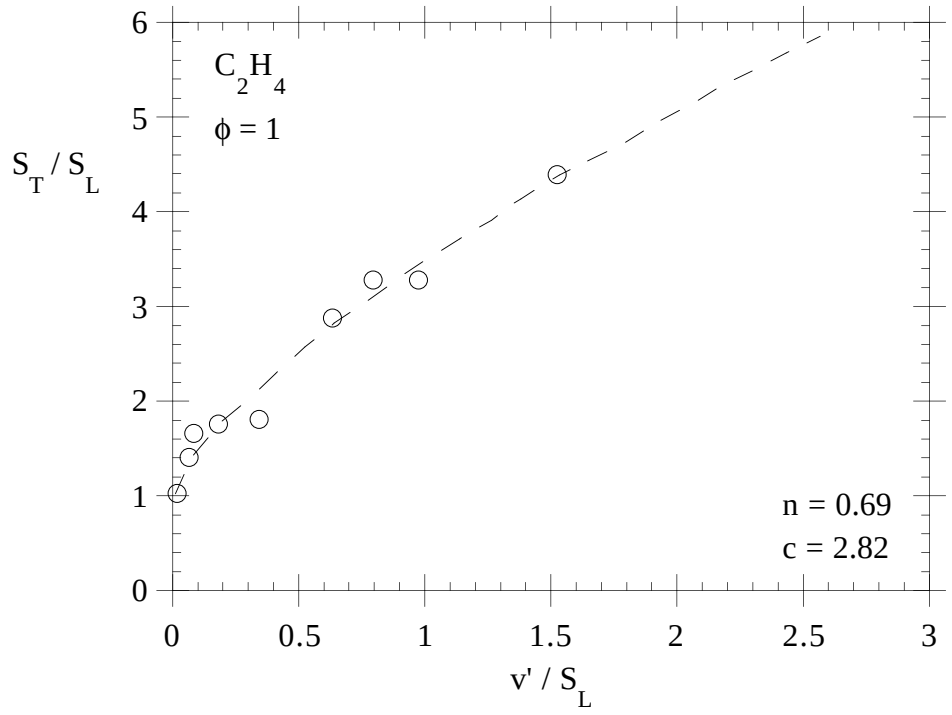

Fig. 15.2 a–b:

1.0 and 4.0. Recent data from Trautwein [15.2] that were obtained in a square piston single stroke compression-expansion machine are shown in Fig. 15.2 a–c.

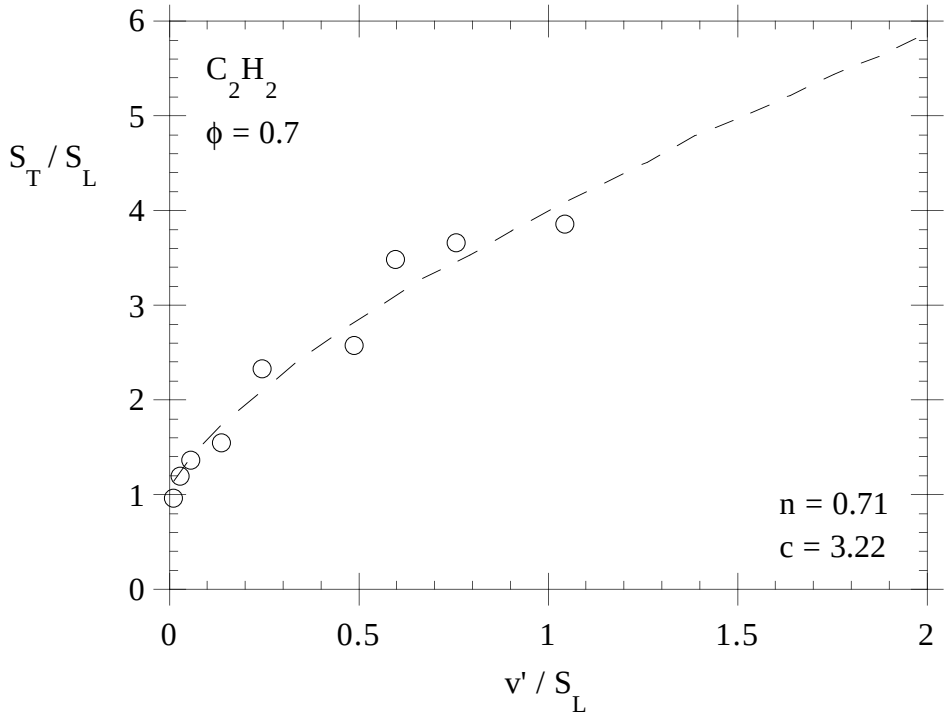

Fig. 15.2 c: Non-dimensional turbulent burning velocity s_T/s_L vs. non-dimensional turbulence intensity v'/s_L for three fuel-air mixtures. The dashed curve represents the best least-square fit for the experimental data according to the relationship $s_T/s_L = 1 + c(v'/s_L)^n$.

The Turbulent Bunsen Flame

The most classical experiment to determine turbulent burning velocities uses the Bunsen burner. The only difference to the laminar Bunsen burner experiment is that the flow is turbulent rather than laminar. This may be achieved by running the experiment with a large enough diameter and velocity to exceed the critical Reynolds number in the pipe of the Bunsen burner or by adding a turbulence grid at the exit of the burner. The second arrangement has the advantage that the turbulence length and velocity scales may be controlled independently while in the case of a turbulent pipe flow they vary in radial direction and depend on whether the pipe flow is fully developed or not. In Fig. 15.3 the turbulent Bunsen cone is shown schematically as a collection of instanteneous flame contours and as a long-time exposure of the fluctuating flame front.

The second picture corresponds to a time-average description and shows the mean flame contour and the flame brush thickness which increases with downstream distances. Also, a mean stream line is shown. Due to thermal expansion in the flame the stream lines are deflected as in a laminar Bunsen flame. As in a laminar Bunsen flame the turbulent burning velocity may be determined by measuring the angle of the mean flame contour with respect to the flow. Since this angle is not constant such a measurement gives only an estimate.

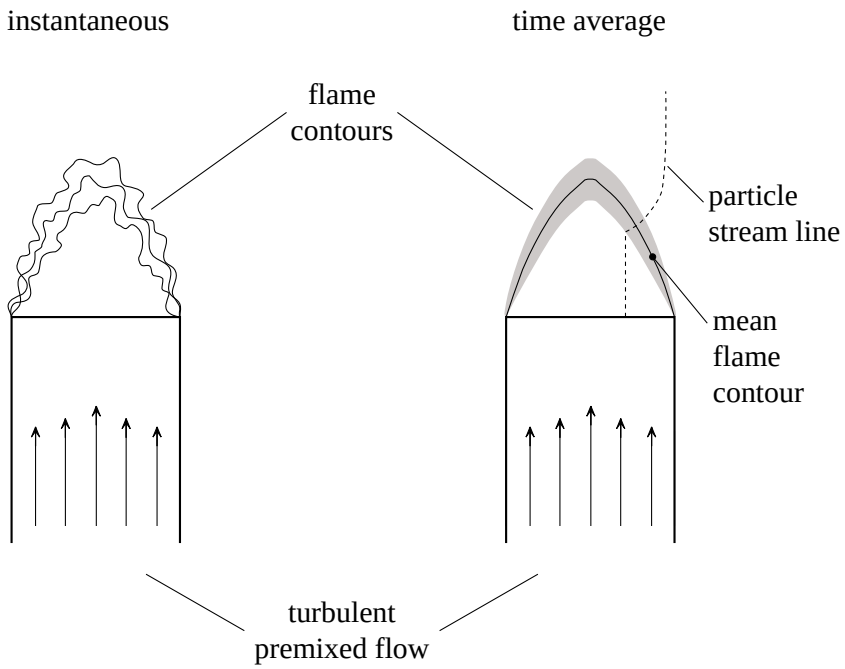

Fig. 15.3. Instantaneous and time averaged Bunsen flames

The **advantages** of this experiment are the following:

- The mass flow rate through the Bunsen cone in known.
- There is an easy optical access to the flame.

The **disadvantages** are:

- The flow field is not uniform in the case of a fully developed pipe flow.
- On the inner and outer side walls of the Bunsen pipe boundary layers develop and create non-uniformities of the flow.
- If the flame is slender parts of the flame surface may interact with each other and with the oncoming flow due to heat expansion.

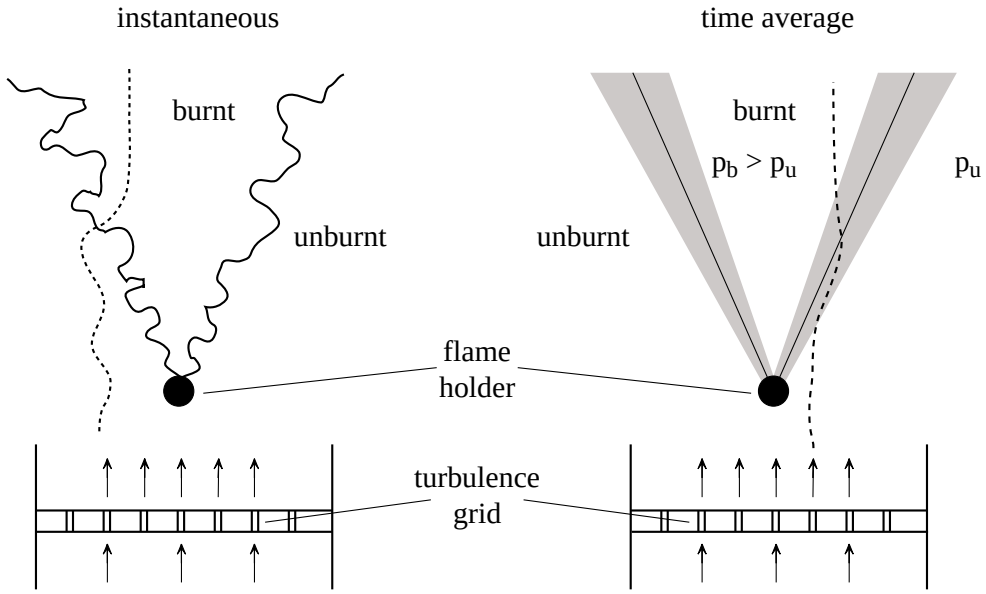

Fig. 15.4. Instantaneous and time averaged V-shaped flames

The V-Shaped Flame

Another classical experiment in premixed turbulent combustion is the V-shaped flame attached to a flame holder in a turbulent flow behind a turbulence grid. An instanteneous and a time average flow contour are shown in Fig. 15.4.

Again a mean stream line and also an instantaneous stream line are shown. Due to the expansion in the flame the pressure in the burnt gas region between the two flame contours is higher than in the unburnt gas outside. This leads to a deflection of the stream lines in the unburnt gas and consequently also of the mean flow contours. Therefore the angle at which the unburnt gas enters into the flame is not known in advance.

The **advantages** of this configuration are the following:

- Due to the turbulence grid the flow and turbulence properties can be controlled and made uniform normal to the flow direction.
- In flow direction the turbulence may be characterized as spatially decaying.

The **disadvantages** are:

- There is a strong deflection of the stream lines of the oncoming flow due to the higher pressure in the burnt gas.
- Effects of the flame holder and the wake developing behind it on the flow and the flame immediate down-stream of it may be considerable.

Turbulent Counterflow Premixed Flames

In the both preceeding flame configurations the flame enters with an angle into the flame. A normal flame that corresponds the closest to the idealized flame discussed above may be established in a divergent axi-symmetric flow between two opposed ducts. In Fig. 15.5 such a flow configuration is shown schematically.

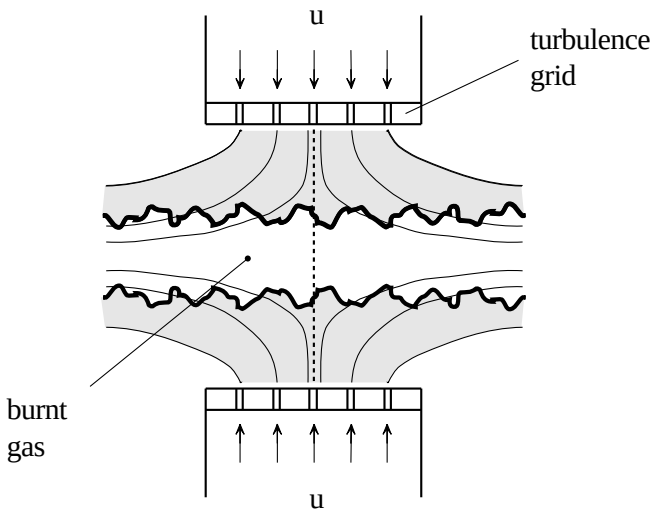

Fig. 15.5. Two turbulent counterflow premixed flames

As in laminar counterflow flames, the flow velocity in axial direction is approximately constant, while the normal velocity increases with radial distance from the centerline. Therefore the two mean flame contours would be approximately normal to the flow, if the turbulence properties were also constant in each plane normal to the flow. This is not necessarily the case because the production of turbulence depends on mean velocity gradients which change with distance from the centerline.

The **advantage** of this configuration is the following:

- Plane steady flames in fully developed turbulence can be stabilized.

The **disadvantages** are:

- The flow-field is non-uniform with mean strain.
- The two flame fronts may interact with each other.

Unsteady Flames Homogeneous Isotropic Turbulence

In order to avoid the influence of non-homogeneities in studying turbulent burning velocities, it is useful to consider unsteady flames. An isotropic turbulence field may, for instance, be established in a fan-stirred combustion bomb shown in Fig. 15.6.

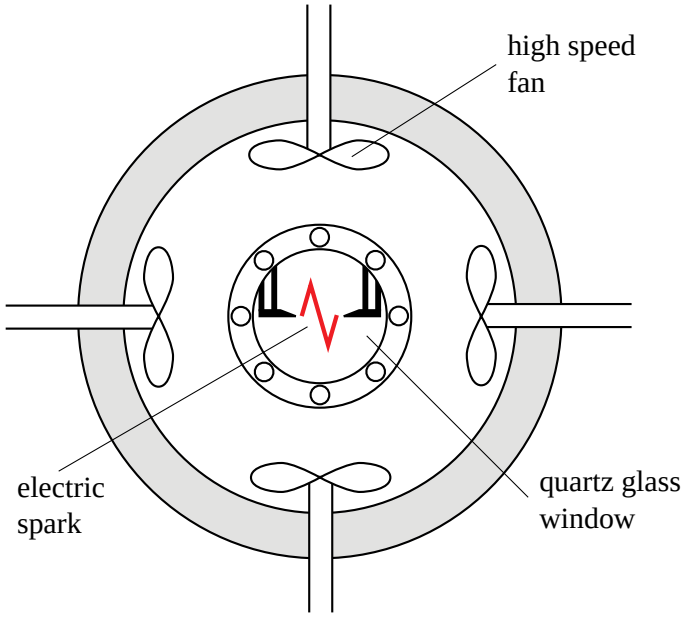

Fig. 15.6: A fan-stirred combustion bomb for premixed turbulent combustion studies

Such a device has been used extensively by D. Bradley and co-workers. Four to six mutually opposed high speed fans create in the center region of the bomb a nearly isotropic homogeneous turbulence field with low mean velocity. A flame kernel is initiated by an electrical spark and propagates radially outwards. It can be observed through quartz glass windows. A similar other device is the single stroke compression maschine with a square piston and a turbulence grid that is pulled through the combustion chamber before ignition. Such a configuration was used by Adomeit and co-workers.

During the flame kernel development the instantaneous flame front interacts with all sizes of turbulent eddies. Therefore, there is a time period during the early flame kernel development, where the interaction of the flame with the turbulent flow field is not fully established. An estimate of this time period will be given below.

The **advantage** of these configurations is the following:

- A nearly isotrop homogeneous turbulence field with high turbulence intensity is established.

The **disadvantages** are:

- The experiment is unsteady and the early flame development must be taken into account.

- The optical access through quartz glass windows is more difficult than in open flames.

15.2 Fractal Analysis of the Turbulent Flame Surface Area

An alternative way to determine the turbulent burning velocity is to use (15.5) and to measure the turbulent flame surface area F_T. The instantaneous flame front can be visualized by using the laser sheet technique. This is shown for the V-shaped flame in Fig. 15.7.

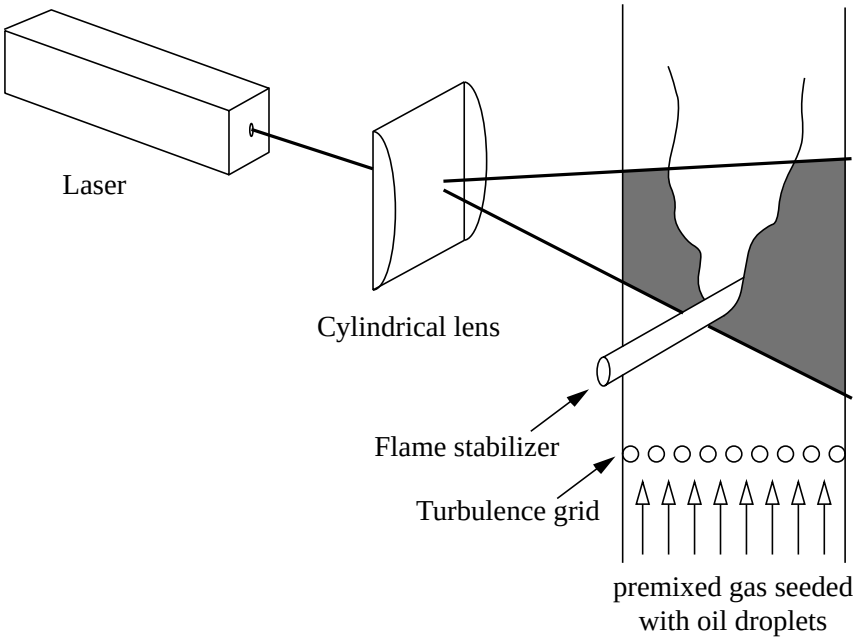

Fig. 15.7: Experimental set-up to visualize the flame surface

The beam of a laser is widened by a cylindrical lens. The premixed gas from the burner is seeded by oil particles and passes through a turbulence grid. The V-shaped flame is stabilized by a rod normal to the flow. The laser light is scattered by the oil droplets which vaporize very rapidly in the flame front. Therefore the instantaneous flame contour is then visualized as the interface between the bright shining region of the unburnt gas and the dark region of burnt gas. It may be recorded either by high speed cinematography or by a CCD camera and may then be processed and digitalized.

The length of the flame contour squared is proportional to the flame surface. The length can be measured by following the contour down to the smallest scales. Since the smallest scales are not always resolved, fractal analysis can be used. The flame length $L(r)$ is then measured by following it with decreasing measuring scales r. The log of $L(r)$ is plotted over the log of r. This is shown in Fig. 15.8.

At measuring scales larger than the integral length the flame contour remains nearly constant. With decreasing measuring scales more and more of the fine structure is resolved and the measured length $L(r)$ increases as r decreses. It reaches a constant value when all scales are resolved for small values of r.

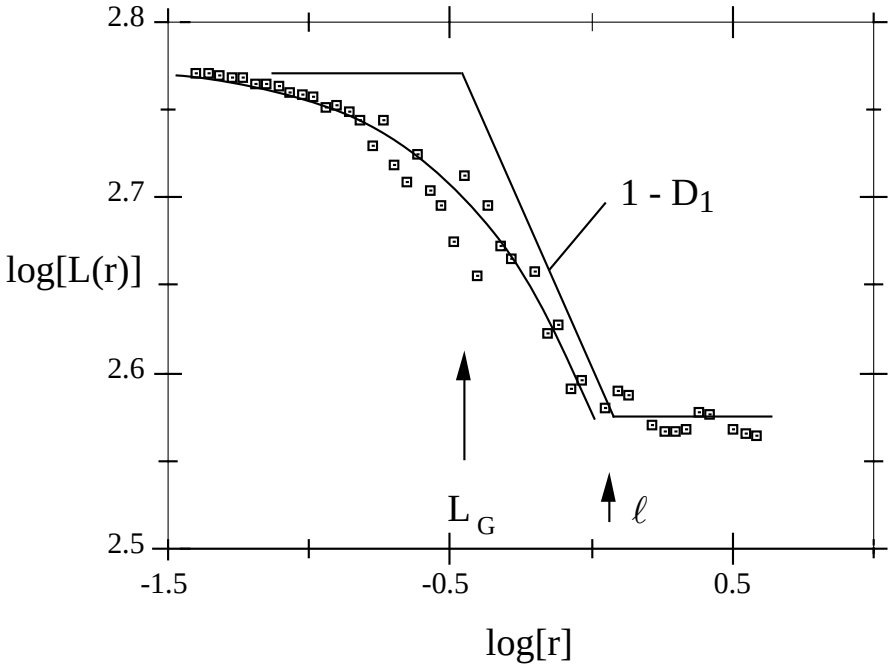

Fig. 15.8: Log-logplot of a measured flame contour and theoretically predicted curve

The diagram in Fig. 15.8 may be idealized by assuming a constant slope region between that integral scale ℓ and the lower cut-off scale which should be the Gibson scale ℓ_G. In such a region with constant slope equal to $1 - D_1$, the turbulent flame contour would behave as a fractal where the fractal dimension of a line is D_1. This is larger than the Euklidian dimension $d = 1$, leading to $1 - D_1 < 0$ and therefore to an increase of $L(r)$ for smaller measuring scales r. A fractal plot of a surface rather than a line would have the slope $2 - D_2$ where $D_2 = D_1 + 1$. From this relation the ratio between the turbulent flame surface area and the cross sectional area are may be calculated as

$$\frac{F_T}{F} = \frac{F(\ell_G)}{F(\ell)} = \left(\frac{\ell_G}{\ell}\right)^{2-D_2} \quad . \tag{15.10}$$

Introducing here the relation between the Gibson scale and the integral length scale from (11.33) one obtains with (15.5)

$$\frac{s_T}{s_L} = \left(\frac{v'}{s_L}\right)^{3(D_2-2)} \quad . \tag{15.11}$$

One may now derive a limiting value for the fractal dimension of the flame surface by considering the mass flux through the flame surface

$$\begin{aligned} \dot{m} &= \rho_u \; s_L \; F \; (\ell_G) \\ &= \rho_u \; s_L \; F \; (\ell_G/\ell)^{2-D_2} \\ &= \rho_u \; F \; v' \; (v'/s_L)^{(3D_2-7)} \end{aligned} \tag{15.12}$$

For very large values of (v'/s_L) the mass flow should be independent of s_L. This leads to

$$D_2 = 7/3 \tag{15.13}$$

and with (15.11) to

$$\frac{s_T}{s_L} = \frac{v'}{s_L} \ . \tag{15.14}$$

This is again Damköhlers's result and is in agreement with the arguments that lead to (14.12) and the first term on the right-hand side of (14.17) in that limit.

15.3 Unsteady Effects During the Increase of the Flame Surface

If an electrical spark ignitiates a flame in a premixed turbulent flow field, the development of the flame surface and therefore the burning velocity needs some time to reach a steady state value. The initial flame kernel grows during this time from values lower than the Gibson scale to values larger than the integral scale. Only when the flame kernel is typically larger than the integral scale, a steady turbulent burning velocity will be reached. Evidents of unsteady effects are found in the data from Trautwein [15.2] shown in Fig. 15.9 where the ratio of the turbulent to the laminar burning velocity is plotted over v'/s_L with the fraction of burnt volume in the chamber as a parameter. As the time and therefore y_b increases, the turbulent burning velocity increases. This increase is more rapid for C_2H_2 which has a much larger laminar burning velocity than C_3H_8 and C_2H_4 and therefore reaches the steady burning velocity earlier. Values for n and c in (15.9) are shown as a function of y_b in Fig.15.10.

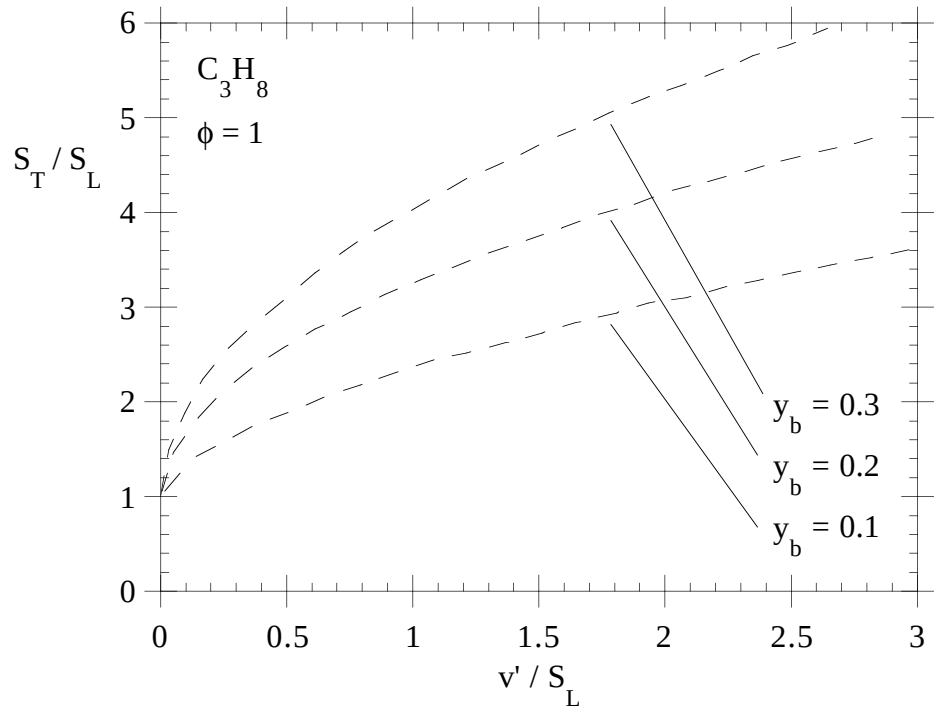

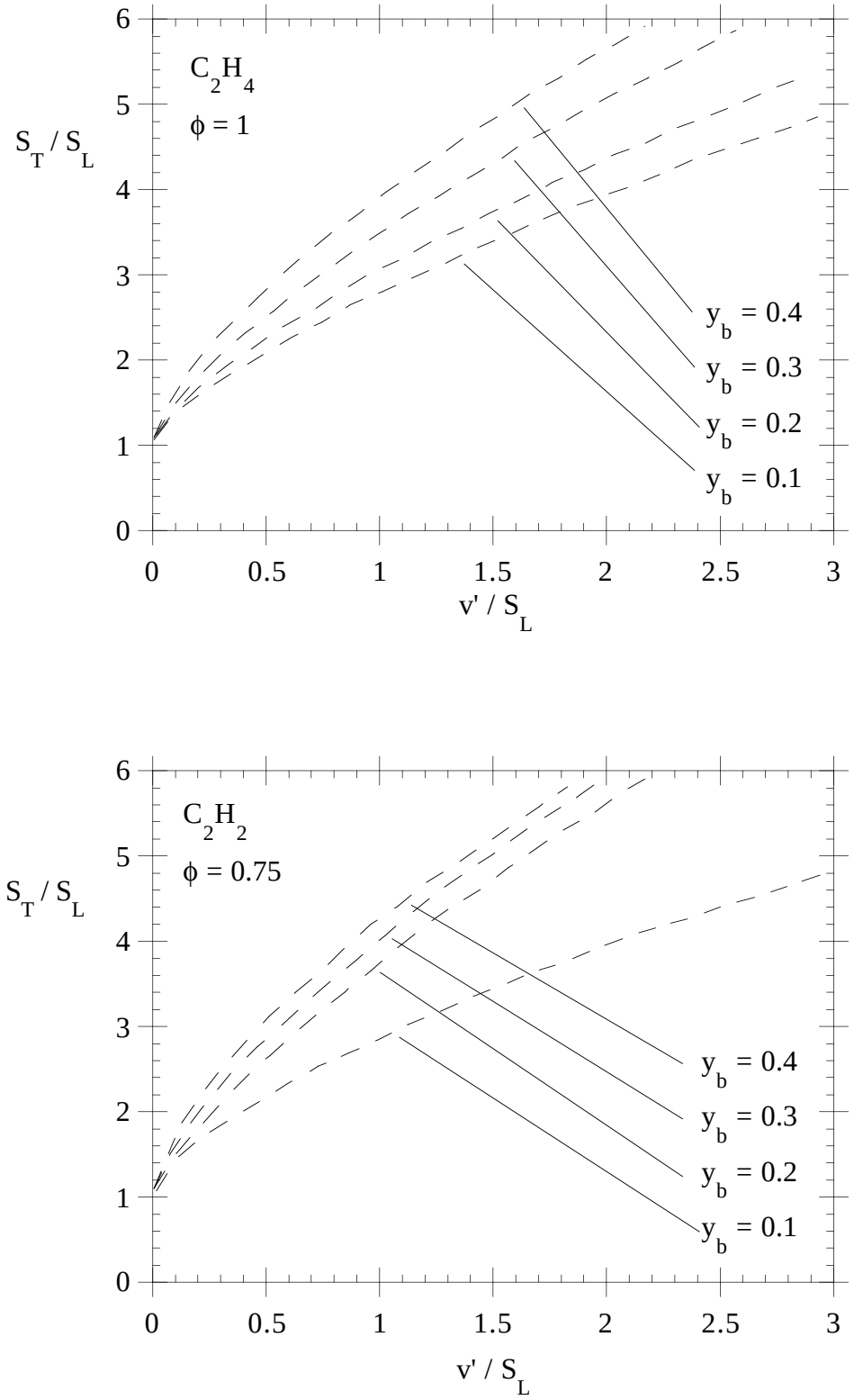

Fig. 15.9: Best least-square fit making use of equation $s_T/s_L = 1 + c(v'/s_L)^n$

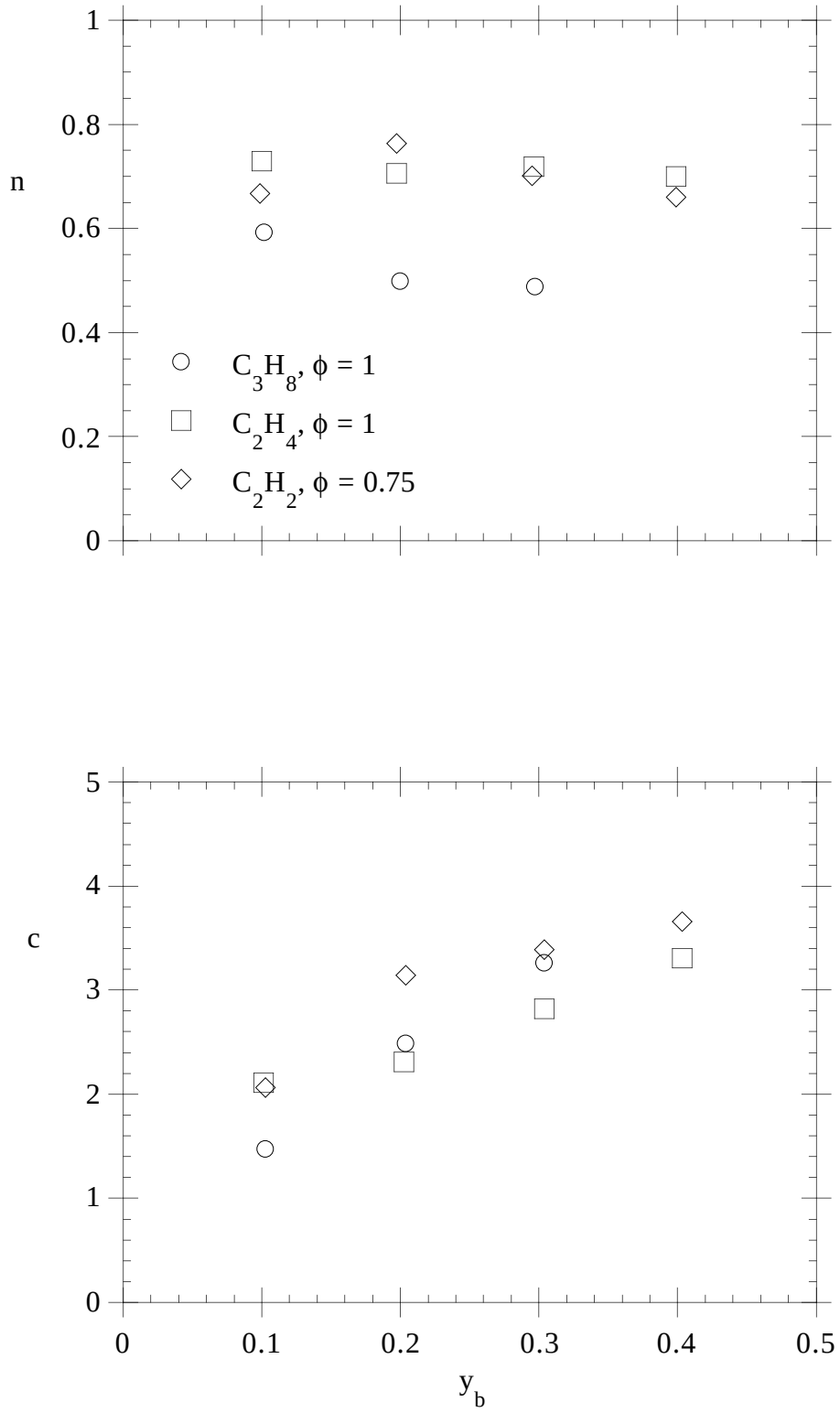

Fig. 15.10: Exponent n and factor c of the relationship $s_T/s_L = 1 + c(u'/s_T)^n$ as obtained from the method of least squares in dependence upon burnt volume fraction y_b.

15.4 An Estimate of Unsteady Flame Kernel Development

If the size of a developing flame kernel is smaller than the integral length scale, the corrugation of its surface can only be caused by eddies of the same or a smaller scale in the spectrum. Since according to (15.5) the turbulent burning velocity depends on the flame surface area, it must be lower than the value of a fully developed turbulent flame. In order to estimate the time needed for a turbulent flame to develop from a flame kernel, we will assume that the increase of the length scale of the flame surface per unit time is essentially due to the straining action of the large eddies. This increase is reduced by the turnover of the eddies of the size than the flame kernel, because this is the largest eddy with which the flame kernel can interact. This is schematically shown in Fig. 15.11.

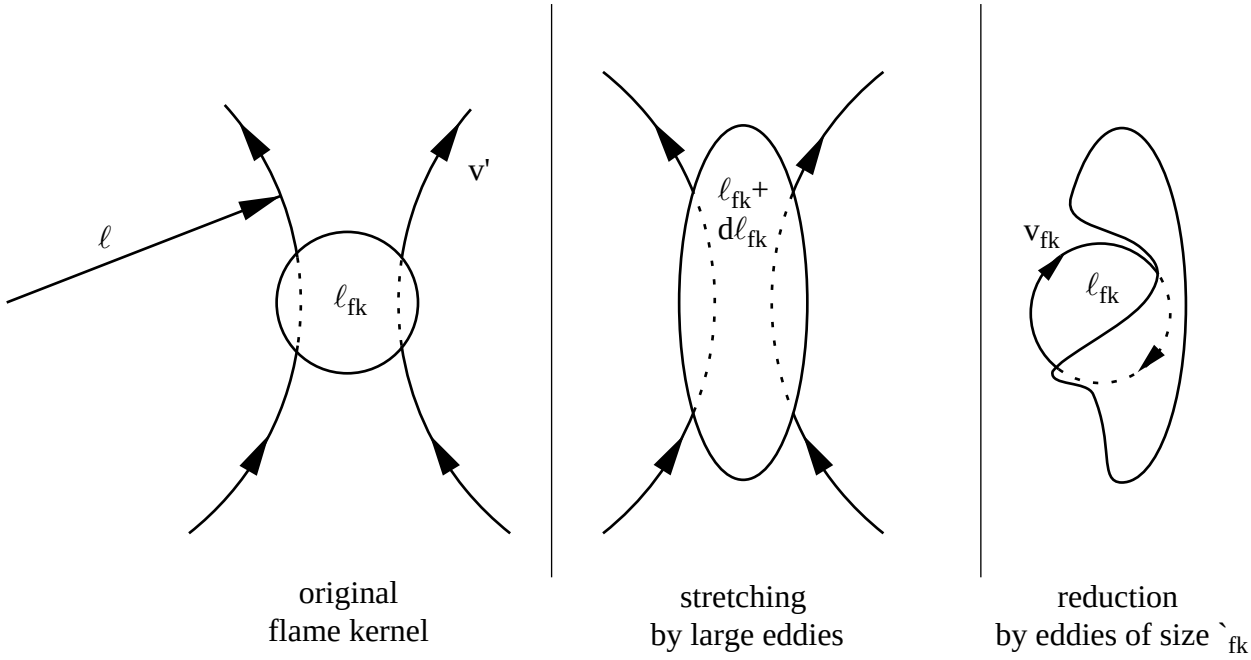

Fig. 15.11: Schematic illustration of the straining and reduction of the size of a flame kernel

This leads to the balance for the temporal change of the size of the flame kernel length scale $\ell_{\rm fk}$

$$\frac{{\rm d}\ell_{\rm fk}}{{\rm d}t} = \alpha\ v' - \beta\ v_{\rm fk} \tag{15.15}$$

where the turnover-velocity of the eddies of the size of the flame kernel is set equal to

$$v_{\rm fk} = v_n = (\varepsilon\ \ell_n)^{1/3} = (\varepsilon\ \ell_{\rm fk})^{1/3}. \tag{15.16}$$

Normalizing (15.15) with the integral length $\ell = c_d\ v'^3/\varepsilon$, it may be written in terms of $x = (c_d\ \beta^3/\alpha^3)\ell_{\rm fk}/\ell$, $\tau = (\beta^3/\alpha^2)\ t\ v'/\ell$ as

$$\frac{{\rm d}x}{{\rm d}\tau} = 1 - x^{1/3} \tag{15.17}$$

which has the solution

$$\tau = 3\left[-\ln(1-x^{1/3}) - x^{1/3} - \frac{1}{2}x^{2/3}\right] . \tag{15.18}$$

This function is plotted in Fig. 15.12 in terms of x over τ. It shows that x increases proportionally to τ for small values of τ when the first term of the r.h.s. of (15.18) is dominating. For large values of τ the limit $x \to 1$ is approached asymptotically. Since τ is proportional to the ratio of the time divided by the turnover time of the large eddies and x proportional to the length scale of the flame front divided by the integral length scale, it follows that the flame surface approaches a value that scales with the integral scale during a time period proportional to the large eddy turnover time. Since the turbulent burning velocity is proportional to the flame surface one obtains a fully developed turbulent flame with a turbulent burning velocity that scales with v' only after this time delay.

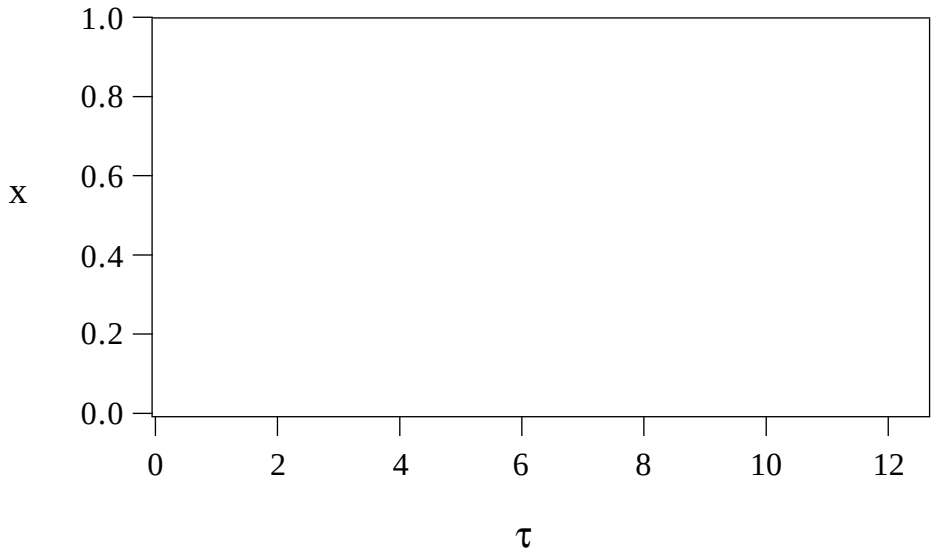

Fig. 15.12. Solution of (15.18)

References

[15.1] Damköhler, G.: Der Einfluß auf die Flammengeschwindigkeit in Gasgemischen, Z. f. Elektroch. No.11; 601–652 (1940).

[15.2] Trautwein, S.E., Untersuchung des Einflusses der Turbulenz auf die Flammenausbreitung unter motorischen Bedingungen, Dissertation Aachen 1989.